University of London
Imperial College of Science, Technology and Medicine

RELIABILITY ANALYSIS OF FATIGUE AND FRACTURE UNDER RANDOM LOADING

by

WANGWEN ZHAO

A thesis submitted for the degreee of Doctor of Philosophy
in the Faculty of Engineering of the University of London

Structural Engineering Section
Civil Engineering Department

March 1989

ABSTRACT

This thesis has developed a methodology for the reliability analysis of structural steel components with pre-existing cracks under the action of random loading. This analysis includes a study of fracture mechanics, fatigue prediction, random load modelling and structural reliability analysis.

Chapter 2 reviews the development of structural reliability theory and presents a refined scheme for the second-order reliability calculation (SORM). Chapter 3 gives the theoretical background of fracture mechanics and the associated design methods, in particular the R6 method. Chapter 4 develops a method by which the reliability analysis of a cracked component under non-cyclic loading can be carried out. In Chapter 5 a new method for determining the probability distribution of the stress range in a structure subjected to stochastic loading is developed, and this is followed in Chapter 6 by a detailed deterministic fatigue analysis. Finally, in Chapter 7, the various techniques are combined to construct a method for the reliability analysis of a structural component failing by fatigue and fracture under random loading.

New contributions include:

1) The formulation of failure functions for reliability analysis of components failing by fatigue and fracture. For assessing the critical state of the structure, the CEGB R6 method has been used, including the treatment of ductile tearing instability.

2) The modelling of basic variables for fatigue and fracture, especially the loading variable. It is found that the stress range distribution derived from the rainflow method can be modelled as the weighted sum of two Weibull distributions whose parameters are functions of the spectral properties of the stress process. Using this model, the equivalent stress range can be calculated and has been found to agree more closely with the simulated results than other empirical models.

3) Improvement to the methods for reliability evaluation. A more efficient scheme for SORM has been implemented in a computer program.

4) Sensitivity studies. The results of sensitivity studies show that for typical steels (a) plastic collapse failure mode is likely to be important in both deterministic and probabilistic safety assessment, (b) for long term fatigue problems, the reliability is not sensitive to the non-fatigue variables such as fracture toughness or yielding stress, so that LEFM approach may be acceptable as a failure criterion. Finally, in structures where the fatigue damage is related to the fundamental natural frequency of the system, uncertainties in either the natural frequency or the frequency of the dominant source of loading can be of extreme importance in governing the reliability of a structure against fatigue.

ACKNOWLEDGEMENTS

I wish to express my deepest gratitude to my supervisor, Mr. M. J. Baker, for his skilful guidance, continuous encouragement and financial support throughout the research, and to my co- supervisor, Prof. C. E. Turner, for his help and inspiration. I am also greatly indebted to Prof. P. J. Dowling, Head of the Department, for his arrangement firstly for the MSc and then for the Ph.D in the Department.

Doing a Ph.D thousands of miles away from home could not be a happy experience without support from family, smiles from friends, and accommodation in the host country. I wish to thank all of those who have helped me and befriended me. I will remember in particular Mr. J. Neale, Mr. G. Scopes and all fellow reseachers in Room 411. I also wish to thank Dr. G. Anagnostides, Dr. M. Chryssanthopoulos and Dr. P. Duxbury with whom I enjoyed many fruitful discussions.

I also wish to thank Mr. R. Turner, Mr. N. Kumar Shetty and Dr. P. Duxbury for reading the draft thesis.

Finally I would like to thank the British Council and the Chinese Ministry of Education for funding the project.

ERRATA

Page No.	Line No.	Error	Correction
Contents	7.5	failuree	failure
1.3	5	treated	be treated
2.16	7		delete one (standard)
3.5	2	initialization	initiation
3.5	last	Westgaad	Westgaard
3.12 Eqn.	3.31,3.32	$\cos^{-1}$	sec
3.14	8	widesread	widespread
3.14	20		delete (will)
3.15	7	set up a	set up
3.15	Eqn.3.37,3.38,3.39.		a is not subscript
3.16	Eqn. 3.43	K	k
3.18	4–5		delete (and in the region where)
3.18	7	where	whether
3.18	16	Pradtl	Prandtl
3.19	5	may	must
3.20	18	function	functions
3.22	11	effects	effect
3.23	4	initialised	initiated
3.25	20	ration	ratio
3.32	26	modules	modulus
4.4	24	Trasca	Tresca
4.7	10	failure	safety
4.7	22	cartisian	cartesian
4.7	27	margin	margins
4.15	10	a	an
5.5	Eqn.(5.3)		add one more double infinite integral sign
5.5	Eqn.(5.7)	$-i$	$+i$
5.20	25,26	ϵ	β_2
5.21	Table 5.3	ϵ	β_2
5.22	10	The the	the
5.22	10	th	the
6.3	19	ranges	range
6.16	13	increase	increased
6.20	9	last	lasts
6.20	15	limit	limits
7.10	31		delete (the)
7.14	2	spectral	spectra
7.14	14	treated a	treated as a

Reference	Error	Correction
3.16	Stones	Stone
3.21	m., and pars	M., and Paris
3.27	Ernst	Ernest
5.3	labes	Labes
5.3	Uncertaities	Uncertainties
5.4	Wirshing	Wirsching
5.9	prduced	produced
5.13	Hydrogrphisches	Hydrographisches
5.14	stochstic	stochastic
5.15	Brabbia	Brebbia
5.28	precesses	processes
6.3	efeect	effect
6.7	thr	the
6.22 Marine technology directorate		Marine Technology Directorate

CONTENTS

Chapter 1

Introduction

1.1

1.1 General Remarks

This thesis has developed a methodology for the reliability analysis of structural components which fail by fatigue and fracture. The author has chosen this work both for its theoretical interest and because of its application potential. The theoretical interest derives from this relatively new approach to safety assessment and the in-depth study of natural phenomena, whereas the application potential results from the urgent need to improve safety standards in industry and to optimise the total cost of design, construction and maintenance.

1.2 The Need For Reliability Analysis

Safety of the living space has always been the prime consideration for human beings. The advance of knowledge, especially in civil engineering, in this century has increased the safety standards for structures dramatically. However in recent years, a series of major disasters have occurred all over the world, for example, the Chernobyl nuclear accident in USSR, the Piper Alpha offshore platform disaster in the UK, the earthquakes in China and the USSR, the hurricanes in the UK and the Caribbean, the floods in Bangladesh etc. The attainment of higher standards of structural safety is obviously a challenge.

In the past, structures have been designed using a simple factor of safety approach to determine the maximum load carrying capacity of a structure, or the length of time that a particular type of load can be sustained. Traditionally, each variable, whether loading or resistance is selected in a conservative way as judged by previous data, experience and, if necessary, human intuition. For different structures (e.g. aircraft, railway, offshore) , the effective safety factors can be quite different.

There is a growing demand from industry to quantify the true safety of structures by statistical calculations. For a good, reliable and durable structure, more initial investment is needed, resulting in reduced maintenance costs. On the other hand, when the initial investment is low, maintenance costs can be expected to rise. The correct balance between these approaches requires knowledge beyond intuition.

In addition, existing structures present an economic maintenance problem. In some cases it is difficult to know how much maintenance is needed to ensure the continuing safety of the structure. This is particularly the case for offshore structures, where maintenance costs are typically very high.

The reliability approach for safety assessment has emerged as a rational method for treating the safety. In this approach, structural failures are events arising from an unfavourable chance combi-

nation of statistical variables which govern the behaviour of the structural system.

More specifically, reliability methods calculate the reliability or probability of failure of the system. In practical situations, the systems are often too complex even for a deterministic approach to incorporate all the factors contributing to the safety of the structure. Thus, the structural system has to be idealised. The reliability calculated in such a way should not treated as an absolute value but rather as a comparative measure of safety.

Research has been pursued by a number of people to minimise the difference between the idealised reliability and actual reliability. Nevertheless, reliability models are often simplified when applied to actual structures. Some of the characteristics, which the application models may have, have been summarised by Duddeck[1.1]:

1. Reality is not portrayed but substituted.

2. Validity is restricted to certain regions of application.

3. Some variables and theories are ignored if the design is insensitive to them.

4. Loads are idealised and limit states are simplified to a few representative ones.

5. The mechanical model is simplified considerably: neglect of imperfections, initial stress, secondary stress concentration, etc.

The above list does not apply to every model of application. In this work effort has been made to maintain high accuracy of reliability calculation with efficiency.

In this thesis, the aim has been to develop reliability methods for application to fatigue and fracture problems. The reliability methodology constructed is intended to aid decision making and to be used as a tool for design. The emphasis is put on efficiency using the latest reliability calculation techniques. Some of the necessary assumptions are discussed in the following text.

1.3 Problems To Be Dealt With When Carrying Out A Reliability Analysis For Fatigue And Fracture Problems

This study has combined developments in fracture mechanics, fatigue analysis, random load and reliability analysis for the purpose of undertaking an integrity analysis of a cracked structural component under random loading.

The methodology includes:

1) fracture mechanics to determine the critical state of a cracked component

2) fatigue crack growth using fracture mechanics to determine the crack size at any time

3) random loading analysis to provide the input cyclic loading or extreme loading

4) statistical modelling of each of the input variables from past experience and data

5) efficient and accurate reliability analysis to determine the probability of failure condition being reached.

When applying reliability to fatigue and fracture integrity assessment, one has to undertake at least the following tasks:

a) to understand the concept of reliability theory for practical and theoretical problems.

b) to understand the physical phenomena of fatigue and fracture process and structural stress or strain history in order to construct failure functions and conduct statistical analysis.

c) to identify basic statistical variables in the failure function and construct their probability distribution functions.

d) to calculate the reliability using an appropriate computer implementation of the physical and statistical models.

To be more specific, for the reliability analysis of fatigue and fracture for a structural steel component under random loading, a number of problems has to be solved:

1) How can reliability theory be adapted for use with fatigue and fracture problems with efficiency and accuracy?

2) If one is to apply the fracture mechanics approach to predict fatigue failure or to assess the integrity of a cracked component, what kind of fracture theory and component failure criteria should be used in order to minimise the model uncertainty?

3) Which basic variables should be used in the fracture mechanics theory? How does one calculate the reliability of cracked components with multiple failure modes, in particular, for the crack instability failure mode? How can one evaluate the results?

4) How can the fatigue loading data input under random loading, e.g. the stress range distribution, be suitably modelled?

5) How does a crack in a welded joint of an offshore structure grow under random loading? What is the efficient way to implement a computer program for the calculation of reliability of a cracked component failing by fatigue?

6) How does one form the integrity analysis of a cracked component under random loading? How can one interpret the results of a reliability analysis ?

The above problems apply both to the analysis of specific structures and to the reliability analysis of fatigue and fracture problems in general.

1.4 Layout Of Thesis

The thesis is arranged in the order given in section 1.3, and attempts to solve the problems of methodology one by one. Because of the wide range of subjects involved, reviews of relevant material are made in each of the Chapters and contributions from this study can be seen separate chapters and also in the way of incorporating all these into a comprehensive methodology.

Chapter 2 reviews the development of reliability theory and provides a refinement for the computational technique for second order reliability analysis. This Chapter explains the concept of reliability in detail, especially first order and second order reliability methods, and thus forms a basis for the later chapters.

Chapter 3 deals with the physical process of fracture, the theoretical explanations of the fracture process and design practice. This Chapter evaluates different fracture theories and design approaches and identifies the uncertainties associated with each of the basic variables. In this Chapter, a failure function has been constructed using the CEGB R6 method and a proper computer implementation is described.

Chapter 4 applies reliability theory to the safety assessment of a cracked component under non-cyclic loading.

Chapter 5 turns to fatigue problems. The fatigue stress cycle distribution derived from the rainflow counting method under random loading has been successfully modelled. The results are compared with data obtained directly by simulation and very close agreement is found.

Chapter 6 deals with the deterministic aspects of fatigue analysis under random loading. The fatigue growth process of cracks in offshore welded joints under random loading is explained in terms of the equivalent stress range concept and is used to build fatigue crack growth models. A proper computer

procedure is implemented for efficient reliability analysis.

In Chapter 7, all the important results from previous chapters are brought together to develop a methodology for the assessment of a cracked component subjected to random fatigue loading, but failing eventually by fracture or plastic collapse under some random overload. A practical example of a welded joint in an offshore structure is examined in detail and the sensitivity of the reliability to the various sources of uncertainty is examined.

Chapter 8 summarises the conclusions from this research and discusses the scope for further work in this important field.

In all, this study has attempted to advance the reliability analysis of components failing by fatigue and fracture and has constructed a methodology for engineering application based of previous work and new research.

Chapter 2

Structural Reliability Theory

Nomenclature

$\mathbf{A}$	transformation matrix
A_i	second order reliability component
b_i	linear function multiplication parameter corresponding to X_i
$\mathbf{B}$	$(b_1, b_2, ..., b_n)$
$\mathbf{C}$	covariance matrix
$Cov[.,.]$	covariance
E	event
$E[\mathbf{X}]$	$\int x\ f_X(x)dx$
$F_X(x)$	cumulative probability distribution function
$f_X(x)$	probability density function
$g(\mathbf{X})$ or $g(\mathbf{Z})$	failure function
∇g	$(\frac{\partial g}{\partial z_1}, \frac{\partial g}{\partial z_2}, ..., \frac{\partial g}{\partial z_n})$
$\|\nabla g\|$	$\sqrt{\sum_{i=1}^{n}(\frac{\partial g}{\partial z_i})^2}$
$\mathbf{I}$	unit matrix
k_i	main curvature of the design point
N_i	co-ordinates of the unit normal vector on the failure surface
$P(.)$	probability
P_f	probability of failure
R	reliability
Var[.]	variance
$\mathbf{V}$	velocity vector
V_i	velocity parameter
X_i	basic random variable
x_i	realisation of basic random variable X_i
$\mathbf{X}$	$(X_1, X_2, ..., X_n)$
$\mathbf{X}^*$ or $\mathbf{Z}^*$	design point
Z_i	standard normal random variable
$\mathbf{Z}$	$(Z_1, Z_2, ..., Z_n)$
z_i	realisation of standard normal variable Z_i
α_i	sensitivity factor of z_i
α	$(\alpha_1, \alpha_2, ..., \alpha_n)$

β	reliability index
β_{HL}	reliability index from Hasofer and Lind algorithm
μ_X	mean value of X
μ'_X	equivalent mean value of X after normalisation
ρ	correlation coefficient
σ_X	standard deviation of X
σ'_X	equivalent standard deviation of X after normalisation
$\phi(x)$	standard normal probability density function
$\Phi(x)$	standard normal cumulative distribution function
Ω	sample space
ω	failure surface
$\in$	contained in

Other symbols are defined in the text.

2.1 Introduction

As early as 1947 Freudenthal[2.1] stated in a pioneering paper: *the purpose of this paper is to analyse the safety factor in engineering structures in order to establish a rational method of evaluating its magnitude*[2.1]. Since then reliability theory and applications have undergone a steady development although even earlier works can be related to reliability theory.

Usually design can be undertaken deterministically by using mathematical models that approximately reflect reality together with appropriate safety factors[2.2]. Limit state design has been introduced to further enhance the treatment of safety[2.3]. However, of far greater significance, is the development of reliability theory, which has made it possible to assess the safety of structures more rationally in terms of probability and thus to optimise their cost[2.4].

The purpose of this chapter is to review the latest development in structural reliability related to the safety assessment of a single cracked structural element. Further improvement in computer programming of reliability theory is developed. The theory and computer algorithm given in this chapter will provide a basis for the following chapters which set up a methodology to calculate the reliability of flawed components using probabilistic fracture mechanics.

Due to the scope of this study and the fast development of reliability methods, it is not appropriate to give a detailed review of structural reliability theory. References are made only to those techniques which have been used in this thesis and to their possible extension in the near future.

2.2 Fundamental Probability Theory

In reliability problems, the calculation of the reliability R is complementary to the calculation of the probability of failure.

$$R = 1 - P_f \tag{2.1}$$

Before proceeding to the reliability theory, some basic axioms of probability will be stated.

A quantity *probability* $P(.)$ is associated with an *event* E, i.e. $P(E)$. An event is a subset of a sample space or a set of sample points. Then:

1) For any event E

$$0 \leq P(E) \leq 1 \tag{2.2}$$

2) For the sample space Ω

$$P(\Omega) = 1 \tag{2.3}$$

3) If $E_1, E_2, ..., E_n$ are mutually exclusive events then

$$P(\bigcup_{i=1}^{n} E_i) = \sum_{i=1}^{n} P(E_i) \tag{2.4}$$

In addition there are two important axioms:

4) The probability of occurrence of event E_1 conditional upon the occurrence of event E_2 is

$$P(E_1|E_2) = \frac{P(E_1 \bigcap E_2)}{P(E_2)} \tag{2.5}$$

5) Event E_1 is said to be statistically independent of E_2 if

$$P(E_1|E_2) = P(E_1) \tag{2.6}$$

Another important theorem is Bayes' theorem . Let the sample space Ω be divided into n mutually exclusive events $E_1, E_2, ...E_n$ and A be an event in the sample space. Then

$$P(E_i|A) = \frac{P(A|E_i)P(E_i)}{\sum_{j=1}^{n} P(A|E_j)P(E_j)} \tag{2.7}$$

In reliability theory, an outcome or an event can be identified as a random variable. Then the probability distribution function of this random variable can be obtained from experiments or observations. For instance a probability distribution function for fracture toughness has been obtained by Gates [2.5] from experimental data. The probability distribution function F_X can be defined as:

$$F_X(x) = P(X \leq x) \tag{2.8}$$

The probability density function (pdf) is then

$$f_X(x) = \frac{dF_X(x)}{dx} \tag{2.9}$$

Also equation (2.7) and (2.9) can be expanded to include more than one random variable. If two variables are correlated to each other, the covariance is :

$$Cov[X_1, X_2] = E[(X_1 - \mu_{X_1})(X_2 - \mu_{X_2})] \tag{2.10}$$

where $E[.]$ and μ are defined at the beginning of this chapter.

And the correlation coefficient is

$$\rho_{X_1X_2} = \frac{Cov[X_1, X_2]}{\sigma_{X_1}\sigma_{X_2}} \tag{2.11}$$

Furthermore, the covariance matrix is defined by

$$\mathbf{C} = \begin{pmatrix} Var[X_1] & Cov[X_1, X_2] & \dots & Cov[X_1, X_n] \\ Cov[X_2, X_1] & Var[X_2] & \dots & Cov[X_2, X_n] \\ \vdots & \vdots & \ddots & \vdots \\ Cov[X_n, X_1] & Cov[X_n, X_2] & \dots & Var[X_n] \end{pmatrix} \tag{2.12}$$

2.3 Reliability Methods

2.3.1 General remarks

In reliability methods, the reliability index or notional reliability may be used to define the safety level of a structure or a component. The second moment method has greatly simplified the calculation of such parameters. The papers by Cornell[2.6], Hasofer and Lind[2.7], and Ditlevsen [2.8] have laid down the theoretical base for the second moment reliability methods.

Reliability methods can be classified into different levels according to the scale of the calculation. For instance in reference [2.4] there are three levels of reliability analysis. Level III obtains the probability of failure by integration over the multidimensional probability space. Level II obtains the reliability index at a selected point of the failure boundary by certain mathematical approximations. Level I defines the safety of the structure by appropriate partial safety factors on the basic variables. However due to the recent developments in reliability theory, these three levels of reliability analysis are often not clearly distinguished. For instance Madsen[2.9] has given 4 levels of reliability analysis depending on the extent of the analysis.

In this thesis, the original level II method is used, with modifications dictated by the requirements of fatigue and fracture failure assessment.

In general structural reliability analysis consists of three basic steps[2.10]:

(1) Choice of basic variables and formulation of failure function , $g(\mathbf{X})$.

(2) Probability modelling of uncertainties in basic variables to give their probability distributions.

(3) Calculation of the reliability index or the probability of failure.

2.3.2 Failure function

Structural behaviour can be idealised into two performance states: failure and non-failure. To define the failure state deterministic failure criteria are used to build the failure boundaries in the multi-

dimensional variable space. A set of variables X , termed as the *basic variables*, are chosen to be the basis of the reliability analysis. They are chosen, on grounds of convenience, availability of data and deterministic equations, to cover all the sources of uncertainty that are relevant to the situation being analysed.

Failure functions are of the form of

$$M = g(\mathbf{X}) \tag{2.13}$$

When $M > 0$, failure does not occur;

when $M \leq 0$, failure does occur.

Therefore, equation (2.1) becomes

$$R = 1 - P(M \leq 0) \tag{2.14}$$

M is called the safety margin.

Given a set of basic variables $X_i, i = 1, 2, ...n$ with probability distribution functions $f_{X_i}(x_i)$, the Level II reliability theory has been developed to calculate the reliability in Eqn. (2.14) both efficiently and accurately.

The function $g(\mathbf{X})$ does not need to be a single explicit equation. It can express the outcome of a lengthy series of calculations. However problems can arise from the type of function which makes convergence of reliability index calculation difficult. In these cases, modification of the failure function can sometimes make the convergence much easier. For instance, if

$$g(\mathbf{X}) = g_1(X_1) - g_2(X_2) = 0$$

does not converge, an equivalent failure function may be adopted

$$g(\mathbf{X}) = \frac{g_1(X_1)}{g_2(X_2)} - 1 = 0$$

2.3.3 Probability modelling of basic variables

The modelling of basic variables is itself a big subject. To discuss all the aspects of basic variable modelling is beyond the scope of this thesis. In addition there are cases where a process e.g. fatigue is taken as being stochastic rather than a basic statistical variable of the fatigue failure functions[2.13]. A number of references are useful[2.4], [2.9], [2.10], [2.12]. The procedure for basic variable modelling is given below:

A Uncertainty classification and recognition of basic variables.

B Choice of distribution type.

C Determination of parameters for distributions

The detailed discussions are as follows:

A. Uncertainty classification and recognition of basic variables

There are normally three types of uncertainties:

1. physical uncertainty: Some physical phenomena are of random nature, for example, wave loading, fatigue crack growth, the measurement of a crack size etc. These uncertainties can be modelled by probability distributions or stochastic processes.

2. statistical uncertainty: The probability or stochastic models may have many parameters. As a result of lack of information, these parameters may themselves be considered as random variables. For example , the seastate spectrum parameters in wave analysis can be taken as random variables.

3. Model uncertainty: No function $g(\mathbf{X})$ could model exactly all the influences of many random variables, except in very simple cases. The models are built up by making some assumptions, or by ignoring some variables due to lack of information, or for reasons of economy, or through inability to incorporate it into the mathematical equation. For instance in elastic plastic fracture mechanics different fracture criteria e.g. CTOD method and the J integral method (see chapter 3) can give different results because each model has emphasis on different physical aspects. Therefore, a model uncertainty should be introduced to take account of the variability from the model to reality. Nevertheless a better model can be achieved with reduced model uncertainties by a better understanding of the physical problem.

B. Choice of distribution type

After the selection of the random variables used to represent the uncertainties in loading and resistance parameters, one has to find a suitable type of probability distribution for each random variable.

There are three ways to determine the distribution types:

1. Choice by accuracy of fit with the available data.

2. Physical reasoning. This is very important because very often the available sample data are insufficient to reflect the nature of the probability distribution.

3. Use of distributions types capable of generating a wide variety of forms. This is a natu-

ral development from the first approach. Many available distribution types, e.g. the three parameter Weibull distribution, the Pearson distribution , have such capacity.

C. Estimation of distribution parameters

The process of parameter estimation can be thought of having three steps:

1. initial inspection of the data

2. application of a suitable estimation procedure

3. final model verification

The first step is to check the data for obvious inconsistencies and errors. For instance in a small population of data, an outlier may be found and must be eliminated for overall assessment of the distribution type.

The second step can be undertaken by many techniques, for instance:

* the method of moments

* the method of maximum likelihood

* various graphic procedures

* use of order statistics

Detailed procedures can be found in a range of references, for instance [2.10], [2.13].

The third step is model verification . Goodness of fit may be judged a) by graphic methods b) by tests from classical statistics, c) by comparing one or more values such as the higher order moments of the distribution and the data.

2.3.4 Calculation of the reliability index or the probability of failure

1) Cornell Reliability index[2.6]

From Eqn. [2.1] and Eqn. [2.14], the calculation of reliability becomes the calculation of P_f in the sample space with the failure boundary defined by setting failure function $g(\mathbf{X}) = 0$.

$$P_f = \int\int\int \dots \int_{M \leq 0} f_{X_1, X_2, \dots, X_n}(x_1, x_2, \dots, x_n) dx_1 dx_2 \dots dx_n \qquad (2.15)$$

where $f_{X_1,X_2,....,X_n}(x_1, x_2, ..., x_n)$ is the joint density function of variables $X_1, X_2, ...X_n$.

Cornell defined a reliability index (or safety index) β_c as

$$\beta_c = \frac{E[M]}{D[M]} \tag{2.16}$$

where $D[M]$ is the square root of the variance of M.

If the failure function is a hyperplane, it is possible to define a linear function

$$g(\mathbf{X}) = b_0 + \sum_{i=1}^{n} b_i X_i = b_0 + \mathbf{B^T X} \tag{2.17}$$

Then, the reliability index takes the value :

$$\beta_c = b_0 + \frac{\mathbf{B^T E[X]}}{\mathbf{B^T C_X B}} \tag{2.18}$$

where $E[\mathbf{X}]$ is the vector of expected value and $\mathbf{C_X}$ is the matrix of covariance of X as defined in Eqn(2.12).

If $g(\mathbf{X})$ is a nonlinear function, $g(\mathbf{X})$ can be approximated by a first order Taylor series expansion. Therefore the failure surface is approximated as a hyperplane and equation (2.17) can be used as before.

2) The Hasofer and Lind reliability index[2.7]

Ditlevsen[2.8] has demonstrated the lack of failure function invariance of the Cornell reliability index. This problem was solved by a mapping technique proposed by Hasofer and Lind.

Hasofer and Lind proposed a nonhomogeneous linear mapping of the set of basic variables into a set of normalised and uncorrelated variables Z_i, which should have the following characteristics:

$$E(\mathbf{Z}) = 0 \tag{2.19}$$

$$C_{\mathbf{Z}} = Cov[\mathbf{Z}, \mathbf{Z}^T] = \mathbf{I} \tag{2.20}$$

The transformation can be written as

$$\mathbf{Z} = \mathbf{A}(\mathbf{X} - E[\mathbf{X}]) \tag{2.21}$$

Using Eqn(2.20), **A** can be obtained using standard linear algebra.

The mean value point in the X space is mapped into the origin of the Z space. The failure surface in the X space is mapped into the Z space. An example of the transformation can be seen in Fig. 2.1.

The perpendicular distance from the origin to the plane of $g(\mathbf{Z}) = 0$ is defined as β. And if the hyperplane is in the standard normal space:

$$P_f = \Phi(-\beta) \tag{2.22}$$

Conversely,

$$\beta = -\Phi^{-1}(P_f) \tag{2.23}$$

The reliability index defined as the shortest distance from the origin to the failure surface is then

$$\beta = min_{\mathbf{Z}\in\omega_\mathbf{Z}}(\mathbf{Z}^\mathbf{T}\mathbf{Z})^{\frac{1}{2}} \tag{2.24}$$

equivalently

$$\beta = min_{\mathbf{X}\in\omega_\mathbf{X}}((\mathbf{X} - \mathbf{E}[\mathbf{X}])^\mathbf{T}\mathbf{C}_\mathbf{X}^{-1}(\mathbf{X} - \mathbf{E}[\mathbf{X}]))^{\frac{1}{2}} \tag{2.25}$$

This reliability index is used to approximate the probability of failure from Equation (2.16).

The solution for $\mathbf{X}$ from equation (2.25) is denoted as $\mathbf{X}^*$, and this point is named the design point. It has been proved that the two definitions for the reliability index β will coincide if this expansion of Taylor series is made about the design point[2.4]. The Hasofer Lind reliability index generalises the concept of reliability index.

3) Non-normal variables

The Hasofer Lind reliability approximation operates in standard normal space. Very often the basic variables are not normally distributed. For independent non-normal variables, the following transformation can be used:

$$\Phi(z_i) = F_{X_i}(x_i) \quad i = 1, 2, ..., n \tag{2.26a}$$

$$\phi(z_i) = \frac{f_{X_i}(x_i)}{\sigma_{X_i}} \tag{2.26b}$$

The inverse transformation is:

$$x_i = F_{X_i}^{-1}(\Phi(z_i)) \quad i = 1, 2, ...n \tag{2.27}$$

Therefore the failure function in the Z space is given in terms of the failure function in the X space as

$$g(\mathbf{X}) = g(F_X^{-1}(\Phi(\mathbf{Z})) \tag{2.28}$$

For the simple transformation of the normal independent variable X into standard normal independent variable Z:

$$z_i = \frac{x_i - \mu_{X_i}}{\sigma_{X_i}} \tag{2.29}$$

For non-normal variables, each may be replaced by an equivalent normal variable X_i' having the following parameters:

$$\sigma_{X_i'} = \frac{\phi(\Phi^{-1}(F_{X_i}(x_i^*)))}{f_{X_i}(x_i^*)} \tag{2.30}$$

$$\mu_{X_i'} = x_i^* - \sigma_{X_i'}\Phi^{-1}(F_{X_i}(x_i^*)) \tag{2.31}$$

With this new failure function in Z space, the Hasofer and Lind reliability index can thus be calculated by means of a computer program. This algorithm is often called the R-F (Rackwitz-Fiessler) algorithm [2.14].

When basic variable are not mutually independent, the Rosenblatt transformation may be used to transform basic variables into standard normal variables[2.15].

4) Closing remarks

The reliability calculation method using hyperplane approximation about the design point is called the First-Order Reliability Method (FORM).

The principle of FORM is simple: transformation of arbitrary random uncertainty vectors into independent standard normal vectors and approximation of the boundaries of the relevant failure domains by linear expansions at certain points on the failure boundary so that failure probability can simply be estimated from the probabilities of linear forms in normal variables.

2.3.5 Algorithm for FORM

In the normalised uncorrelated Z space, **Z** can be expressed as

$$\mathbf{Z} = \beta\alpha \tag{2.32}$$

where α is the normal unit vector thus:

$$\sum_{i=1}^{n} \alpha_i^2 = 1 \tag{2.33}$$

$$\beta = (\mathbf{Z}^{\mathrm{T}}\mathbf{Z})^{\frac{1}{2}} \qquad (\mathbf{Z} \in \omega) \tag{2.34}$$

$$\alpha_i = -\frac{\frac{\partial g(\mathbf{Z})}{\partial z_i}}{\sqrt{\sum_{i=1}^{n}(\frac{\partial g(\mathbf{Z})}{\partial z_i})^2}} = \frac{\partial \beta}{\partial z_i} \tag{2.35}$$

where

$$\frac{\partial g(\mathbf{Z})}{\partial z_i} = \sum_{j=1}^{n} \frac{\partial g(\mathbf{X})}{\partial x_j}\frac{\partial x_j}{\partial z_i}$$

If the basic variables are independent $\frac{\partial x_j}{\partial z_i}$=0 when $i \neq j$. Furthermore if the basic variable X_i is normal variable, $\frac{\partial x_i}{\partial z_i} = \sigma_{X_i}$.

If the basic variables are not independent, $\frac{\partial x_j}{\partial z_i}$ must be obtained from the Rosenblatt transformation, or from a Jacobian matrix co-ordinates rotation if the variables are normally distributed.

α is then the sensitivity measurement of the reliability index to variations in the value of z_i at the point of minimum distance $\mathbf{Z}^*$.

To determine the design point in Eqn(2.24), i.e. the minimum value of β, an iteration procedure must be used from equations (2.32), (2.34) and (2.35).

The procedure is as follows:[2.9]

1) Initially, a trial set of values of **Z**, preferably in the neighbourhood of $\mathbf{Z}^*$, is selected.

2) α is calculated from Eqn (2.35) . α_i can be calculated numerically using a small step increment $\triangle z_i$ of each z_i in turn.

3) A new point Z_{new} is found from:

$$\mathbf{Z_{new}} = (\mathbf{Z}^{\mathrm{T}}\alpha)\alpha - \frac{g(\mathbf{Z})}{\sqrt{\sum_{i=1}^{n}\frac{\partial g(\mathbf{Z})}{\partial z_i}}}\alpha \tag{2.36}$$

In the basic variable space,

$$\mathbf{X}_{new} = E[\mathbf{X}] + C_{\mathbf{X}} \nabla g(\mathbf{X}) \frac{(\mathbf{X} - E(\mathbf{X}))^T \nabla g(\mathbf{X}) - g(\mathbf{X})}{\nabla g(\mathbf{X})^T \mathbf{C}_{\mathbf{Z}} \nabla g(\mathbf{X})} \tag{2.36a}$$

4) repeat 2) and 3) to achieve convergence.

5) evaluate β from Eqn(2.34).

A computer program based on this algorithm is available at Imperial College, which has facilitated this study greatly. However this algorithm does not automatically ensure convergence, so that care should be taken in applications.

2.4 Further development

2.4.1 Second Order Reliability Method(SORM)

FORM has provided a fast way of calculating the reliability by approximating the failure surface as a hyperplane at the design point - that is, the point which has the shortest distance from the origin to the failure surface in the standard normal space. The Taylor expansion of the failure surface at the design point is only to the first order. However, this approximation can be misleading when the failure function has appreciable contributions from higher order terms.

Fiessler *et al*[2.16] proposed to approximate the g- function by a quadratic g-function instead of a linear function in a normalised Z space. In general , by including the second order partial derivative of $g(\mathbf{Z})$ in the analysis, SORM can produce more accurate P_f estimates than $\Phi(-\beta)$. However this accuracy depends on the qualities of the quadratic approximation of $g(\mathbf{Z})$.

For the special case of the failure function having its global minimum at $\mathbf{Z} = \mathbf{Z}^*$ only, Tvedt[2.17] has derived a three- term approximation to the reliability, based on a study by Breitung[2.18], as

$$P_f = A_1 + A_2 + A_3 \tag{2.37}$$

where

$$A_1 = \Phi(-\beta) \prod_{j=1}^{n-1} (1 - \beta k_j)^{-1/2}$$

$$A_2 = [\beta\Phi(-\beta) - \phi(\beta)]\{\prod_{j=1}^{n-1} (1 - \beta k_j)^{-1/2} - \prod_{j=1}^{n-1} (1 - (\beta + 1)k_j)^{-1/2}\}$$

$$A_3 = (\beta + 1)[\beta\Phi(-\beta) - \phi(\beta)]\{\prod_{j=1}^{n-1} (1 - \beta k_j)^{-1/2} - Re(\prod_{j=1}^{n-1} (1 - (\beta + i)k_j)^{-1/2})\}$$

In the above formula, i is square root of -1, k_i is the main curvature at the design point of the failure surface. To obtain the main curvatures, formulae from differential geometry have to be used.

Calculation of main curvatures

First define the curvature as being positive when the curve rotates inwards; otherwise it is negative.

i.e. the unit normal vector:

$$\mathbf{N} = \frac{\nabla g}{\|\nabla g\|}$$
$$= \left(\frac{\frac{\partial g}{\partial z_1}}{\|\nabla g\|}, \frac{\frac{\partial g}{\partial z_2}}{\|\nabla g\|}, \ldots\ldots, \frac{\frac{\partial g}{\partial z_n}}{\|\nabla g\|}\right) \tag{2.38}$$

So

$$N_i = \frac{\frac{\partial g}{\partial z_i}}{\|\nabla g\|} \tag{2.39}$$

The main curvatures are the eigenvalues of the Weingarten map [2.19] $L_p : S_p \longrightarrow S_p$ for a unit normal vector oriented (n-1)-surface in n space and the point p on surface S.

If the failure surface S is defined by $g(\mathbf{Z}) = 0$, the Weingarten mapping[2.19] is:

$$L_p(\mathbf{v}) = -\nabla_{\mathbf{v}}\mathbf{N}$$
$$= -(\nabla_{\mathbf{v}}\mathbf{N}_1, \nabla_{\mathbf{v}}\mathbf{N}_2, \ldots\ldots, \nabla_{\mathbf{v}}\mathbf{N}_n) \tag{2.40}$$

For a (n-1) surface in n space, there exist (n-1) independent vectors along the surface. Therefore

$$\mathbf{V} = \begin{pmatrix} V_1 \\ V_2 \\ \vdots \\ V_{n-1} \end{pmatrix} \tag{2.41}$$

If z_i are independent variables, set V_i is the velocity vector along the z_i axis direction, we can obtain:

$$L_p(\mathbf{v}) = -\begin{pmatrix} \frac{\partial N_1}{\partial z_1} & \frac{\partial N_2}{\partial z_1} & \cdots & \frac{\partial N_{n-1}}{\partial z_1} \\ \frac{\partial N_1}{\partial z_2} & \frac{\partial N_2}{\partial z_2} & \cdots & \frac{\partial N_{n-1}}{\partial z_2} \\ \vdots & \vdots & \ddots & \vdots \\ \frac{\partial N_1}{\partial z_{n-1}} & \frac{\partial N_2}{\partial z_{n-1}} & \cdots & \frac{\partial N_{n-1}}{\partial z_{n-1}} \end{pmatrix} \bullet \begin{pmatrix} V_1 \\ V_2 \\ \vdots \\ V_{n-1} \end{pmatrix} \tag{2.42}$$

$$= \mathbf{L} \bullet \mathbf{V}$$

In general terms :

$$L_{ij} = -\frac{\partial N_i}{\partial z_j} \tag{2.43}$$

$$= -\frac{\frac{\partial^2 g}{\partial z_i \partial z_j}\|\nabla g\|^2 - \frac{\partial g}{\partial z_i}\sum_{k=1}^{n}(\frac{\partial g}{\partial z_k}\frac{\partial^2 g}{\partial z_k \partial z_j})}{\|\nabla g\|^3} \tag{2.44}$$

The eigenvalues are the solution of

$$\mathbf{L} \bullet \mathbf{V} - \lambda \mathbf{I} \bullet \mathbf{V} = 0 \tag{2.45}$$

If the basic variables $\mathbf{X}$ are independent normal variables

$$\frac{\partial g}{\partial z_i} = \frac{\partial g(\mathbf{X})}{\partial x_i}\sigma_{X_i} \tag{2.46}$$

and

$$\frac{\partial^2 g}{\partial z_i \partial z_j} = \frac{\partial g^2(\mathbf{X})}{\partial x_i \partial x_j}\sigma_{X_i}\sigma_{X_j} \tag{2.47}$$

If the basic variables are correlated a more complicated form of transformation is needed. This involves the use of Rosenblatt transformation or orthogonal transformation if all the variables are normally distributed.

Each term in equation (2.44) can be obtained from analytical differential solution or numerical finite differentiation. In the reliability analysis of fatigue and fracture the value $g(\mathbf{X})$ is usually calculated implicitly by numerical procedure rather than explicitly in one or more equations. This calculation process sometimes involves a large amount of computer time for each value of $g(\mathbf{X})$ in the iterative procedure, for instance, the cycle by cycle calculation of crack growth.

The standard scheme for finite differentiation for second order derivatives for n variables needs the function g to be evaluated at $2n + 4\frac{n(n-1)}{2} + 1$ points. In this study, in equation (2.44) , only first order and second derivatives at one point of the surface are of interest. If we assume the g function is second order continuous and smooth, by choosing a small mesh size, a further simplification can be obtained by the mesh scheme shown in Fig 2.2 for two dimensional space.

The second order partial derivatives can be approximately assessed by the following equations:

$$\frac{\partial^2 g}{\partial x_1 \partial x_2} = \frac{g(\mathbf{X}_{t12}) - g(\mathbf{X}_{t1})) - g(\mathbf{X}_{t2}) + g(\mathbf{X}_0)}{dx_1 dx_2} \tag{2.48}$$

The point of differentiation is the point within the square of $t12, t1, 0, t2$ as shown in Fig. 2.2.

For n-dimensional problems

$$\frac{\partial^2 g}{\partial x_i \partial x_j} = \frac{g(\mathbf{X}_{ij}) - g(\mathbf{X}_{ti}) - g(\mathbf{X}_{tj}) + g(\mathbf{X}_0)}{dx_i dx_j} \tag{2.49}$$

The accuracy of this scheme is dependent on the mesh size dx_i, dx_j and the local shape of the failure surface. The number of $g(\mathbf{X})$ values needed according to this scheme is only $2n + \frac{n(n-1)}{2} + 1$. Using this numerical scheme computation time is reduced significantly.

One example is taken from data group 2 for crack fracture reliability in chapter 4. Probability calculations have been conducted by SORM from the standard standard finite difference scheme and the present scheme. From Table 2.1 very little difference can be found between results obtained from the present scheme and the standard scheme.

From the above description, only if the design point has already been determined and the failure surface is continuous up to second order, can the probability of failure be obtained from SORM using equation (2.37). One further point that should be mentioned is that because the design point is the shortest distance from the origin to the failure surface in the standard normal space, the main curvatures are therefore $\leq 1/\beta^*$.

2.4.2 Three parameter normal tail approximation

Based on the usual normalisation procedure as proposed by Rackwitz and Fiessler[2.14], Chen and Lind [2.20] proposed using a three parameter normal tail approximation. The R-F algorithm can result in serious discrepancy when the failure surface is very skew.

Let

$$z^* = \frac{(x^* - \mu_X)}{\sigma_X} \tag{2.50}$$

and a function scaled from a standard normal CDF be

$$F_X(x) = \eta\Phi(\frac{(x - \mu_x)}{\sigma_x}) \tag{2.51}$$

Three conditions should be met:

$$F_X(x^*) = \eta\Phi(z^*) \tag{2.52}$$

$$\frac{\partial F_X(x^*)}{\partial x} = \frac{\partial(\eta\Phi(z^*))}{\partial x} \tag{2.53}$$

$$\frac{\partial^2 F_X(x^*)}{\partial x^2} = \frac{\partial^2(\eta\Phi(z^*))}{\partial x^2}, \tag{2.54}$$

Note that the additional condition to the R-F algorithm is the equality of the second derivative in the approximate normal distribution and the original independent variable distribution as in Eqn. (2.54). By introducing the third condition, a third variable η should also be introduced.

This algorithm is only suitable for independent variables and original hyperplane surface in the X space. Care should also be taken that $f_X(x)$ should be positive in the upper tail and negative in the lower tail. Otherwise, the original R-F algorithm should be used without the additional condition equation (2.54).

Solving these equations , gives:

$$\frac{z^*\Phi(z^*)}{\phi(z^*)} = -\frac{F_X(x^*)f'_X(x^*)}{[f_X(x^*)]^2} \tag{2.55}$$

The solution for z^* from equation (2.55) is found to be of the form

$$Z_i = \delta_i\beta = \frac{a_i\sigma_{X_i}}{[\sum_{i=1}^{m}(a_i\sigma_{X_i})^2]^{1/2}}\beta \tag{2.56}$$

where $a_1, a_2, a_3, ..., a_m$ are determined from curve fitting and can be found from Chen and Lind[2.20].

After solving for $\mathbf{Z}^*$ from equation (2.55), the result for lower tail approximation is (one can have rotational symmetry results for the upper tail):

$$\eta = \frac{F_X(x^*)}{\Phi(z^*)} \tag{2.57}$$

$$\sigma'_X = \frac{F_X(x^*)\phi(z^*)}{f_X(x^*)\Phi(z^*)} \tag{2.58}$$

$$\mu'_X = x^* - z^*\sigma_x \tag{2.59}$$

For linear cases,

$$\beta = \beta_{HL}\prod_{i=1}^{n}\eta_i \tag{2.60}$$

and η can be calculated at the end of the routine.

Wirsching[2.21] used the Chen-Lind three parameter approximation principle but obtained the parameters through least square calculation and thus claimed to have a more precise result.

2.4.3. Sensitivity analysis

In Eqn(2.28) α at the design point can measure the sensitivity of the reliability index to uncertainties in the value of Z_i . From eqn(2.35), α_i can be interpreted as the fraction of uncertainty caused by the uncertainties described through z_i at the design point.

The values of sensitivity factors can provide information for further analysis:

1) For large α_i, z_i can have large uncertainty and thus it is of interest for analysts to undertake further investigation.

2) For small α_i, the contribution of z_i to the reliability index is small. Depending on the required accuracy of the FORM index, the basic variables with small sensitivity factors can be omitted.

Madsen[2.22] found that for independent basic variables, with $|\alpha_i| \leq 0.14$, the relative error in the reliability index by replacing a basic variable by its mean value is less than 1%. Madsen then proposed using an omission algorithm, i.e. at each step after the first iteration a variable Z_i with $|\alpha_i| < \alpha_t$ is replaced by the deterministic value $\beta_m \alpha_i/2$. β_m is updated every step, but α_i can be taken from the first iteration. However caution must be taken when the numerical iterations are complicated procedures.

In conventional design codes, partial safety factors are presented to designers. Partial safety factors are decided from the calibration and optimisation of the weighted probability of failure in relation to the target probability of failure. This process involves the calculation of sensitivity factors.

In this study, the sensitivity factors are studied to judge relative importance of the various basic variables in fatigue and fracture.

2.4.4. Multiple failure modes and system reliability

This is currently a very active area of reliability research. This part is given a less emphasis In this thesis, because the calculation of reliability is only for the structural element . However, in the R6 method of fracture mechanics, two failure modes, [2.23] i.e. plastic collapse and fracture, are combined into one failure function. The failure surface may have two or more places which are locally the shortest distance to the origin. Either the multiple integration technique or the system bounds theory should be used.

Let the failure sets be $F_1, F_2, F_3, ...F_n$ and

$$F = \bigcup_{i=1}^{n} F_i \tag{2.61}$$

Ditlevsen has given general bounds for a structural system[2.24]:

for the upper bound

$$P(F) \leq \sum_{i=1}^{n} P(F_i) - \sum_{i=2}^{n} max_{j<i} P(F_i \bigcap F_j) \tag{2.62}$$

for the lower bound

$$P(F) \geq P(F_1) + \sum_{i=2}^{n} max[\{P(F_i) - \sum_{j=1}^{i-1} P(F_i \bigcap F_j)\}; 0] \tag{2.63}$$

For independent normal variables Z_i[2.25]:

$$Cov(g_i, g_j) = \sum_{k=1}^{n} (\frac{\partial g_i}{\partial z_k})(\frac{\partial g_j}{\partial z_k}) \tag{2.64}$$

$$\sigma_{g_i} = \sqrt{\sum_{i=1}^{k} (\frac{\partial g_i}{\partial z_k})^2} \tag{2.65}$$

From Eqn. (2.11),

$$\rho_{ij} = \frac{Cov(g_i, g_j)}{\sigma_{g_i} \sigma_{g_k}} = \sum_{k=1}^{n} \alpha_{ik} \alpha_{jk} \tag{2.66}$$

If

$$P(F_i \bigcap F_j) = \Phi(-\beta_i, -\beta_j; \rho_{ij}) \tag{2.67}$$

Set

$$P(A) = \Phi(-\beta_1)\Phi(-\frac{\beta_2 - \rho\beta_1}{\sqrt{1-\rho^2}}) \tag{2.68}$$

$$P(B) = \Phi(-\beta_2)\Phi(-\frac{\beta_1 - \rho\beta_2}{\sqrt{1-\rho^2}}) \tag{2.69}$$

If $\rho > 0$,

$$max[P(A), P(B)] \leq P(F_i \bigcap F_j) \leq P(A) + P(B) \tag{2.70}$$

If $\rho < 0$,

$$0 \leq P(F_i \bigcap F_j) \leq min[P(A), P(B)] \tag{2.71}$$

2.5 Concluding Remarks

This chapter has reviewed the methodology for general structural reliability analysis. The rational assessment of structural performance in probabilistic terms is explained. A reliability calculation algorithm is presented which has been used in the applications to fatigue and fracture reliability discussed in later chapters. An extension has been made to the second order reliability method and has been implemented in the available level 2 reliability computer program. A new scheme with significant reduction of computer time to calculate the main curvatures of the failure surface is proposed . For a full reliability study of fatigue and fracture, the following tasks remain:

1) Formulation of the failure function for failure by fatigue and fracture.

2) Determination of the probability distributions for the basic variables.

3) Approximation of the probability of failure in nonlinear failure surfaces.

Table 2.1 Comparison of Probability of Failure from FORM, SORM by Standard Finite Difference Scheme (SORM.SFD) and SORM by Approximate Finite Differenc e Scheme (SORM.AFD)

LOG*10*(Pf) For data group 2 of series 1 in Chapter 4

mean point	FORM	SORM.SFD	SORM.AFD
1	-16.75607	-16.75535	-16.75535
2	-15.02572	-15.02439	-15.02439
3	-13.35106	-13.34880	-13.34880
4	-11.73164	-11.72788	-11.72788
5	-10.16423	-10.15793	-10.15793
6	-8.64078	-8.62994	-8.62994
7	-7.14531	-7.12610	-7.12610
8	-5.64926	-5.61483	-5.61483
9	-4.10813	-4.05340	-4.05339
10	-2.61955	-2.58225	-2.58225
11	-1.53626	-1.51568	-1.51563
12	-.76435	-.75843	-.75843
13	-.30402	-.30518	-.30518
14	-.08803	-.08430	-.08811

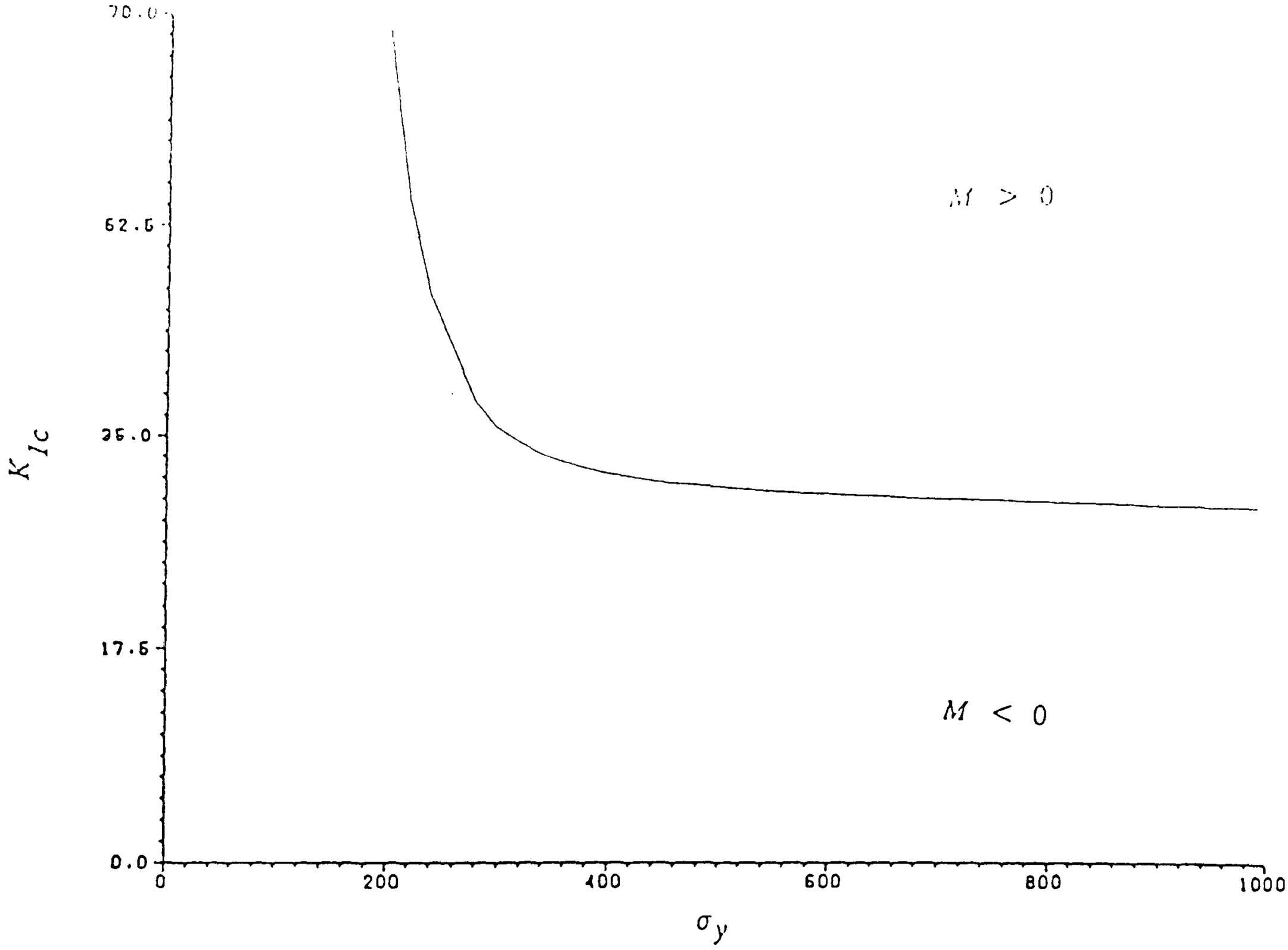

FAILURE SURFACE

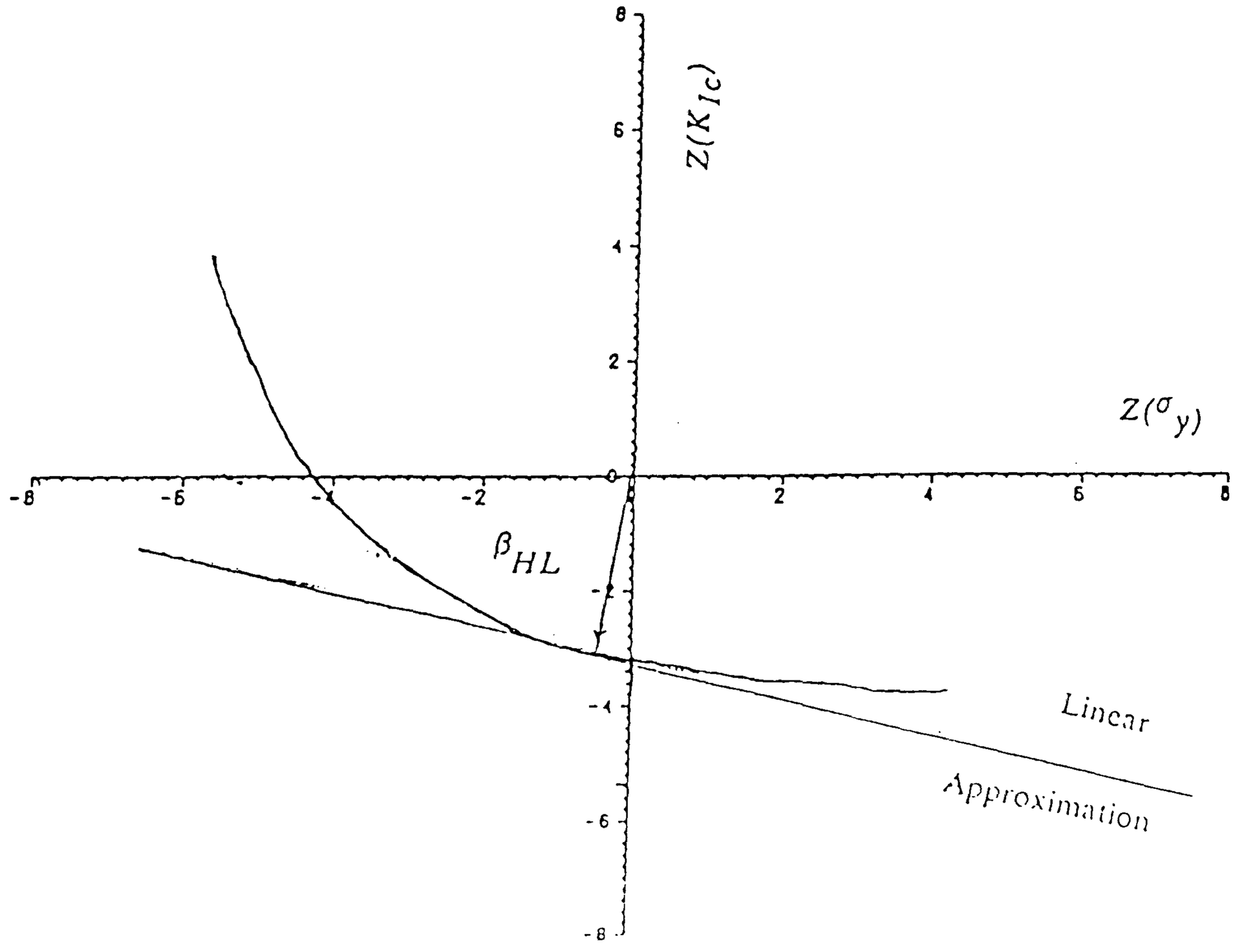

FAILURE SURFACE IN THE STANDARD NORMAL SPACE

Fig. 2.1 Transformation from basic variable space to standard normal space

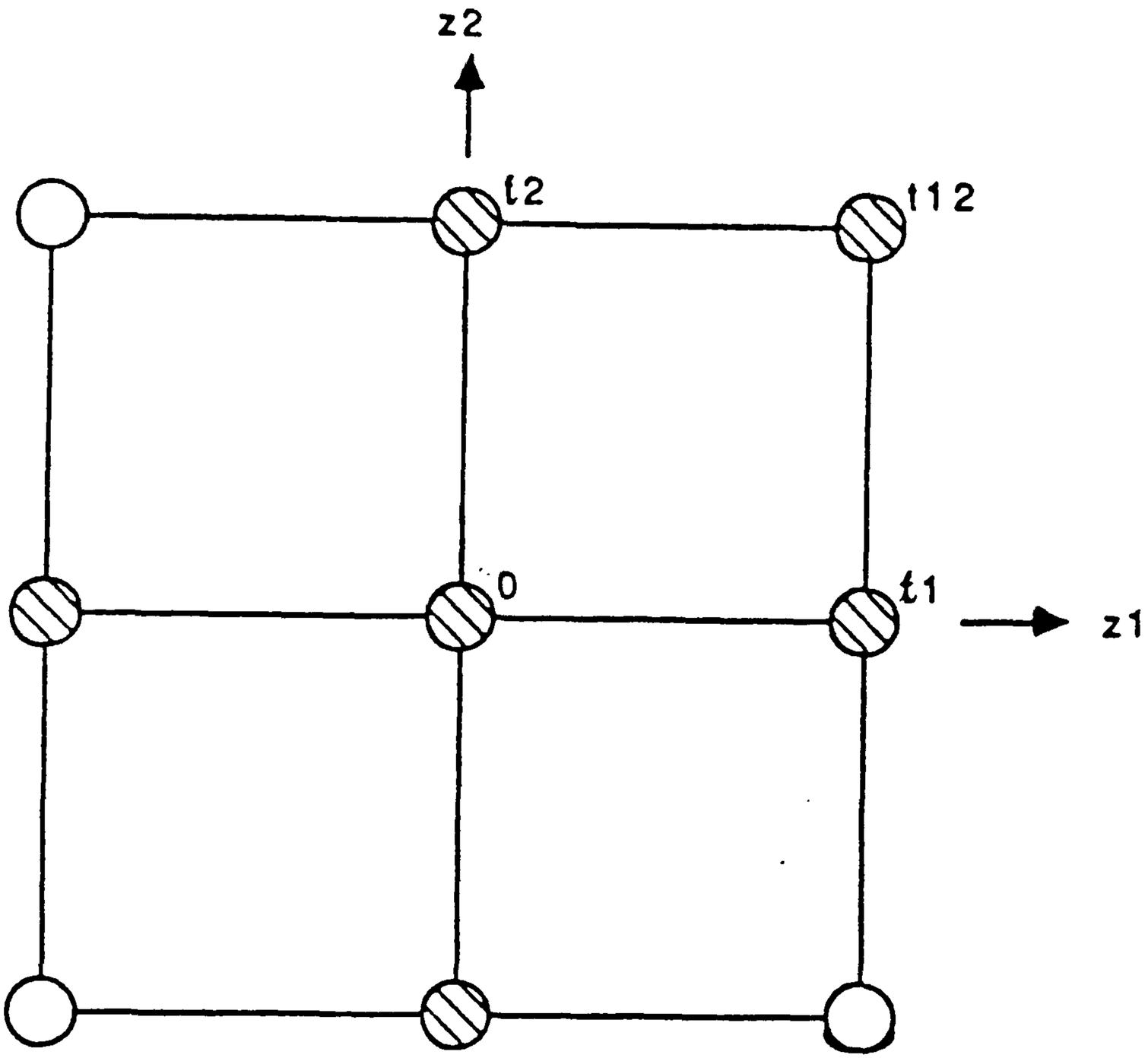

Any circle -- standard Finite Difference Scheme
Filled circle -- points needed for proposed scheme

Fig.2.2 Two dimensional finite difference scheme

Chapter 3

Deterministic Fracture Mechanics and Design

Nomenclature

a	crack size
$\triangle a$	crack extension
B	specimen thickness
b	ligament thickness
C	compliance
CTOD	crack tip opening displacement
CVN	Charpy V-notch test energy
E	Young's modulus
EPFM	elastic plastic fracture mechanics
F	external force
G	energy release rate
f	local stress
HRR field	crack stress field by using J proposed by Hutchinson, Rice and Rosengren
K	stress intensity factor
K_{1d}	dynamic plane strain fracture toughness
LEFM	linear elastic fracture mechanics
M	failure margin
m	multiplication factor of σ_y for stresses ahead of the crack tip
P	potential energy
R	zone size beyond which HRR unique stress and strain field can apply
r_p	radius of plastic zone
q	load line displacement
U	strain energy
u	displacement
W	energy required to produce crack growth
w	overall width of the specimen
Y	crack geometry factor
δ	CTOD
ϵ	strain
η	f(geometry,hardening) for calculation of J
ν	Poisson's ratio

ρ	plastic zone size or plasticity correction factor in R6
σ	stress

Subscripts:

ee	external energy
el	elastic
ie	internal energy
ini	initiation
pl	plastic
y	yielding
1*c*	critical in plane strain mode
c	critical

Other parameters are defined in the text.

3.1 Introduction

3.1.1 General remarks

When a structural component has a crack the strength of the component under tensile stresses will decrease rapidly for which the main reason is that the crack leads to fracture by stress or strain concentration.

Fracture is the separation of a solid body into two or more parts under stresses. The fracture process initiates at the weakest point where there are large stress concentrations and low material resistance. When stressed part of the body cannot sustain the locally concentrated stress, the solid body will be deformed and some atomic bonds will be broken, so that a macro crack can be formed and grow. In places where a crack or a notch already exists , the crack will be made even larger. The crack may develop to total separation of the solid body or may stop growing at some point depending on circumstances.

There are two kinds of fracture:

1) **BRITTLE FRACTURE** in which after initiation there is rapid crack propagation followed by breakage of the component with little gross deformation.

2) **DUCTILE FRACTURE** in which after initiation there is an appreciable amount of plastic deformation prior to or during crack propagation. In ductile fracture a crack may stop due to the energy absorption through active plasticity without increase in applied load.

In brief, the distinction between brittle fracture and ductile fracture in the sense of mechanics is the ability to sustain large strains, i.e. plastic deformation, during the fracture process.

It is important that the difference between micro aspects of brittle fracture and ductile fracture and the macro aspects of brittle fracture and ductile fracture should be noted. In the micro sense, brittle fracture is the separation of crystals with only negligible deformation, whereas ductile fracture is the growth and coalescence of microvoids. In the macro sense, brittle fracture usually occurs by the sudden acceleration of the crack growth up to complete separation prior to general plastic deformation. Ductile fracture on the other hand is the stable tearing of the crack which may stop at some point or finally tear in an unstable manner. The speed of ductile crack growth is much slower than the brittle one from start to final fracture. Usually in ductile fracture some time may elapse between initiation and final separation of the solid body, while the brittle fracture occurs suddenly. In some metals notably in steel in the transition region, a micro brittle separation after macro general deformation occurs.

As far as fatigue is concerned, crack growth cannot be described as the break of the solid body

bonds. It is now well accepted that the deformation of crystals under a cyclic loading occurs by slip or shear displacement of one atom plane past to an adjacent plane. The initialisation point of a fatigue crack is determined by the type of crystal and by the presence of a discontinuity in the form of a microcrack, foreign particle, or a void. The fatigue process has yet to be described in mathematical terms partly due to insufficient knowledge of the solid body or inability to interpret fatigue data. However over the past twenty years, fracture mechanics, for instance the Paris' law, has been widely and relatively successfully applied to help to explain the fatigue process and to predict fatigue life.

3.1.2 Scope of the Chapter

In this thesis, fracture mechanics is taken as the best defined mathematical and physical tool to study fatigue and as the reference for the final failure of a cracked structural component. Consequently linear elastic fracture mechanics and ductile fracture mechanics should be understood to a sufficient extent. This section is intended to clarify some basic concepts of Linear Elastic Fracture Mechanics (LEFM) and Elastic Plastic Fracture Mechanics (EPFM).

Firstly, LEFM will be introduced and briefly reviewed in section 3.2.2. LEFM is relatively well established theory and will lay a base for EPFM studies.

EPFM will be discussed in section 3.2.3. Due to the complexity of EPFM and vast literature in EPFM, only relevant parts of the EPFM studies are presented and critically discussed. J is an important parameter in this study acting both as the characterisation for the crack tip stress field and the energy release rate. J should also be viewed with uncertainties for the HRR stress field and the energy for crack growth.

Section 3.3 presents and evaluates one of the fracture design method , the R6 method in detail .

3.2 Background of Fracture Mechanics

3.2.1 General remarks

Although this section will not cover any original work directly, it is important in a fracture or fatigue study to understand the basis for physical models before one could treat the problem in terms of probability. The development of fracture mechanics has given new directions as well as confusions. The author of this review attempts to present the related literature in a logical way. As a result, the reliability analysis for design can be carried out with integrity.

3.2.2 Linear Elastic Fracture Mechanics

For brittle fracture, LEFM analyses the stress concentration in the region of the crack tip and the correspondence between concentrated stress and fracture occurrence. So far , LEFM is a well established theory within its limiting conditions[4.1].

3.2.2.1 Stress Intensity Factor

In LEFM, the stress intensity factor K is used to characterise the crack tip stress field. The critical value of K corresponding to fracture behaviour is called the fracture toughness. More about fracture toughness will be in section 3.2.2.3.

The principle of the stress intensity theory is that:

> the distribution of the elastic stress field in the vicinity of the crack tip is invariant in all structural components subjected to this type of deformation and that the magnitude of the elastic stress field can be described by the single parameter, K, i.e. the stress intensity factor.

For Mode I opening crack fracture

$$K = constant \times \sigma \times \sqrt{a} = Y\sigma\sqrt{a} \tag{3.1}$$

where σ is the nominal applied stress perpendicular to the crack plane, Y is often called LEFM shape factor.

The Y factor depends on the crack size, shape and orientation and the structural configuration associated with structural components. Various methods of finding it are available:

1) Analytical methods for only relatively simple geometries(e.g. Westergaad stress function)

2) Green's function

3) Weight function techniques

4) Boundary collocation

5) Finite element method

6) Integral equations

7) Boundary method

8) Compounding method

9) Experimental methods

Each method has its own advantages and disadvantages. And each method can be suitable for some special cases. For common crack geometries, there are many solutions in Handbooks[3.2]. It should also be noted that there will be no ideal solution in practical situations due to the diversity caused by the assumptions each method has to make. Therefore , the solutions have uncertainties to a greater or lesser extent. Further discussion on those uncertainties can be found on section 3.2.2.6.

3.2.2.2 Energy consideration

With an understanding of the stress concentration at the crack tip and the singularity of the stress field characterised by K, the question then arises about the critical energy value for the crack to extend. Historically, the energy consideration came before the crack tip characterisation. But in this thesis because emphasis has been put on the application of fracture mechanics, the K factor is explained first.

The stress concentration will store a large amount of energy in the cracked body. Griffith[3.3] confined his attention to a brittle material containing a single crack of length $2a$. He then considered the energy changes in the system associated with an incremental extension of the crack. He stated that *a crack will propagate when the decrease in elastic potential energy is at least equal to the energy required to create the new crack surface.* Therefore for perfect linear elastic material the following condition must be met:

The total energy of the system must be reduced by an incremental extension of the notch.

In the crack growth process the sum of the energies will be $U+W-Fe$. The variation of $U, W, U+W$ can be shown schematically when in fixed displacement condition where external energy $Fe = 0$ in Fig. 3.1.

In the graph, W increases linearly because the energy to break an atomic bond is assumed to be constant.

From Griffith's theory , the crack will extend uncontrollably when

$$\frac{\partial(W+U)}{\partial a}=0 \tag{3.2}$$

i.e.

$$-\frac{\partial U}{\partial a}=\frac{\partial W}{\partial a}=constant \tag{3.3}$$

Set

$$G=-\frac{1}{B}\frac{\partial U}{\partial a}\bigg|_q \tag{3.4}$$

G is then referred as the crack *driving force.* A critical value of G can be defined as G_{crit} , at which unstable crack propagation will occur. G_{crit} can be a material property since $\frac{\partial W}{\partial a}$ is a constant.

$$G_{crit}=\begin{cases} G_c=\dfrac{\sigma_c^2\pi a}{E}, \quad \text{for plane stress} & (3.5)\\ \\ G_{1C}=\dfrac{\sigma_c^2\pi a}{E}(1-\upsilon^2), \quad \text{for plane strain} & (3.6)\end{cases}$$

Also G has a direct relationship with the compliance of the structure which is defined as:

$$C=\frac{\text{displacement}}{\text{force}}=\frac{u}{F} \tag{3.7}$$

i.e.

$$u=CF \tag{3.8}$$

In fixed-grip condition , the strain energy release rate per unit thickness for crack extension is $-1/2u\delta F$. In fixed-load condition , the strain energy release for crack extension is -1/2 $F\delta u$. So, for a small crack extension the energy per unit thickness:

$$U_{fixed\ grip}=-\frac{1}{2}u\delta F=-\frac{1}{2}CF\delta F=-\frac{1}{2}F\delta u=U_{fixed\ load} \tag{3.9}$$

For the fixed-grip condition,

$$G=-\frac{\partial U_{fixed\ grip}}{\partial a}=-\frac{1}{2}CF\frac{\delta F}{da} \tag{3.10}$$

$$=\frac{1}{2}F^2\frac{\partial C}{\partial a} \tag{3.11}$$

In this way G can be obtained from the interpretation of compliance measurement from the load displacement record on the cracked specimen.

Irwin [3.4] found that the relation between K and G is

$$K^2 = E'G \tag{3.12}$$

where

$$E' = \begin{cases} E & \text{for plane stress} \\ \frac{E}{(1-\upsilon^2)} & \text{for plane strain} \end{cases}$$

From this equation, one can see that K_{1C} (see section 3.2.2.3) will be a material property since G_{1C} is a material property.

3.2.2.3 Fracture Toughness

In equation(3.1), σ, a, Y affect the value of K, but do not change the stress field distribution. From this feature, it is possible to correlate the laboratory test results with practical design by using the fracture toughness concept:

> unstable fracture occurs when the stress intensity reaches a critical value. For mode I deformation and for the plane strain condition, the critical stress intensity factor for fracture instability is called K_{1C}.

Various experimental methods are used to determine K_{1C}, .e.g. ASTM designation E 399-78.[3.5].

Specimen Size Requirement A typical crack configuration is shown at Fig. 3.2. It is found that K_c and G_c are strongly thickness dependent.

K_C values change very much when thickness is small and after certain value of thickness become stable. The reason is that when B is small , the failure mode is plane stress condition; when B becomes bigger , the failure mode approaches a plane strain condition. The plane strain fracture toughness , K_{1C}, is the minimum of the K_C values. This minimum fracture toughness is a material constant.

The condition for K_{1C} to be a constant for a flat fracture is for the crack to have a plane strain opening behaviour. Empirically [3.6]:

$$a, B, \frac{w}{2} \geq 2.5 \left(\frac{K_{1C}}{\sigma_y}\right)^2 \tag{3.13}$$

Or in other words the plastic zone, to be discussed in section 3.2.2.4, is to be restricted within an elastic stress field. That is:

$$\rho \leq \frac{B}{50} \tag{3.14}$$

where ρ is the plastic zone size as e.g. defined in equation (3.21).

Charpy tests

The K_{1C} tests recommended by the ASTM committee and other laboratory test methods [3.7] are often not convenient for large complex structures. Some *auxiliary* methods have to be used. One of the most popular fracture toughness tests since the early stage of fracture mechanics application is the Charpy test.

The Charpy V-notch(CVN) impact fracture toughness test specimen is widely used as a general reference specimen as well as in actual toughness specification. It is simple, inexpensive and easy to conduct. Similarly, the CVN slow-bend test is carried out but with a different loading rate.

There are some empirical correlations between the CVN test result and fracture toughness K_{1c}.

K_{1C}-CVN upper shelf correlation

Based on experimental results from a number of investigators, Barsom and Rolfe [3.8] suggested the relationship of K_{1C} and CVN as

$$\left(\frac{K_{1C}}{\sigma_y}\right)^2 = \frac{5}{\sigma_y}(CVN - \frac{\sigma_y}{20}) \tag{3.15}$$

for K_{1c} in ksi$\sqrt{\text{in}}$, $\sigma_y$in ksi, CVN in ft-lb;

or

$$\left(\frac{K_{1C}}{\sigma_y}\right)^2 = \frac{38.7}{\sigma_y}(CVN - \frac{\sigma_y}{3.9}) \tag{3.15a}$$

for K_{1c} in MPa$\sqrt{\text{m}}$, $\sigma_y$in MPa, CVN in J.

K_{1C} and CVN transition region correlation

The prediction of K_{1C} by the CVN in the transition temperature region is more complicated than in the upper shelf. The correspondence between K_{1C} and CVN energy absorption

values at a particular test temperature and at the same strain rate for both the K_{1C} and CVN can be approximated as[3.9]:

$$\frac{K_{1C}^2}{E} = A(CVN) \tag{3.16}$$

The constant A incorporates the effects of specimen size and notch acuity. It can be decided by correlating to the experimental data.

temperature shift

In order to incorporate K_{1d} value for K_{1C} under different test conditions, temperature shift is needed

to take account of the different loading rates[3.10]. The magnitude of the temperature shift between dynamic($\dot{\epsilon} \approx 10sec^{-1}$) and slow-bend ($\dot{\epsilon} \approx 10^{-5}sec^{-1}$) is:

$$T_{shift} = 215 - 1.5\sigma_y \quad for \quad 36 \ \text{ksi} < \sigma_y < 140\text{ksi} \tag{3.17}$$

$$T_{shift} = 0 \quad for \quad \sigma_y > 140 \ \text{ksi} \tag{3.18}$$

or

$$T_{shift} = 215 - 0.218\sigma_y \quad for \quad 248 \ \text{MPa} < \sigma_y < 965\text{MPa} \tag{3.17a}$$

$$T_{shift} = 0 \quad for \quad \sigma_y > 140MPa \tag{3.18a}$$

The magnitude of the temperature shift between dynamic($\dot{\epsilon} \approx 10sec^{-1}$) and intermediate strain rate ($\dot{\epsilon} \approx 10^{-3}sec^{-1}$) was found to be 75% of the shift between dynamic and slow-bend curves.

A detailed procedure can be seen in Ref. [3.10]. As an engineering approach, the CVN test results are effectively used but empiricism and uncertainty will inevitably prevail.

3.2.2.4 Plasticity effect

The stress concentration around the crack tip will reach the yielding criteria and will create a plastic zone. LEFM is based on the elastic assumption which cannot be possible in any case. Because fracture mechanics concentrates its study on the region around the crack tip, the effect of plasticity on the fracture of the component will be profound.

The determination of a precise plastic zone size and shape in mode I needs a large amount of computation either by finite element method or any other method and need the detail of the geometry. However , there are two main approximate plastic zone models, namely,

1) Irwin's plastic zone model

2) Dugdale's plastic zone model

Irwin [3.11] assumed that a *notional crack* extends beyond the real crack tip to the centre of the yielding plastic zone and that the stresses in the zone equals the yielding stress. This crack extension is given by:

$$r_p = \frac{1}{2\pi}(\frac{K_I}{m\sigma_y})^2 \tag{3.19}$$

where K_I is the stress intensity factor for mode I

$$m = \begin{cases} 1 & \text{for plane stress} \\ \sqrt{3} & \text{for plane strain} \quad \text{(empirically)} \end{cases} \tag{3.20}$$

One can have the actual plastic zone size:

$$\rho = 2 * r_p = \frac{1}{\pi}(\frac{K_I}{m\sigma_y})^2 \tag{3.21}$$

Dugdale [3.12] assumed that the plastic zone ahead of the crack could be treated as if the actual crack extends through it and the portion of the extended crack situated in the plastic zone experiences a constant , negative pressure of the same magnitude as yield stress.

Because the stress singularity of the plastic zone dimension ρ, the superposition of the stress intensity factors by remote stress with the extended crack and by the plastic closure negative stress should be zero. If K_σ and K_{σ_y}, the stress intensity factors from σ and σ_y,

$$K_\sigma + K_{\sigma_y} = 0 \tag{3.22}$$

$$K_\sigma = \sigma\sqrt{\pi(a+\rho)} \tag{3.23}$$

$$K_{\sigma_y} = -2\sigma_y\sqrt{\frac{a+\rho}{\pi}}arccos(\frac{a}{a+\rho}) \tag{3.24}$$

Hence,

$$\frac{a}{a+\rho} = cos(\frac{\pi\sigma}{2\sigma_y}) \tag{3.25}$$

When $\sigma \ll \sigma_y$,

$$\rho = \frac{\pi}{8}(\frac{K}{\sigma_y})^2 \tag{3.26}$$

Comparing equation (3.26) with (3.21), the values are with small difference for plane stress case $m = 1$.

It should also be emphasised that the approximations for equations (3.21) and (3.26) strictly lack theoretical basis and exclude such effects as work hardening and large strains. If in the zone ahead of the crack $m\sigma_y$ is used rather than σ_y, then the Dugdale model is correct until the total load on the section exceeds limit load because Dugdale model is based on an infinite plate. These will be discussed with other aspects in later section for (EPFM).

3.2.2.5 Design Procedure

Under the conditions of LEFM, to minimise the possibility of brittle fracture in a given structure, the designer has three primary factors to control:

1. Material toughness at the particular service temperature and loading rate (K_{1C})

2. Nominal stress level (σ)

3. Flaw size present in the structure (a)

Equation (3.1) gives a combination of the three factors. For the safety of the structure:

$$K < K_{1C} \tag{3.27}$$

The safety margin is :

$$M = K_{1C} - K = K_{1C} - Y\sigma\sqrt{a} \tag{3.28}$$

When $M > 0$ the component is safe

When $M \leq 0$ the component is unsafe

The limiting stress is

$$\sigma \leq \frac{K_{1C}}{Y\sqrt{a}} \tag{3.29}$$

The limiting crack size is

$$a \leq (\frac{K_{1C}}{Y\sigma})^2 \tag{3.30}$$

In the same way as in equation (3.28), safety margin equations for limiting stress and limiting crack size can be constructed.

A example graph is shown in Fig 3.3. It is interesting to compare this diagram with the column instability Euler curve diagram. It seems that both share the same trend with increase in a or slenderness ratio.

If a is modified to become $a + \rho$ from the Dugdale's model with

$$a + \rho = a\ cos^{-1}(\frac{\pi}{2}\frac{\sigma}{\sigma_y}) \tag{3.31}$$

The new K, denoted as K^*, is

$$K^* = Y\sigma\sqrt{a\ cos^{-1}(\frac{\pi}{2}\frac{\sigma}{\sigma_y})} < K_{1C} \tag{3.32}$$

which leads to

$$\frac{K^2}{K_{1C}^2} < cos(\frac{\pi}{2}\frac{\sigma}{\sigma_y}) \tag{3.33}$$

where K is originally defined in Eqn. (3.1).

If

$$K' = (\frac{K}{K_{1C}}) \quad and \quad S' = (\frac{\sigma}{\sigma_y})$$

equation (3.33) then becomes:

$$K'^2 < cos(\frac{\pi}{2}S') \tag{3.35}$$

This is very similar to the Failure Assessment Diagram to be discussed later in the R6 method except the R6 method will introduce plasticity and redefine the S' .

3.2.2.6 Discussion

LEFM is a well established theory but contains many idealisations. Generally it is only suitable to be directly applied to brittle fracture design. The main assumptions for LEFM are:

1. homogeneous material

2. no plasticity effect

3. K_{1C} value can be used for large scale structure although obtained from small laboratory test specimen.

Those assumptions will inevitably bring uncertainties to the engineering design:

(1) **Plasticity Effect** LEFM assumes that small scale yielding occurs in the crack tip region. The plastic zone size from Irwin's and Dugdale's models are without convincing theoretical base. If there is large plasticity, then LEFM cannot be applied. These problems lead to the use of EPFM.

(2)**Notch Effect** In practical situations , the crack may not be of uniform length or even all through the thickness, but the Y factors in equation (3.1) are taken from empirical equations or graphs containing surface and backface geometrical corrections. Newman, J.R.[3.13] reviewed 14 of the commonly used surface crack K equations and graphs. By employing a brittle epoxy as an ideal material for brittle fracture, Newman was able to get the variation of each representation of K. They are ranked $\pm$ 20% to $\pm$ 10 % standard deviation with 95 % of the data analysed.

(3)**Scaling Effect** LEFM theory assumes that the fracture behaviour of a real crack component can be predicted by scaled smaller size laboratory specimen. A survey conducted by Sinclair, G.B . and Chambers, A.E. for brittle fracture mechanics found that the physical agreement with the strength predicted from LEFM is not valid especially when there are appreciable changes in scale. In their extrapolation, fracture toughness may not be a material property.

LEFM is related to simple and idealised materials. It is widely used as a theoretical base for codes of practice and many primary investigation of brittle fracture mechanics. In fatigue study, LEFM is now widely used for crack growth predictions due to cyclic elimination of the plasticity effects.

Many real fracture problems will not be so ideal. EPFM will take the yielding into account and thus extend the view and applicability of fracture mechanics.

3.2.3 Elastic Plastic Fracture Mechanics(EPFM)

3.2.3.1 General remarks

In many cases fracture will occur after widesread plasticity in the crack tip region. LEFM cannot explain and thus solve these problems. In the last 20 years people have come to realise the need for EPFM. However, due to the engineering complexity and uncertainties in various aspects, EPFM is much less established than LEFM[4.1]. Fortunately, the consequence of ductile fracture may not be as serious as brittle fracture because the higher ductility of the cracked body material makes the crack growth detectable before final fracture. The high ductility will be important in limit state design for the large reserve of capacity against failure in ductile fracture and thus important for reliability analysis.

Two concepts are widely used to explain EPFM; the Crack Tip Opening Displacement (CTOD) and J-integral methods.

In LEFM the entire energy provided by the external force will be stored by the elastic strain and then can be released through fracture. In EPFM, part of the energy from external force will cause plasticity of material and will thus will not be recovered. The size restraint effects resulting in nonidealised plane stress or plane strain conditions and the redistribution of stress and strain will make the plasticity even more complex so that the fracture mechanics of the crack will become more difficult to analyse.

The first problem to encounter is again the characterisation of crack tip state, which in LEFM is by the stress intensity factor. In EPFM, CTOD uses the geometric state of the crack tip region, while the J-integral uses the strain energy around the crack tip to characterise the crack tip state. Many of the design methods are derived from these two concepts. Further investigation has shown these two concepts can be related to each other.

This section is intended to give a systematic review of the EPFM theory which will be the theoretical basis of design methods and serve for the understanding of uncertainties in the reliability assessment of cracked components.

3.2.3.2 CTOD method

The basic assumption of the CTOD method is that the crack state is characterised by the opening distance right behind the crack tip. The relationship between this displacement and the critical fracture state has been shown in a large number of experiments [3.15] [3.1], while the theoretical base for CTOD could be the Dugdale stress yield line model.

The Dugdale plasticity model was discussed in the LEFM as in Eqn. (3.26). If relating the Dugdale model to the geometry of the crack tip, one could set up a mathematical criteria for fracture.

Dugdale [3.12] showed the length of the plastic region $(a_1 - a)$ was

$$(a_1 - a) = a[sec(\frac{\pi\sigma}{2f}) - 1] \tag{3.36}$$

where a_1 is the extended crack including plastic region

f is the local stress system

Burdekin and Stone[3.16] evaluated the displacement at the tip of the real crack for the line plasticity model by combining with the elastic solutions and found

$$\delta = 2\nu_a = \frac{8f_a}{\pi E} ln(sec\frac{\pi\sigma}{2f}) \tag{3.37}$$

If the $ln(sec)$ term is expanded

$$\delta = \frac{8f_a}{\pi E}[\frac{1}{2}(\frac{\pi}{2}\frac{\sigma}{f})^2 + \frac{1}{12}(\frac{\pi}{2}\frac{\sigma}{f})^4 + ...] \tag{3.38}$$

and taking only the first term gives,

$$\delta = \frac{8f_a}{\pi E}[\frac{1}{2}(\frac{\pi}{2}\frac{\sigma}{f})^2] \tag{3.39}$$

In plane stress

$$\delta = \frac{\pi\sigma^2 a}{Ef} = \frac{G}{f} \tag{3.40}$$

and

$$G = \frac{K^2}{E} = \frac{\sigma^2\pi a}{E} \tag{3.41}$$

From the above equation, $G = \delta f$.

$$f = m\,\sigma_y \tag{3.42}$$

Burdekin and Stone also evaluated the overall strain in plane stress by assuming $f = \sigma_y$:

$$\frac{\epsilon}{\epsilon_y} = \frac{E}{\pi}\{2n\,coth^{-1}[\frac{1}{n}(\frac{k^2+n^2}{1-K^2})^{\frac{1}{2}}] + (1-\nu)cot^{-1}(\frac{k^2+n^2}{1-K^2})^{\frac{1}{2}} + \nu cos^{-1}k\} \tag{3.43}$$

where

$$n = \frac{a}{y}$$

$$k = cos\frac{\pi\sigma}{2f}$$

$$\epsilon_y = \frac{\sigma_y}{E}$$

The document of BSI PD6493 [3.15] in 1980 has used CTOD to assess crack integrity by using the non-dimensional factor ϕ. However the design curves in BSI PD6493 were drawn from experiments.

$$\phi = \frac{\delta}{2\pi\epsilon_y a} = (\frac{\epsilon}{\epsilon_y})^2 \quad for\frac{\epsilon}{\epsilon_y} < 0.5 \tag{3.44}$$

$$\phi = \frac{\delta}{2\pi\epsilon_y a} = (\frac{\epsilon}{\epsilon_y}) - 0.25 \quad for\frac{\epsilon}{\epsilon_y} < 0.5 \tag{3.45}$$

Criticisms of the CTOD method are 1) the theoretical assumptions of Dugdale model, 2) the inadequacy for large scale plasticity and 3) the reliability of data obtained in hostile environment and for complex geometry.

Several features of the Dugdale model are noticeable:

(1) the stress state is illustrated as a yielding stress line which is only nearly true for plane stress.

(2) the stress field is without any work hardening.

Although many efforts have been made on the modification of the CTOD method since it first appeared, the essential limitation of this model on large scale plasticity, which will result in strain hardening and size restraint effects, cannot be effectively removed.

3.2.3.3 J-Integral Method

The J-integral concept was first introduced into engineering practice in the United States by Rice[3.17] Mathematically, the J-integral is the integration of the strain energy on a contour around the crack tip, which actually ignores the part right in the crack tip, i.e. considers only the non-linear aspects. It measures the energy flow in a contour about the crack.

By definition

$$J = \int_{\Gamma} \{Z\ dy - T_i \frac{\partial U_i}{\partial x}\} ds \tag{3.46}$$

where Z is strain energy density, $Z = \oint \sigma_{ij} d\epsilon_{ij}$, or density of stress working if the recoverable sense of the term strain energy is to be avoided.

T_i is the component of surface tractions

U_i is the displacement component at the surface

s is the distance along any contour

Several important features of J can then be verified:

1. It is path independent for nonlinear elastic material but for the incremental laws of plasticity can only be used providing the contour is sufficiently large enough, i.e. away from the crack tip. This feature is important for the uniqueness of computation.

2. Through HRR [3.18] [3.19] unique stress and strain field, J is able to characterise the crack tip state, i.e.

$$\left.\begin{aligned}
\sigma_{ij} &= \sigma_y \left(\frac{JE}{I\alpha\sigma_y^2 a}\right)^{\frac{1}{N+1}} \frac{1}{\left(\frac{r}{a}\right)^{\frac{1}{(N+1)}}} \tilde{\sigma}_{ij}(\theta) \\
\epsilon_{ij} &= \epsilon_y \alpha \left(\frac{JE}{I\alpha\sigma_y^2 a}\right)^{\frac{N}{N+1}} \frac{1}{\left(\frac{r}{a}\right)^{\frac{N}{(N+1)}}} \tilde{\epsilon}_{ij}(\theta) \\
U_{ij} &= \epsilon_y \alpha \left(\frac{JE}{I\alpha\sigma_y^2 a}\right)^{\frac{N}{N+1}} \left(\frac{r}{a}\right)^{\frac{1}{(N+1)}} \tilde{U}_{ij}(\theta)
\end{aligned}\right\} \tag{3.47}$$

$$\frac{\epsilon_{pl}}{\epsilon_y} = \alpha \left(\frac{\sigma}{\sigma_y}\right)^N \tag{3.48}$$

where $\sigma_{ij}, \epsilon_{ij}$ is the tensor vector of stress and strain.

α, N are the constants to represent the work hardening state.

I is the normalising constant depending on the symmetry of the field and on whether plane strain or plane stress hold as the tip approaches.

Several restrictions have to be put on this model[3.20]:

(2.a) In the fracture process zone where voids are produced and void coalescence occurs, and in the region where the solution from finite strain theory does not meet that from small strain theory for HRR. Let R be the zone of dominance in the singular fields beyond which HRR can apply. It depends on where plane strain or plane stress is assumed, on load, on strain hardening and on configuration.

For mode I plane strain, McMeeking[3.21] found that R is 2 or 3 times the CTOD assuming that the fracture process zone is also within the radius

$$R > 3 \times CTOD \tag{3.49}$$

Shih[3.22] calculated that in plane strain with light or moderate strain hardening.

$$COD \approx 0.6 \times \frac{J}{\sigma_y} \tag{3.50}$$

or

$$COD \approx \frac{1}{m} \times \frac{J}{\sigma_y} \tag{4.51}$$

(2.b) Under large scale yielding triaxiality may occur. For instance, in fully yielded bend type specimen where Pradtl field prevails

$$R \approx 0.07b \tag{3.52}$$

$$R > 1.8\frac{J}{\sigma_y} \tag{3.53}$$

$$b > 25\frac{J}{\sigma_y} \tag{3.54}$$

But in cases where the high triaxiality state of stress ahead of the crack is lost such as the centre-cracked strip in plane strain tension.

$$R \approx .01b \tag{3.55}$$

$$b > 200\frac{J}{\sigma_y} \tag{3.56}$$

Since the high triaxiality associated with J dominance generally gives the most critical answer for initiation and advance at lowest level for a given material, most effort in the past was put into the former case to a lower bound of J.

(2.c) In stable crack growth, additional restriction may be satisfied to ensure that the HRR field outside the immediate vicinity of the crack tip where elastic unloading and strongly non-proportional plastic deformation occur. i.e.

$$\triangle a < R \tag{3.57}$$

$$\text{and} \quad D < R \tag{3.58}$$

where D is the zone size of elastic unloading and the non-proportional deformation.

$$\frac{1}{D} = \frac{1}{J_{Ic}}(\frac{dJ_R}{da})_c \tag{3.59}$$

For fully bend type specimen under plane strain

$$\frac{\triangle a}{b} = 0.07 \tag{3.60}$$

$$\frac{b}{J_{Ic}}(\frac{dJ_R}{da})_c > 14 \tag{3.61}$$

Parts of HRR model uncertainty can come from those restrictions discussed above. In addition, it should be pointed out that the HRR model is originated from an infinite plate so that although all the conditions are more or less met and they are used reasonably well from the engineering point of view, they do not indicate the real state of the crack tip.

3. The energy meaning of J can be compared with G in LEFM. In LEFM the characterisation parameter K is related to the energy balance with G. The J-integral is the amount of energy flow in the contour area.

For non linear elastic material:

$$J = -\frac{dP}{Bda} \tag{3.62}$$

or

$$J = -\frac{\partial U}{B\partial a} \tag{3.62a}$$

In LEFM $J = G$. In EPFM, some of the energy may be dissipated by the plasticity or non-linear effect.

3.2.4 η factors

As pointed out by Sumpter and Turner in 1976 [3.23], J can be expressed in the form

$$J = J_{el} + Jpl$$

$$J = \frac{\eta_{el} U_{el}}{(w-a)B} + \frac{\eta_{pl} U_{pl}}{(w-a)B} \tag{3.63}$$

where η_{el}, η_{pl} are dimensionless geometry constants for J_{el} and J_{pl}. U_{el} and U_{pl} are the elastic strain energy and the plastic strain energy.

The introduction of η factors provides a convenient relationship for the analysis of several fracture problems.

$$\eta_{el} = \frac{\partial C}{\partial a}\frac{b}{C} \tag{3.66}$$

Furthermore, from the expression for C in K or Y, the η_{el} can be derived as:

$$\eta_{el} = \frac{Y^2 a}{\int Y^2 a da} b \tag{3.67}$$

For plastic η_{pl} , it will be more complicated. A general condition for the existence of η_{pl} was discussed in a paper by Paris, Ernst and Turner[3.24]. If:

$$P = \frac{b^2}{w} F_1\left(\frac{\delta_{pl}}{w}, \frac{a}{w}, \ldots, etc.\right) \tag{3.68}$$

$$\text{and} \quad F_1\left(\frac{\delta_{pl}}{w}, \frac{a}{w}, \ldots, etc.\right)$$

can be separated to be equal to the multiplication of two different variable function as:

$$F_1\left(\frac{\delta_{pl}}{w}, \frac{a}{w}, \ldots, etc.\right) = G_1\left(\frac{\delta_{pl}}{w}, \ldots\right) \times H_1\left(\frac{a}{w}, \ldots.\right) \tag{3.69}$$

then a genuine solution of η_{pl} can be obtained

$$\eta_{pl} = \left(2 - \frac{b}{L}\frac{\partial H_1}{\partial\left(\frac{a}{w}\right)}\frac{1}{H_1}\right). \tag{3.70}$$

The existence of η_{pl} then depends on the separation of function F_1.

3.2.5 Determination of J by experiments

3.2.5.1 Introduction

In brittle fracture, the fracture toughness is the stress intensity factor at the onset of the crack extension as stated in section 3.2.2.1. The testing methods can be found from the recommendation in ASTM E399-78 [3.5] or BS.5447 [3.7].

However in ductile fracture, it is expected that after crack initiation, some stable crack growth should occur prior to the failure of the specimen. Therefore, the fracture resistance with crack growth must be studied as a parameter to characterise the crack growth process and the final fracture.

In the experiments, usually three parameters are important, i.e. load F, displacement q or u, and the crack length.

3.2.5.2 J for stationary crack tip

When the J test is for the initialisation of crack growth, (J_{1C}), stationary crack tip J tests are carried out to meet the condition of path independence of J with no unloading.

1) *Compliance* J

As explained in section 2.3.3, J may be expressed for nonlinear elastic material with no crack advance as

$$J = -\frac{1}{B}\frac{\partial U}{\partial a}\bigg|_q \tag{3.71}$$

$$= \frac{1}{B}\frac{\partial C}{\partial a}\bigg|_F \tag{3.72}$$

where $U = \oint F dq$ the work done

Or in case of plasticity

$$J = -\frac{1}{B}\left(\frac{\partial U_{el}}{\partial a}\bigg|_q + \frac{\partial U_{pl}}{\partial a}\bigg|_F\right) \tag{3.73}$$

2) *Rice-Paris-Merkle method*

The above compliance method needs multi-crack experiment and is often expensive . Rice *et al*[3.25] has found an alternative J test method employing the same theoretical principle as the above one.

For deep notched bending specimen, the angle of bend, θ, is only the function of the applied moment, M, and the square of the remaining ligament, b.

$$\theta = f\left(\frac{M}{b^2}\right) \tag{3.74}$$

The potential energy in equation (3.71) is

$$U = \int_0^{\theta} M \, d\theta \tag{3.75}$$

The solution for J from equation (3.71), (3.74) and (3.75) is

$$J = \frac{2}{Bb}\int_0^{\theta} M \, d\theta \tag{3.76}$$

Recalling to the η factor defined in section 3.2.4, one can see that for bend type specimen η is equal to 2.

3) *tension effects*

In the bending test the tension effects, which does exist in a small proportion is ignored. To take account of this effect, Sumpter and Turner [3.23] suggested that

$$J = J_{el} + J_{pl}$$

$$= \frac{\eta_{el} U_{el}}{Bb} + \frac{\eta_{pl} U_{pl}}{Bb} \tag{3.7}$$

Clark *et al* [3.26] used elastic perfectly plastic flow properties to estimate the contribution of the tension component in the compact speciemen test.

$$J = \frac{\eta U_T}{Bb} \tag{3.78}$$

where

$$U_T = U_{el} + U_{pl}$$

$$\eta = \frac{\eta_{el} + \eta_{pl}}{2}$$

It is found that

$$\eta = 2\left(\frac{1+\alpha}{1+\alpha^2}\right) \tag{3.79}$$

or

$$\eta \simeq 2 + 0.522\frac{b}{w} \qquad for \quad 0 \leq \frac{b}{w} \leq 0.5 \tag{3.80}$$

where

$$\alpha = \sqrt{(\frac{2a}{b})^2 + 2(\frac{2a}{b}) + 2} - \{(\frac{2a}{b}) + 1\} \tag{3.81}$$

3.2.5.3 J for the growing crack

When the crack is initialised, J can be no longer tested by the stationary test. The technique to test the growing crack resistance curve, named R-curve, has been developed in the last twenty years. It should be recognised that the difference between the stationary and growing crack J tests cause much difficulty both in the experimental technique and the analysis. The following section will review briefly the current practice.

deformation J

Due to the fact that in the testing process the crack is growing, the load versus load point displacement record will not follow the correct path to indicate the work done by the external force as shown in the last section. Rather the curve slips from the initial crack length $F - v$ curve into $F - v$ curve of the following crack length. So

$$J = \frac{\eta}{Bb} \oint_0^v F \, dv \tag{3.82}$$

For growing if J is expressed as internal energy W

$$J_{ie} = \frac{\eta W}{Bb} \tag{3.83}$$

Hence

$$\frac{dJ_{ie}}{da} = \frac{\eta}{Bb}\frac{dW}{da} + \frac{J}{b}(1 + \frac{b}{\eta}\frac{d\eta}{da}) \tag{3.84}$$

If we put

$$f(\eta) = (1 + \frac{b}{\eta}\frac{d\eta}{da}) \tag{3.85}$$

$$dW = dU - BJda \tag{3.86}$$

$$\frac{dJ_{ie}}{da} = \frac{\eta}{Bb}\frac{dW}{da} + \frac{J}{b}f(\eta) \tag{3.87}$$

Or

$$\frac{dJ_r}{da} = \frac{dJ_{ie}}{da} = \frac{\eta}{Bb}\frac{dU}{da} + \frac{J}{b}g(\eta) \tag{3.88}$$

Where

$$g(\eta) = f(\eta) - \eta \tag{3.89}$$

For external energy,

$$\frac{dJ_{ee}}{da} = d(\frac{\eta U}{Bb}) = \frac{\eta}{Bb}\frac{dU}{da} + \frac{J}{b}f(\eta) \tag{3.90}$$

From equation (3.86),

$$\frac{dJ_{ee}}{da} = \frac{dJ_{ie}}{da} + \eta\frac{J}{b} \tag{3.91}$$

The solution for J from external energy and internal energy would be different. However if

$$\frac{dJ}{da}\frac{b}{J} \gg f(\eta)$$

then $\triangle W \approx \triangle U$

$$\triangle J_{ee} = \triangle J_{ie} = \triangle J_r$$

If approximately , we set

$$\frac{dJ_r}{da} = \frac{\eta}{Bb}\frac{dU}{da} \tag{3.92}$$

A correction should be made as follows

$$J_r = J_{r(approx)} * \{1 + \frac{\triangle a}{b}g(\eta)\} \tag{3.93}$$

Ernst [3.27] proposed a general form:

$$J_{I+1} = \{J_i + (\frac{\eta}{b})_i A_{i,i+1}\}\{1 - (\frac{\gamma}{b})_i(a_{i+1} - a_i)\} \tag{3.94}$$

where J_i is the J from crack length a_i J_{i+1} is the J at crack length a_{i+1} $A_{i,i+1}$ is the increment of area under the load displacement record between lines of constant displacement at a_i and a_{i+1}

For a compact specimen

$$\eta_i = 2 + 0.522b_i \tag{3.95}$$

$$\gamma_i = 1 + 0.76(\frac{b_i}{W}) \tag{3.96}$$

For the deeply cracked bend specimen η=2 and$\gamma = 1$ independent of crack length.

The following conditions must be imposed for the above R-curve formula:

1)

$$\omega \gg 1 \tag{3.96}$$

2)

$$(\frac{\triangle a}{b}) \ll 1 or (\frac{\triangle a}{b}) \simeq .1 \tag{3.97}$$

3)

$$B, b > 25\frac{J}{\sigma_{flow}} \tag{3.98}$$

A modified J from computational analysis for larger $\triangle a/b$ is proposed by Ernst [3.28]:

$$J_M = J_D - \int_{a_0}^{a_f} \frac{\partial(J-G)}{\partial a}\Big| \atop v_{pl}da \tag{3.99}$$

where J_D is the deformation plasticity J Or for the case of compact specimen,

$$J_M = J_D + \int_0^a \gamma\frac{J_{pl}}{b}da \tag{3.100}$$

3.3 The R6 method

3.3.1. Introduction

Fracture mechanics has undergone many developments as partly seen in section 3.2. The maturity of fracture mechanics had led to the widespread applications in design and safety assessment. In this section, one of the major application methodology for engineering design practise, the R6 method is presented and evaluated for the purpose of assessing the structural integrity and calculating the reliability of flawed structural components.

When a structural component under tensile stress has a crack, the component can either fail by fracture or plastic collapse. The usual fracture mechanics design methods only predict failure in the fracture mode. The Two-Parameter Fracture Criterion (TPFC) constructs a failure prediction method polarising the brittle fracture and plastic collapse to give a general failure mechanism[3.29]. Based on this TPFC method, the Central Electricity General Board (CEGB) has gradually developed R6 method from revision 1 in 1979 and revision 2 to revision 3 in 1985. R6 revision(rev.) 1 constructed a relationship between S_r, which is the ratio of applied load to the flow load, and K_r, which is a ration of stress intensity factor to fracture toughness, in a ln(sec) function derived from the expression in TPFC for CTOD. The R6 rev. 2 updated R6 rev. 2 but still use the same expression. The R6 rev.. 3 [3.30] uses the J- integral as a valid parameter for characterising crack initiation and crack growth to construct a method for elastic plastic fracture prediction with brittle fracture and plastic collapse on both ends. The R6 method rev. 3 treats the stable ductile tearing (slow crack growth) and load instability by using a resistance curve approach. Also work in CEGB and EPRI have developed fully plastic solutions (deformation theory) [3.31] for fracture specimens. The CEGB R6 method rev. 3 stated that a tensile specimen could either fail by brittle fracture or plastic collapse and these two mechanism are connected by an interpolation curve based on J-integral study and experimental data. In R6 rev. 3, the abscissa S_r in R6 rev. 1 is replaced by L_r which is the ratio of the applied load to the yield load.

The R6 method is used in this thesis as the failure criterion for the final failure of a cracked component. R6 method provides a safety margin function for cracked components for use in reliability analysis. In this thesis, when reference is made to the R6 method, R6 revision 3 has generally been used unless other revisions are specified.

3.3.2. Definitions

As a methodology to apply in engineering practice, the R6 method defined many new parameters in addition to the commonly used fracture mechanics parameters. Some parameters in R6 rev. 3 are listed below.

1. Crack size

$\triangle a_g$ maximum amount of ductile crack growth at which valid data can be derived from test specimens

a_g $a_{ini} + \triangle a_g$

$\triangle a_j$ postulated amount of ductile crack growth

a_j $a_{ini} + \triangle a_j$

2. Stresses

σ^p stresses arise from loads which contribute to plastic collapse

σ^s stresses arise from loads which do not contribute to plastic collapse

$\bar{\sigma}$ flow stress

3. F factors (load factor related)

$$\text{loadfactor} F^L = \frac{\text{the load which could produce a limiting condition}}{\text{the applied load in the assessed condition}}$$

F^L_{ini}, F^L_g load factors for flaw sizes a_{ini}, a_g respectively

4. J factors

J_{app} value of J due to the applied loading

J_{mat} value of J due to material resistance

5. K factors

K^p_I, K^S_I value of K_I due to loads giving rise to σ^P, σ^s respectively

$K_{0.2}$ fracture toughness relating to K at 0.2 mm crack extension

K_g fracture toughness after $\triangle a_g$ of the ductile crack growth

K_{mat} material fracture toughness as indicated in individual cases

$K_\Omega(\triangle a)$ fracture toughness after $\triangle a$ of ductile crack growth

6. Ordinate in the FAD

$$K_r = K^p_r + K^s_r$$

$$K_r^p = \frac{K_I^p(a_{ini})}{K_{mat}}$$

$$K_r^s = \frac{K_I^s(a_{ini})}{K_{mat}} + \rho(a_{ini})$$

ρ plasticity correction factor for σ^s stresses

$K_{rg} = K_{rg}^p + K_{rg}^s$

$$K_{rg}^p = \frac{K_I^p(a_g)}{K_g}$$

$$K_{rg}^s = \frac{K_I^s(a_g)}{K_g} + \rho(a_g)$$

7. Abscissa in the FAD

$$L_r = \frac{\text{total applied load giving rise to } \sigma^P \text{ stresses}}{\text{plastic yield load of the flawed structure}}$$

$$L_r^{max} = \frac{\text{flowstress}}{\sigma_y}$$

8. strain

ϵ_{ref} uniaxial strain at load level $L_r \times \sigma_y$

3.3.3. Failure Assessment Diagram (FAD)

In the R6 method, the limiting conditions for load, flaw size and fracture toughness or yielding stress are all combined in one diagram called the Failure Assessment Diagram(FAD). The abscissa is L_r, the ordinate is K_r. To set up the fracture failure criterion, the J-integral is used.

$$J = J_{el} + J_{pl}$$

J_{el} can be obtained from various elastic fracture handbooks or can be calculated from the methods discussed in section 3.3. J_{pl} can be obtained through:

1. elaborate J-integral calculation,

2. the fully plastic solution for flawed structure developed by EPRI.

3. approximation from numerical or experimental data.

Corresponding to these three levels of calculation R6 method has three options of Failure Assessment Line(FAL) function. Option 1 need elaborate calculation of J. Option 2 is subject to the availability of the fully plastic solution for flawed structure of interest, i.e. the availability of ϵ_{ref} which is the uniaxial strain at stress of $L_r \times \sigma_y$. In option 3 an empirical curve, which acts as the lower bound of data from numerical and experimental analysis for K_r, can be formulated as:

$$K_r = (1 - 0.14L_r^2)[0.3 + 0.7exp(-0.65L_r^6)] \quad for \;\; L_r \leq L_r^{max} \tag{3.101}$$

$$K_r = 0 \qquad for \;\; L_r > L_r^{max} \tag{3.102}$$

This formula constructs a direct relationship between K_r and L_r without complicated calculation and reference to other parameters. Among the three options the option 3 is the most convenient but with greater inaccuracy. It is suitable for all materials which do not exhibit a yield discontinuity in the stress strain curve and which do not have high initial work hardening rate . It can be used for initial screening test with only σ_y and flow stress needed to be known. The option 3 FAL is called the general curve in R6. The general curve is illustrated in Fig.3.4. In this thesis, option 3 FAL has been used for reliability analysis.

Depending on the material fracture toughness, a cracked specimen can fail by brittle fracture or ductile tearing. The ductile tearing can have large reserved load capacity. To deal with different modes of fracture failure, the R6 method has three categories of fracture analysis.

Category 1. When failure is by brittle fracture and significant ductile tearing is absent, K_{mat} can be taken as K_{1c} or K_c. If failure is by ductile mechanisms but no benefit is taken of the increase in toughness due to ductile tearing, $K_{mat} = K_{0.2}$. The co-ordinate (L_r, K_r) can thus be calculated and should be below the Failure Assessment Line (FAL) for safety. The limiting condition is that the point of interest must be on the FAL.

Category 3. When failure is by ductile mechanisms and benefit should be taken from the reserved load capacity due to increased fracture toughness, a J-integral resistance curve should be found.

$$K_{mat} = K_\Omega(\triangle a) = \{EJ(\triangle a)\}^{1/2} \tag{3.103}$$

The experimental procedure for the determination of the fracture resistance of ductile steels can be seen from the R6 rev. 3 and more detail from Neale,B.K *et al* [3.32].

The locus with crack size extending under fixed load condition is called crack extension locus and has been used in the category 3 analysis. The safe condition of category 3 for stable crack growth is that at the applied load a part of the crack extension locus falls within the FAL . The limiting condition is therefore that the locus is tangential to FAL.

Category 2. As an intermediate treatment between category 1 and category 3, category 2 performs the tearing analysis at two points only:

a. $K_{mat} = K_{0.2}$

b. $K_{mat} = K_g$

The limiting condition is defined for two sets of conditions:

$$F_g^L \geq 1.1 \tag{3.104}$$

and

$$\frac{F_g^L}{F_{ini}^L} \geq 1.2 \tag{3.105}$$

The first condition requires that there is a 10% margin on load to extend the crack by $\triangle a_g$. The second condition ensures that the difference between the applied crack driving force and the material fracture resistance is sufficient to make the result relatively insensitive to variations in the resistance curve data.

The detailing procedure of R6 method is shown in Fig.3.5 as a chart form from the R6 rev. 3.

3.3.4 Evaluation of R6 method

(1) Comparison of prediction results with other methods

The development of fracture mechanics has led to many methods of failure prediction by investigating different aspects of fracture. Some commonly used fracture design methods can be found in references [3.1,3.34].

Rhee,H.C. *et al*[3.35] compared the CTOD method from the BSI document [3.15] and the R6 FAD from rev 1 and rev 3 option 2 by using J -integral crack instability analysis as the reference. The experimental specimens include 1) the centre-cracked tension panel(CCT) , the single-edge notched panel(SENP) and a pipe with internal circumferential flaw to study the geometry effects; 2) single-edge notch panel with three point bending (SENB) , with pure tension (SENT) and combined tension and bending to study the loading mode effects.

From the comparison of prediction results, it was found that R6 FAD method has better behaved

solutions with relatively narrow bands with or without crack extension being considered than the CTOD method has. If the crack extension is considered, the solution scatter bands will also be reduced compared to that obtained without crack extension. The CTOD design curve from BSI can result in unconservative results for certain problems and can be influenced significantly by the loading modes and the geometric characteristics of the problem.

In 1985 an ASTM Committee E24.06.02 Task Group [3.34] conducted a round robin study on fracture to evaluate and to document various elastic-plastic failure load prediction methods. 18 participants using 13 different failure prediction methods from United States and United Kingdom joined the round robin study. The CEGB R6 method was presented by Bloom as Deformation Plasticity Failure Assessment Diagram (DPFAD).

The experimental fracture data for the round robin were gathered by NASA Langly Research Centre and Westinghouse Research and Development Laboratory. The tested materials were 7075-T651 aluminium alloy, 2024-T351 aluminium and 304 stainless steel. The data provided to each participant were:

a) tensile properties (σ_y, σ_u, E and full stress strain curve.)

b) fracture properties results from test on compact specimen (maximum failure loads, typical load displacement records, K_R- curve, and J_R curve.)

c) fracture analysis data from compact, middle-crack tension, and the three-hole-crack tension(THT) specimens (all specimen dimensions, a_{ini}, K solution for THT specimen.)

The predictions from all the participants are ranked according their order of variation of predicted failure load to the experimental failure load. The results are summarised in Table 3.1 after reference [3.34].

To compare the accuracy of the participants as well as their applicability , a new comparison can be made:

1) excluding the prediction methods which do not predict failure on all specimens.

2) for each specimen, giving a score equal to the number of the rank in each specimen and summing up.

3) all the prediction methods are ranked in the inverse order of the amount of their score.

Therefore according to the above rules and by studying the ASTM summary, first participants 3, 10, 11, 12, 17, 18, are excluded from this comparison. The table below shows the subsequent comparison

Table 3.2 Ranking of ASTM round robin participants

Participants	7075-T651	2024-T351	304	Score
14	3	3	2	7
K_R-curve and limit load				
6	2	4	4	10
R6 DPFAD				
4	7	1	3	11
TPFC (one parameter)				
15	1	10	1	12
K_R-curve and limit load				
5	8	2	7	17
TPFC				
13	4	9	5	18
K_R-curve and limit load				
9	10	5	9	24
Theory of Ductile Fracture				
2	6	8	12	26
LEFM (plastic zone)				
8	12	6	8	26
Theory of Ductile Fracture				
16	9	11	6	26
K_R-curve and limit load				
1	5	12	11	28
LEFM (size effects)				
7	11	7	10	28
Theory of Ductile Fracture				

results.

It should be noted that participants 13,14,15,16 used different approaches for different material i.e.

K_R-curve for 7075-T651 aluminium

K_R-curve and limit load for 2024-T351 aluminium

limit load for 304 stainless steel

These tables clearly shows that within the reach of the ASTM round robin study, the R6 DPFAD has relatively good accuracy and consistency when compared with the experimental results.

(2) Features of R6 method

Ever since the R6 method revision 1 came out in 1976, the prime aim of the R6 method has been concentrated on the engineering applicability and accuracy of failure prediction by using the latest development of fracture mechanics. The R6 method has been undergoing constant review and updating. R6 rev. 3, uses the J- integral and fracture resistance curve concept and incorporates the most modern development in fracture mechanics which were current up to april 1985. The form of the R6 method enables it to be modified to take into account any new advances in fracture mechanics.

The treatment of secondary stress of σ^s which has no role in plastic collapse failure in R6 has facilitated the applications. The combined load effects can be easily taken into account by the calculation of ρ factor. Ainsworth calculated the ρ factors for general use by using the reference stress technique and the concept of an equivalent mechanical load which produces the same deformation as the combined loading[3.36]. In R6 rev. 3 , the ρ factors are standardised as listed below:

$$\left.\begin{aligned}
&\rho = \rho_1 \quad L_r < 0.8 \\
&\rho = 4\rho_1(1.05 - L_r) \quad 0.8 < L_r < 1.05 \\
&\rho = 0 \quad 1.05 < L_r \\
&\rho_1 = 0.1x^{0.714} - 0.007x^2 + 0.00003x^5 \quad x < 5.2 \\
&\rho_1 = 0.25 \quad x > 5.2 \\
&x = \frac{K_1^s}{\frac{K_1^p}{L_r}}
\end{aligned}\right\} \tag{3.106}$$

The adjustment by ρ is because at low value of L_r the curve of FAL of combined loading rises above the curve of FAL for σ^p loading only because at any given L_r the small scale plasticity effects by the combined loading are greater than those by the σ^p only. Validation literatures by either theoretical analysis or numerical and experimental analysis can be found in reference [3.34].

In the R6 method the adaptation of ductile tearing into the FAD is made by the technique of crack extension locus as in the category 3 analysis. This procedure to accommodate the stable crack growth in the R6 method is proposed and validated by Milne [3.37]. By comparing with other ductile fracture criterion e.g. the tearing modules theory and by experiment, Milne was able to conclude that the limiting condition for category 3 analysis is valid and conservative.

The R6 method is in a standard format and relatively easy to use. Extensive validity studies have been conducted and further advances have been under pursuit. Large number of variables like crack location, material properties, flaw characterisation, loading regime, etc. could be analysed quickly and cheaply. A sensitivity study can thus be conducted directly. These qualities very well suit for a reliability analysis which calculates the safety index of the integrity structure by treating every parameter and the model itself as statistical variable.

It was also pointed out by Rhee *et al* in their comparison of R6 method and the BSI CTOD procedure [3.15] that the most desirable feature of the R6 method is its predictability as critical load parameter which is demonstrated by the narrow scatter band and the most significant challenge for R6 method is the quantification of the level of conservatism.

In the opinion of the author of this thesis, these features of the R6 method make it particularly suitable for reliability assessment. The results are more meaningful because there is a low model uncertainty and the parameters are clearly defined and consistent from brittle fracture to plastic collapse. In addition, the reliability analysis can help to quantify the uncertainties by conducting statistical investigations and sensitivity studies. More discussions of the uncertainties of the R6 method, their quantification and the reliability analysis can be seen in a later chapter dealing with probabilistic fracture mechanics.

(3) Limitations of the R6 method

When applying the R6 methods , the following limitations exist:

a. Limits on J controlled crack growth

The R6 method is an adapted form of J-R curve method. The applicability of R6 method is thus under the same restriction for J controlled crack growth. Those restrictions have been discussed in section 3.2.3.3.

b. The accuracy of the prediction of crack instability

It seems that there is a lack of accuracy for the prediction of ductile instability compared with the K-R curve method in the ASTM round robin study[3.34]. The uncertainties could be from the fracture extrapolation from Milne which was only for maximum load and is conservative. Also uncertainties may arise from the tedious numerical calculation which involves transferring J values into K values and finding the tangential points. This uncertainty can be due to uncertainty of J-R theory as well as the transformation in R6 FAD. A more exact instability load should be found from I theory [3.38] or other relevant literature.

c. Availability of fully plastic solutions for flawed structures of interest

The current plastic solutions for J_{pl} is limited to two-dimensional and axial symmetric flawed configuration. This would involves treating the material stress strain data explicitly and taking full account of the structural component geometry. More work relating to this aspect needs to be carried out.

d. Applicability for various failure mode in practical situations

The R6 method has shown explicitly the failure mechanism of fracture and plastic collapse in one direction of the crack. However, the failure of a structural component in practical situations often involves the combination of several failure mechanisms. For instance , the leak before break analysis, the fatigue crack growth, the change of fracture mode other than the mode I crack opening fracture etc. are not fully implemented. R6 rev. 3 did recommend some solutions for some of these problems but is yet to be satisfactory.

3.4 Conclusions

This chapter has reviewed developments in LEFM and EPFM, and discussed R6 design method in detail. The purpose is to provide the physical basis for statistical analysis of basic variables, and to provide a failure function model of cracked components for reliability analysis.

In the review for LEFM, emphasis is on stress intensity factor: its characterisation of the crack tip, and its relation with energy. Based on K, the concept of fracture toughness K_c has been built. The size requirement of a steady K_{1c} has been discussed. The Charpy tests are briefly presented. The design method using LEFM are discussed. In the end, some of the uncertainties associated with K_{1c} applications are discussed. LEFM is important for brittle fracture analysis.

For ductile fracture analysis, EPFM should be used. Comparison is made between J-integral method and CTOD method. J-integral method is used in this thesis for its features in mathematical integration, crack tip characterisation, and energy meanings. Some experimental procedures to determine J have also been briefly reviewed. The restrictions and limitations of J-integral method have also been discussed.

The R6 method, specially R6 Rev. 3, is evaluated and selected to be the design method for reliability assessment for cracked components. The R6 method analyses the safety of cracked components in an integrity manner and can be updated with the development of fracture mechanics. The R6 method provides a relatively consistent and relatively reliable fracture failure criterion for reliability analysis. In this chapter the limitation and features of R6 method are also discussed. Therefore in later chapters the reliability assessment of cracked components will use failure function from R6 method.

Table 3.1 Ranking of participants in order of minimum standard order on the three material for all predictions (from ref. [3.34])

7075-T651		2024-T351		304	
Participant	Standard Error	Participant	Standard Error	Participant	Standard Error
11	0.072[a]	4	0.043	11	0.042[a]
15	0.088	11	0.046[b]	15	0.079
17	0.089	17	0.047	17	0.096[a]
14	0.104	5	0.054	14	0.106
13	0.108	10	0.063	4	0.109
12	0.113[a]	14	0.100	6	0.113
10	0.117	6	0.100	13	0.148
18	0.141[a]	18	0.117[a]	16	0.160
6	0.148	3	0.138[a]	5	0.161
1	0.166	9	0.162	18	0.176[a]
2	0.221	8	0.163	3	0.189[b]
4	0.225	7	0.165	8	0.244
5	0.247	2	0.168	9	0.246
16	0.255	13	0.190	7	0.246
3	0.386[a]	15	0.198	1	0.262
9	0.597	16	0.259	2	0.279
7	0.611	12	0.364[a]	10	...[c]
8	0.637	1	0.380	12	...[c]

[a]Participant did not predict failure on all specimens.
[b]Participant submitted predictions on only the compact specimens.
[c]Participant did not predict failure on this material.

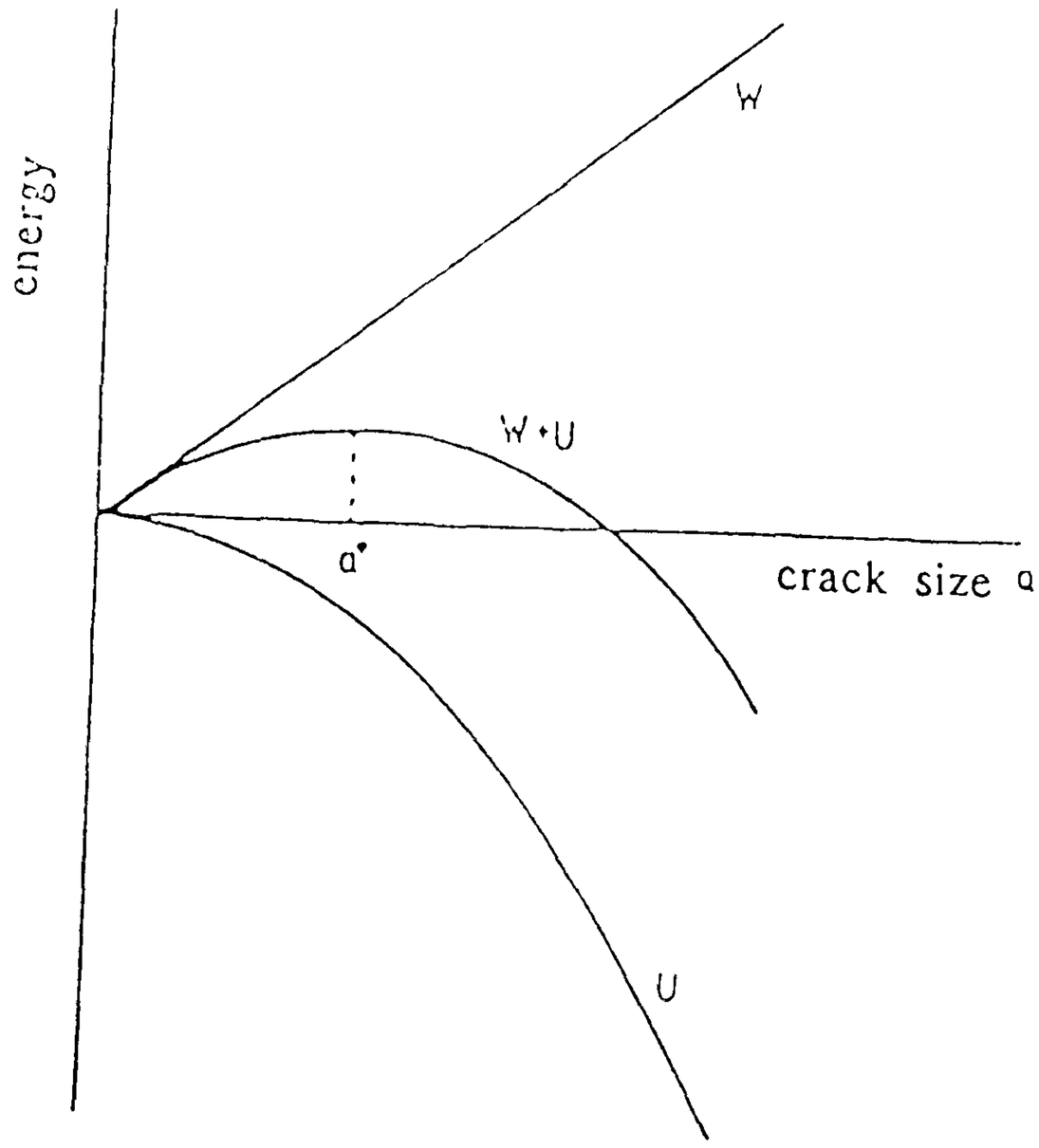

Fig. 3.1 Relationship between energy and crack size

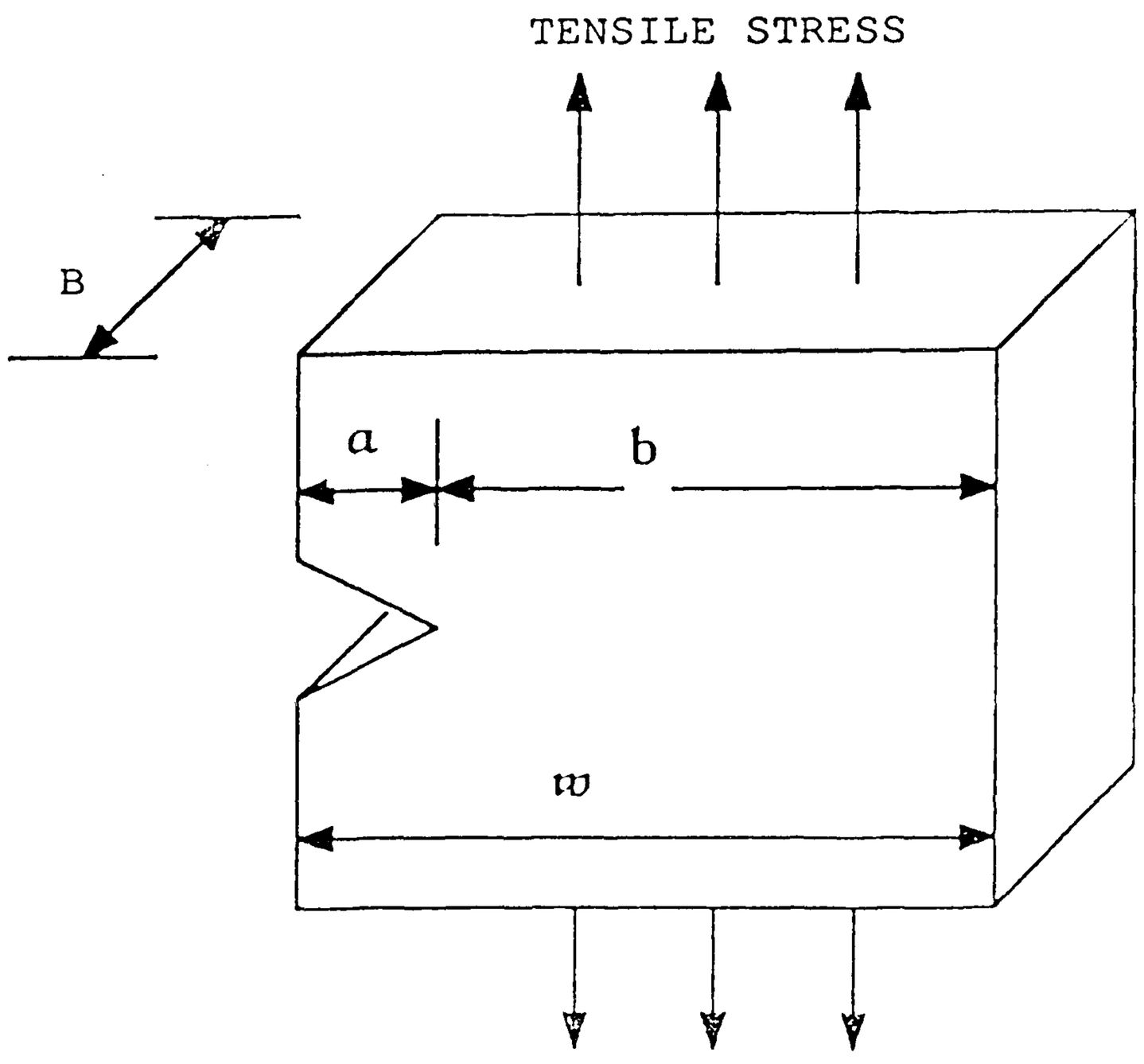

Fig. 3.2 A typical crack configuration

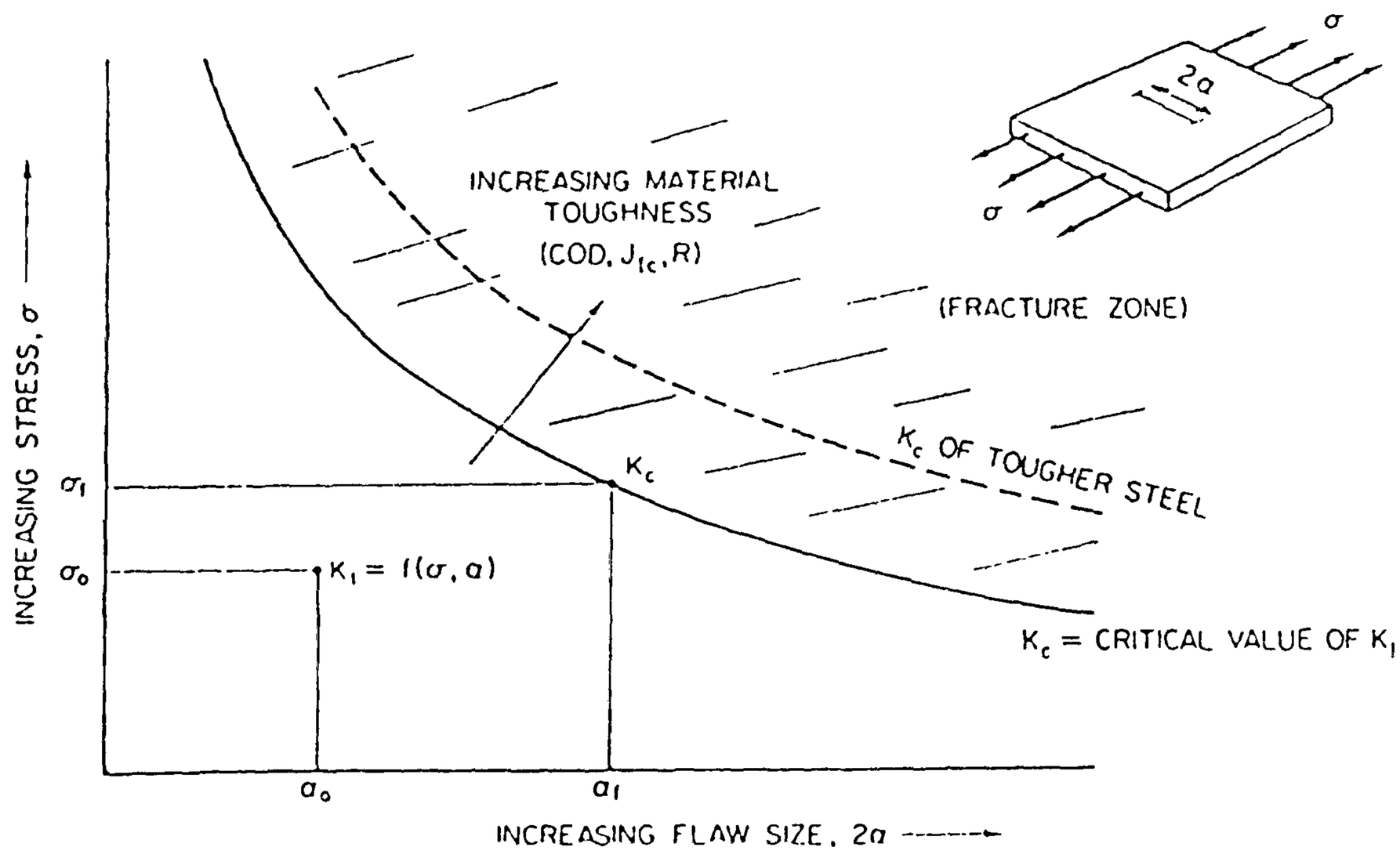

Fig. 3.3 Relation ship between critical stress and critical crack size

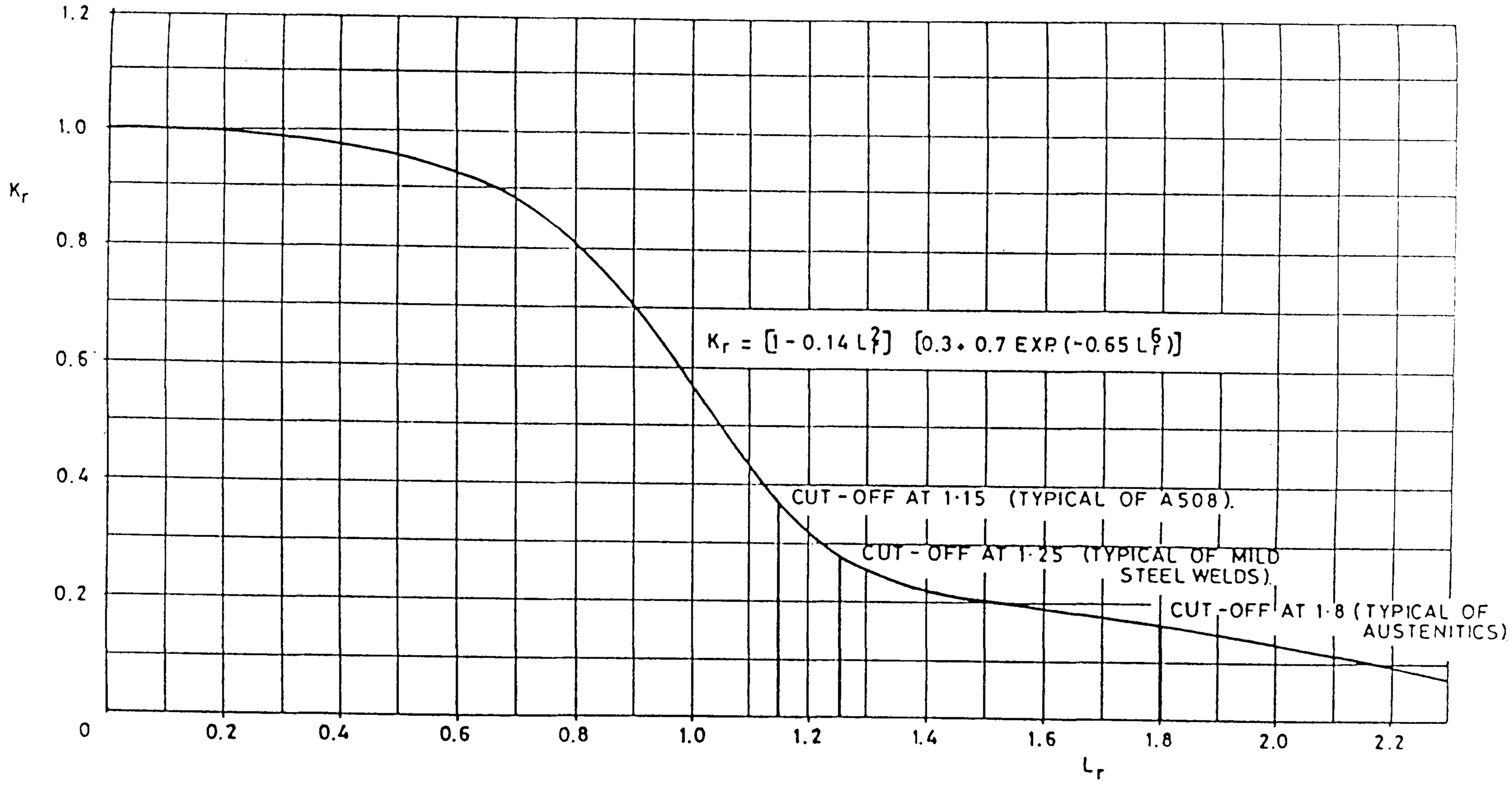

Fig. 3.4 The general failure assessment diagram (option 1) (from ref. [3.30])

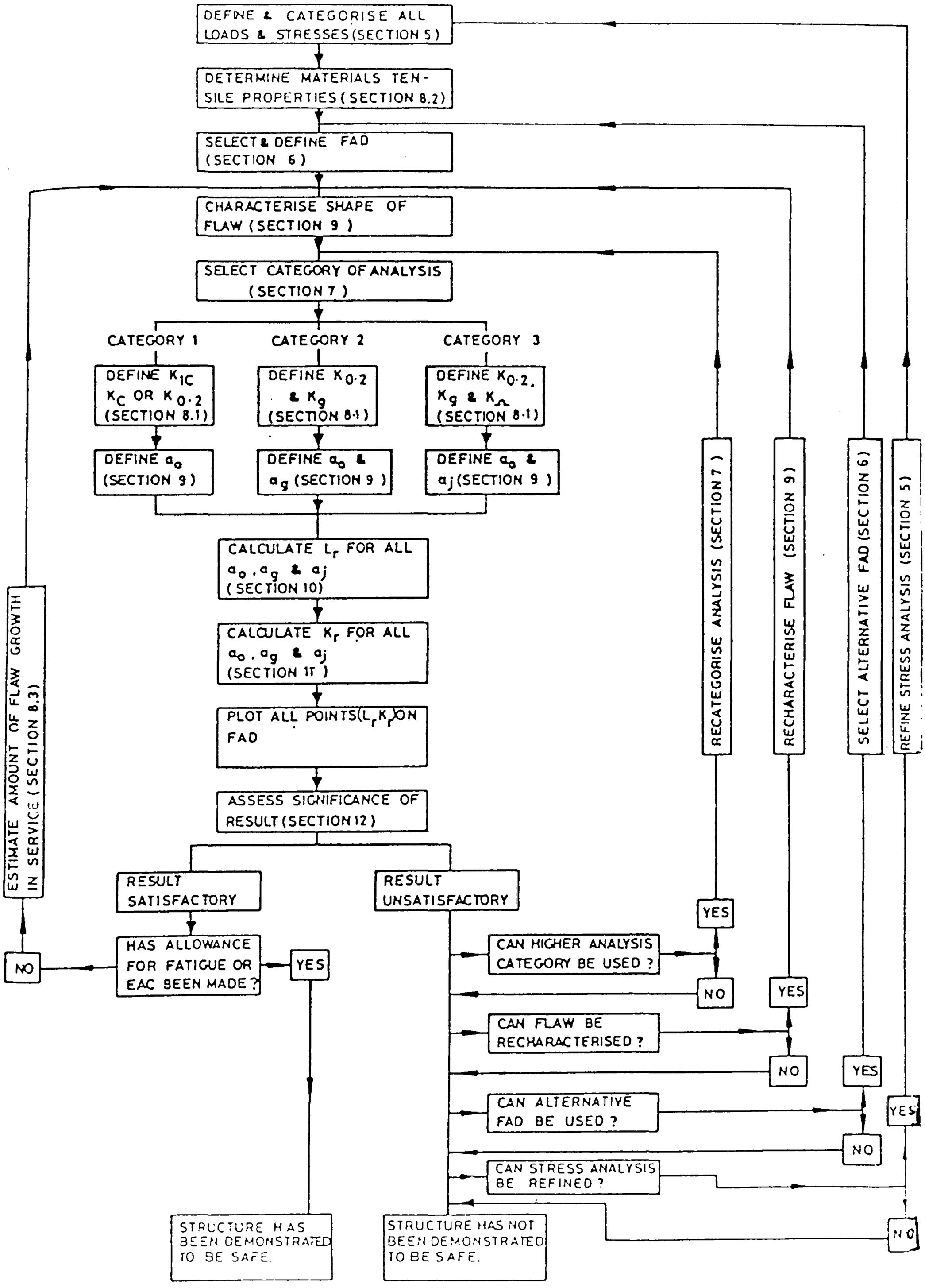

Fig. 3.5 Failure assessment procedure flow chart (from ref. [3.30])

Chapter 4

The Reliability Assessment Of Cracked Components Under Tensile Loading

Nomenclature

a	crack size
a_0	average measured crack size
a_{ini}	initial crack size
$\bar{a}$	mean crack size
$\triangle a$	crack extension
c	half of crack length
$Cov[.,.]$	covariance matrix
E	Young 's modulus
F	geometry correction factor
F^L	load factor
FAL	failure assessment line
$J_{0.2}$	J integral fracture resistance with 0.2mm crack growth.
K_{1c}	brittle fracture toughness.
K_r	ordinate in R6. Rev. 3 FAD.
L_r	ratio of applied load to plastic collapse load
N	number of NDT inspections
M	safety margin
P	load
$P(F)$	probability of failure
w	specimen thickness
Y	crack geometry factor
β	reliability index
σ_{x_i}	standard deviation
σ	stress
σ^p	stress with effects on plastic collapse
σ^s	stress without effects on plastic collapse
σ_y	yield stress

Other parameters are defined in the text.

4.1 Introduction

In this chapter, each of the basic variables appearing in the fracture failure function has been examined for its statistical variability. With the failure functions for crack initiation and crack instability proposed in chapter 3 and the Level 2 reliability analysis method explained in chapter 2, the approximate probability of failure or the reliability index can be calculated efficiently .

When a structural component has a crack resulting either from fabrication or from service, the component may fail by fracture or by plastic collapse under tensile loading. The integrity of the component is affected by a number of variables. Fig. 4.1 shows the failure paths which a cracked component can follow[4.1].

The deterministic safety assessment in the R6 method is carried out by the measurement of the load factor . The load factor in the R6 method is defined as the ratio of the applied load which produces a limiting condition against the applied load in the assessed condition. In normal cases, the limiting load is evaluated by changing the value of the specified load until the assessed point lies on the Failure Assessment Line(FAL). The deterministic sensitivity analysis for each variable is carried out by plotting a relation between the variable and the load factor over a range of values while keeping the other variables fixed.

In a realistic environment, all the variables of the structural failure function such as loading, crack geometry, material resistances may be considered to be randomly distributed. By using a probabilistic model for each variable with parameters based on statistical analysis of the sample data, reliability theory can be used to calculate the probability of failure for a certain assessment point in a deterministic study (which is called the mean point in reliability study) to a sufficient accuracy and efficiency.

With appropriate computer implementation, the reliability calculation can be a routine exercise for engineering purposes. With the benefit of reliability analysis, some of the characteristics of safety assessment can be expressed explicitly. For instance, a sensitivity factor can be obtained for each statistical variable from the co-ordinates of the design point (see chapter 2). Furthermore, in the case of more than one failure mode, the dominant mode can be determined by finding which reliability index is the smallest.

4.2 Failure Mode Identification

As Fig. 4.1 (from Ref. [4.1]) shows, a cracked body can follow a number of failure paths. The final failure modes are brittle fracture, ductile fracture , and plastic collapse. In each particular path, the failure mode will depend on material properties, loading conditions, geometry of the structure and other factors.

If the material is brittle, immediately after crack initiation the structure will fail by rupture. In this case, failure paths 1 and 2 are followed. If the material has a high fracture toughness and a low yield stress, the cracked body may reach plastic collapse before fracture occurs. In this case failure path 6 is followed.

If the material can sustain a certain amount of slow stable crack growth after initiation, failure paths 3, 4 or 5 may be followed. Failure path 3 is particularly dangerous, because after a seeming period of ductile stable crack growth, by increasing the triaxiality or crack velocity or by temperature shift, a sudden brittle fracture occurs. For engineering purposes, this is treated as in failure path 2 to exclude cleavage fracture from ductile analysis.

Therefore for the present analysis, if the material is brittle or with little ductility, it may be assumed that failure occurs either when crack initiation occurs or when plastic collapse occurs. This series system of failure modes is shown in Fig. 4.2. as series 1. Series 1 follows failure paths 1,2,3 by crack initiation or failure path 6 by plastic collapse. If the material is ductile, failure occurs after slow stable crack growth by plastic collapse or tearing instability. This series system of failure modes is shown in Fig.4.2 as series 2. Series 2 follows failure path 4, or 5 or 6. Failure path 4 and 5 in the R6 method can be determined only by the calculation of the maximum load for instability.

4.3 Discussions on The Probability Distributions for The Basic Variables

4.3.1 General remarks

In this chapter, only four types of parameters are considered to be statistical variables: 1) the fracture toughness K_{1c} or $J_{0.2}$ and the slope of the fracture resistance curve, 2) the yield stress, 3) the crack size and 4) the applied stress . Other parameters appearing in the failure function are either deterministic or have little statistical variation and so are of little importance. Model uncertainty is not considered yet because of the difficulty of having sufficient data to determine probability distribution parameters . Nevertheless model uncertainty remains a great challenge for future study.

4.3.2 Fracture toughness

Factors influencing the variability of the fracture toughness include:

1) Microstructural variability, i.e. the within-specimen variability including metallurgical structure and thickness effects etc.

2) Between-specimen variability, e.g. the non-uniformity in the fatigue pre-crack, material from different suppliers etc.

3) Measurement errors

4) Other factors. As discussed in chapter 3, K_{1c} is a parameter in LEFM to define the critical level of stress intensity factor for brittle fracture. There are 3 main effects which may cause inaccuracy in its determination 1) plasticity effect 2) notch effect 3) scaling effect .

Gates *et al* [4.2] [4.3] have demonstrated a normal distribution forK_{1c}, $J_{0.2}$ and the slope of the R curve.

4.3.3 Yield stress

For yield stress, the first three sources of uncertainty are the same as for fracture toughness. In addition, different yield stress criteria, for instance von Mises or Trasca criteria, can cause uncertainty. The usual assumption for yield stress is the normal or lognormal distribution or Weibull distribution. The lognormal distribution has the advantage of precluding negative values[4.4].

The parameters of probability distributions for fracture toughness and yield stress are estimated from data collection. From [4.4], the yield stress can be modelled by a lognormal distribution. In this study, the fracture toughness is assumed to be normally distributed and the yield stress is assumed to be lognormally distributed.

4.3.4 Correlation of fracture toughness and σ_y

It is found for some steels that a high fracture toughness for cleavage is associated with low yield stress. There is no clear trend for this association in ductile fracture. Although this phenomenon appears in a wide range of steel, it is not clear how much the fracture toughness correlates with yield stress.

In this chapter, in one example for brittle fracture it is assumed that for cleavage fracture the correlation coefficient of K_{1c} and σ_y is -0.1. Otherwise, the correlation coefficient has been assumed to be 0.

4.3.5 Crack size

The uncertainties in the crack size distribution results from the following sources:

1) the size distribution inherent from manufacture,

2) the error in measuring the size of the crack associated with the non-destructive testing technique e.g. ultrasonic testing,

3) the probability of not detecting such cracks in the course of subsequent pre-service inspections,

4) the extension of cracks in service e.g. due to fatigue.

In this chapter the crack is assumed to have been inspected at some stage of service so that only the second source is considered.

The Welding Institute [4.5] has carried out a survey of the errors associated with the ultrasonic inspection of planar defects. Their results suggested that defects sizing errors are partly systematic and partly random.

* There is a systematic undersizing of defects by 1mm.

* There is a random error with a standard deviation of 2.5mm. Thus if an operator makes N scans, the standard deviation of the mean is $2.5/\sqrt{N}$.

It is assumed that the NDT errors are normally distributed, then the probability distribution function of mean crack size $\bar{a}$ is

$$f_a(\bar{a}) = \frac{1}{2.5}\sqrt{\frac{N}{2\pi}} exp - \left\{ \frac{N(\bar{a} - a_0 - 1)^2}{12.5} \right\} \qquad (4.1)$$

where a_0 is the average measured crack size.

4.3.6 Loading

The probability distribution of applied stress depends on the environment and the overall structural system . It is assumed in this study that the applied stress is tensile and normally distributed with a coefficient of variation of 0.1. It is further assumed in this chapter that residual stress is a deterministic parameter.

4.3.7 Component geometry

The dimensions of the cracked component in this chapter are assumed to be deterministic because their variations are small in comparison with the crack size and crack length.

4.4 Construction Of The Failure Function

4.4.1 Series 1 for brittle material

For failure series 1 in Fig 4.2 failure criteria are crack initiation and plastic collapse. For crack initiation, from R6. Rev. 3 discussed in chapter 3:

$$M = \frac{Y(\sigma + \sigma_{res})\sqrt{\pi a}}{K_{1c}} + \rho - [1 - 0.14L_r^2][0.3 + 0.7exp(-0.65L_r^6)] \tag{4.2}$$

where for tensile applied stress σ, and for the case where yield load equals $\sigma_y(W - a)$

$$L_r = \frac{\sigma w}{\sigma_y(W - a)} \tag{4.2a}$$

and where ρ is plasticity correction factor.

The other failure mode is plastic collapse. In the R6 method a cut off value of L_r^{max} is defined as:

$$L_r^{max} = \frac{\text{flow load}}{\text{yield load}} \tag{4.3}$$

The critical condition is $L_r = L_r^{max}$. For A508 steel chosen for this chapter L_r^{max} is 1.15. So,

$$M = 1.15 - L_r \tag{4.4}$$

4.4.2 Series 2 for ductile material

1) Discussion on R6 Rev.3 category 3 analysis

As seen in chapter 3, the R6 Rev.3 category 3 analysis has the following steps:

(a) Plot the reserve factor on load, F^L, as a function of the postulated crack extension.

(b) Repeat the analysis for different values of a_0 to establish the sensitivity of the results to initial crack size and plot these on the same graph.

(c) Explore the effects of changing the other variables specified in the reserve factors.

The main reason for such an extensive analysis is due to the complicated nature of ductile fracture and the fact that reserve factors can depend on each other and should not be considered in isolation. The failure criterion of the category 3 analysis can be presented as :

$$J_{app} \leq J_{mat} \tag{4.5}$$

$$\frac{\partial J_{app}}{\partial a} \leq \frac{dJ_{mat}}{da} \tag{4.6}$$

The instability load point or the limiting condition in category 3 is when both the above equations are satisfied as equalities. It is from these formula that Milne [4.8] set up the crack extension locus procedures to treat ductile crack instability together with some experimental validation. From Milne it is known that the maximum loading has a crack extension locus tangential to the crack initiation FAL.

Despite the R6 category 3 analysis advantages of giving a detailed picture of the safety against crack ductile instability, there are certain shortcomings:

A failure assessment line cannot be provided for general use in ductile instability. The instability point depends on both the R curve and the crack initiation FAL. There will be a different FAL for each different fracture resistance R curve in the (L_r, K_r) cartisian co-ordinate system. Also sensitivity analysis is carried out with little global view of the inter-relation of the many variables in the fracture governing system equations.

The failure series 2 in Fig 4.2 is for ductile tearing. Assuming that the specimen is under load controlled condition, the maximum stress is either the ductile tearing instability stress or the plastic collapse stress, whichever is the lowest. Thus the safety margin are:

$$M = \sigma_{max}(\text{maximum stress from ductile fracture analysis}) - \sigma \tag{4.7}$$

and

$$M = L_r^{max} - L_r \tag{4.8}$$

One of the impediments in applying the R6 method is the tedious procedure used for considering crack stable tearing. The procedure in the R6 method involves plotting the reserve factor on load, F^L as a function of the postulated crack extension to find the maximum F^L [4.6].

The R6 method presents an analysis in a schematic graphical manner. It should be understood that these graphical procedures were made for practitioners to visualise and to apply in a uniform way. Reliability methods can be introduced to investigate the interrelation of various variables and their relative sensitivities, in a more rational and more efficient way. However, the procedure to quantify failure margin in R6 Rev. 3 is not suitable for such a numerical iterative process of the reliability analysis.

To quantify the reserve capacity (+ or -) of the flawed ductile component a mathematical failure indicator should be established. If the new failure indicator can be proved to be applicable, general use of it should be made.

2) Numerical procedure to calculate the instability maximum load

In this study, the procedure for finding the maximum load point is a numerical program to get the maximum F^L efficiently and directly instead of the schematic procedure suggested in R6 Rev 3.

In Fig. 4.3, the failure assessment line (FAL) of R6 is plotted with three crack extension loci. These three crack extension loci differ only in the applied load with $P_1 < P_2 < P_3$.

Crack extension locus 1 intersects with the FAL twice. In fact, the crack will stop growing at point a. Crack extension locus 3 does not meet the FAL, so that the crack will extend in an unlimited way until final collapse. Crack extension locus 2 is tangential to the failure assessment line. According to the definition in R6 rev 3, this is the critical limiting condition.

It is evident that

if $P > P_2$ the crack extension locus will not meet the failure assessment line and the crack state is unstable.

if $P \leq P_2$ crack extension locus will meet the failure assessment line and the crack state is either stable or critical.

In order to obtain the critical P value i.e. P_2, the following algorithm is proposed:

1) Input the set of variable values and find the position in the R6 FAD for this set of data.

2) Calculate the value of M from equation (4.2).

3) If $M > 0$, the assessed point is inside the frame of R6 FAD. The load is then increased with the increment being either the last increment or a third of the last decrement until the assessed point is outside the R6 FAD frame i.e. $M < 0$.

4) If $M < 0$, the assessed point is outside the frame of R6 FAD; fix the applied load and go to the next step of crack extension (step 5 below).

5) Increase only the crack size to see whether the crack extension locus will fall inside the frame of the R6 FAD by calculating the M value from equation (4.2) for each point.

6) If any of the M values in the crack extension locus is greater than 0, the crack state is stable; then go to step 3.

7) If none of the M values in the crack extension locus is greater than 0, the crack extension locus is outside the frame of R6 FAD and is unstable. Decrease the applied load by an amount equal to either a third of the last increment or to last decrement.

8) If crack extension is equal to 0, repeat step 5.

9) The magnitude of last increment or decrement is changed each time the crack extension locus is drawn, and becomes smaller and smaller. If pp is the magnitude of last increment or last decrement, the difference between the last stable load and the last unstable load is either pp or 2pp. So $|P_{estimated} - P_2| \leq$ 2pp. pp can therefore be taken as a indicator for convergence. If pp is less than some preset criterion, the computational procedure can be stopped and the P_2 can thus be taken as the estimated value.

The convergence and the accuracy depend on the situation and the amount of computation. They are controlled in the program by the preset criterion of parameter pp. The main strategy in this algorithm is the minimisation of pp. A flow chart is shown in Fig. 4.4. The results of an example calculation are shown in Fig. 4.5.

4.5 Example of Reliability Calculation for Brittle Material(series 1)

4.5.1 Dimensions

A structural component has a thickness, w, of 22mm. A semi-elliptical surface crack is found (see Fig. 4.2). For this example, it is assumed that $a = c$ so that the crack has a semi-circular shape. Furthermore, a or c is much less than w.

4.5.2 Stresses

There are two sources of stresses: 1) applied uniform tensile stress 2) residual stress. The applied stress σ^p has an effect on plastic collapse while residual stress σ^s has no effect.

4.5.3 Stress intensity factor

For a semi-elliptical surface crack in a finite plate , the stress intensity factor according to Newman-Raju [4.7] is:

$$K = \sigma\sqrt{\frac{\pi a}{Q}}F \tag{4.9}$$

where

$$Q = 1 + 1.464(\frac{a}{c})^{1.65} \quad \text{for} \quad \frac{a}{c} \leq 1 \tag{4.10}$$

$$Q = 1 + 1.464(\frac{c}{a})^{1.65} \quad \text{for} \quad \frac{a}{c} > 1 \tag{4.11}$$

$Q = 2.464$ in this case.

$$F = [M_1 + (\sqrt{Q} - M_1)(\frac{a}{w})^p + \sqrt{Q}(M_2 - 1)(\frac{a}{W})^{2p}]f_w \tag{4.12}$$

where $p = \sqrt{\pi}$, and f_w is the finite-width correction factor. If the specimen width is much bigger than c, then $f_w = 1$. And $M_1 = 1.13 - 0.1 = 1.03$ and $M_2 = \sqrt{\frac{\pi}{4}}$.

4.5.4 Plastic yielding load

In this case it is assumed that $P_y = \sigma_y(w - a)$ for a surface through crack. In practical cases, the plastic yielding load may have a more complicated form.

4.5.5Data preparation

For crack size, assume N=25, a_0 = 11mm. So the average crack size $\bar{a}$ = 12mm. The standard deviation of crack size is 0.5mm.

Gates conducted a study on probabilistic elastic plastic fracture mechanics[4.2], where three different sets or groups of data have been used in order to study the relation between load factor and the probability of failure in three regions of the R6 FAD, i.e. the LEFM region, the plastic collapse region and the intermediate region. However, the analysis by Gates[4.2] was based on a thorough integration of the probability density function and the early revision of R6 method, R6 Rev. 1, rather than a clearly defined level 2 reliability method and the latest R6 revision, R6 Rev. 3. In R6 Rev. 3, the yield stress and ultimate stress are used instead of flow stress in R6 Rev. 1. These three different data group from [4.2] are taken for investigation in this chapter, with the flow stress equal to the yield stress here, for two reasons: 1) numerical convenience, 2) the strong correlation between flow stress and yield stress. The data by Gates[4.2] give the best estimates and 95% lower bounds. So in this example, the mean values are the best estimates and the standard deviations are calculated on the assumption that the lower bound corresponds to the 2.5 % fractile of a normal distribution.

Table 4. 1 data for analysis without ductile tearing

(SD : standard deviation, X : positive multiplying factor)

parameter	type of distribution	data group 1 linear elastic	data group 2 elastic plastic	data group 3 plastic
K_{1c} (mean)	normal	50 MPa $\sqrt{m}$	70 MPa $\sqrt{m}$	210 MPa $\sqrt{m}$
K_{1c} (SD)		5.10 MPa $\sqrt{m}$	7.14MPa $\sqrt{m}$	21.4MPa $\sqrt{m}$
σ_y (mean)	lognormal	830 MPa	415 MPa	415 MPa
σ_y (SD)		55.10 MPa	27.55 MPa	28.05 MPa
a (mean)	normal	12mm	12mm	12mm
a (SD)		.5mm	.5mm	.5mm
σ^p(mean)	normal	33 X MPa	33 X MPa	33 X MPa
σ^p(SD)		3.3 X MPa	3.3 X MPa	3.3 X MPa
σ^s		31 X MPa	31 X MPa	31 X MPa
w		22 mm	22 mm	22mm

The mean values for these three groups of data are shown in Fig 4.6 for various values of the scale multiplier X.

The load factor is an inverse relation between applied stress and maximum stress which is specified in R6 Rev. 3. For illustrative purposes, in this chapter, a nominal safety parameter is defined in Fig. 4.7. It should be noted that with the definition used, an increase in the safety parameter

corresponds to an increase in the probability of failure.

4.5.6 Reliability calculation procedures

From the structural reliability theory discussed in chapter 2 and the failure functions discussed in section 4.4 of this chapter, an iterative computer program has been developed. The program is described in the flow chart in Fig. 4.18.

4.6 Results and Discussion

Figs. 4.8, 4.9 and 4.10 show the correspondence of safety parameter with $log_{10}P(F)$ calculated from FORM , SORM and FORM with negative correlation of K_{1c} and σ_y for data groups 1 ,2 and 3. Fig. 4.11 presents results obtained by FORM for all three data groups in one diagram.

From these figures, some obvious statements can be made:

1) There is very little difference in the reliability calculated by FORM and SORM. This is because the local shape of the failure surface in the standard normal space is relatively flat.

2) There is a small decrease in probability of failure due to the negative correlation between fracture toughness and yield stress in data group 2, i.e. the intermediate region in the R6 FAD. There is very little influence of the correlation in the LEFM region and plastic collapse region.

3) There is not a unique relationship between safety parameter or load factor [4.2] and probability of failure. The differences in the value of $log_{10}P(F)$ decrease with an increase in the values of the safety parameter. The differences in $log_{10}P(F)$ are more than 1.0 until $log_{10}P(F)$ reaches a value of about -3.0 at a value of the safety parameter around 0.7. As seen in Fig. 4.11 the increase of the safety parameter corresponds only to the general trend of increase in probability of failure.

Because of the wide scattering of the reliability results, this findings confirm that a comprehensive reliability analysis is thus necessary, rather than using safety parameters or load factors to indicate the safety of the structure. Further variations in safety levels can of course occur as a result of variations in statistical parameters between different structures but this is beyond the scope of this example.

Figs. 4.12, 4.13, and 4.14 present the results of sensitivity factors at the design points which govern the reliability. If more than one failure mode is considered, the design point is chosen as the design point of the mode with the lowest reliability. It is known from chapter 2 that the absolute value of sensitivity factor reflects the contribution of the variation of that variable to the probability of

failure.

4) For data group 1, the sensitivity factor of K_{1c} is much larger than that of σ_y. When K_{1c} and σ_y are assumed to be negatively correlated, sensitivity factors of σ_y change from negative to positive. Comparatively, the sensitivity factors of a, σ and σ_y are much less than that of K_{1c}. K_{1c} has a dominant role in deciding the reliability in the LEFM region.

5) For data group 2, the absolute value of the sensitivity factor of K_{1c} decreases dramatically while the other three increase sharply when the safety parameter is more than 0.5. The order of absolute sensitivity values of these four variables are σ, K_{1c}, a and σ_y. There seems to be no overall dominant variable.

6) For data group 3, the sudden change of the slope of sensitivity factors is due to the change of dominant failure modes. The plastic collapse failure modes determine the reliability when safety factors are more than 0.4. In the plastic failure mode, there is no fracture toughness variable.

7) For data group 3, sensitivity factor of K_{1c} is 0 or a small value when K_{1c} and σ_y are correlated. The sensitivity factor of yield stress has an important role on the value the reliability.

8) With K_{1c} and σ_y are correlated, the sensitivities of resistance variable K_{1c} and σ_y are related to each other. When one of them is dominant, the other may take a positive value.

4.7 Reliability of Component Failing by Ductile Fracture(series 2)

When material is at the upper shelf temperature, it behaves in a ductile manner. There will be a large reserve of capacity. Much effort in the past has been put into the investigation of the R-curve both by means of global analysis and micromechanism. Gates *et al* [4.3] have conducted a statistical analysis and found the statistical properties for one group of material investigated, by assuming a linear relation between J and crack extension $\triangle a$.

$$J = J_{0.2} + \triangle a \frac{dJ}{da} \tag{4.13}$$

where $J_{0.2}$ is the J value with 0.2 mm crack extension. The relation between $J_{0.2}$ and K_{1c} is

$$K_{1c} = \sqrt{E' J_{0.2}} \tag{4.14}$$

For the material of an A508 forging, it was found from tests on six specimens that the mean value and standard deviation are[4.3]:

$\mu_{J_{0.2}} = 182.2$kN/M and $\sigma_{J_{0.2}} = 33.84$kN/M

$\mu_{dJ/da} = 658$MPa and $\sigma_{dJ/da} = 209$MPa

These quantities are both assumed to be normally distributed. Together with the above data group, it is also assumed that

$\mu_{\sigma_y} = 1400$MPa and $\sigma_{\sigma_y} = 140$MPa

and that σ_y is lognormally distributed.

For this material, it is assumed that $L_r^{max} = 1.2$. The crack dimensions , σ^p and σ^s are the same as in the study for series 1. This data group has mean points seen in Fig 4.15.

Fig. 4.16 shows the increased reliability (decreased probability of failure) when ductile tearing is taken into account. For this example, the difference of probability of failure as judged by initiation and by ductile tearing is as much as two orders of magnitude.

Fig. 4.17 compares the sensitivity factors for the failure mode of initiation and plastic collapse(series 1) and the failure mode of ductile instability and plastic collapse(series 2). For the data group in the intermediate region, for the former case, $J_{0.2}$ and σ_y have sensitivity factors with similar magnitude. But for the latter case with ductile tearing, the sensitivity factors for $J_{0.2}$ and dJ/da are 0. This can be explained for the following reasons:

In Fig.4.15 the design point from FORM with corresponding assessment point (or mean point) are shown. The design point for FORM is the point with the shortest distance to the mean point in the standard normal space. Because the failure surface for ductile tearing is further from the assessment point than the failure surface for plastic collapse, the plastic collapse failure mode governs the failure probability.

The variation in the slope of the J-R curve appears not to be important in this particular case. The failure probability may be sensitive to the J-R curve in some other cases when the J-R curve has much lower mean values or the data group is in the LEFM region.

This result can be compared with a deterministic study by Milne [4.9] where a range of material with more or less ductility was found to fail finally by plastic collapse. Those failures may not be caused by the initial crack but with the crack extension all fail near the state of plastic collapse.

However, the study by Milne [4.9] should not be confused with this study. Milne found that all the specimens in that study failed near the plastic collapse limit after certain crack extension in a deterministic condition. In this study, for a group of mean points in the R6 FAD, with the assumed statistical distributions, the *most probable* mode of failure is plastic collapse. There is

still a possibility of ductile tearing instability. This study and Milne's study point out the need to investigate further the failure mode of plastic collapse.

4.8 Conclusions

A reliability method has been set up for conducting the safety assessment of a structural steel component with a crack. For failure by crack initiation or plastic collapse example cases with three typical series of data for LEFM region , plastic collapse region and the intermediate region are analysed. For ductile tearing instability plus plastic collapse, only one group of data is analysed. Some general conclusions can be drawn from the results:

1) In the context of fracture assessment, an algorithm to calculate ductile instability load is proposed. The maximum stress can be calculated by a iterative scheme. The sensitivity factors can be calculated from reliability analysis.

2) In the context of reliability calculation a detailed formula and a simplified numerical scheme to calculate second order reliability has been proposed. It is found that reliability calculated from SORM differs very little from FORM for the examples considered, confirming the adequacy of FORM for general purposes.

3) In the context of safety assessment for fracture without ductile tearing , it is found that a single safety parameter or load factor[4.2] as used in R6 method can not give a satisfactory indication of safety. The failure probability can vary drastically with the same safety parameter. In the intermediate region, the probability of failure can be decreased by the negative correlation between fracture toughness and yield stress. In the near plastic collapse region, the plastic failure mode is the dominant failure mode.

4) In the context of sensitivity analysis, it is found that the sensitivity factors for different variables vary dramatically from region to region. In the LEFM region, fracture toughness has a very high sensitivity factor while yield stress has a low sensitivity factor. The opposite happens in the data group for the plastic region. These facts can have a serious implication if one is to consider giving a partial safety factor for each variable in the future.

5) In the context of ductile fracture reliability analysis, it is found for the example, that there is a large difference of failure probability with and without ductile tearing. The plastic collapse failure mode is found to be dominant if considering ductile tearing. To this extent, this implies that only the mean values of the slopes of the J-R curves are of importance in most cases. However, considering that the failure mode of ductile tearing instability is much less catastrophic than the other two failure modes, especially brittle fracture failure, the academic

interest in pursuing the R-curve distributions may be justified.

6) For future study, a number of topics can be mentioned: 1) the reliability in the transition region between the two extremes of brittle fracture and ductile fracture, 2) the statistical distributions of basic variables, 3) the modelling of model uncertainties 4) investigation of the plastic collapse failure mode 5) application to more specific material and component configurations.

Fig. 4.1 The different failure paths which a cracked body can follow (from ref. [4.1])

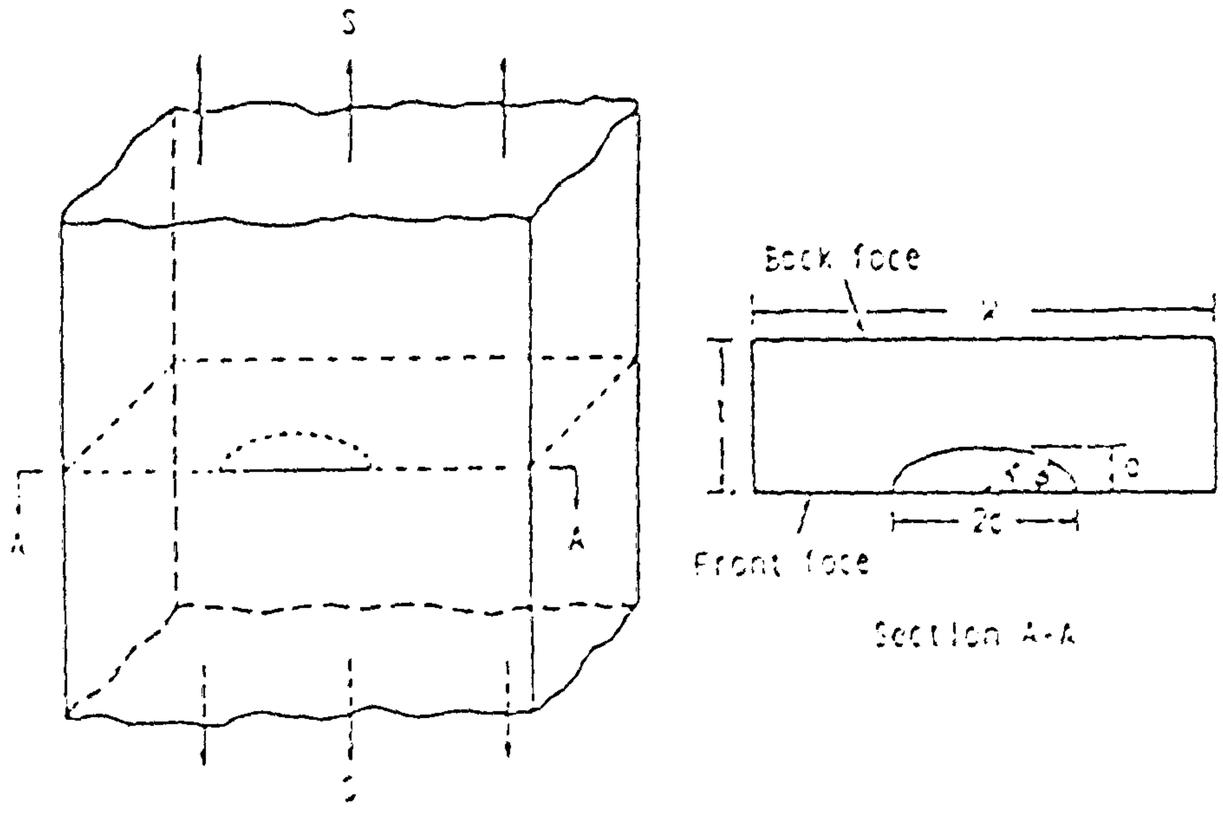

Initial state of a cracked component under tensile stress

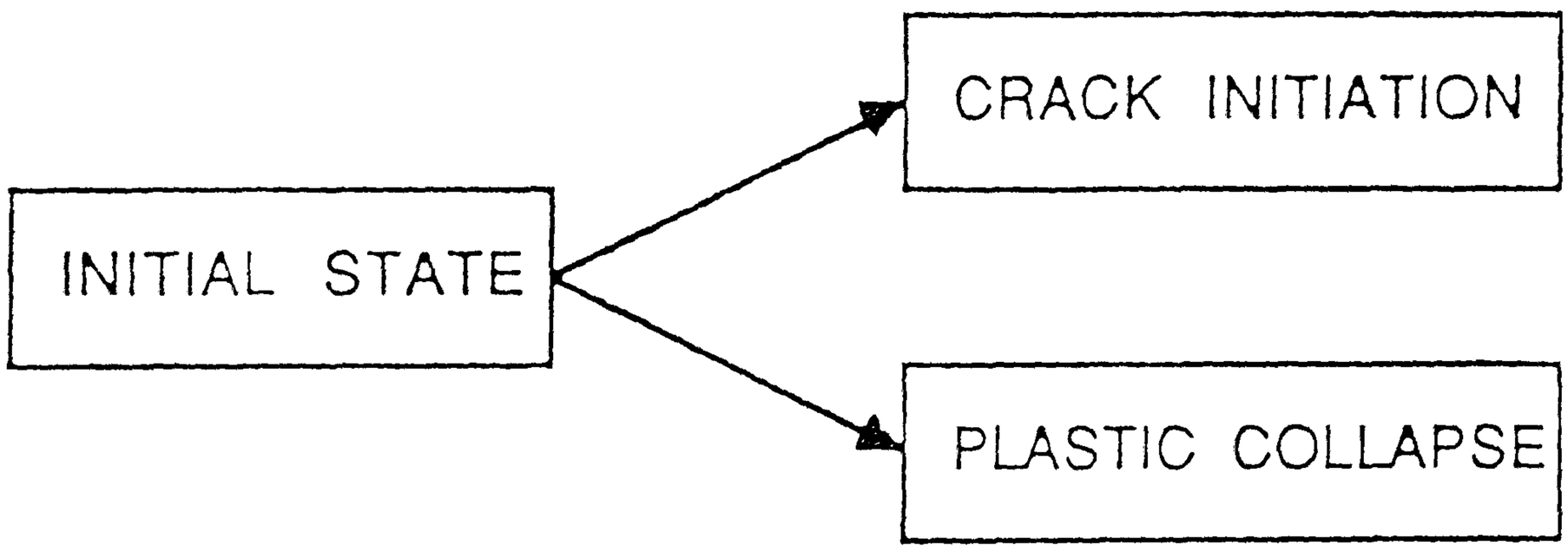

SERIES 1 (for brittle material)

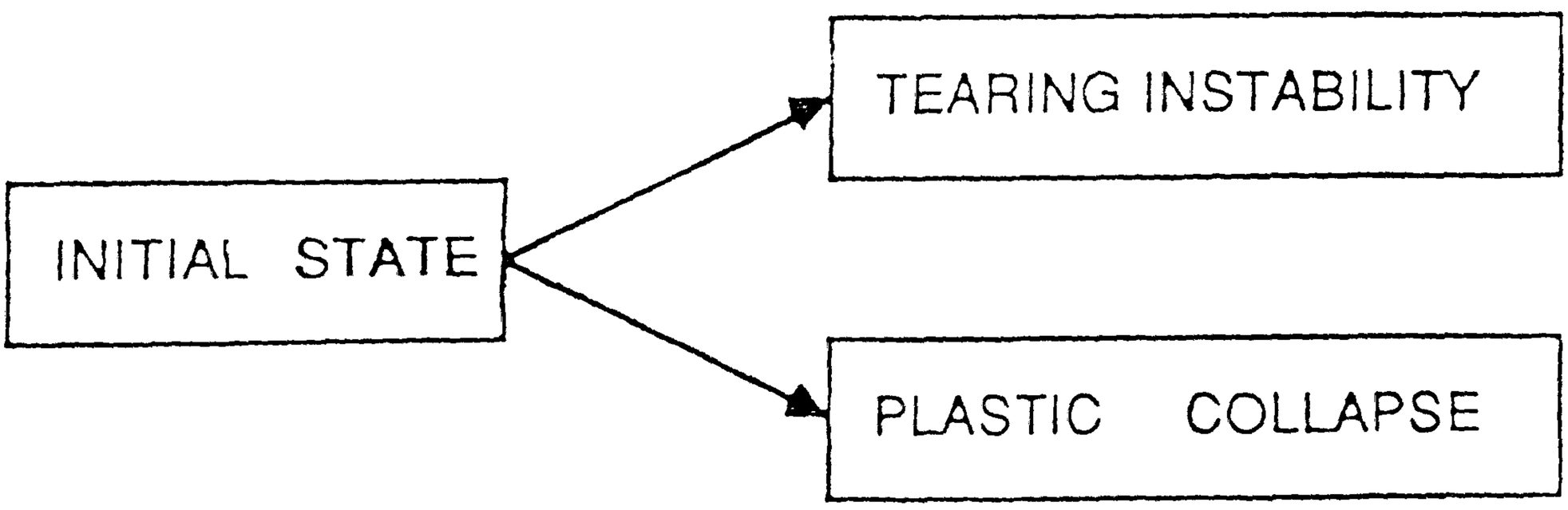

SERIES 2 (for ductile material)

Fig. 4.2 Series system of failure mode

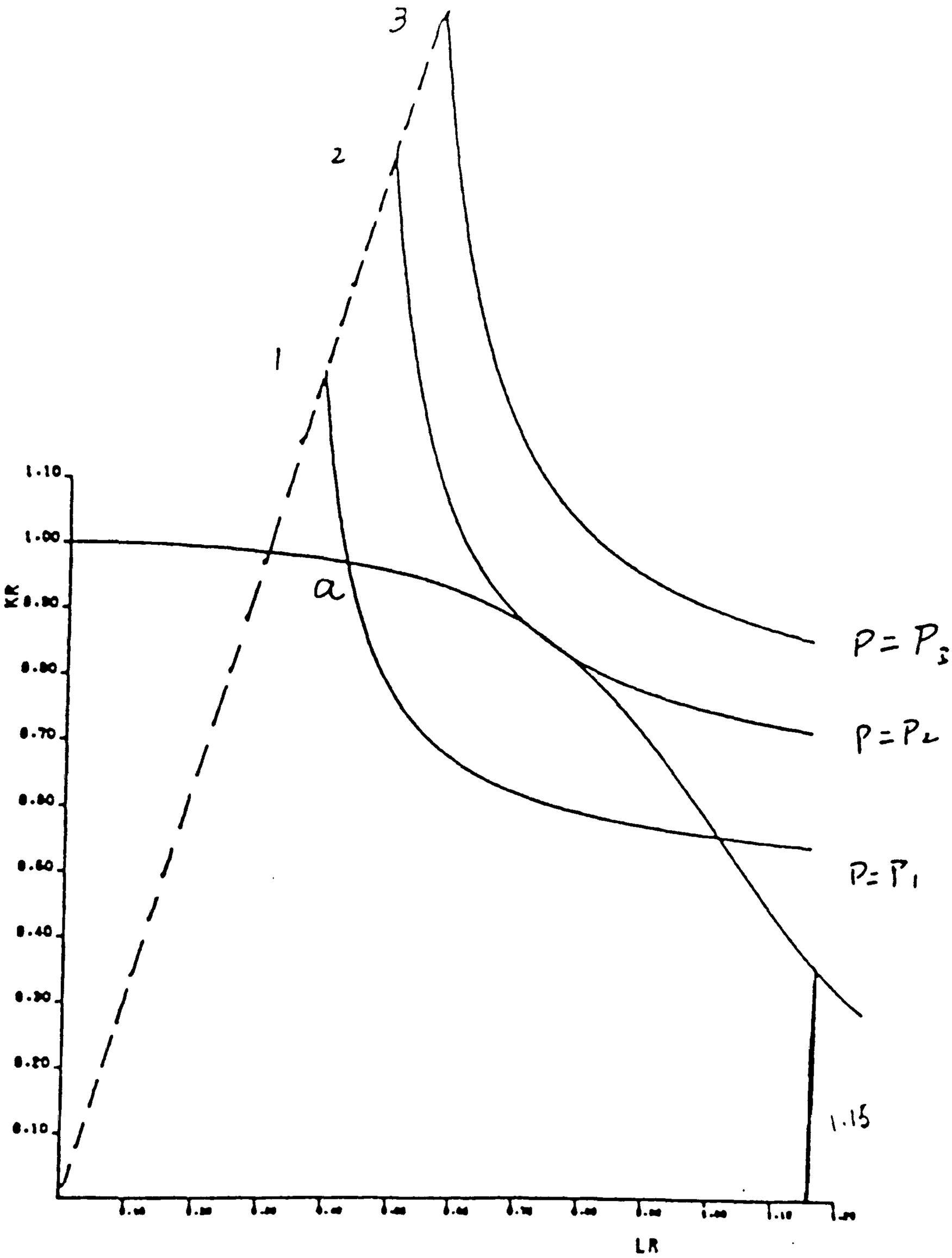

Fig. 4.3 Crack extension loci and R6 general curve

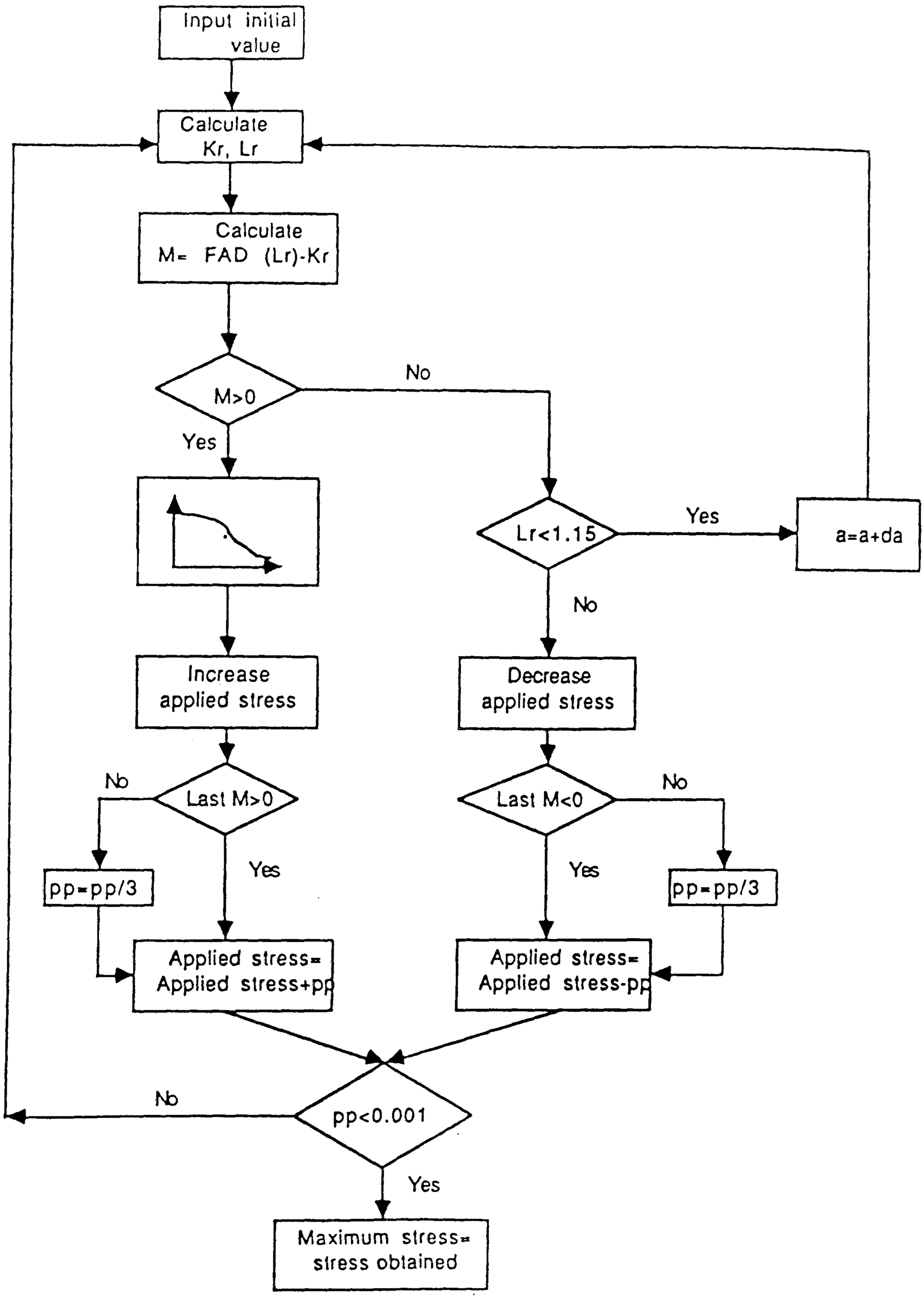

Fig. 4.4 Flow chart for computing maximum stress for crack instability

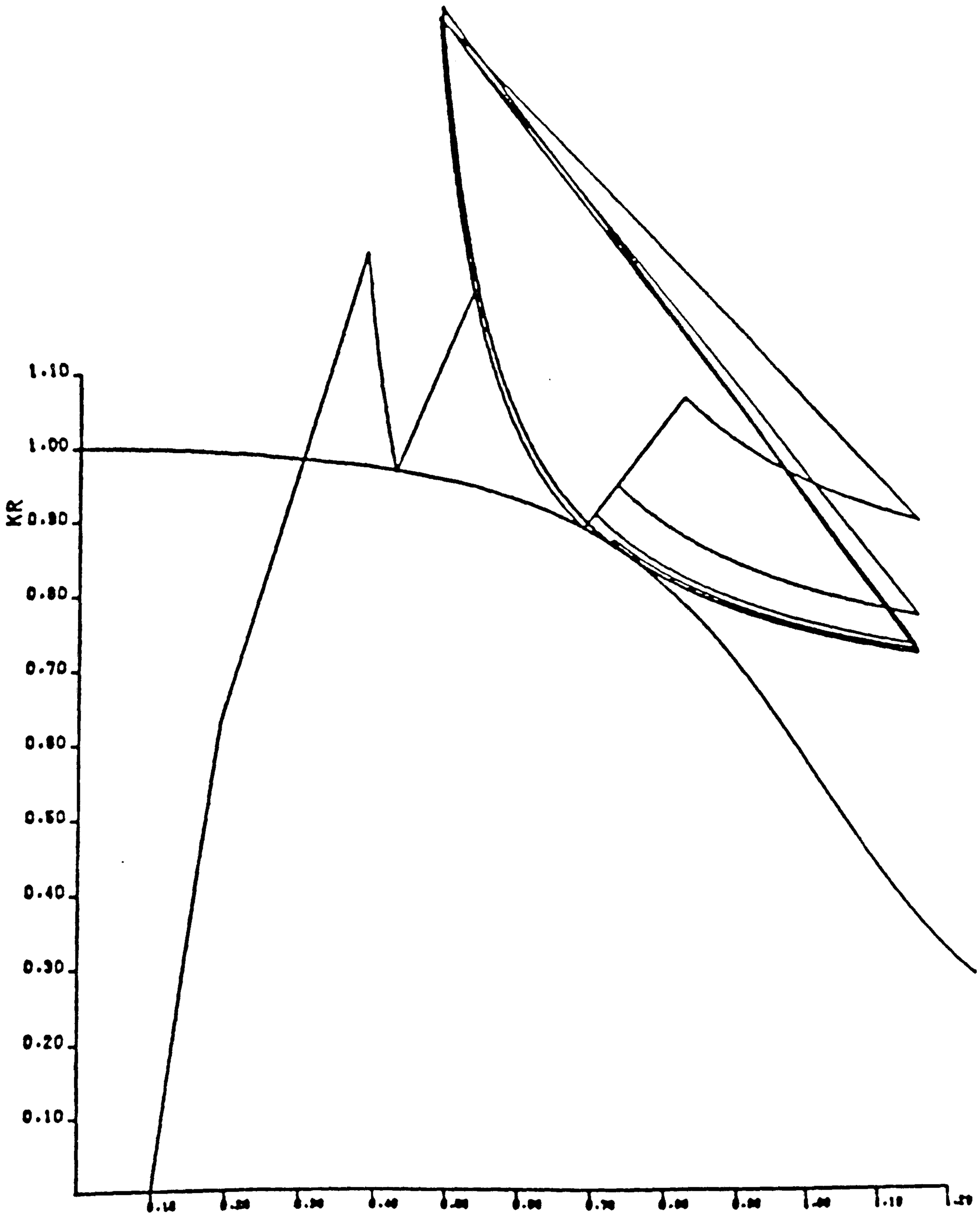

Fig. 4.5 Demonstration to find the maximum stress for crack instability

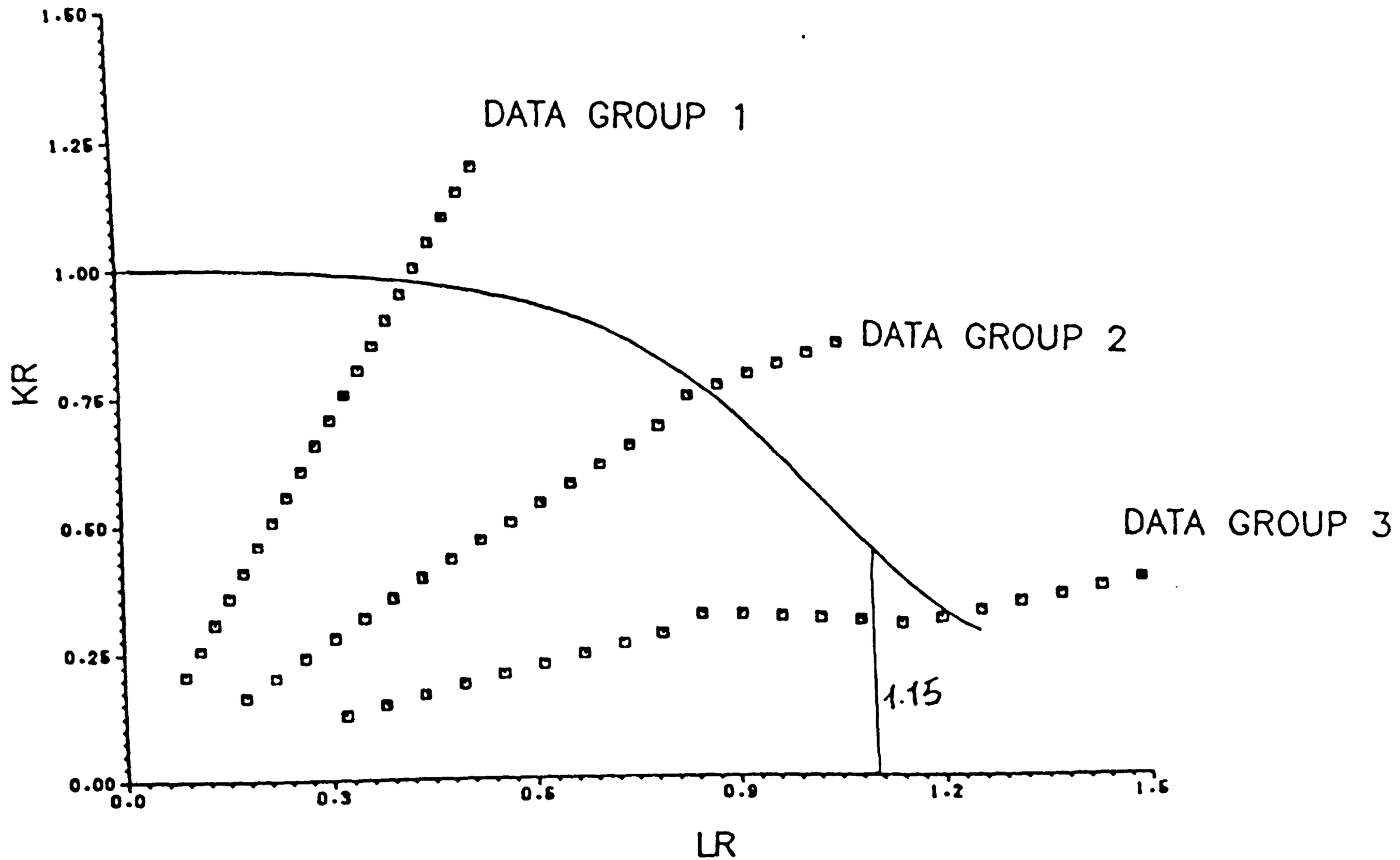

Fig. 4.6 Data groups in R6 FAD

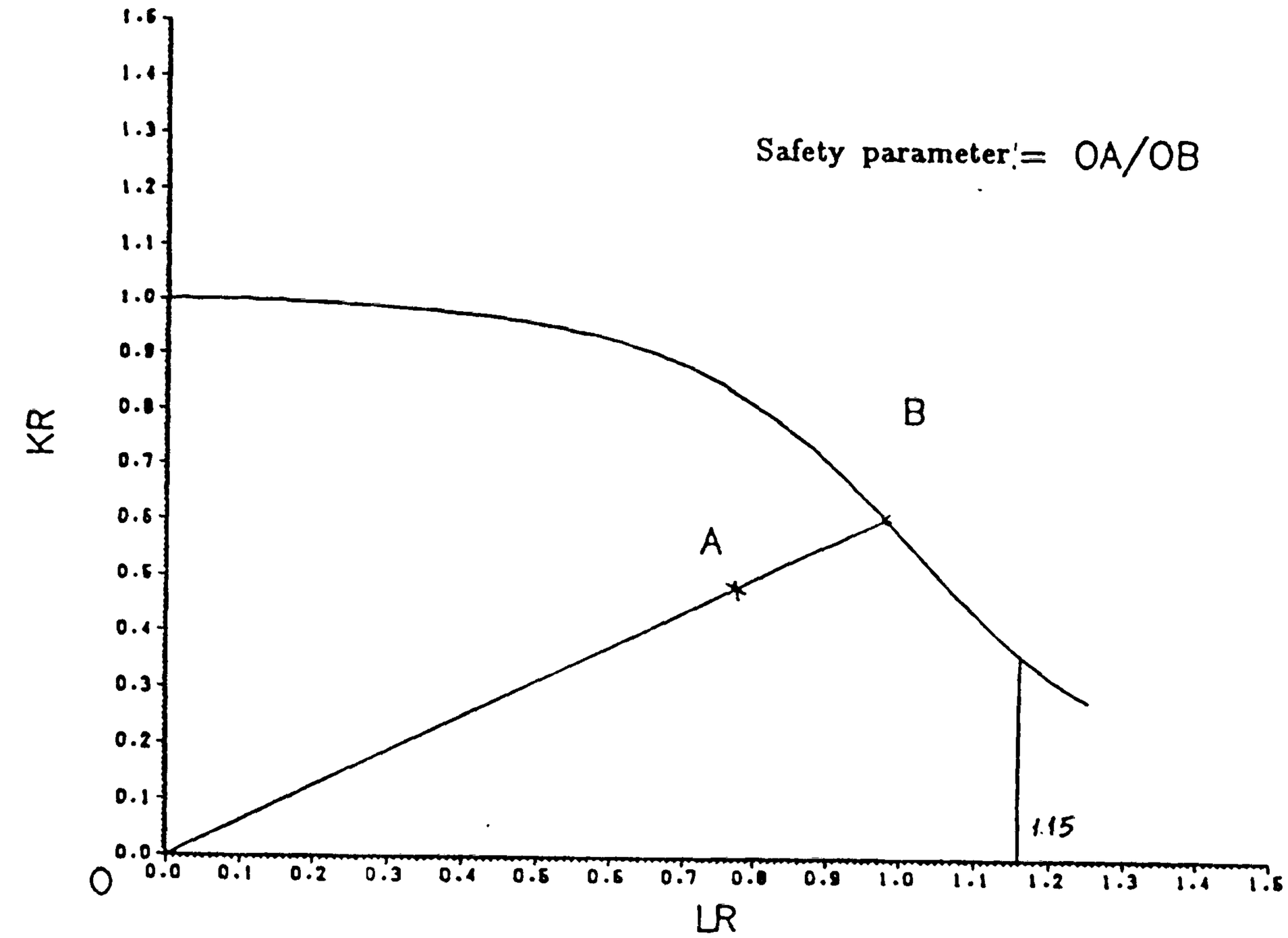

Fig. 4.7 Definition of safety parameters with the R6 general curve

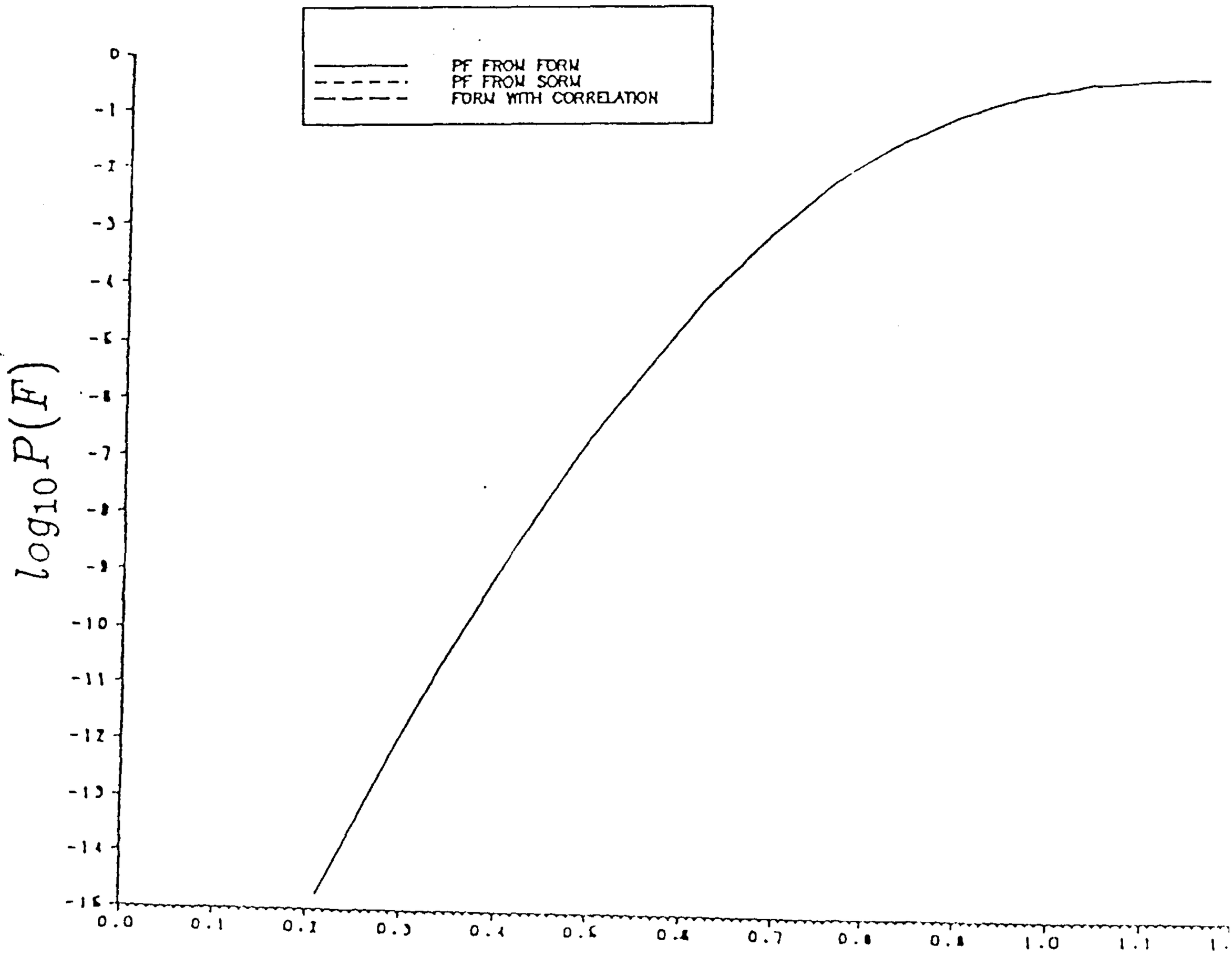

Fig. 4.8 Relationship between safety parameter and probability of failure for data group 1

DATA GROUP 2

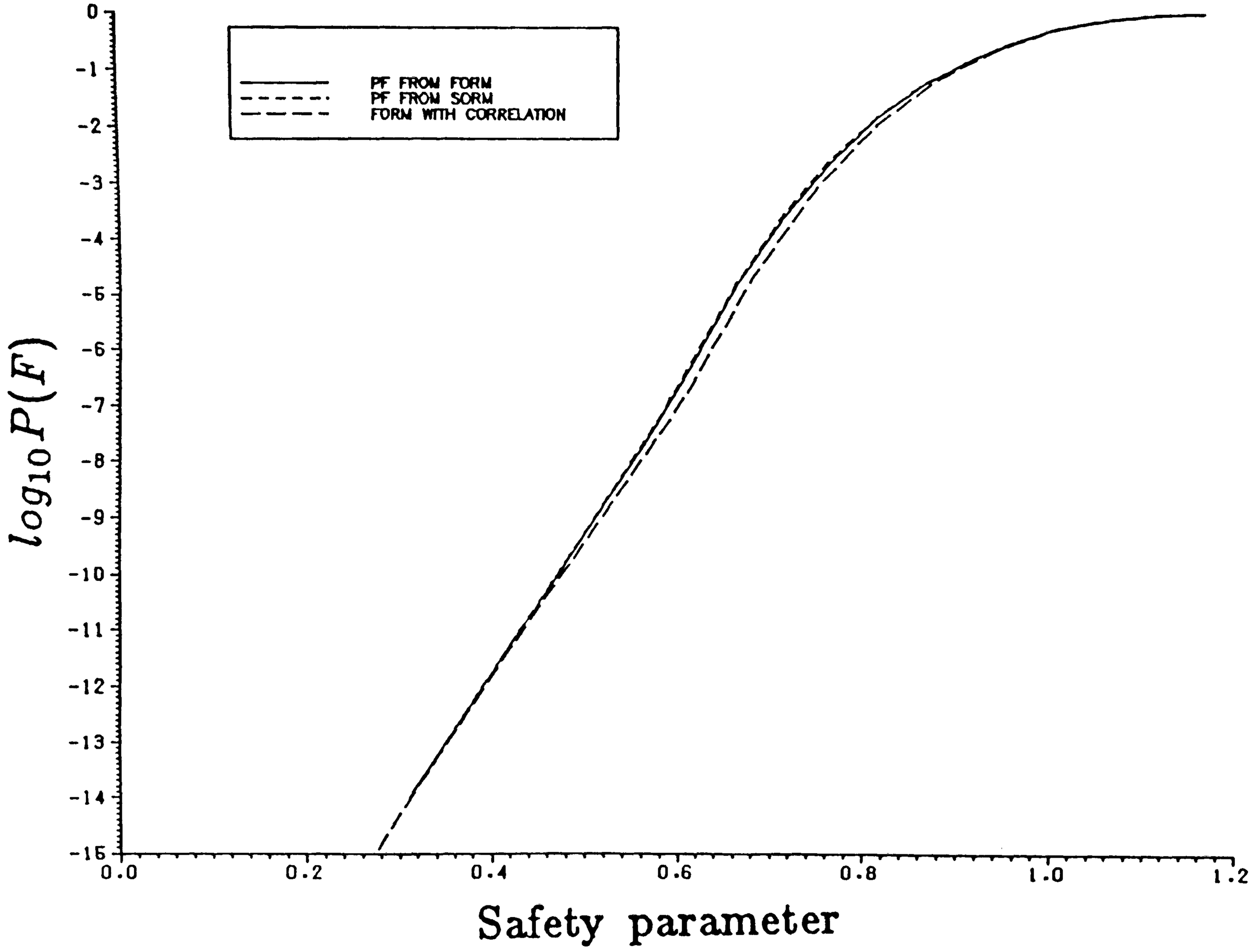

Fig. 4.9 Relationship between safety parameter and probability of failure for data group 2

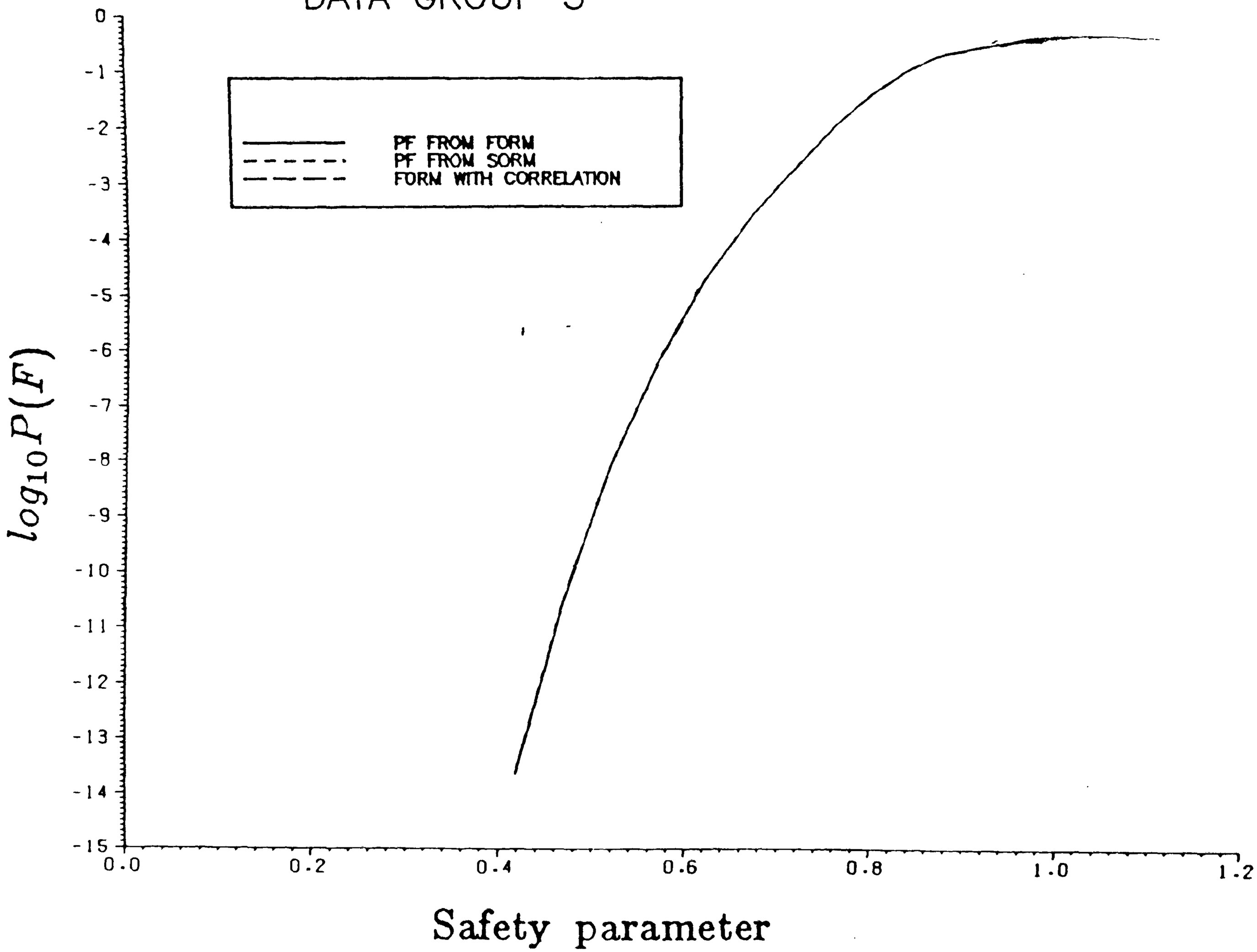

Fig. 4.10 Relationship between safety parameter and probability of failure for data group 3

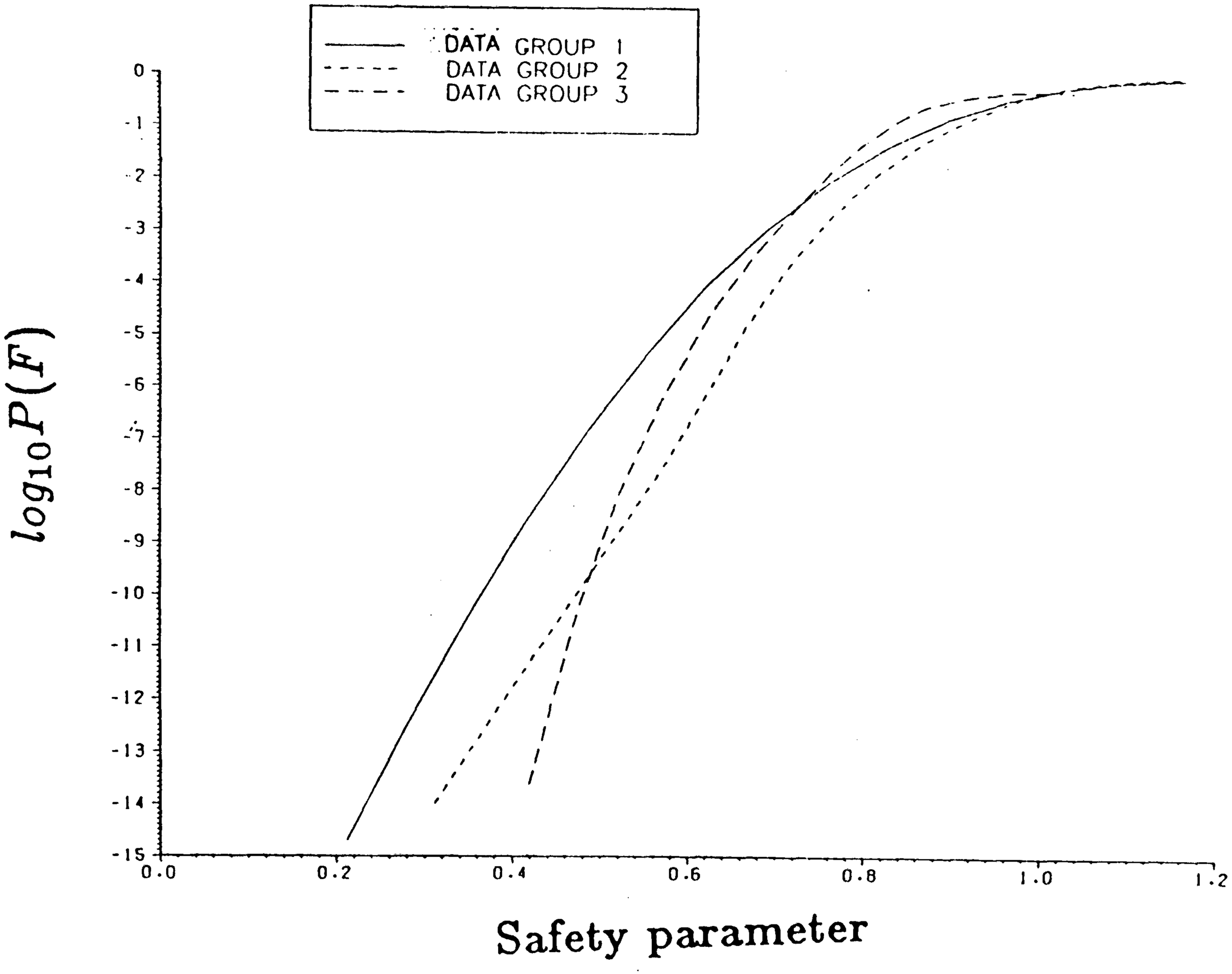

Fig. 4.11 Relationship between safety parameter and probability of failure for data group 1, 2 and 3 by FORM

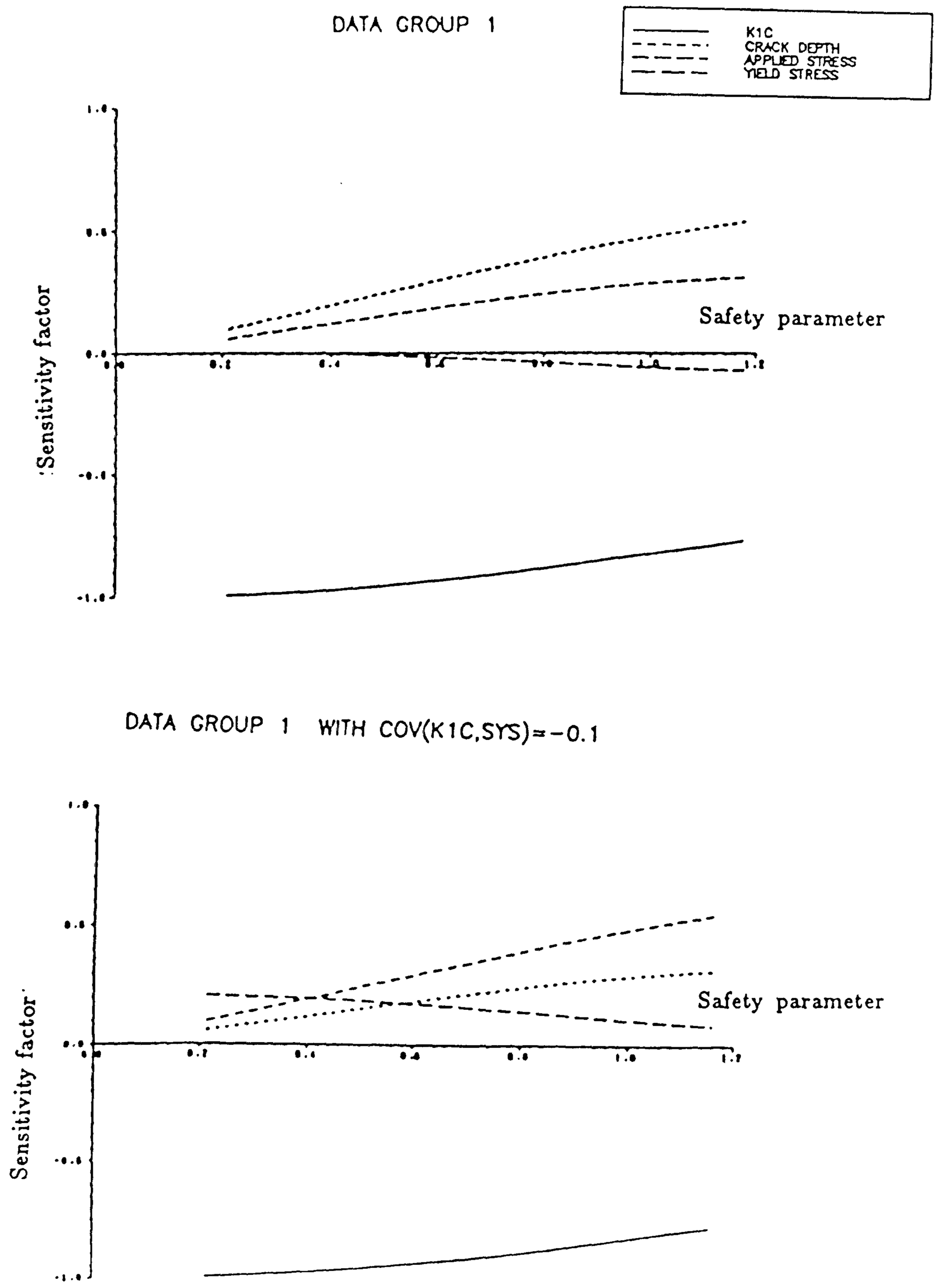

Fig. 4.12 Sensitivity factors for data group 1

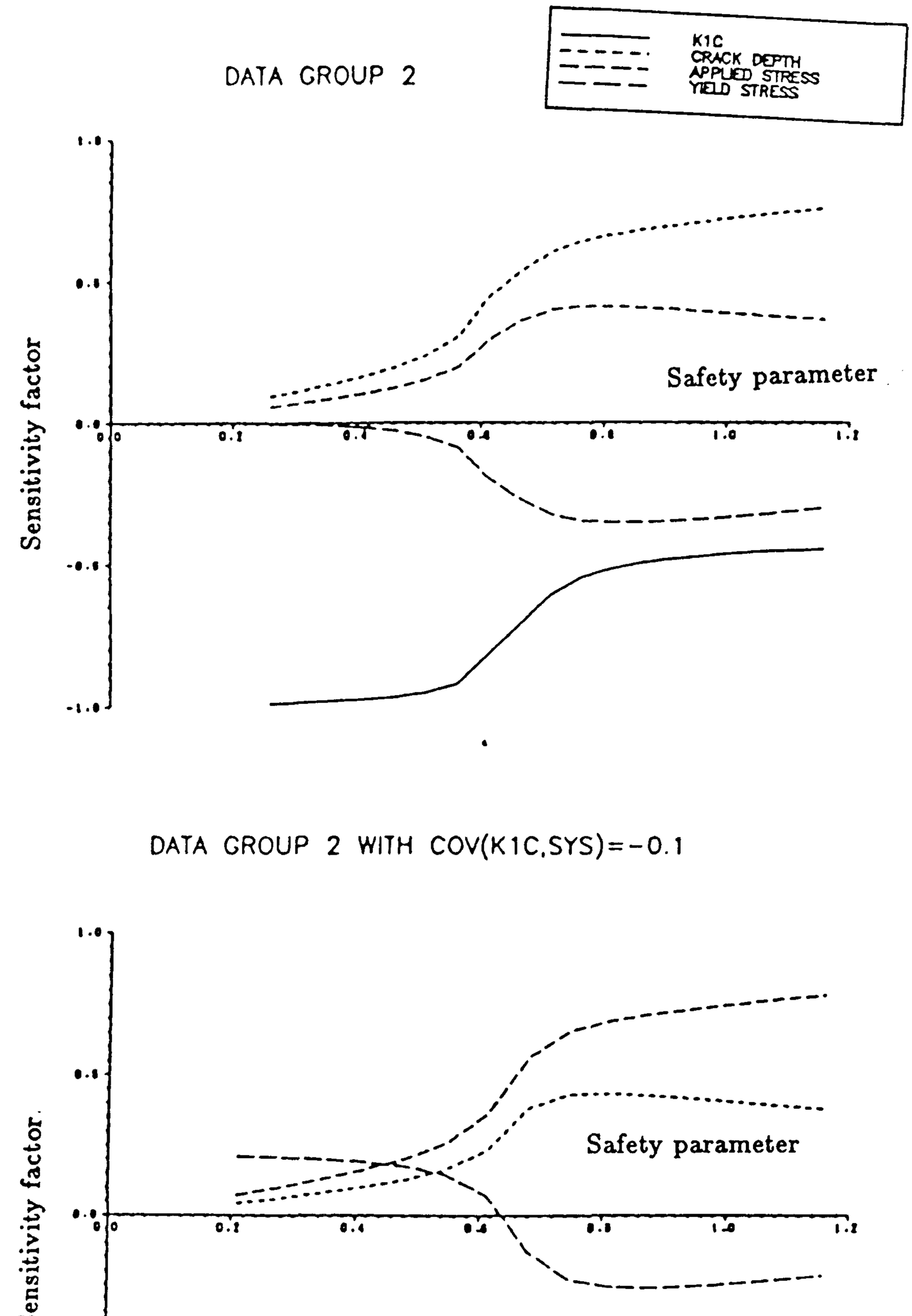

Fig. 4.13 Sensitivity factors for data group 2

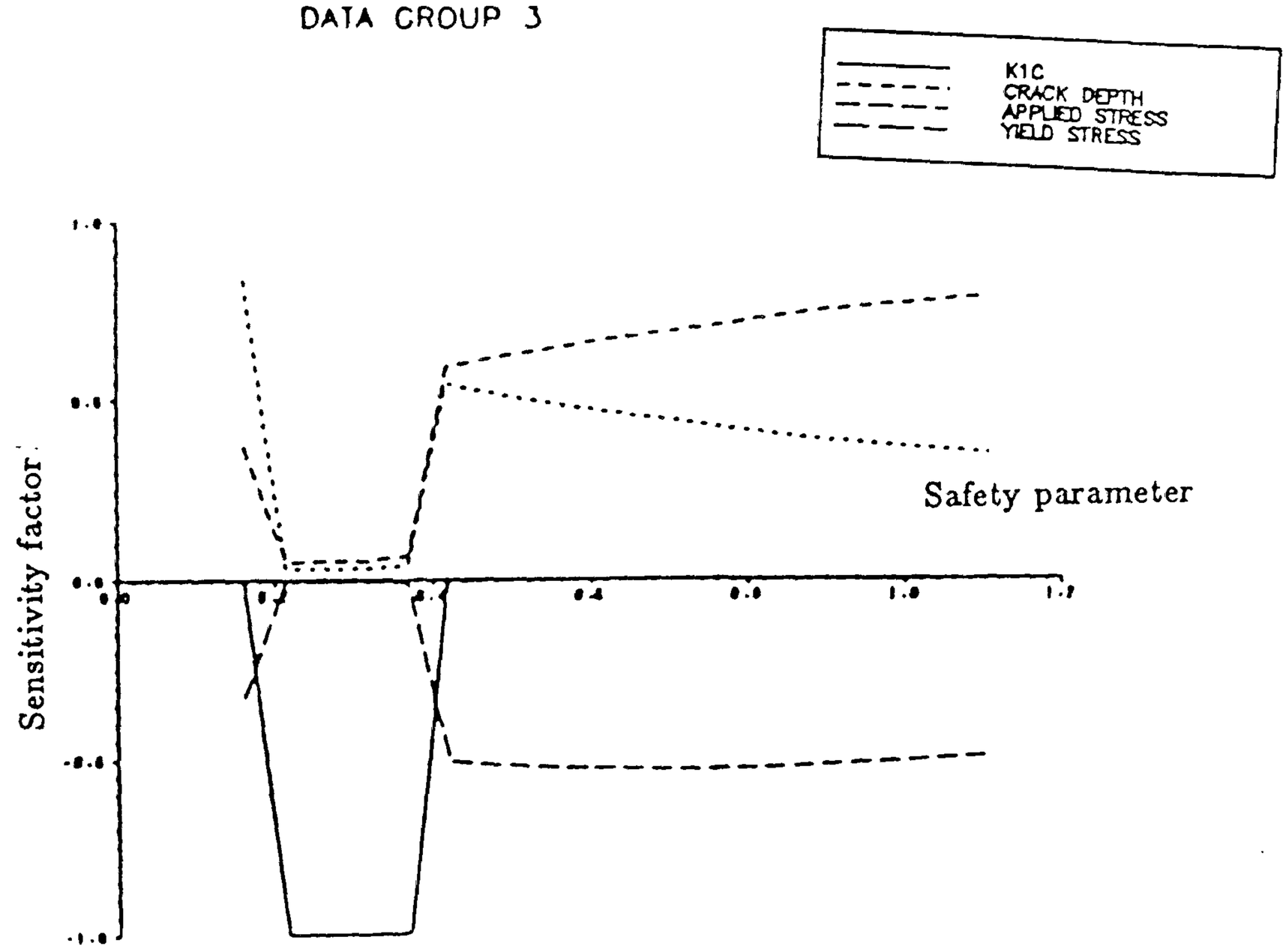

Fig. 4.14 Sensitivity factors for data group 3

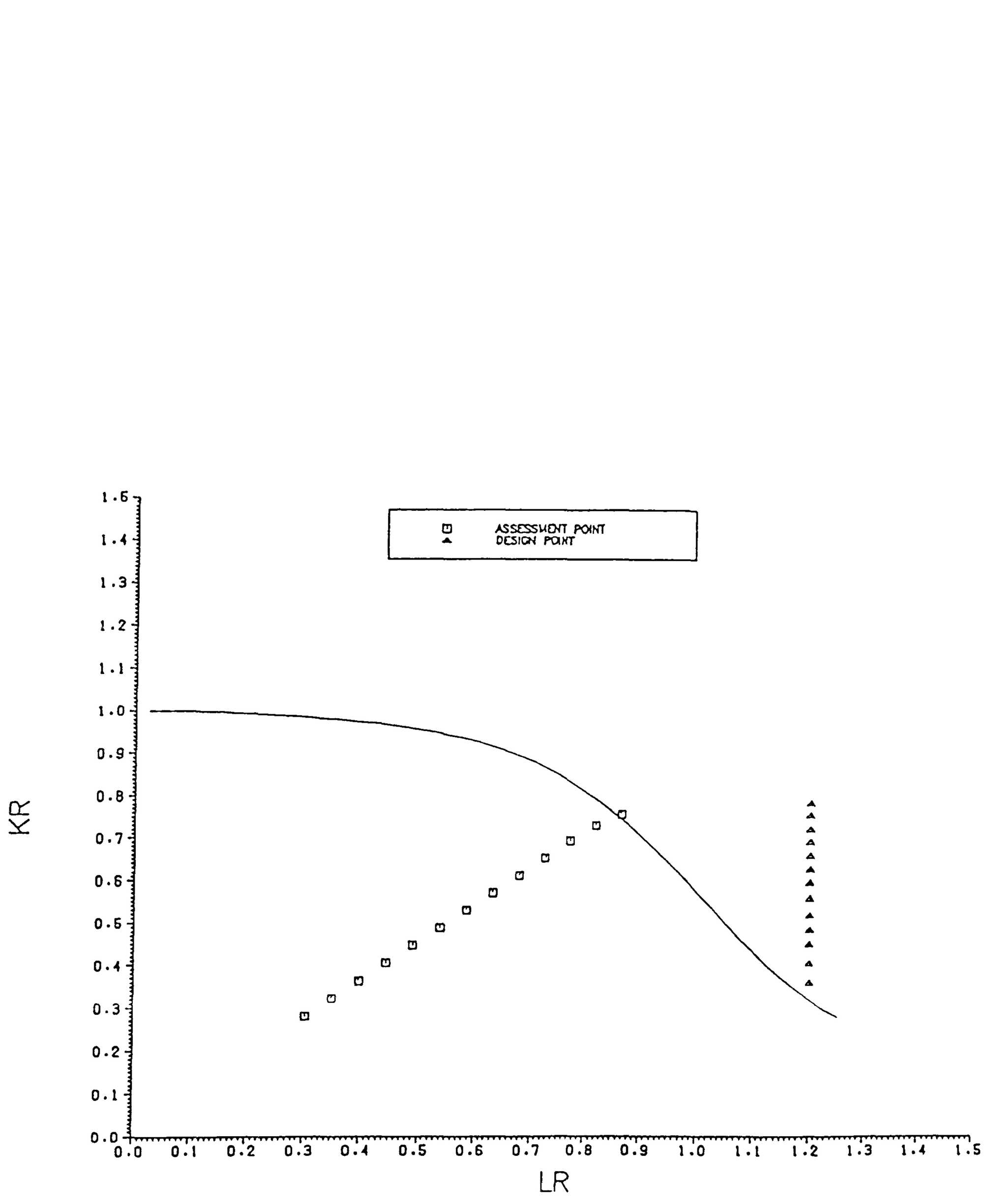

Fig. 4.15 Data group and design points in R6 FAD for reliability analysis with ductile material

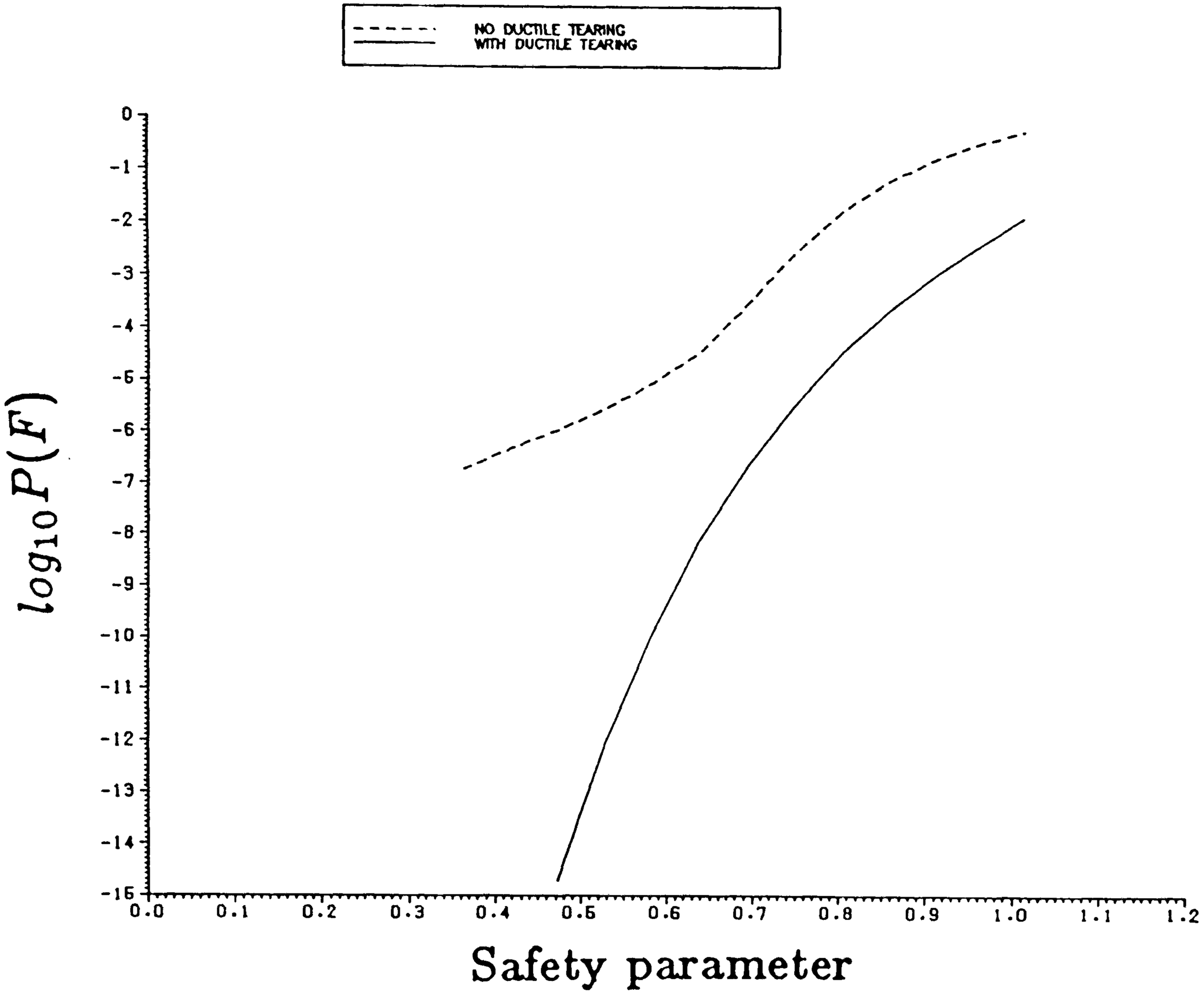

Fig. 4.16 Calculated probability of failure for data of ductile material

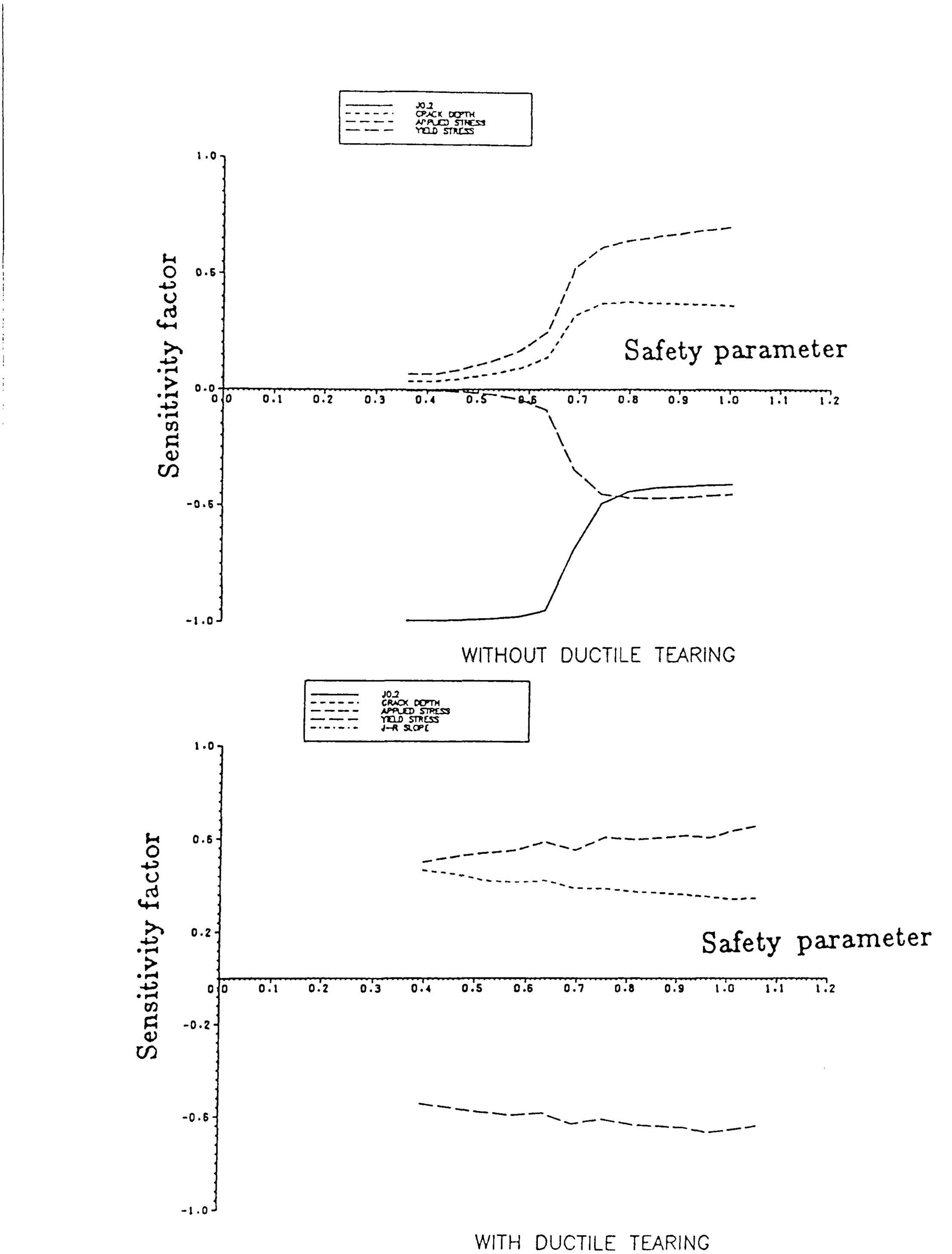

Fig. 4.17 Sensitivity factors for ductile material

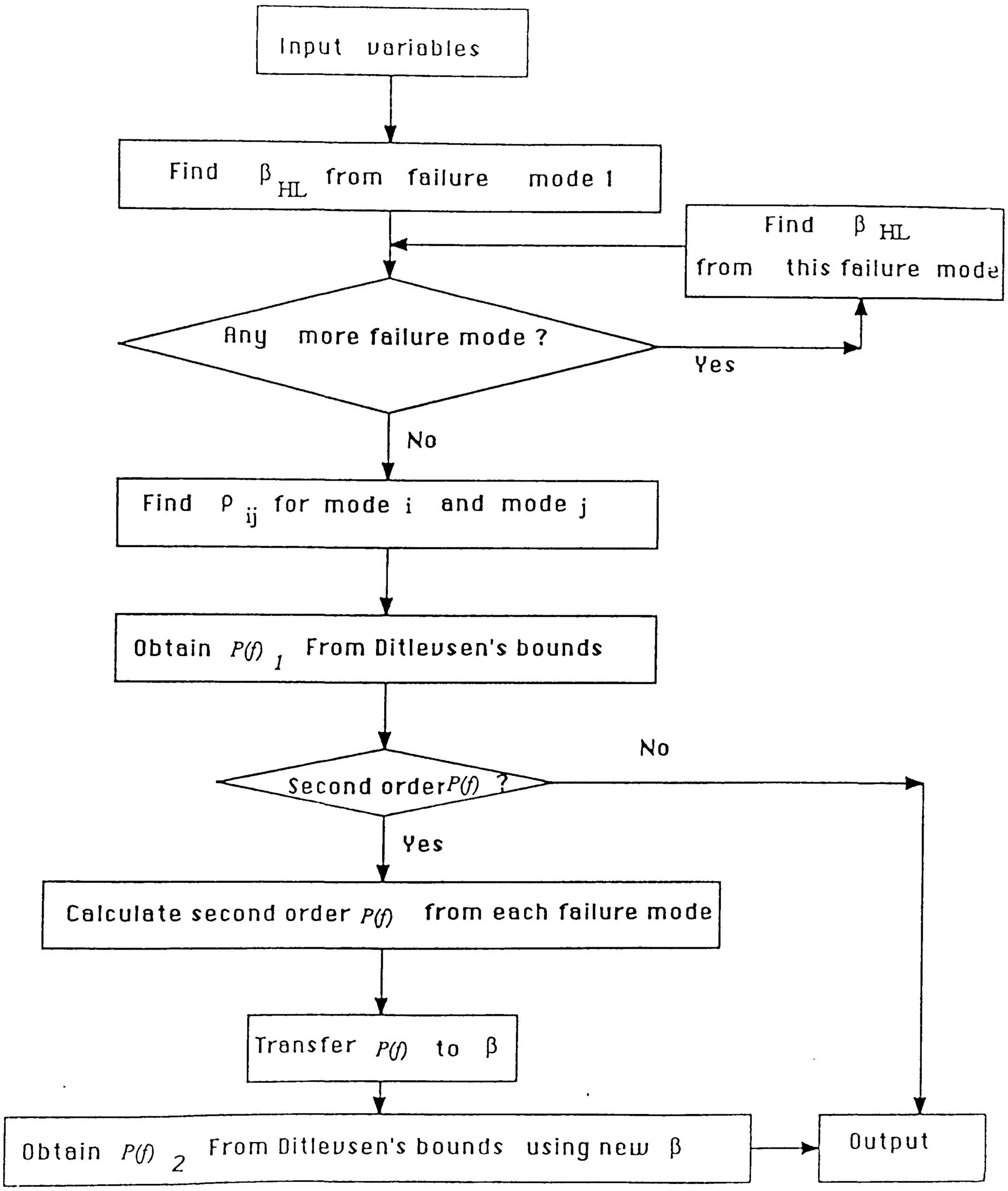

Fig. 4.18 Flow chart of REFF (Reliability calculation of Fatigue and Fracture)

Chapter 5

Modelling Of Stress Range Under Stochastic Loading For Fatigue Analysis

Nomenclature:

$a_1, b_1,$	
a_2, b_2	parameters in $f(s)$
B, C	parameters in Wirsching's spectrum
C_i	constants in autoregressive simulation
D	damage indicator
$E[.]$	mean
$e_1, ..., e_k$	values of the theoretical stress range pdf
f	frequency in Hz.
f_{max}	maximum frequency in target spectrum of simulation.
$f(x)$	probability density function of parameter x
f_W	weighting factor in $f(s)$
g	acceleration due to gravity
H_s	significant wave height
I	irregularity factor
m_i	ith power integration of spectral density function from Eqn. (5.41)
n_i	number of applied cycles for stress range S_i
N_i	number of cycles to failure for stress range S_i
$nc_1, ..., nc_k$	frequencies of simulated stress range
q	value of χ^2 probability validity test
$R_{\eta\eta}(\tau)$	stationary process auto-correlation function
S	stress range
s	normalised stress range
$s(t)$	random structural stress response
$S'_{\eta\eta}(\omega)$	spectral density of mean square
$S(.,.)$	spectral density function
t	time
T_D	dominant period
x_i	parameters in $f(s)$
$X(t)$	sea profile above some arbitrary datum
α, β	parameters in P-M spectrum
β_b	alternative bandwidth parameter

ω	frequency in rad/sec
τ	time interval
λ	correction factor defined in Eqn. (5.38)
σ	root mean square
$\triangle(\omega)$	normalised force spectral function
ω_{in}	natural frequency of the ith mode
ψ_i	damping factor for the ith mode
η	sea profile elevation
ϵ	bandwidth parameter

Other symbols are defined in the text.

5.1 Introduction

5.1.1 General remarks

Let $s(t)$ denote a continuous, random function of time t representing, for example, the random structural stress response at some point in a structure. The probability distributions of the maxima and minima of a stochastic process have been investigated to a considerable extent[5.1], [5.2]. However in fatigue studies, the problem of determining the stress range distributions is yet to be solved. Related to this is the problem of defining stress ranges.

The primary loading on many structures is of a stochastic nature. For many types of structures, extensive data collection has made it possible to obtain analytical models for the processes giving rise to the loads (e.g. wave spectrum) or, alternatively, stress spectra directly.

Under stochastic primary loading the structural response is also stochastic -namely a random function of time $s(t)$. Fatigue loading data may be obtained directly from structure monitoring records, in the form of strain gauge records[5.3]. However, in many cases, this is not possible or economical. Alternatively, the loading data for fatigue analysis of a structure under random amplitude loading can be compiled in the following way:

(i) specification of primary loading (e.g. wind, wave, traffic, machinery, etc.).

(ii) determination of the structure's stress or strain response.

(iii) quantification of stress or strain for fatigue analysis (e.g. stress or strain ranges, mean value of each range, order of ranges).

In this thesis, offshore structures under random wave loading have been examined. The ocean wave processes can be divided into a series of stationary processes corresponding to separate sea states that give rise to the loads. The transfer function from wave height to the actual response of the structure is generally complex and thus for normal engineering purposes a number of simplifying assumptions are often made[5.4]. Nevertheless, for the purpose of this thesis, it is assumed that the response spectra in terms of stress are available, as required.

In fatigue life prediction under random loading, it is generally recognised that uncertainty can result in part from the cycle counting method used. In the work described here, the rainflow method has been used as a reference procedure, by which to compare other methods, since this gives a better fit to experimental fatigue data than other cycle counting methods.

Usually, approximate methods are used to quantify stress ranges for the purpose of fatigue analysis [5.5], [5.6], [5.7], [5.8], rather than using direct simulation and cycle counting, which involves an appreciable amount of numerical computation[5.9], [5.10]. However, these methods can be shown to

give rise to considerable inaccuracies when compared with the results from simulations. A number of previous attempts have also been made to derive analytical solutions for stress range probability distribution functions but they either require excessive computer time, or need sufficient statistical information.

This chapter presents a set of simple empirical models, which enable close approximation to the true probability distributions of stress range for use in fatigue analysis. They are derived directly from the properties of any response spectrum, without recourse to simulation and cycle counting. This chapter will serve as the basis for fatigue reliability analysis under random loading, with later work in this thesis taking full advantage of this better understanding of fatigue loading.

5.2. Loading Process

5.2.1 General remarks

Development has led to the definition of various kinds of spectra for describing the loading process in offshore structures. Time series can thus be simulated from these spectra.

The response spectrum proposed by Wirsching[5.4] in 1976 has been widely accepted as a convenient form for research and application. Some of the assumptions originally set out by Wirsching may not be necessary in all cases. It is beyond the scope of this thesis, which is intended to be generally applicable to reliability analysis, to investigate the validity of each assumption.

To obtain a response spectrum for an offshore platform under wave loadings, Wirsching has made the following basic assumptions:

1. The structure is linear. Damping is small and can be linearised. The response is also linear.

2. The seastate is two dimensional with the worst case for the structure occurring when the wave direction is orthogonal to one side of the structure.

3. Motion of the platform is negligible.

4. The wave force is concentrated at the mean water level.

5. In computing the wave force on the structure, the structure has zero width relative to the wave.

Having obtained the general spectrum of structural response, e.g. the stress in the structural component, the stochastic loading process should be reproduced from these spectra. In order to simulate the loading history, some simulation technique has to be used. An exact transfer from power spectrum in the frequency domain, to time series in time domain may not be possible. The closer the

features of simulated process are to original spectrum, the more computer time is needed. However, the most important features in the time series for fatigue study are the maxima and minima, which can then form loops. Autoregressive simulation can provide a self-motivated time series without periodical effect and only requires limited computation.

5.2.2 Loading spectra

5.2.2.1 Sea state spectra

Wave loading has been chosen as an example for modelling because fatigue damage in offshore structures is mainly caused by wave loading. Waves are generated by wind blowing over the surface of the sea. The sea profile above some arbitrary datum, $X(t)$, at any point is a random process [5.11]. The mean value is

$$\mu_X(t) = E(X(t)) = \int_{-\infty}^{\infty} x f_X(x,t)\, dx \tag{5.1}$$

where $f_X(x,t)$ is the first-order density function of X.

The auto-correlation function $R_{XX}(t_1,\ t_2)$ is defined by:

$$R_{XX}\ (t_1,t_2) = E[X(t_1)\ X(t_2)] \tag{5.2}$$

$$= \int_{-\infty}^{\infty} x_1 x_2 f_X(x_1,\ x_2;\ t_1,t_2)\, dx_1\, dx_2 \tag{5.3}$$

When the first order and second order distribution of X(t) are independent of absolute time, the process is said to be weakly stationary. i.e. when

$$R_{XX}(t_1,t_2) = R_{XX}(\tau) \tag{5.4}$$

where $\tau = |t_1 - t_2|$

The conditions in the open sea are not stationary throughout. However, within a finite period of time, these conditions can be considered to be stationary.

If $\eta(t)$ is the wave surface elevation above mean still water level, this quantity may be modelled as a zero mean, continuous space, continuous time stochastic process, which over a short period of time is stationary. And,

$$R_{\eta\eta}(\tau) = E[\eta(t)\eta(t+\tau)] \quad -\infty \le \tau \le +\infty \tag{5.5}$$

The spectral density of mean square can be defined as:

$$S'_{\eta\eta}(\omega) = \frac{1}{2\pi}\int_{-\infty}^{\infty} R_{\eta\eta}(\tau) e^{-i\omega\tau} d\tau \quad -\infty \le \tau \le \infty \tag{5.6}$$

where $R_{\eta\eta}(\tau)$ has an inverse Fourier relationship with $S'_{\eta\eta}(\omega)$, i.e.

$$R_{\eta\eta}(\tau) = \int_{-\infty}^{\infty} S'_{\eta\eta}(\omega)\ e^{-i\omega\tau} d\omega \quad -\infty \le \omega \le \infty \tag{5.7}$$

When $\tau = 0$,

$$R_{\eta\eta}(0) = E(\eta(t)^2) = \int_{-\infty}^{\infty} S'_{\eta\eta}(\omega)\ d\omega \tag{5.8}$$

$$E[\eta(t)^2] = \sigma_\eta^2 + \mu_\eta^2 \tag{5.9}$$

When $\mu_\eta = 0$, as it is assumed for the wave surface elevation, then

$$\sigma_\eta^2 = \int_{-\infty}^{\infty} S'_{\eta\eta}(\omega)\ d\omega \tag{5.10}$$

Setting $f = \omega/2\pi$ as the frequency in Hertz, and putting

$$S_{\eta\eta}(f) = S'_{\eta\eta}(\omega) \quad \text{where} \quad f = \omega/2\pi \tag{5.11a}$$

gives

$$\sigma_\eta^2 = \int_{-\infty}^{\infty} S'_{\eta\eta}(\omega)\ d\omega = 2\pi \int_{-\infty}^{\infty} S_{\eta\eta}(f)\ df \quad -\infty \leq f \leq \infty \tag{5.11}$$

For engineering purposes, the single sided spectrum is used. Thus,

$$\sigma_\eta^2 = 2\pi \int_0^{\infty} S_{\eta\eta}(f)\ df \quad 0 \leq f \leq \infty \tag{5.12}$$

From the assumption that $\mu_{\eta(t)} = 0$, Eqn. (5.9) becomes

$$E[\eta(t)^2] = \sigma_\eta^2 \tag{5.9a}$$

The left side of equation (5.9a) can be obtained from a simulated random process; while the right side can be calculated from Eqn. (5.10), Eqn. (5.11) and Eqn. (5.12). A random process $\eta(t)$ from simulation, should have similar, if not equal statistical properties, to its original spectral function. Eqn (5.9a) could be used to check how close the statistical properties of the simulated time series is, to those of the response spectra in a simple way.

A number of empirical spectral formulations of the water elevation, which are known as the seastate spectra, are in common use, e.g. the Pierson-Moskowitz (P-M) and the JONSWAP spectrum[5.12], [5.13]. For a fully developed sea, the P-M spectrum is often used. The P-M spectrum is defined by wind speed and two dimensionless constants α, β.

$$S'_{\eta\eta}(\omega) = \frac{\alpha g^2}{\omega^5} exp^{-\beta[\frac{\omega_0}{\omega}]^4} \tag{5.13}$$

where

$$\omega_0 = \frac{g}{\mu_{19.5}}$$

$\mu_{19.5}$ is the wind speed in m/s at a height of 19.5m above the mean still water level

α is equal to 0.0081

β is equal to 0.74

Alternatively , the P-M spectrum may be expressed in terms of the seastate parameters , H_s , the significant wave height and, T_z, the mean zero crossing period [5.11] or T_D the dominant period.

5.2.2.2 Response spectra

A response spectrum can be represented in a number of different ways:

a) as an explicit function of frequency[5.12]

b) implicit in terms of an input spectrum and transfer function (often involving a linearisation)[5.14]

c) in numerical form.

In many cases, however, exact analytical expressions do not exist for other than simple structures.

In offshore structures, when the seastate spectrum is obtained, if the structure is linear, the ordinates of the response spectrum for each frequency will be the product of the seastate spectrum and the transfer function as in Eqn (5.15).

The transfer function depends on mass , stiffness and damping of the system, apart from the external loading[5.11], [5.14]. Many factors should be included e.g. water elevation, deck mass, soil stiffness, pile geometry, pile flexibility, batter, damping force, water particle velocity, platform velocity etc. The exact solution will require considerable computation efforts [5.8], [5.14], [5.15]. For the purposes of preliminary design and reliability fatigue analysis, a simple algorithm was proposed by Wirsching [5.4], to provide the mechanism for the efficient introduction of probabilistic design theory.

Wirsching claimed to have a much simplified response spectrum, which is summarised in the following paragraphs[5.4], without resorting to extensive computation. For each mode of structural response, the natural frequency can be identified. A filter equation can be made to include most of the effects discussed in the second paragraph of this section, and to transfer the seastate spectrum to the response spectrum.

For the ith mode of structural dynamic response, from the P-M seastate spectrum, if $\Delta(\omega)$ is defined as the normalised force spectral density function from the sea state spectrum, derived from P-M

spectrum, we have:

$$\Delta(\omega) = \frac{Bc}{T_D^c \omega^{c+1}} exp^{\{\frac{-B}{T_D^c \omega^c}\}} \quad for \;\; \omega > 0 \tag{5.14}$$

where $B > 0$, $c > 0$, (for example $B = 1050, c = 4$ as in the Bretschneider example [5.4]) and

$$\int_0^\infty \Delta(\omega)\, d\omega \;=\; 1$$

Multiplying the force spectrum by the transfer function, the response spectrum is:

$$S(\omega) = \frac{\Delta(\omega)}{(1-\gamma_i{}^2)^2 + (2\xi_i\gamma_i)^2} \tag{5.15}$$

where

$$\gamma_i = \frac{\omega}{\omega_{in}}$$

and ξ_i is the damping factor for the ith mode

Based on the response spectrum of equation (5.15), if

$$f = \frac{\omega}{2\pi}, \qquad f_n = \frac{\omega_{in}}{2\pi}$$

$$S(f) = AH_s{}^{\varphi} \frac{1}{T_D{}^4} \frac{exp^{[\frac{-B}{(2\pi T_D f)^4}]}}{(2\pi f)^5[\{1-(\frac{f}{f_n})^2\}^2 + \{\frac{2\xi f}{f_n}\}^2]} \tag{5.16}$$

where $B = 1050$

$\varphi = 3.25$ in this study

A is scaling factor of 5580 when H_s is in metres

$\xi = 0.02$ in this study

The 11 seastate spectra are shown in Fig. 5.1 according to data provided by Table 5.1 from ref.[5.30]. By choosing f_n=0.286 the 11 response spectra are shown in Fig. 5.2.

Fig. 5.3 shows each spectrum separately to illustrate the change of band width. It is obvious that spectrum 1 has a relatively wide band width whilst spectrum 11 is relatively narrow band.

Table 5.1 Sea states

Sea state	Significant wave height H_s(m)	Dominant period T_D(sec)	Fraction of time
1	16.01	17.3	3.68×10^{-5}
2	14.48	16.5	9.32×10^{-5}
3	12.96	15.8	3.70×10^{-4}
4	11.43	14.7	2.20×10^{-3}
5	9.90	13.6	7.30×10^{-3}
6	8.38	12.7	1.35×10^{-2}
7	6.86	11.6	2.65×10^{-2}
8	5.33	10.3	6.01×10^{-2}
9	3.81	9.1	2.00×10^{-1}
10	2.28	7.7	4.90×10^{-1}
11	0.76	4.4	1.90×10^{-1}

5.2.3 Loading process simulation

5.2.3.1 Introduction

To relate the statistical properties of the structural response spectrum to a real time history, a direct numerical simulation has been conducted. It is virtually impossible to simulate the exact time history which will satisfy all the statistical properties e.g. the moments of the power spectrum to a very high level. In fatigue study, the most important features of the loading history are the peaks and troughs, from which the stress ranges can be obtained. By using current knowledge, the loading peaks and troughs process can be approximated to a sufficient extent. The time interval for simulation has been taken as half the reciprocal of the maximum frequency in Hertz, so that the minor differences can be ignored.

5.2.3.2 Normal methods

In the past, the simulation of peaks and troughs from the sample functions of the random process has been a very cumbersome task, as shown by Shinozuka [5.16]. In the late sixties, the Fast Fourier transform(FFT) was developed. Yang [5.17] then used the FFT technique to generate discrete time series which could serve as artificial random signals, as in the following explanation.

From Eqn (5.6) and Eqn (5.7) for a stationary process, the spectral density and auto-correlation function of the process forms an inverse Fourier relationship. If the random process is stationary and Gaussian with zero mean and spectral density $S'_{\eta\eta}(\omega)$, put

$$X_0(t) = \int_{-\infty}^{\infty} e^{i\omega t}\, d\bar{x}_0(\omega) \tag{5.17}$$

where $d\bar{x}_0(\omega)$ is an orthogonal random process with zero mean and

$$E[d\bar{x}_0(\omega_1)d\bar{x}_0^*(\omega_2)] = 0 \quad for \;\; \omega_1 \neq \omega_2 \tag{5.18}$$

$$E[|d\bar{x}_0(\omega)|^2] = S'_{\eta\eta}(\omega)\; d\omega \tag{5.19}$$

The asterisk denotes the complex conjugate.

Using condition (5.17), one can see

$$R_{\eta\eta}(\tau) = \; E[\eta(t)\eta(t+\tau)] = \int_{-\infty}^{\infty} S'_{\eta\eta}(\omega)e^{i\omega\tau}\; d\tau \tag{5.20}$$

If

$$S(\omega) = 2S'_{\eta\eta}(\omega)$$

$$R_{\eta\eta}(\tau) = \int_0^{\infty} S(\omega)\; cos\omega\tau\; d\tau \tag{5.21}$$

So from equation (5.18), if one defines

$$dU(\omega_K) = \; [2S(\omega)\; \triangle\omega_K]^{\frac{1}{2}} cos\psi_K \tag{5.22}$$

$$dV(\omega_K) = -[2S(\omega)\; \triangle\omega_K]^{\frac{1}{2}} sin\psi_K \tag{5.23}$$

where ψ_K $(K = 1,2....)$ are independent and identically distributed random phase angles with a uniform density function $1/2\pi$ in $[0,2\pi\,]$, then

$$\triangle\omega_K = \; \omega_{K+1} - \omega_K \tag{5.24}$$

$$X_0(t) = cos(\omega t)\; dU(\omega) + sin(\omega t)\; dV(\omega) \tag{5.25}$$

will satisfy conditions (5.18), (5.19).

Therefore, for a stationary random process

$$s(t) = X_0(t) = \sum_{K=1}^{N} [2S(\omega_K)\triangle\omega_K]^{\frac{1}{2}} cos(\omega_K t + \psi_K) \tag{5.26}$$

From equation (5.26), by selecting $\Delta\omega_K$, a pseudo-random process can be achieved.

The computational cost of simulation will depend on the length of the required loading process and the shape of the spectrum. If all $\Delta\omega_K$ are equal, $X(t)$ will be periodic with a period equal to the reciprocal of the minimum frequency of the input spectral density. To avoid this periodic problem, two ways have been proposed:

(1) Make $\Delta\omega_K$ small, hence N is big and the period is bigger than the length of the simulation loading process (J.N. Yang) [5.17].

(2) Choose random $\Delta\omega_K$. (P. Wirsching) [5.8].

The first way will raise the computation cost depending on the length of record wanted, while the latter approach might miss some significant spectrum points which, for example, may happen in the second narrow peak of the double peak offshore response spectrum.

5.2.3.3 Autoregressive simulation

May [5.18] generated wind records which specify a particular power spectrum using an autoregressive filter. The same approach is used by Anagnostides [5.19] for earthquake simulation. This autoregressive method makes a time series system oscillating under its own internal random forces. Therefore the problems from Ref. [5.17] and [5.8] can be avoided. Consider the random process $s(t)$ formed by a moving linear combination of another random process X_q:

$$s(t) = C_o X_q + C_1 X_{q-1} + ... + C_k X_{q-k} \tag{5.27}$$

where $C_o, C_1 .... C_k$ are constants.

If Δt is the increment of the series then the power spectra of $s(t)$ and X_q are related as shown in [5.18] by spectral density values:

$$S_s(f) = |Y(f)|^2 S_X(f) \tag{5.28}$$

where $|Y(f)|^2$ is the transfer characteristic of the autoregressive filter, given by:

$$|Y(f)|^2 = b_o + 2b_1 cos\omega\Delta t + 2b_2 cos 2\omega\Delta t + ... + 2b_k cos k\omega\Delta t \tag{5.29}$$

where

$$\begin{pmatrix} b_0 \\ b_1 \\ \vdots \\ b_{k-1} \\ b_k \end{pmatrix} = \begin{pmatrix} C_0 & C_1 & \dots & C_{k-1} & C_k \\ C_1 & C_2 & \dots & C_k & 0 \\ \vdots & \vdots & \ddots & \vdots & \vdots \\ C_{k-1} & C_k & \dots & 0 & 0 \\ C_k & 0 & \dots & 0 & 0 \end{pmatrix} \begin{pmatrix} C_0 \\ C_1 \\ \vdots \\ C_{k-1} \\ C_k \end{pmatrix} \tag{5.30}$$

Hence, a time series with a specific power spectrum can be generated as follows:

(1) Initially, a sequence of independent random numbers μ_i with uniform distribution in the interval (0,1) is obtained using a standard sub-routine in the computer.

(2) A new sequence of independent random numbers $\{X_i\}$ with a Gaussian distribution having zero mean and unit variance is obtained with the transformation [5.20].

$$\begin{aligned} X_i &= (-2\ln\mu_i)^{\frac{1}{2}} cos(2\pi\mu_{i+1}) \\ X_{i+1} &= (-2\ln\mu_i)^{\frac{1}{2}} sin(2\pi\mu_{i+1}) \end{aligned} \tag{5.31}$$

where i is an odd number.

(3) From Eqn (5.28), by transformation of Eqn (5.27), the transfer characteristic of the required autoregressive filter is

$$|Y(f)|^2 = \frac{S_s(f)}{S_X(f)} \tag{5.32}$$

where $S_s(f)$ is the target spectrum, for instance, $S(f)$ equation (5.16). The power spectral density function of the ensemble form has the function[5.20]:

$$S_X(\omega) = S_0 \frac{6 - 8cos(\omega\triangle\tau) + 2cos(2\omega\triangle\tau)}{(\omega\triangle\tau)^4} \tag{5.33}$$

$$S_X(f) = 2\pi S_0 \frac{6 - 8cos(2\pi f\triangle\tau) + 2cos(4\pi f\triangle\tau)}{(2\pi f\triangle\tau)^4} \tag{5.34}$$

where

$$S_0 = \frac{\triangle\tau}{\pi}$$

$\triangle\tau$ is the time interval of the white number μ_i.

If we set

$$\triangle\tau = \frac{1}{2f_{max}} \tag{5.35}$$

there will be no local maximum or minimum between two points because it must require a period less than $\Delta\tau$, which is impossible, for f_{max} is the maximum frequency in Hertz.

(4) The coefficients $(b_0, b_1, ..., b_k)$ in equation (5.29) are obtained by the solution of equation (5.29) for $(k+1)$ values of ω and so $S_s(f), S_X(f)$ and $|Y(f)|^2$. The coefficients $(C_0, C_1, ..., C_k)$ of the autoregressive filter can then be obtained by solving the non-linear equations (5.30) by using Newton-Raphson's method.

(5) The most costly part of computation in autoregressive simulation is to solve the non-linear equations (5.30). Any random process $s(t)$, can be efficiently generated through Eqn (5.27), with any random number set μ_i, and hence with the random number set X_i.

The autoregressive filter only needs one set of C_i for a target spectrum to produce any length of time series. The eleven spectra referred to in Section 5.2.2 have their C_i solutions in Table 5.2 with $f_{max} = 0.34$, and $k = 60$.

Accordingly, time series have been generated for the 11 spectra listed in Table 5.1. Two of them , spectrum 1 and spectrum 11, which represent the wide band spectrum and narrow band spectrum, are shown in Fig. 5.4 and Fig. 5.5.

5.2.2.4 Discussion

Random loading process simulations are complicated. However, the peaks and troughs process could be easily simulated from the spectral properties by the autoregressive simulation method as shown in this section.

The autoregressive simulation method has been adopted for this study because of its efficiency in generating large numbers of process points. Only if the solution of transformation coefficients of selected frequency spectral density are obtained, can the loading process be generated from the addition of zero mean unit variance random numbers. Furthermore, the autoregressive simulation is not restricted by the form of the target power spectrum, so that any other fatigue random loading can be generated in the same way. Clearly, the autoregressive simulation method has the advantages over the other method in section 4.2.3.2.

The general problem, however, is to obtain a solution for stress range frequencies having similar accuracy, but without resorting to time-consuming simulation. The easily generated loading process, provides a route for further study of stress ranges, to build up a semi-empirical model by observations of a number of generated records of different spectra. This shall be discussed in the following sections.

5.3 Cycle Counting Methods

5.3.1 General remarks

In order to calculate the fatigue damage caused by a variable loading process, the primary information required is the number of stress cycles or strain loops. For a variable amplitude loading process, there are a number of methods to define a cycle. Different definitions of stress cycles lead to different cycle counting methods and somewhat different results. The rainflow method is used in this study because of its highly reliable performance in the prediction of fatigue life under random loading compared with other methods.

5.3.2 Rainflow Algorithm

The rainflow method identifies small strain ranges or stress ranges associated with closed hysteresis loops. From that, a complex loading process is divided into many small stress reversals or strain loops. At the present time the rainflow method is widely used in fatigue analysis of weldable structural steels[5.21].

In the rainflow method, the stress history should be first converted to a series of peaks and troughs as shown in Fig. 5.6, with peaks numbered at consecutive even number. The time axis is then viewed as a sequence of roofs with rain falling on them. The rainflow paths are defined according to the following rules [5.8], [5.21].

(a) A rainflow path is started at each peak and trough.

(b) When a rainflow path started at a trough, comes to the tip of the roof, the flow stops if the opposite trough is more negative than that at the start of the path under consideration (e.g. paths [1-8] and [9-10]..). A path started at a peak is stopped by a peak which is more positive than that at the start of the rain path, (e.g. path [2-3], path [4-5] and path [6-7]...).

(c) If the rain flowing down a roof intercepts flow from a previous path, the present path is stopped, (e.g. paths [3-3a] and [5-5a]...).

(d) A new path is not started until the path under consideration has stopped. Half cycles of trough originated stress ranges magnitudes S_i are projected on the stress axis (e.g. [1-8], [3-3a], [5-5a] etc.). It should be noted that for time series sufficiently long, any trough originated half cycle will be followed by another peak originated half cycle for the same range.

In a fatigue study, those points in a loading process without reversal, where the structural component has a monotonic loading increase or decrease, will not have any cyclic effect. Fatigue damage accumulation is therefore insensitive to the elimination of those points. In the rainflow method those points should be eliminated before the rainflow algorithm can be applied.

In practical situations, a time history is unlikely to begin at the highest peak or lowest trough. In these cases, an ideal loop will not be formed . As in normal practice, the time history should be reset, moving the time origin to the highest peak or lowest trough, whichever occurs first, while the time series before the origin should be moved to the end of the whole time history.

After the elimination and the resetting of the time history, a simple computer program can be created; let the range of each peak and valley be identified as follows:

X = range under consideration;

Y = previous range adjacent to X.

As each peak or valley is encountered, it is stored in the computer.

Rainflow counting then proceeds according to the following steps:

1. Find the highest peak or the lowest valley in the process.

2. Set the time history origin at the highest peak or the lowest valley, whichever is the first, and move the parts of the time series before origin to the end.

3. Rainflow starts at the time series origin.

4. Read the next peak or valley (if out of data, stop)

5. Form ranges of X and Y (if at the beginning, less than three points are available, go to step 4).

6. Compare ranges X and Y.

   a) if $X < Y$, go to step 4

   b) if $X \geq Y$, go to step 7

7. Store each range Y. Discard the peak or valley of Y. Go to step 5.

5.3.3 Other cycle counting methods

In addition to the rainflow method, some commonly used cycle counting methods are peak counting and range counting methods [5.22].

Peak counting method

All the local maximum above zero are counted and paired with local minimum of the same size below zero. It is thus implied that the pdf of $f_{max}(x)$ and $f_{min}(-x)$ of local maxima and minima satisfies:

$$f_{min}(-x) = f_{max}(x) \tag{5.36}$$

The relative location of local maxima and minima are ignored. The pdf for a stress range is:

$$f_s(s) = f_{max}(\frac{s}{2}) \tag{5.37}$$

In section 5.4.4, one can see that the above equation only holds true in narrow band stationary process.

Range counting method

Each stress range, i.e. the difference between two successive local extremes, is counted as one half stress cycle. The range counting method only use the local information about the stress process, as each local extreme is only combined with the preceding and the following local extreme. This method

* does not refer to the mean level of stress cycle,

* takes every small cycle into account,

* breaks large ranges into several smaller ones.

5.3.4 Evaluation of rainflow method and other methods

Dowling[5.23] examined a number of cycle counting methods with a test of 83 specimens of 2024-T4 steel and found that the rainflow method gave the best results. Predicted fatigue lives using the rainflow method, were within a factor of three of the actual lives for all the tests. For all the tested specimens, the summations of the cycle ratios were all between 0.36 to 1.5. The rainflow method has been widely used as a cumulative damage procedure and counting method for fatigue research and applications. Also, the rainflow method is used in British Standard 5400, as the practice for fatigue design and assessment of steel, concrete and composite bridges.

As shown in this section, the rainflow method has the advantage over peak counting method by taking the relative location of a local maxima and local minima into account, and the advantage over the range counting method is that by considering the whole loops of stress cycles, the bigger stress ranges are not ignored. This would suggest that the peak counting method tends to overestimate stress cycles and that the range counting method tends to underestimate stress cycles, while the rainflow method predicts results in between.

However, whereas the peak counting method and range pair method can directly use results from statistical maxima distribution or order statistics, the rainflow method needs extensive simulation and counting, so it is very cumbersome. This thesis will demonstrate a way to achieve a stress range distribution function directly from a response spectrum. The distributions so obtained, can be shown to closely approximate the distributions obtained by simulation and rainflow counting.

5.4 Construction Of The Stress Range pdf Models

5.4.1 General remarks

For structures under random loading fatigue damage is often approximated using a narrow band loading assumption. This avoids the loading simulation and rainflow counting procedure. Wirsching[5.5] has defined the fatigue damage rate correction factor λ as:

$$\lambda = \frac{\text{damage rate by rainflow analysis}}{\text{damage rate by Rayleigh analysis}}$$

$$\lambda = \frac{D_{\text{rainflow}}}{D_{\text{narrow band}}} \tag{5.38}$$

Fig. 5.7 shows the correlation between the bandwidth parameter ϵ, which is defined by equation (5.40), and fatigue damage rate from three different simulation studies [5.6]. The trend of those points in relation to the bandwidth parameter, suggests that the stress range probability distribution should be a function of spectral properties. Due to the complexity of the loading process and the nature of the rainflow method, attempts in the past to model the stress range pdf have not been entirely successful.

With a narrow band loading process, the stress range probability distribution approaches the Rayleigh distribution as each positive peak would correspond to a negative trough. However as seen in Fig 5.8, the simulated stress range probability distribution from spectrum 11, which is relatively narrow band with ϵ =0.167, deviates significantly from the Rayleigh distribution (shown as the smooth curve). For a wide band spectrum as shown in Fig. 5.9, the shapes of the simulated histograms are far from the Rayleigh distribution. Therefore the approximation of the relationship

between damage rate and bandwidth is not satisfactory. In this section the stress range probability distribution is investigated from a different direction.

(1) The parameters of the distributions are assumed to be functions of stress range amplitude and an alternative bandwidth parameter.

(2) The Stress Range Probability Density Functions (SRPDF) $f(s)$ are treated empirically as the sum of two weighted Weibull probability density functions.

(3) Constants in $f(s)$ are obtained through careful adjustment to fit the model with the stress range histograms over a wide range of spectra.

(4) The validity of the semi-empirical $f(s)$ are tested against the results obtained by simulation and rainflow counting using the χ^2 test.

This technique is called Combined Distribution Technique(CDT) which starts directly from the study of stress range frequency of occurrence, obtained from simulation and rainflow counting. This is a more fundamental approach than previous studies. A series of ready made solutions, for general spectrum in practical application, can be provided.

5.4.2 Literature review

Early work by Cartwright and Longuet-Higgins [5.1] studied the statistical distributions of the maximum values of a random function, which is the sum of an infinite number of sine waves with random phases. By mathematical derivation from Rice [5.24], the probability distribution of the height of maxima above the mean level, η, is:

$$f(\eta) = \frac{1}{(2\pi)^{\frac{1}{2}}}[\epsilon e^{\frac{1}{2}\eta^2/\epsilon^2} + (1-\epsilon^2)^{\frac{1}{2}}\eta e^{-\frac{1}{2}\eta^2}\int_{-\infty}^{\eta(1-\epsilon^2)^{\frac{1}{2}}/\epsilon} e^{\frac{-1}{2}x^2}dx] \tag{5.39}$$

$$\begin{cases} \epsilon^2 = \dfrac{m_0 m_4 - m_2^2}{m_0 m_4} \\ m_i = \int_0^\infty S(f) f^i df \end{cases} \tag{5.40}$$

ϵ is shown to represent the relative width of the power spectrum - the so-called bandwidth parameter. In reference [5.1], two extreme cases of ϵ were discussed:

1) when $\epsilon \longrightarrow 0$, the spectrum is narrow band

$$f(\eta) = \begin{cases} \eta e^{-\frac{1}{2}\eta^2} & (\eta \geq 0) \\ 0 & (\eta \leq 0) \end{cases} \tag{5.41}$$

which is the Rayleigh distribution;

2) when $\epsilon \longrightarrow 1$, the spectrum is wide band

$$f(\eta) = \frac{1}{(2\pi)^{\frac{1}{2}}} e^{-\frac{1}{2}\eta^2} \tag{5.42}$$

which is a Gaussian distribution.

The proportion of negative maxima, γ, is a function of ϵ given by

$$\gamma = \frac{1}{2}(1 - (1 - \epsilon^2)^{\frac{1}{2}}) \tag{5.43}$$

Also, it was shown that the mean height of the $1/n$ highest proportion of the wave series is a function of ϵ, but tends to decrease with increasing ϵ.

The work done by Borgman [5.25], and later by Moe and Crandall [5.26], gave an asymptotic probability density of normalised local maximum to be a two phase distribution, which is of Rayleigh distribution in the high maximum part, but exponential in the low maximum part.

Based on the extreme value theory, as in equations (5.1), (5.4) and (5.5), Choudhury and Dover [5.7] proposed a general theoretical form for the probability density of peak amplitude as the combination of a Rayleigh density function and a Gaussian density function, for different seastates.

The works mentioned above all relate stress range to the local maxima or minima distribution. For a fatigue study, it is more important to study the stress range from rainflow counted stress ranges. Using the direct simulation method as in Section 3.2, Wirsching explored the stress ranges of rainflow counting approach for various forms of spectral density function [5.8]. Because the Weibull distribution has been widely used in engineering practice, of which the Rayleigh distribution is a special case, the former was investigated as a possible fit to the data used in that study. However, it was recognised that the probability distribution of stress ranges is not Weibull in general.

Because of difficulties in getting the SRPDF for random loading, the fatigue damage rate as defined by equation (5.20), has to be approximated by various methods [5]. Wirsching related damage rate λ to ϵ, while Lutes *et al* related λ to a more general term β_b as defined in Eqn (5.44).

Recent work of Rychlic [5.27], [5.28] and Ford [5.29] has attempted to give a analytical solution. Rychlic redefined the rainflow counting procedure and approximated the loading process as a Markov chain. Ford used time series theory to calculate range pair exceedance probability and then related the theory into the stress range from the rainflow method. Both of them need appreciable numerical effort and sufficient statistical information.

5.4.3 The new models

5.4.3.1 Selection of parameters

Wirsching [5.5] found that the damage rate of fatigue (see equation 5.2) is related to ϵ. However, the data also indicates a significant scattering from the mean line, which was discovered by Lutes *et al* from a comprehensive study of several simulation results[5.6]. To accommodate the variation of λ, Lutes *et al* inferred that a general form of bandwidth parameter can be related to the damage rate. Those bandwidth parameters are defined as:

$$\beta_b = \frac{m_b}{(m_0 m_{2b})^{\frac{1}{2}}} \tag{5.44}$$

where m_i is defined by Eqn. (5.40).

For any $b > 0$, β_b can be considered as a bandwidth parameter. β_b has some obvious characteristics:

(i) $0 \leq \beta_b \leq 1$

(ii) $\beta_b = 1$ if the power spectrum contains only one frequency.

(iii) When $b = 2$, $\beta_b = \sqrt{1 - \epsilon^2}$.

On a purely empirical basis, Lutes *et al*[5.6] found that if using the Paris' law to predict the crack growth with Paris' parameter $m = 3$, λ shows a stronger correlation with $\beta_{0.75}$ than with other β values as shown in Fig 5.10. Comparing Fig 5. 10 with Fig 5.7 , one can see that the plotted data have less variation from the mean line with $\beta_{0.75}$ than with ϵ. It is also pointed out by Lutes *et al* that $\beta_{0.75}$ is not the only bandwidth parameter to adequately correlate with λ value. There can be other alternative bandwidth parameters, similar in form to β_b, which may be appropriate for some other situations.

Since the Paris' parameter $m = 3$ is the most common value for steels, it may be presumed from the above discussion that $\beta_{0.75}$ is a more suitable value to model the probability distributions of stress ranges than ϵ.

By using the 11 offshore response spectra from reference [5.30], the value of the parameters $\beta_{0.75}$ and ϵ have been calculated and are listed in Table 5.3.

From the Table 5.3, one can see that ϵ changes rapidly from about 0.5 to nearly 1, while $\beta_{.75}$ changes only a small amount.

Table 5.3 Statistical values of the 11 spectra

Sea state	Peak rate E(P) Hz	ϵ	$\beta_{0.75}$	RMS σ (MPa)
1	.244	.506	.689	47.65
2	.247	.534	.698	41.31
3	.250	.559	.704	35.17
4	.254	.603	.717	29.79
5	.257	.651	.733	24.81
6	.260	.693	.746	19.86
7	.264	.693	.746	15.51
8	.268	.809	.787	11.68
9	.271	.862	.807	7.86
10	.275	.917	.827	4.33
11	.283	.986	.852	1.69

5.4.3.2 Structure of the new models

Fig. 5.9 illustrates the distribution of stress ranges simulated from three typical structural response spectra, (spectrum 1, spectrum 6, and spectrum 11 from Table 5.1), using 9,000 time interval points ($\triangle\tau = 1/2f_{max}$) in Eqn (4.36). In the figure, the normalised stress range is:

$$s = \frac{S}{2\sigma_x} \tag{5.45}$$

where S is the real stress range

If the simulated process has normalised stress ranges between s_i and $s_i + ds$ k times, and has the total number of stress ranges equal to n, then the ordinate in Fig. 5.9. is determined by:

$$f(s_i) = \frac{k}{n}\frac{1}{ds} \tag{5.45a}$$

The ordinate is then called the Normalised Probability Density of Stress Range (NPDSR) $f(s)$.

Fig. 5.20 shows the stress range frequencies of the 11 selected spectra by simulation and rainflow cycle counting.

From Fig. 5.20, one can see that the frequencies of the small stress range gradually become smaller, while the frequencies of the middle stress range gradually become larger, from spectrum 1 to spectrum 11, when the value of $\beta_{0.75}$ increases. Interestingly, the Weibull distribution function has the same trend. Seven typical Weibull probability density functions are plotted for different values of parameters a and b in Fig. 5.11.

The two parameter Weibull probability density function has the form

$$f(x;a,b) = \begin{cases} abx^{b-1}e^{-ax^b} & x > 0;\ a > 0\ b > 0 \\ 0 & x \leq 0 \end{cases} \tag{5.46}$$

From Fig. 5.11, one can see that when $b < 1$, the Weibull density function has a maximum value only at $s = 0$; when $a = 1$, and $b > 1$, the bigger b is , the further away the peak of $f(s)$ is from the axis $s = 0$.

Setting $b = 2$ in Eqn(5.46) gives

$$f(x;a,b) = \begin{cases} 2axe^{-ax^2} & \text{for } x > 0;\ a > 0 \\ 0 & x \leq 0 \end{cases} \tag{5.47}$$

which is the Rayleigh distribution. Four typical Rayleigh distributions are shown in Fig. 5.12. In Fig. 5.12, one can see that the larger a is, the closer the peak of $f(s)$ is to $s = 0$.

Also from Fig. 5.20 it can be seen that $f(s)$ has a strange shape which is not identical to any of the Weibull distributions. The the frequencies of th large stress range (about $s > 1.6$) remain to be almost the same. In a fatigue study, it is very important to study the effect of high stress range s, while the low stress range s may not cause any damage at all. The high tail parts of $f(s)$ are thus significant.

However, from the flexibility of two parameter Weibull distribution, the sum of two weighted Weibull distribution functions may be taken to model the individual stress range distribution frequencies and their progressive changes closely.

A model for $f(s)$ may therefore be assumed to be

$$f(s) = f_W a_1 b_1 s^{b_1-1} e^{-a_1 s^{b_1}} + (1 - f_W) a_2 b_2 s^{b_2-1} e^{-a_2 s^{b_2}} \tag{5.48}$$

$s > 0; a_1 > 0, \quad b_1 > 0; \ a_2 > 0, \quad b_2 > 0$

'a_1, b_1 are adjusted so that as $\beta_{0.75} \longrightarrow 0$ (i.e. the spectrum becomes more wide band), the primary peak of $f(s)$ appears in the position $s \longrightarrow 0$. a_2, b_2 are to maintain the second peak in $f(s)$. For a narrow band spectrum, the two Weibull distributions will both become Rayleigh distributions. The parameter f_W is used to give the correct weight of the two Weibull functions. A typical function of $f(s)$, from Eqn. (5.48) is shown in Fig. 5.13 where the first term curve and the second term curve are also clearly shown. Therefore the problem of finding $f(s)$ has simply become that of finding suitable sets of the parameters a_1, b_1, a_2, b_2, f_W. The technique is called the Combined Distribution Technique(CDT).

5.4.3.3 Determination of a_1, b_1, a_2, b_2, f_W

a_1, b_1, a_2, b_2, f_W in equation (5.48) are constants for a single spectrum but must change with the changes of spectral properties to model the change in $f(s)$. The purpose of this section is to make a_1, b_1, a_2, b_2, f_W as functions defined by spectral properties in order to make $f(s)$ in equation (5.48) fit with the simulated distribution of stress range for any general spectrum.

By definition the integral of any Weibull distribution function from zero to infinity equals 1. Therefore, from equation (5.48):

$$\int_0^\infty f(s)ds = f_W + (1 - f_W) = 1$$

As discussed in Section 5.3.1, $f(s)$ should be treated as $f(s; \beta_{0.75})$. Therefore a_1, b_1, a_2, b_2, f_W should be functions of $\beta_{0.75}$. When $\beta_{0.75} \longrightarrow 1$, the power spectrum is narrow band so that the stress range pdf should approach the Rayleigh pdf, which implies that $b_1, b_2 \longrightarrow 2$.

The 11 seastate response spectra selected, range from wide band to narrow band. The spectral properties are listed in Table 5.1, Table 5.2. Simulated stress range frequencies of occurrence, from spectrum 1, spectrum 6 and spectrum 11 are shown in Fig. 5.9.

The following procedure has been adopted to determine the values of a_1, b_1, a_2, b_2, f_W. This procedure is a graphical fit procedure.

(1) *choose some initial values for* a_1, b_1, a_2, b_2, f_W For instance, with two Weibull distribution functions, equal weight may be given to each of them (i.e. f_w=.5), and for the second peak, $b_2 = 2$.

(2) *choose the remainder of the parameters* a_1, b_1, a_2, b_2, f_W *as functions of* $\beta_{0.75}$ *and undecided exponents* x_i The function can initially be set intuitively, and can be altered according to the situation to fit with the simulated $f(s)$. The number of undecided exponents x_i should be big enough to accommodate the changes of different $f(s)$ resulting from different spectra, and should be simple enough to manipulate.

(3) *determine the undecided exponents* x_i *to fit* $f(s)$ *for general spectrum* This can be carried out by fitting the curve for frequencies from the wide band spectrum 1, and then fitting the curve for frequencies from the narrow band spectrum 11 without changing the values of parameters for spectrum 1, and then fitting for frequencies from other spectra without changing much the values of parameters for previous spectra. Normally if $f(s)$ curves for spectrum 1, spectrum 6 and spectrum 11 fit with the simulated results, the rest of the curves will grossly fit with the simulated results.

(4) *go to step 2 and try a new set of* a_1, b_1, a_2, b_2, f_W

(5) *repeat step (3)*

(6) *compare the results*

(7) *check validity by* χ^2 *test* It could be a further enhancement to the step 3 graphical fit.

As a first attempt:

(1) Assume $b_2 = 2$ and $a_2 = 0.5$ from which the second term in the right side of Eqn(5.48) is a Rayleigh distribution.

(2) Assume $b_1 = 1+\beta_{0.75}^{x_1}$, where x_1 is a constant which makes $b_1 \longrightarrow 2$ when $\beta_{0.75} \longrightarrow 1$ and $b_1 \longrightarrow 1$ when $\beta_{0.75} \longrightarrow 0$. Also it can be assumed that :

$$a_1 = \frac{(2-\beta_{0.75}^{x_2})^{x_3}}{b_1} \tag{5.49}$$

where x_2, x_3 are constants. When $\beta_{0.75} \longrightarrow 1, a_1 \longrightarrow 0.5$, f_W is constant

(3) By trial and error, x_1, x_2, x_3, and f_W were determined to be 4, 2, 4 and 0.55 to fit the simulated results.

$$\left.\begin{aligned} b_1 &= 1+\beta_{0.75}^4 \\ a_1 &= \frac{(2-\beta_{0.75}^2)^4}{b_1} \\ b_2 &= 2 \\ a_2 &= 0.5 \\ f_W &= 0.55 \end{aligned}\right\} \tag{5.50}$$

This is called **model 1**. The $f(s)$ from this model are compared with the simulated results for spectra 1, 6 and 11 in Fig. 5.14. The 11 $f(s)$ of model 1 for the 11 spectra are shown in Fig. 5.15.

(4) In model 1, a_2, b_2 are invariables with $\beta_{0.75}$. In order to obtain a better model for $f(s)$, a_2 is now taken as a decreasing function of $\beta_{0.75}$ while b_2 remains equal to 2; f_W is also a variable, taken as a function of $\beta_{0.75}$.

(5) Set

$$a_2 = \frac{(2-\beta_{0.75})^{x_2}}{b_2}$$

Also, f_W is to be a function of $\beta_{0.75}$. By repeating the same approach as in (3), one obtains:

$$\left.\begin{aligned} b_1 &= 1 + \beta_{0.75}^4 \\ a_1 &= \frac{(2 - \beta_{0.75}^2)^5}{b_1} \\ b_2 &= 2 \\ a_2 &= \frac{(2 - \beta_{0.75})^{.25}}{b_2} \\ f_W &= 0.2 + 0.35\sqrt{\beta}_{0.75} \end{aligned}\right\} \tag{5.50}$$

This will be called **model 2**. The $f(s)$ from this second model are compared with the simulated results for spectra 1, 6 and 11 in Fig. 5.16. The 11 $f(s)$ of model 2 for the 11 spectra are shown in Fig. 5.17.

In a fatigue analysis, the stress ranges of high value will have more severe effect and thus should be paid higher attention. So in a new round of curve fitting, in step (3) the manipulation is specially aimed to fit the stress ranges densities in the high tail with a_2 being an increasing function of $\beta_{0.75}$. By adopting the same strategy, it is then decided that:

$$\left.\begin{aligned} b_1 &= 1 + \beta_{0.75}^4 \\ a_1 &= \frac{(2 - \beta_{0.75}^2)^5}{b_1} \\ b_2 &= 2 \\ a_2 &= \sqrt{(1 + \beta_{0.75}^6)} \\ f_W &= 1.3 - 1.1\beta_{0.75} \end{aligned}\right\} \tag{5.51}$$

This will be called **model 3**. The $f(s)$ from model 3 in comparison with the simulated results for spectra 1, 6 and 11 are shown in Fig. 5.18. The 11 $f(s)$ of model 3 for the 11 spectra are shown in Fig. 5.19.

(7) Validity tests are to be carried out in Section 5.4.4.

(8) The application of equivalent stress range is carried out in chapter 6.

5.4.4 Validity test

The models for $f(s)$ obtained by CDT were determined on the basis of a graphical fit with the simulated histogram of stress ranges. The validity of these assumed distributions should be verified statistically by goodness-of-fit tests.

One of the commonly used goodness-of-fit tests is the χ^2 test for distribution [5.31].

Consider a sample of n simulated values of the stress ranges. The χ^2 goodness-of-fit compares

Table 5.4 χ^2 test results

$$\frac{\chi^2_{399}}{399} = \sum_{i=1}^{400} \frac{(nc_i - e_i)^2}{e_i} \frac{1}{399}$$

Sea state	model 1	model 2	model 3	Rayleigh
1	.959	1.169	1.095	69.294
2	.846	1.012	.943	52.900
3	.869	.993	.993	56.538
4	.831	.902	.920	44.211
5	.869	.880	.884	40.973
6	.905	.878	.910	32.360
7	.960	.912	.893	25.206
8	1.050	1.010	.923	22.081
9	1.036	1.000	.906	14.410
10	1.163	1.170	1.042	14.064
11	1.299	1.364	1.192	10.964

the simulated frequencies $nc_1, nc_2, ..., nc_k$ of k values of the stress ranges with the corresponding frequencies $e_1, e_2, ..., e_k$ from the proposed theoretical models of equation (5.48). The quantity in this comparison is:

$$q = \sum_{i=1}^{k} \frac{(nc_i - e_i)^2}{e_i} \tag{5.52}$$

which approaches the chi-square (χ_f^2) distribution with ($f = k-1$) degrees of Ωfreedom as $n \longrightarrow \infty$. Values of χ^2_f are tabulated for various significance levels[5.31]. If q is less than the value of χ^2 then the model is acceptable at that significance level. It should also be pointed out that the results of χ^2 test be treated in relative terms rather than in absolute terms as there is arbitrariness in the choice of significance level.

For each spectrum, (i.e. for each value of $\beta_{0.75}$ and σ_x), there is a set of a_1, b_1, f_W, a_2, b_2, for each of the three models. $f(s)$ can be obtained from equation (5.48) so $e_1, e_2, ..., e_k$ can be calculated. Taking $k = 400$ and $s_{max} = 4$,

$$e_i = f(s_i)ds_i \times number\ of\ stress\ ranges$$

By simulation and counting for each of the 11 spectra, $nc_1, nc_2, ..., nc_k$ can be obtained with 90,000 points generated. The results of χ^2 test results on the three proposed models together with Rayleigh distribution test results are shown in Table 5.4.

The Rayleigh distribution has very large test results, which gradually become smaller as the spectrum approaches the narrow band spectrum. With $k = 399$, all the test values from three proposed models are very similar and much smaller than those from the Rayleigh distribution. All the $q/399$

values are within the band of [0.831, 1.364] . The significance level of 0.50 has a test result of 1.0. With k as big as 400, this χ^2 test results show that the proposed models all have χ^2 test result close to 1., and .thus are satisfactory.

It can be seen that in these three models there is no single set of parameter a_1, b_1, f_W, a_2, b_2 which is absolutely superior to the other sets. The constants x_i, in the set, are all simple integer numbers or values with not more than two decimal points. This can be explained partly by the empiricism of each model and by the probabilistic nature of stochastic loading processes, in which any model would only fit for a random number set, within certain bands of confidence.

5.5 Conclusions

The fatigue effects of a random cyclic loading process, especially for offshore structural response, have been investigated. The loading variables are treated as numbers of cycles of stress ranges, derived from the rainflow method, subjected to the random cyclic loading process. A set of new models for stress range pdf $f(s)$ obtained by the combined distribution technique (CDT) have been found to fit the simulated stress range frequency of occurrence. The validity test and graphical demonstration show that pdf $f(s)$ is almost exact in most cases.

It is found that the stress range pdf $f(s)$ from the rainflow counting method can be considered as the sum of two weighted Weibull distributions with parameters defined by the spectral properties. Therefore, without going through cumbersome simulation and cycle counting, one can obtain the numbers of cycles of stress ranges directly from the response spectrum, knowing its spectral properties. This discovery saves time in reaching a solution for fatigue effects under random loading.

In this chapter, only offshore structural response spectra are studied in detail. It is important to stress that any other power spectrum in the frequency domain could be generated as a time series in this way for fatigue study, and thus the probability distribution models developed in this chapter will not be limited only to offshore applications. In fact, various workers in the past have generated time series for other spectra to study fatigue performance[5.5],[5.6] and found that there is a general trend between damage correction factor λ and spectral properties. The only parameters which are of significance in the time series generation are the mathematical properties of the spectra no matter what sources the spectra are from. However, when applying to other kinds of spectra, if the results are not quite satisfactory, the strategy adopted in section 5.4.4.2 can be used to form a new kind of $f(s)$. The analytical solution for $f(s)$ would be expected to have a complex form. However the $f(s)$ obtained in the thesis is relatively simple and easy to apply.

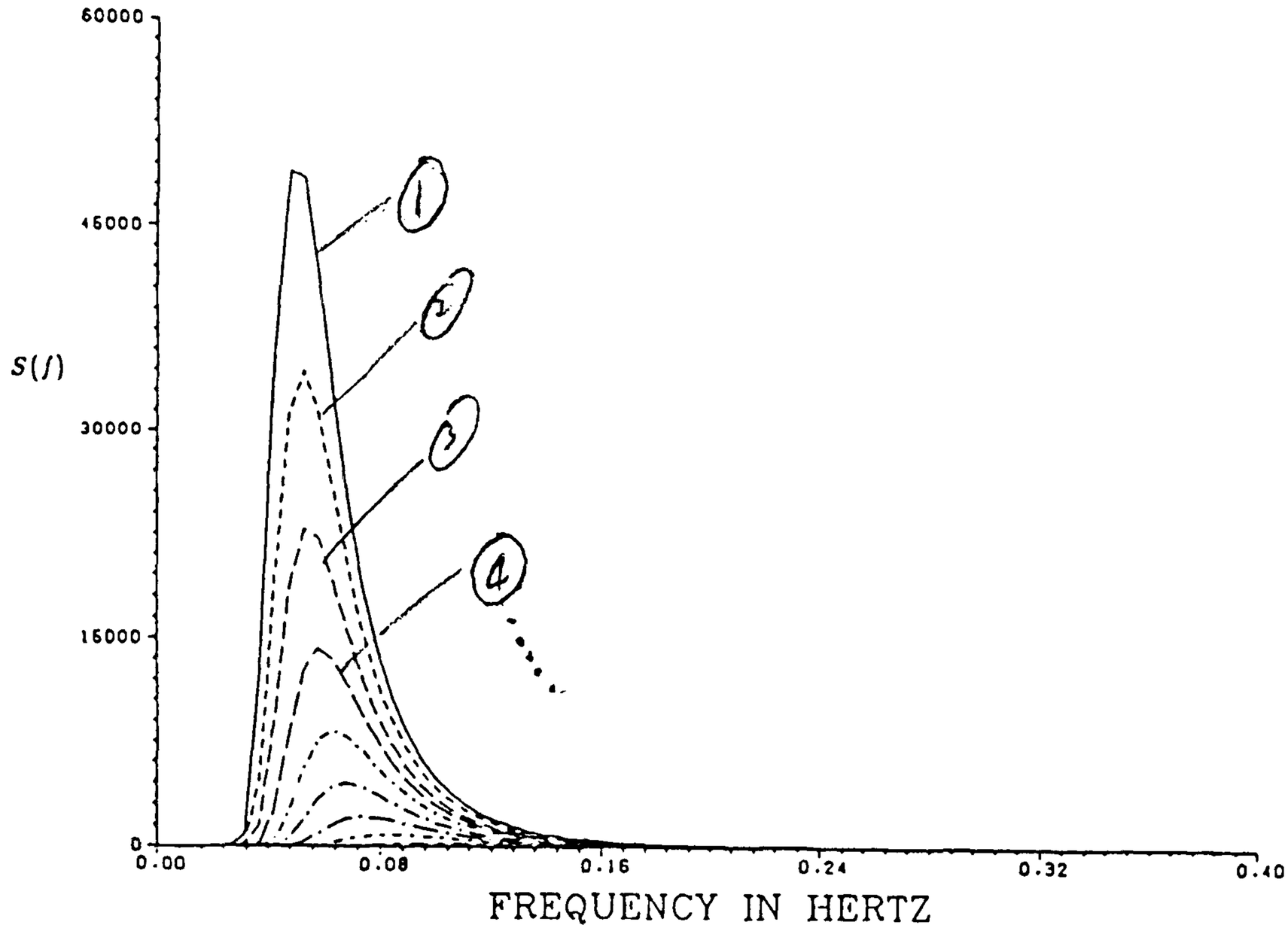

Fig. 5.1 Seastate spectra

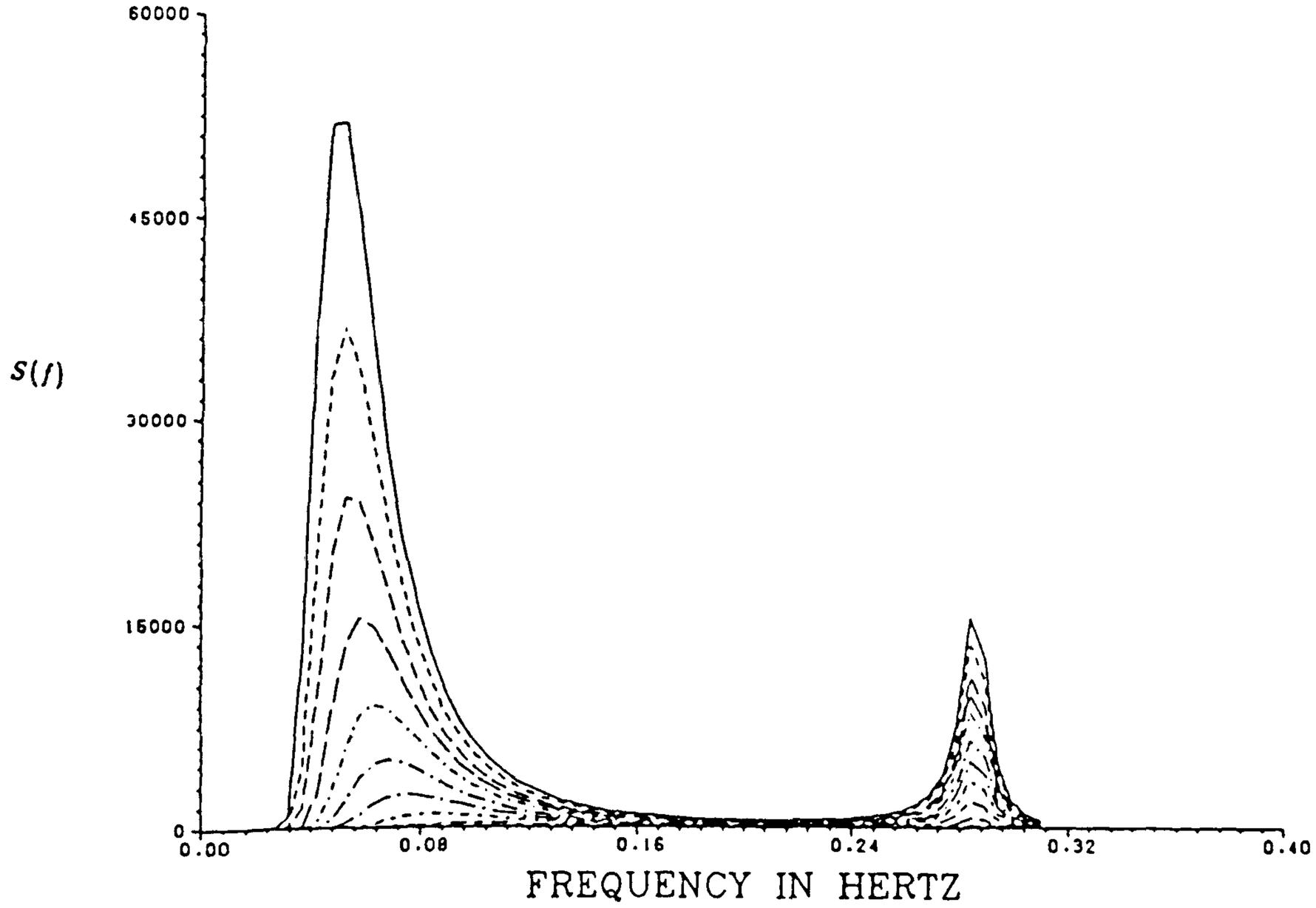

Fig. 5.2 Double peak response spectra

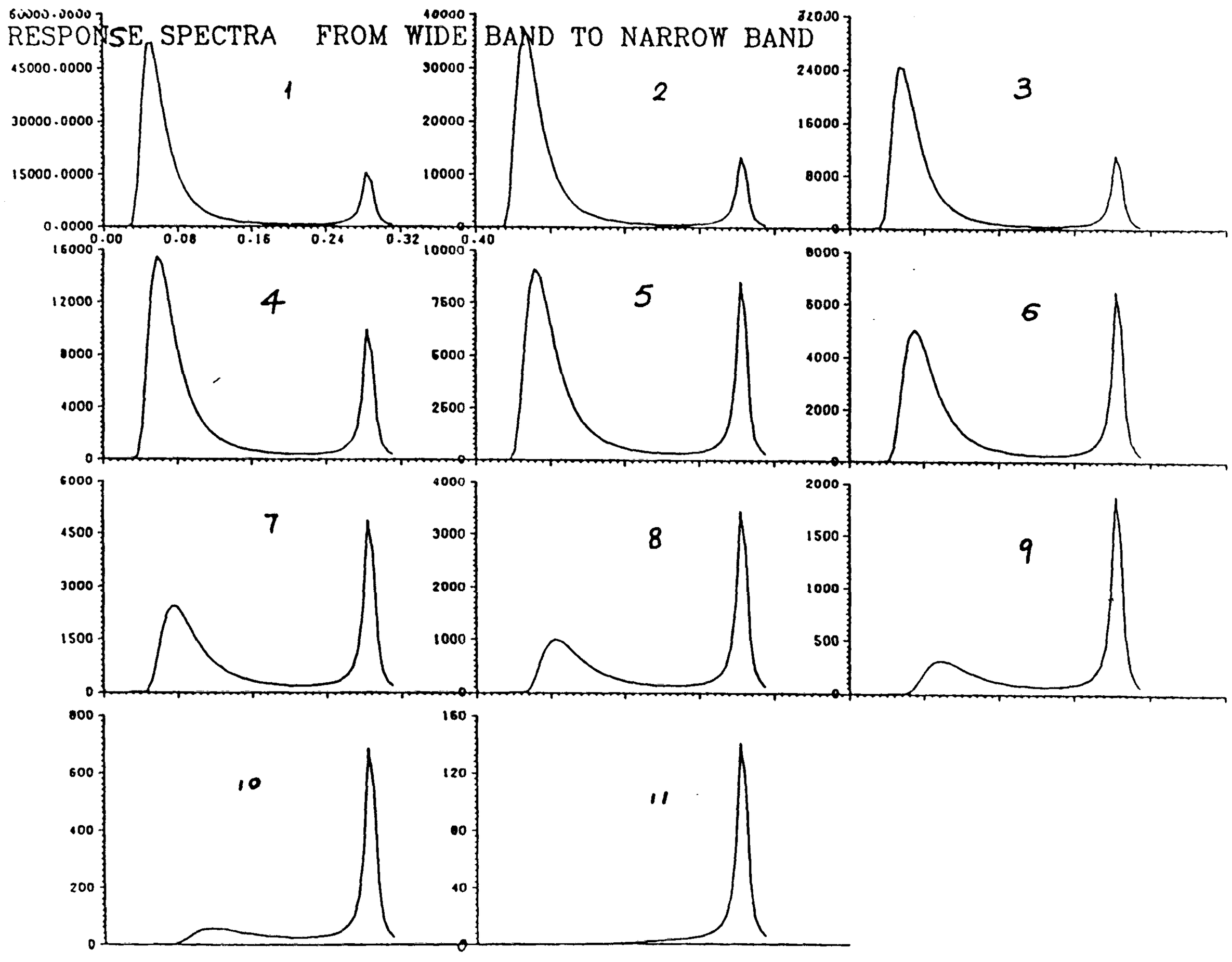

Fig. 5.3 Separated response spectra

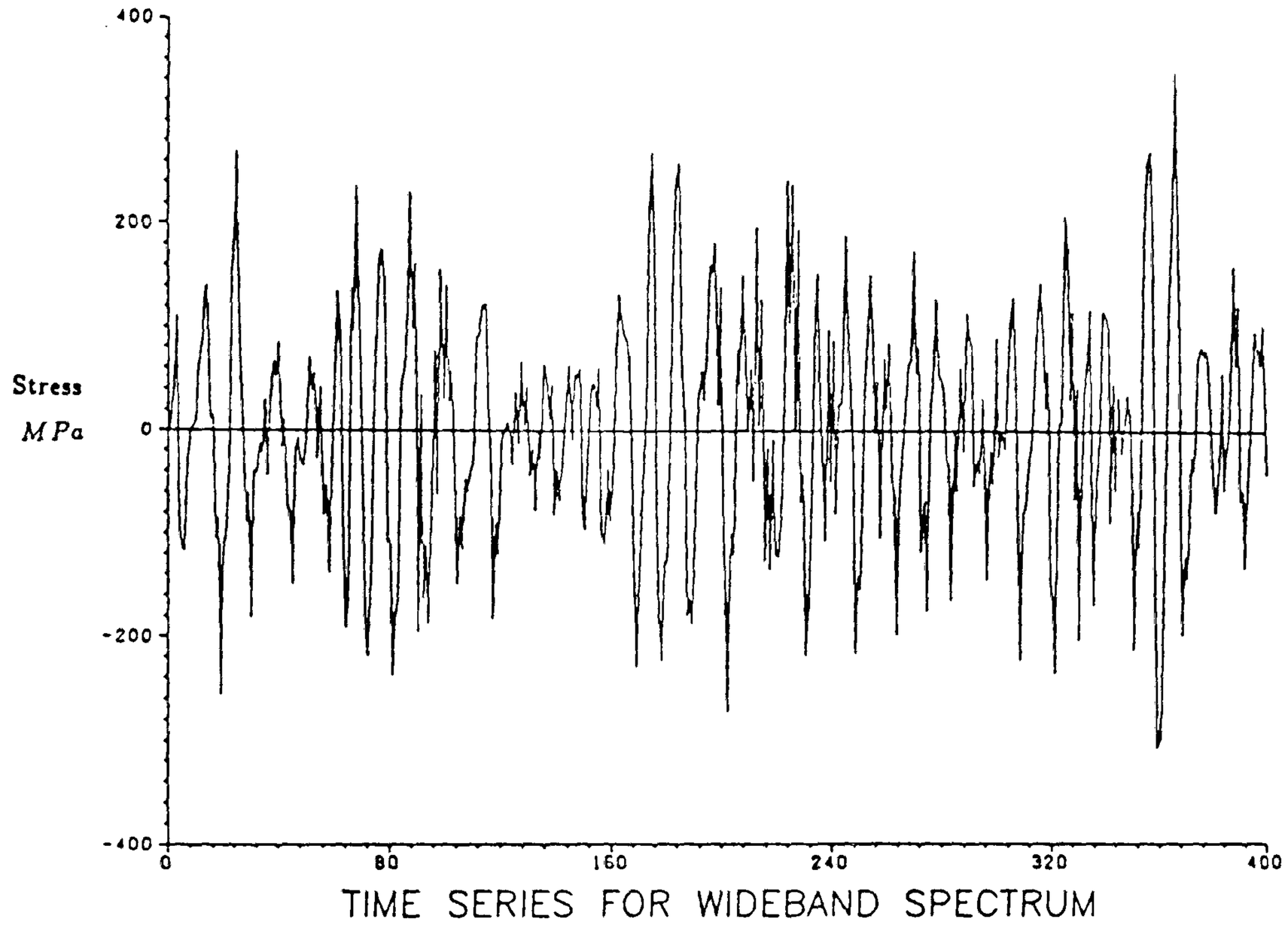

Fig. 5.4 Time series from spectrum 1

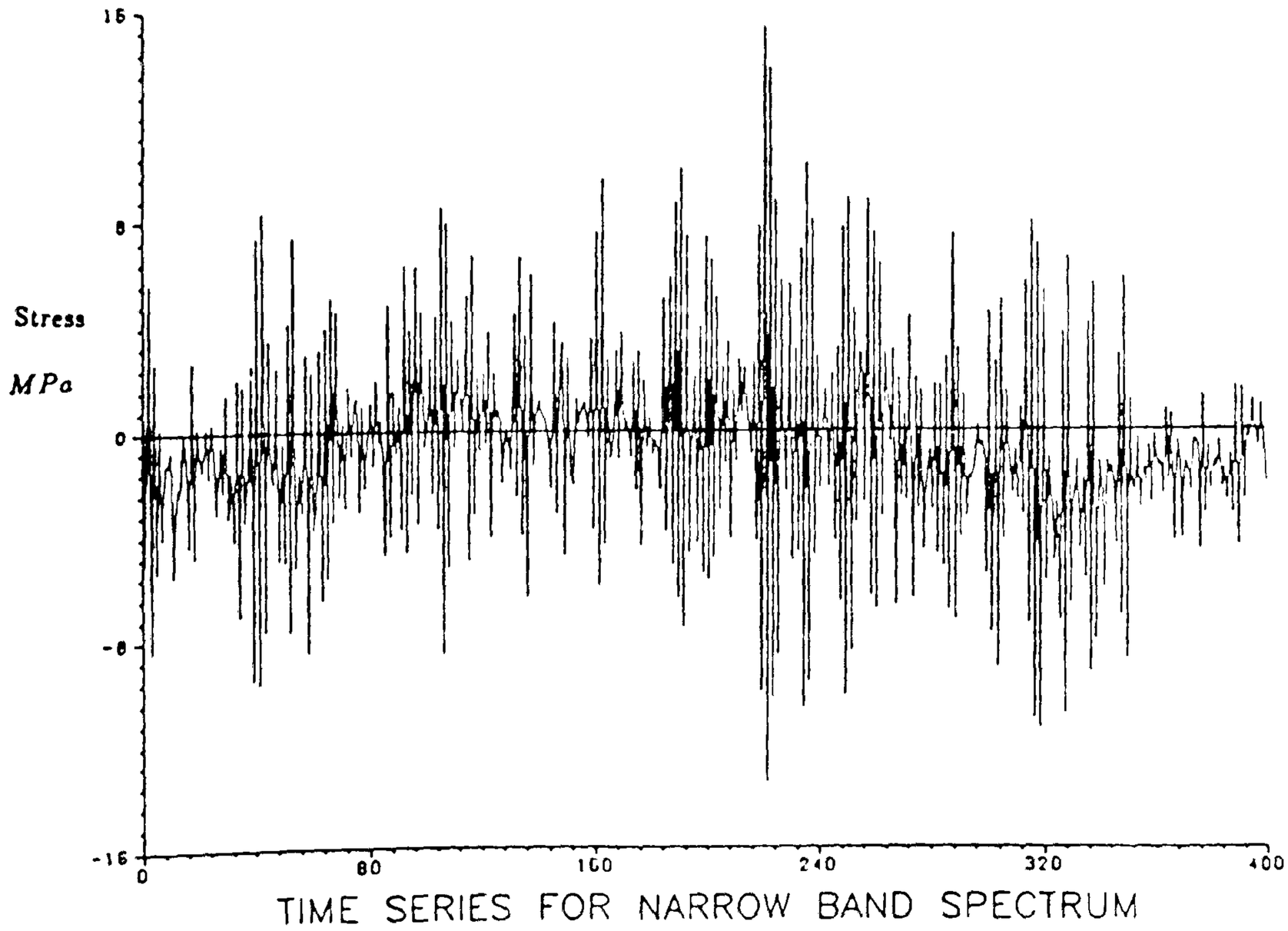

Fig. 5.5 Time series from spectrum 11

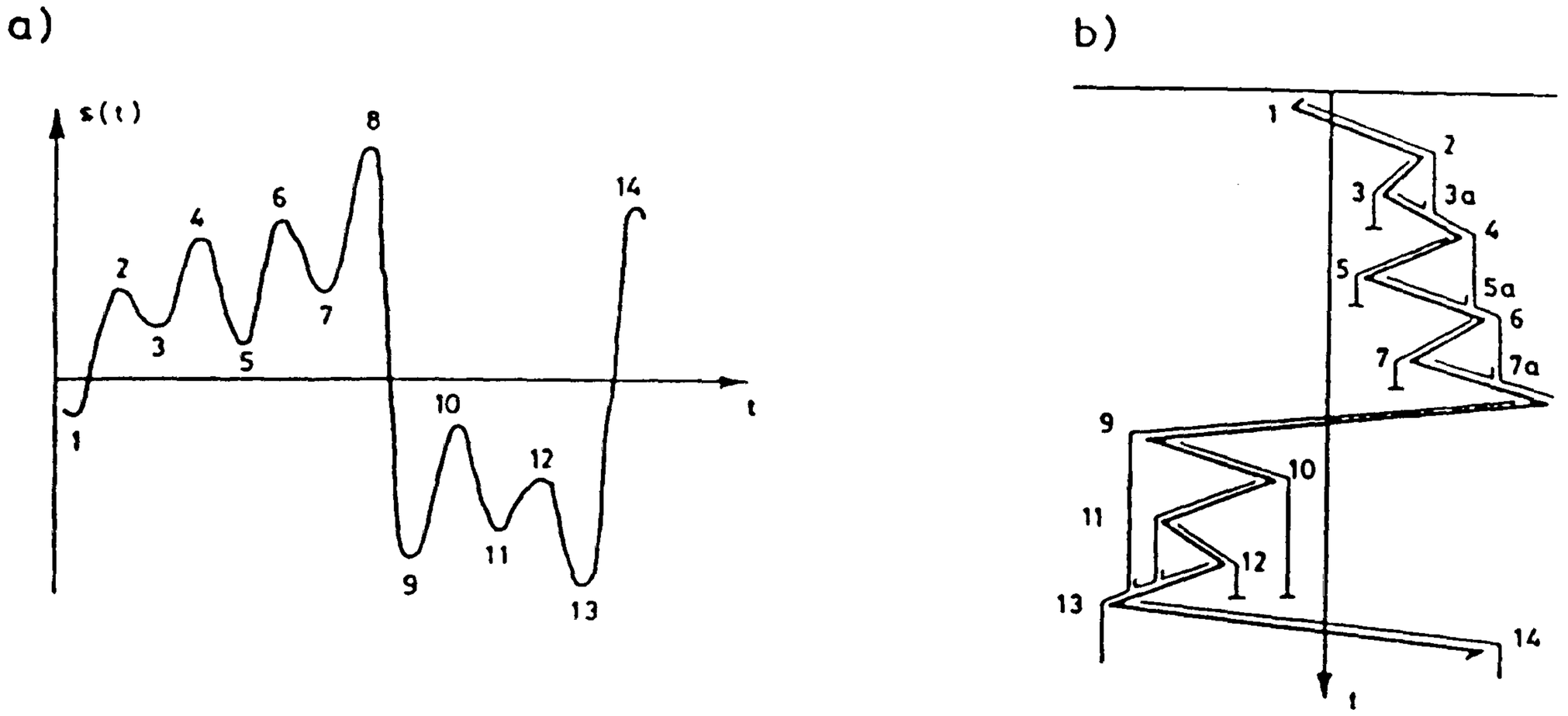

Application of rain-flow counting to a stress history

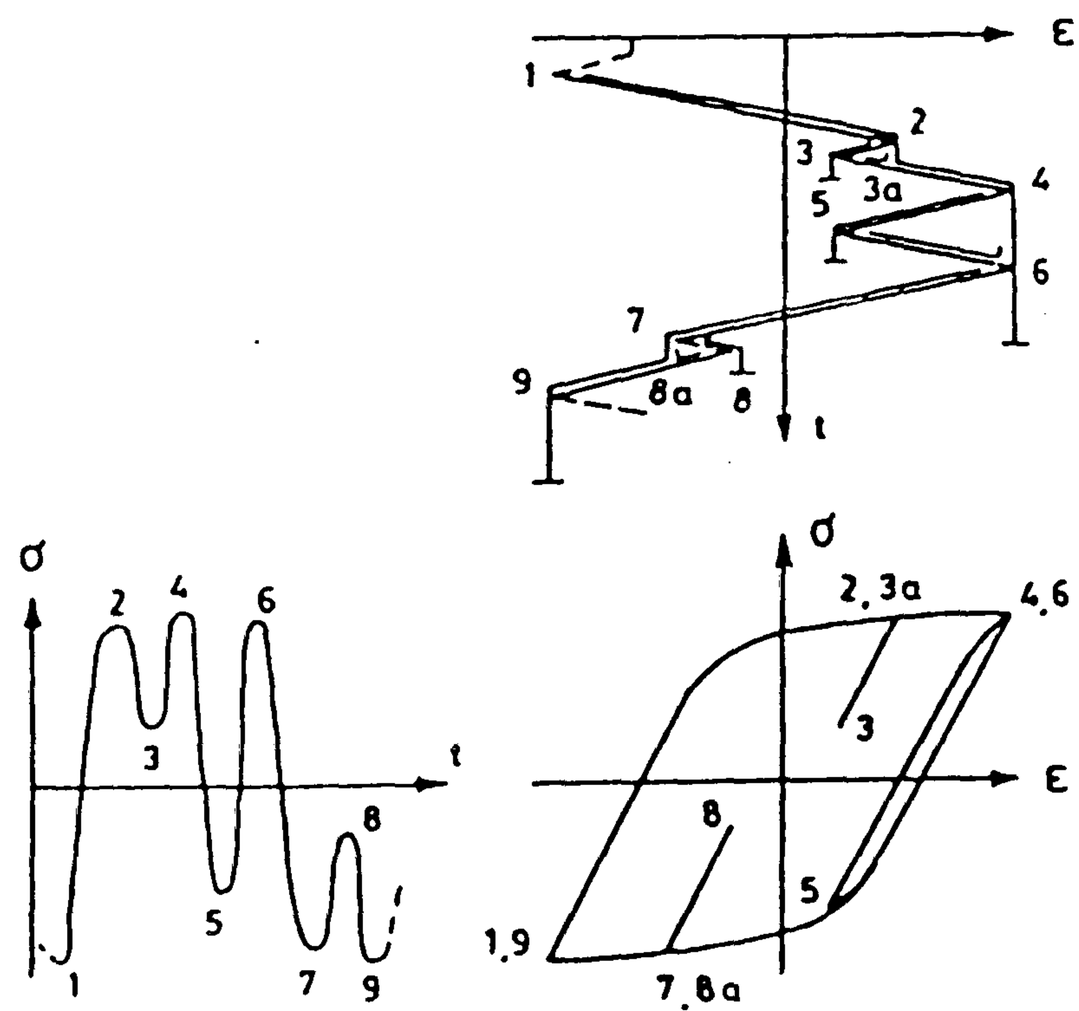

Application of rain-flow counting to a low-cycle high strain history

Fig. 5.6 Illustration of the rainflow counting method from ref. [5.8]

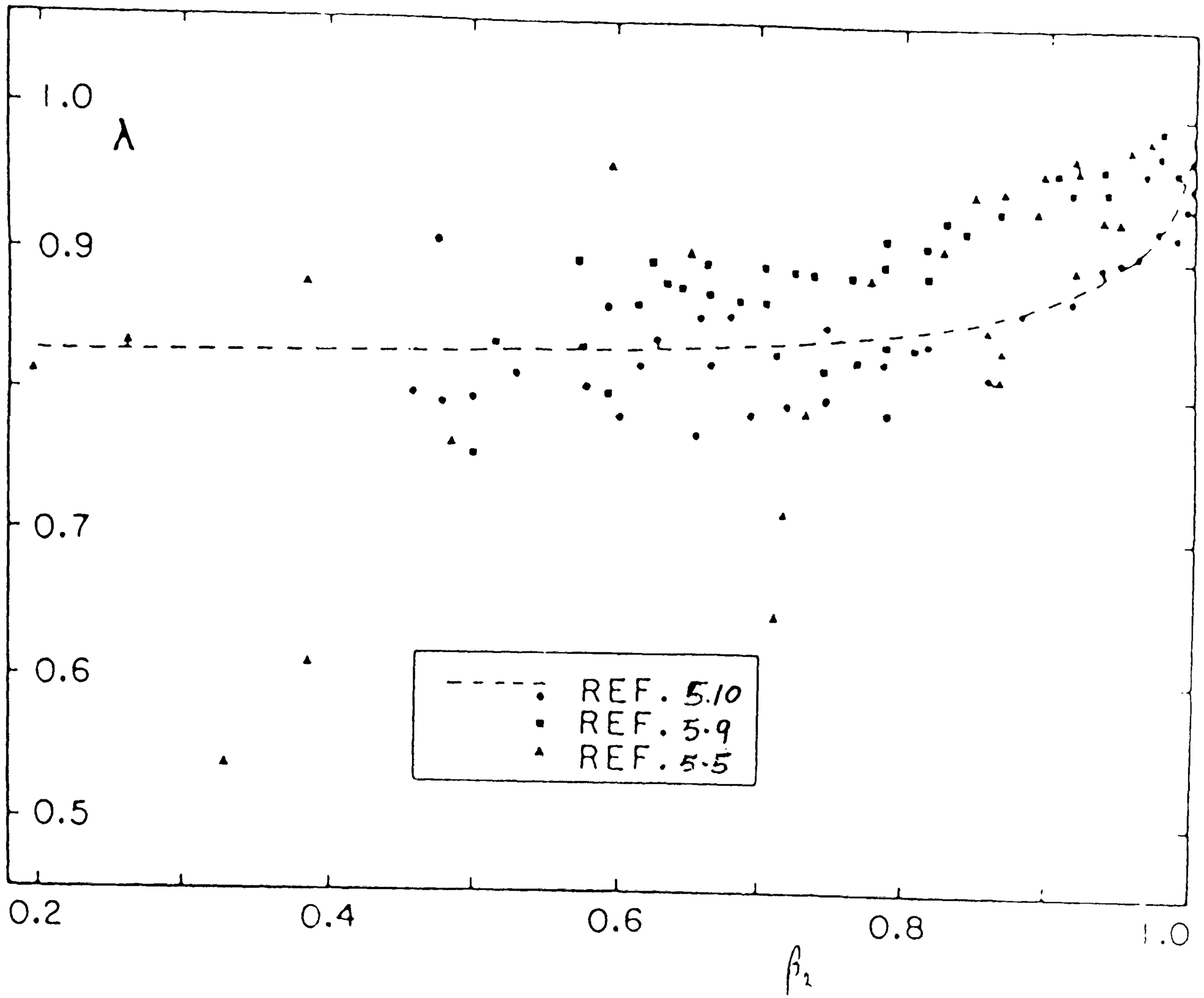

Fig. 5.7 Effect of bandwidth on correction factor

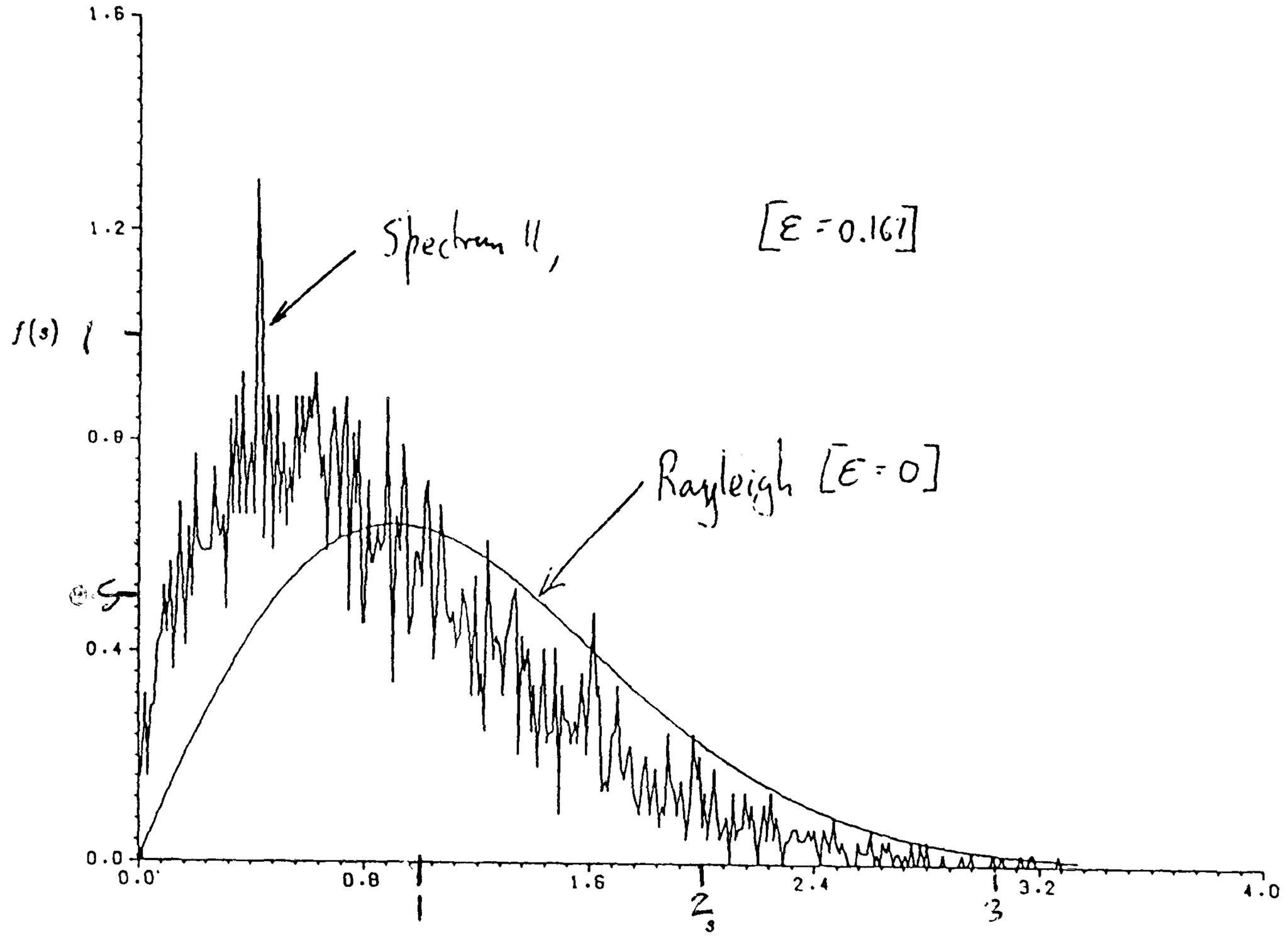

Fig. 5.8 Comparison of Rayleigh distributions and stress range distribution of spectrum 11 from simulation

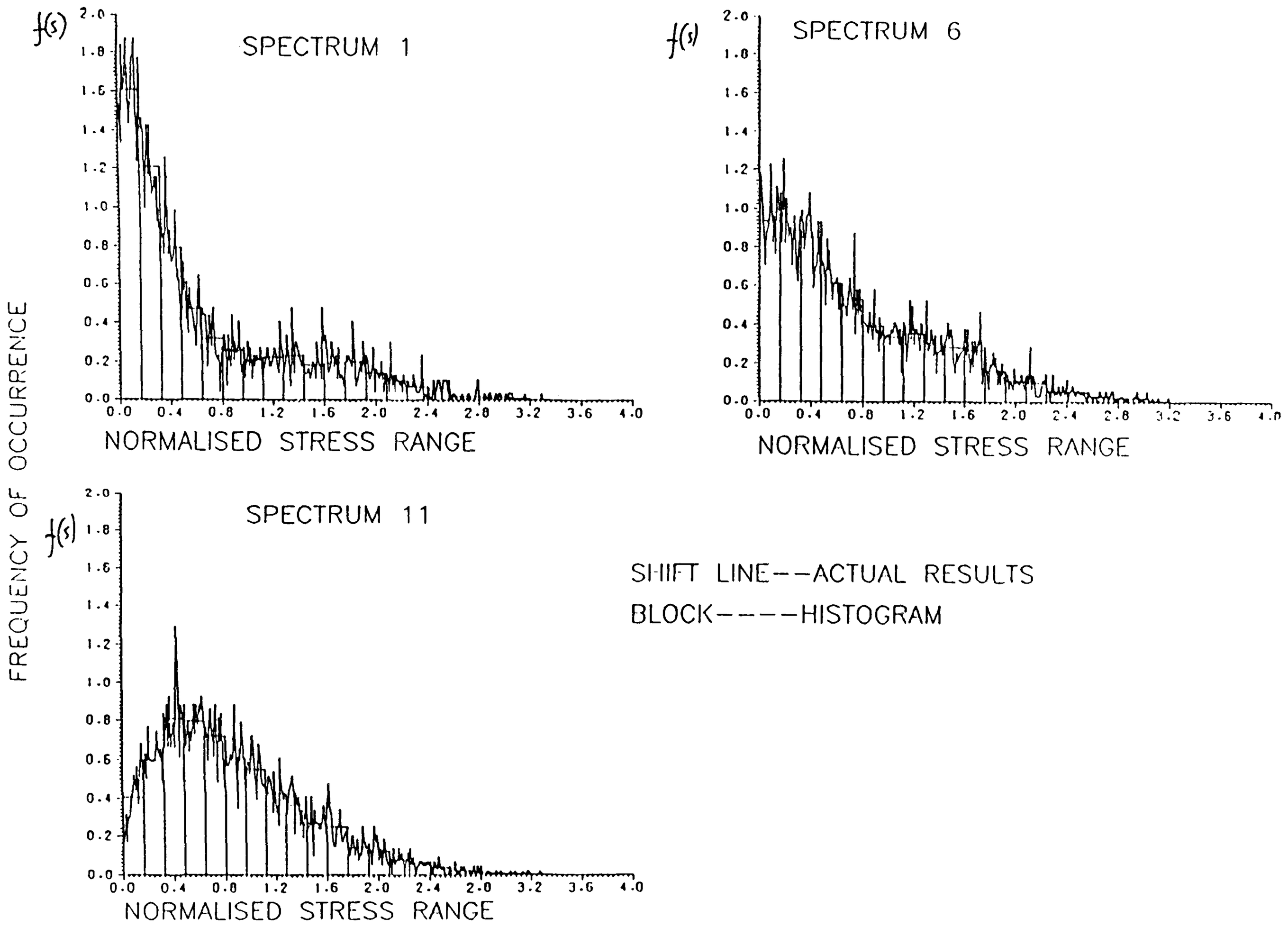

Fig. 5.9 Stress ranges histograms for spectra 1, 6 and 11

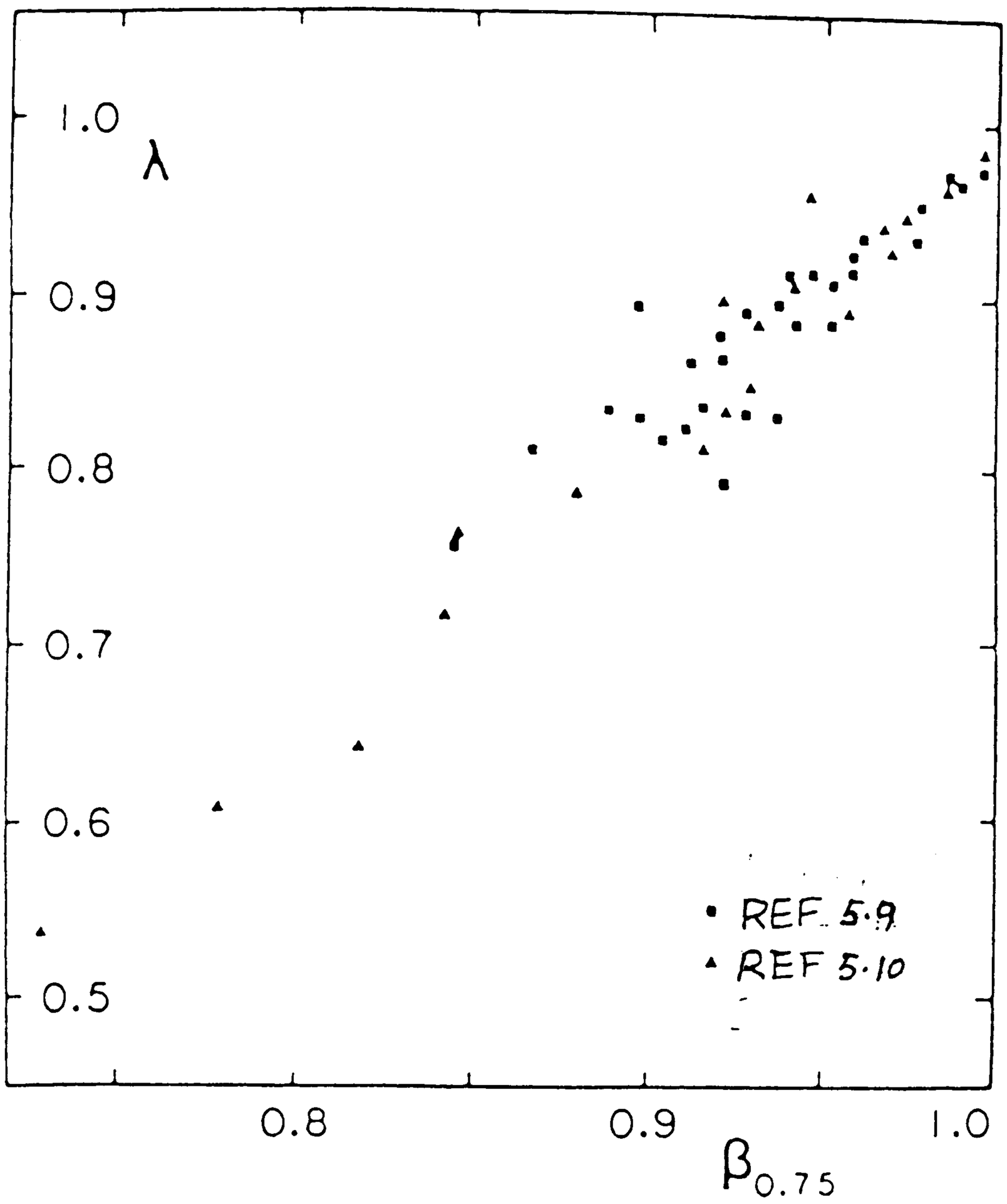

Fig. 5.10 Effect of alternative bandwidth on correction factor

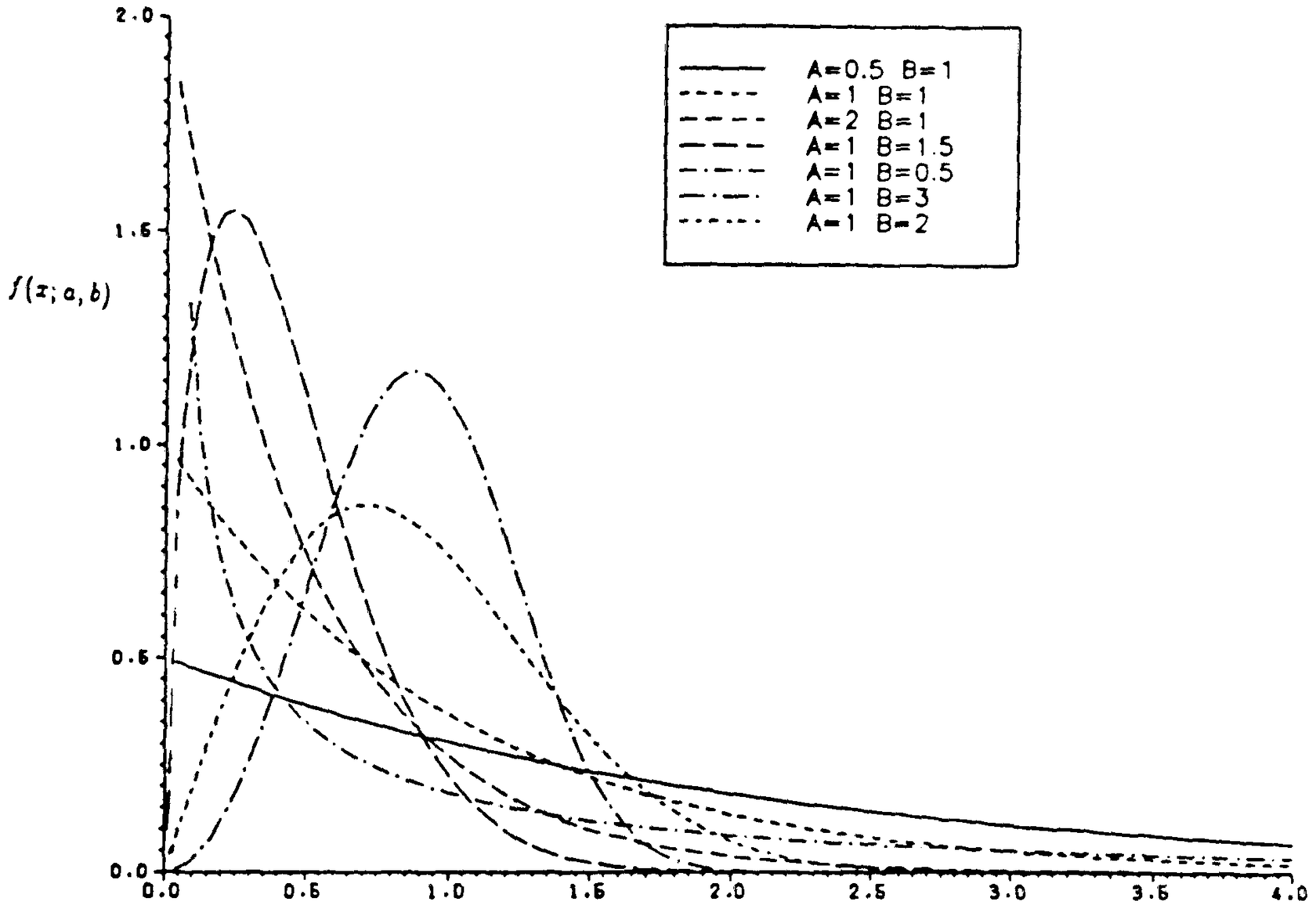

Fig. 5.11 Weibull distribution

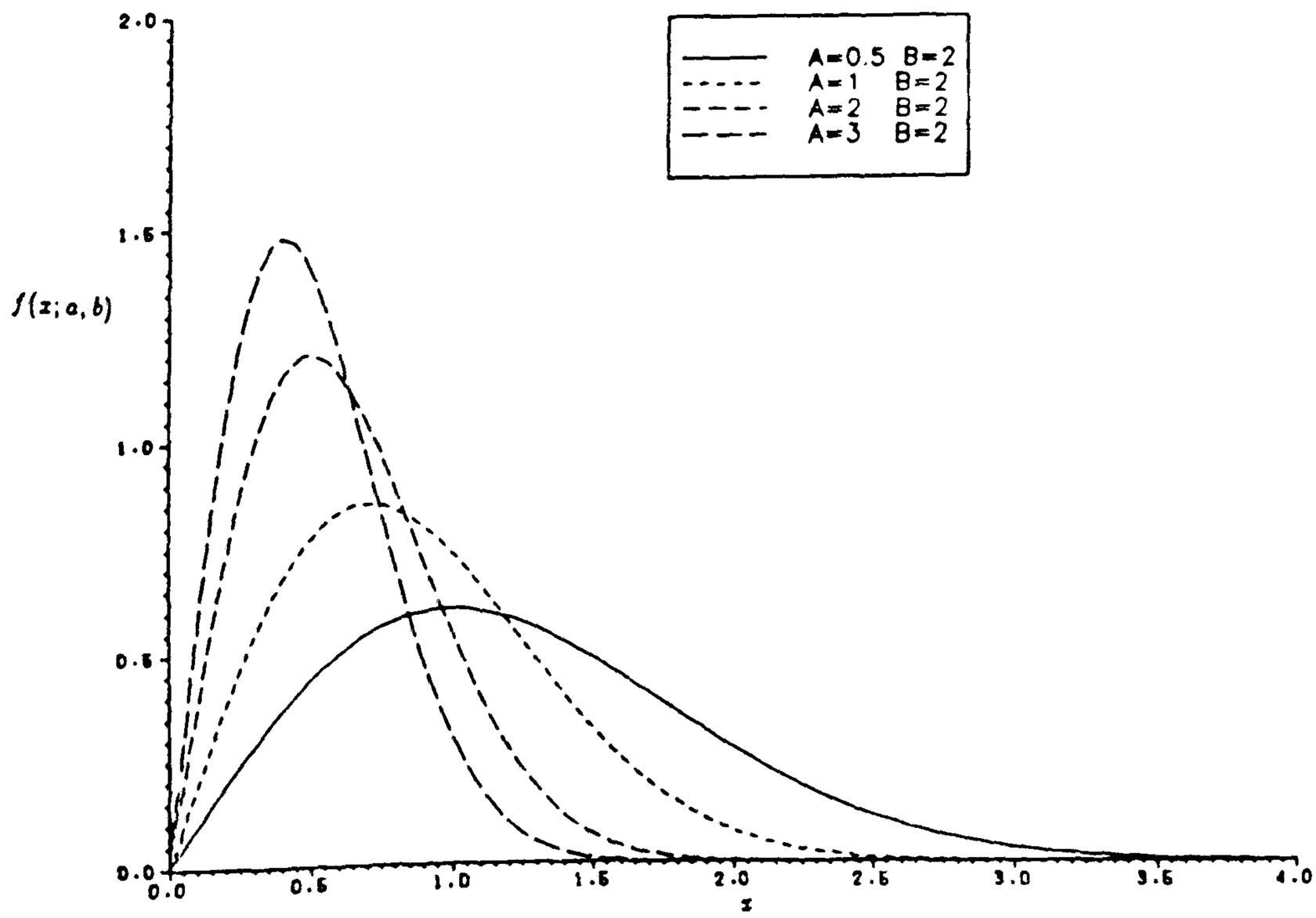

Fig. 5.12 Rayleigh distribution

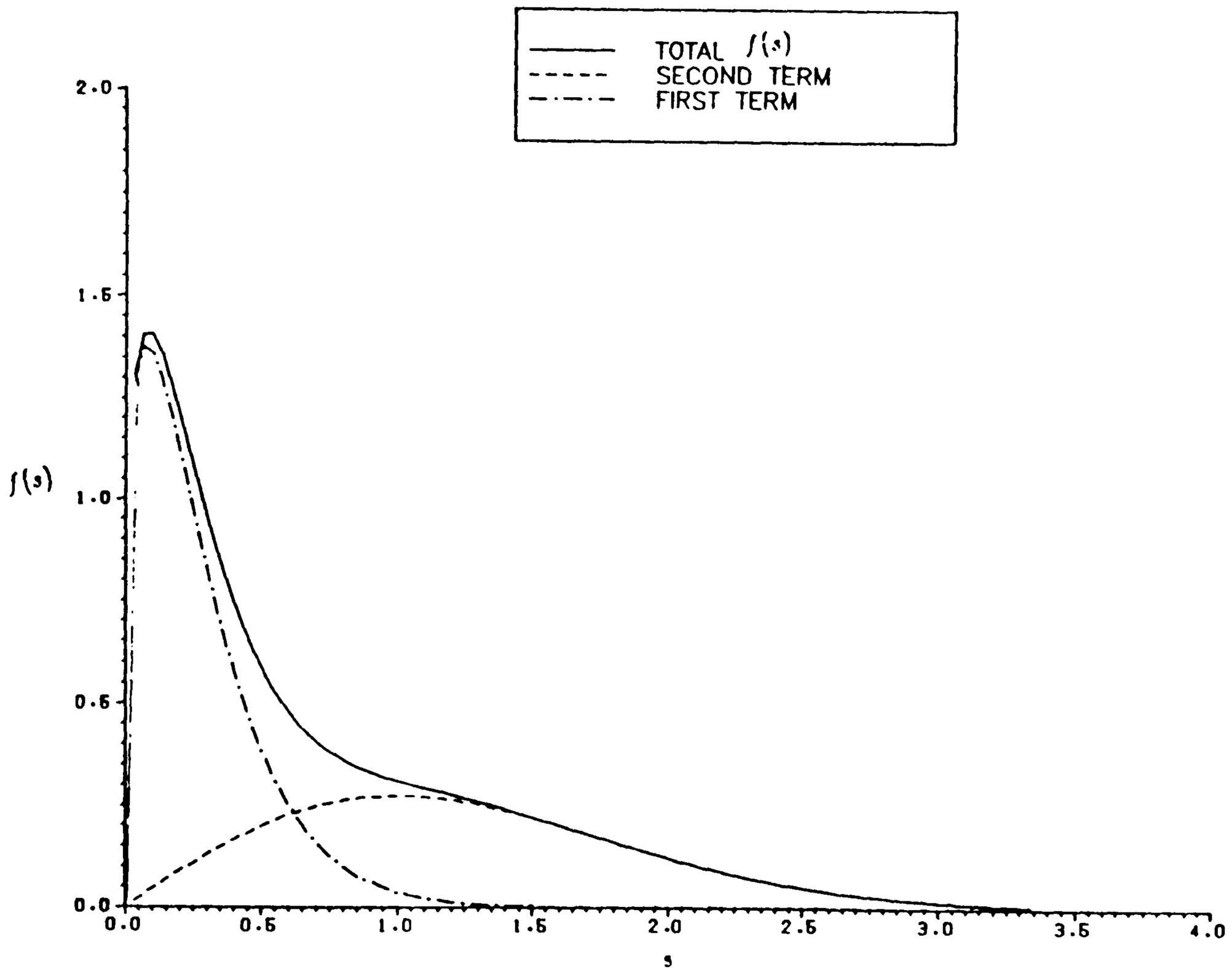

Fig. 5.13 Structure of the new $f(s)$

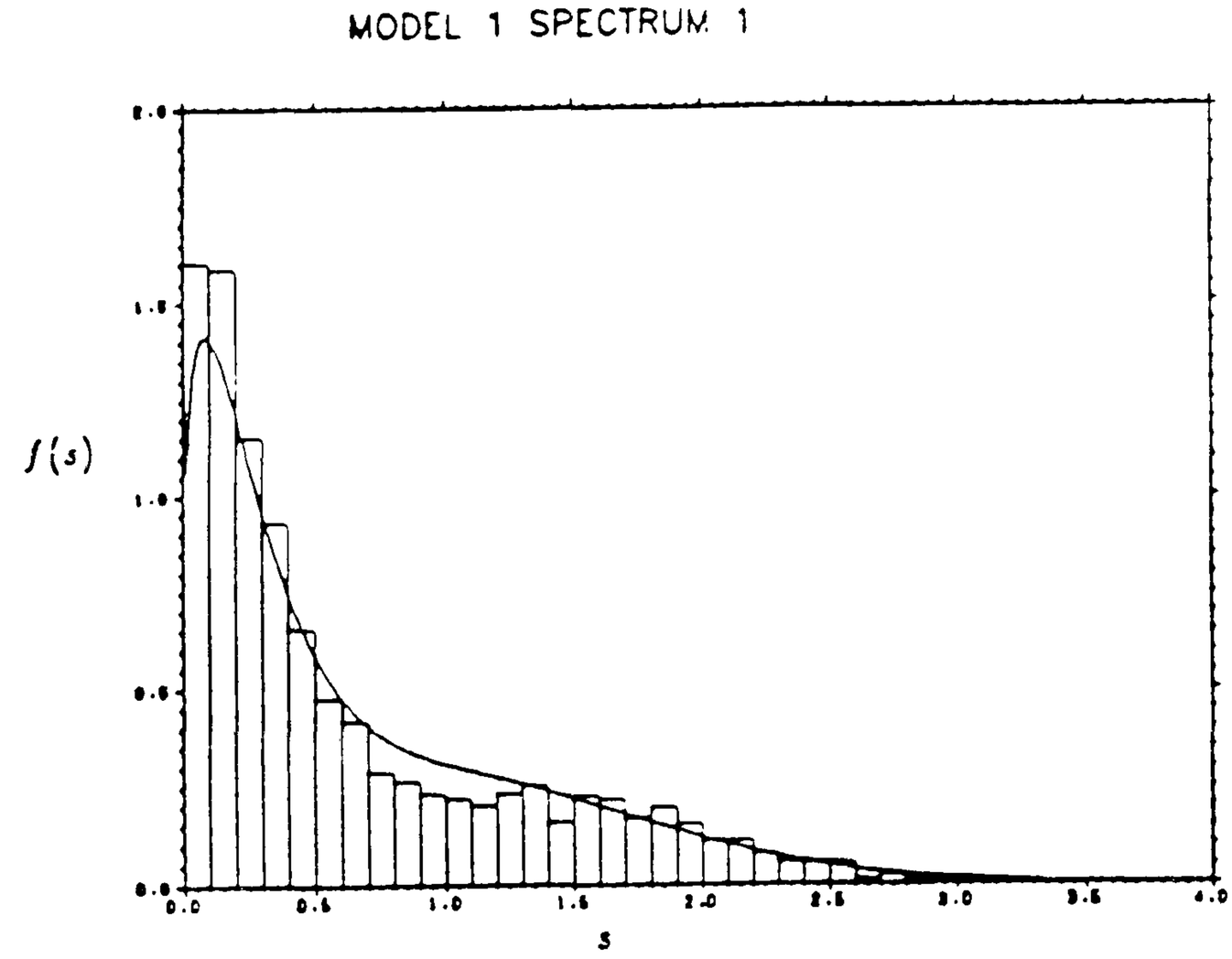

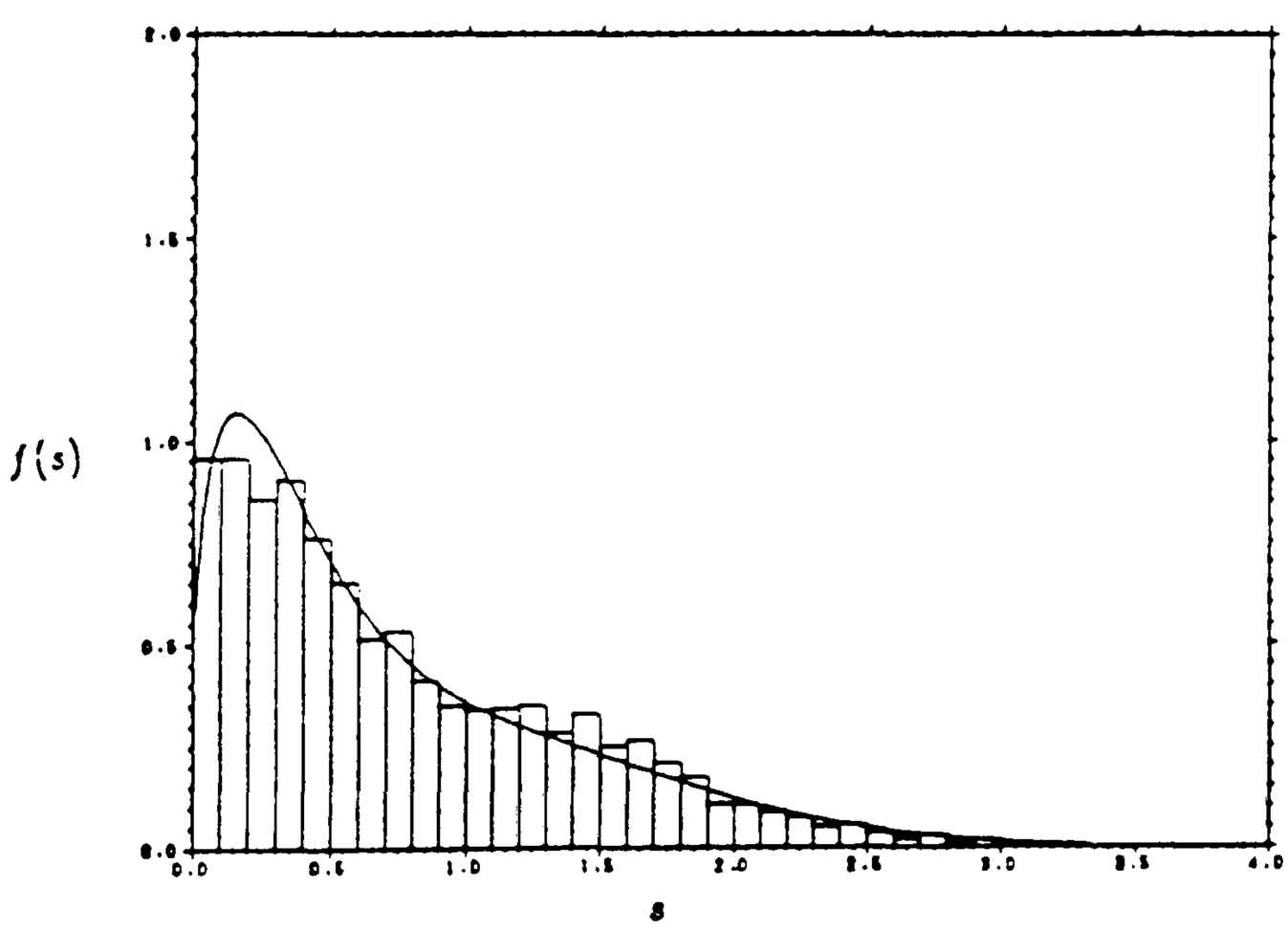

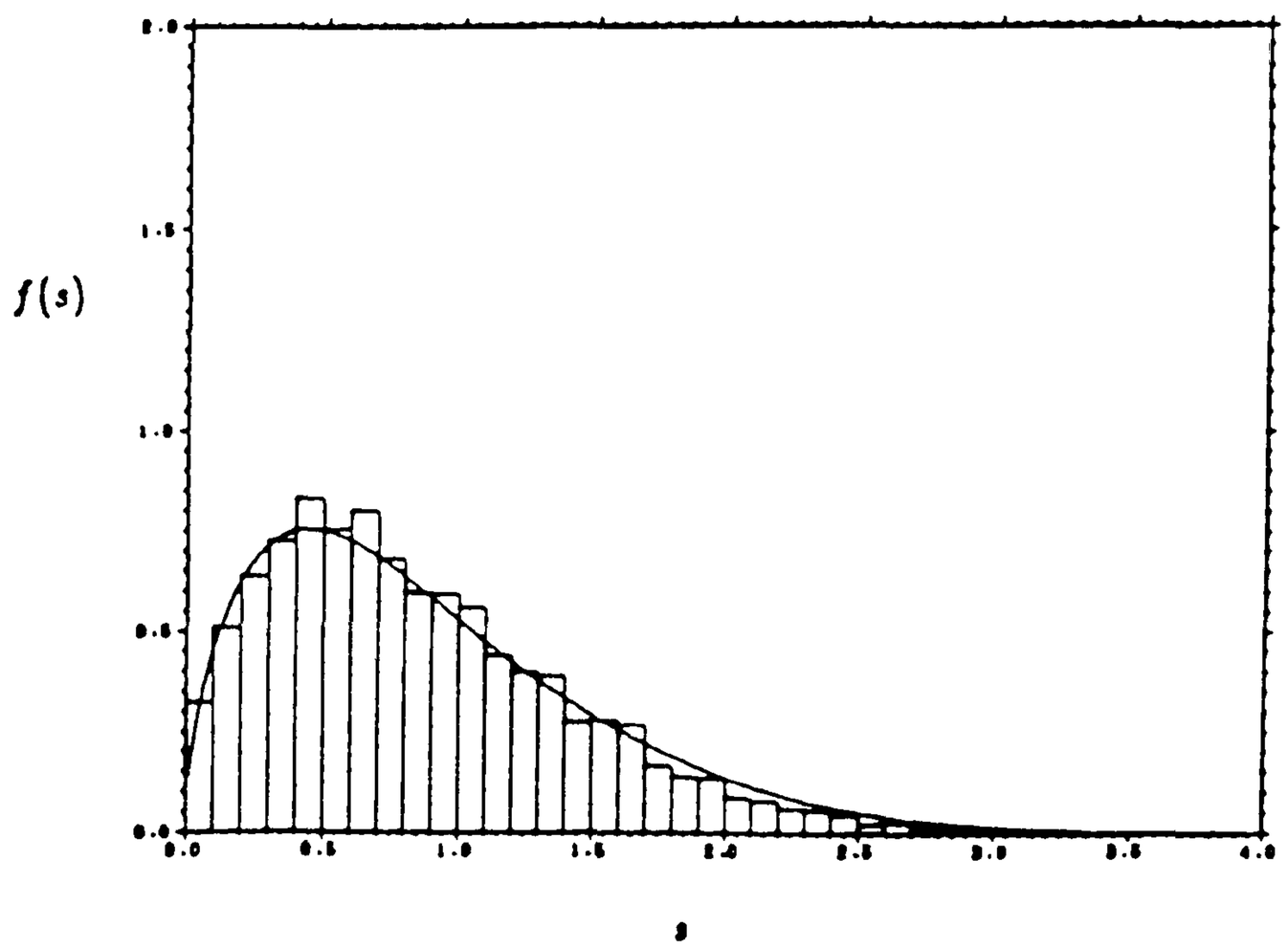

Fig. 5.14 Proposed model 1 for $f(s)$ for spectra 1, 6 and 11

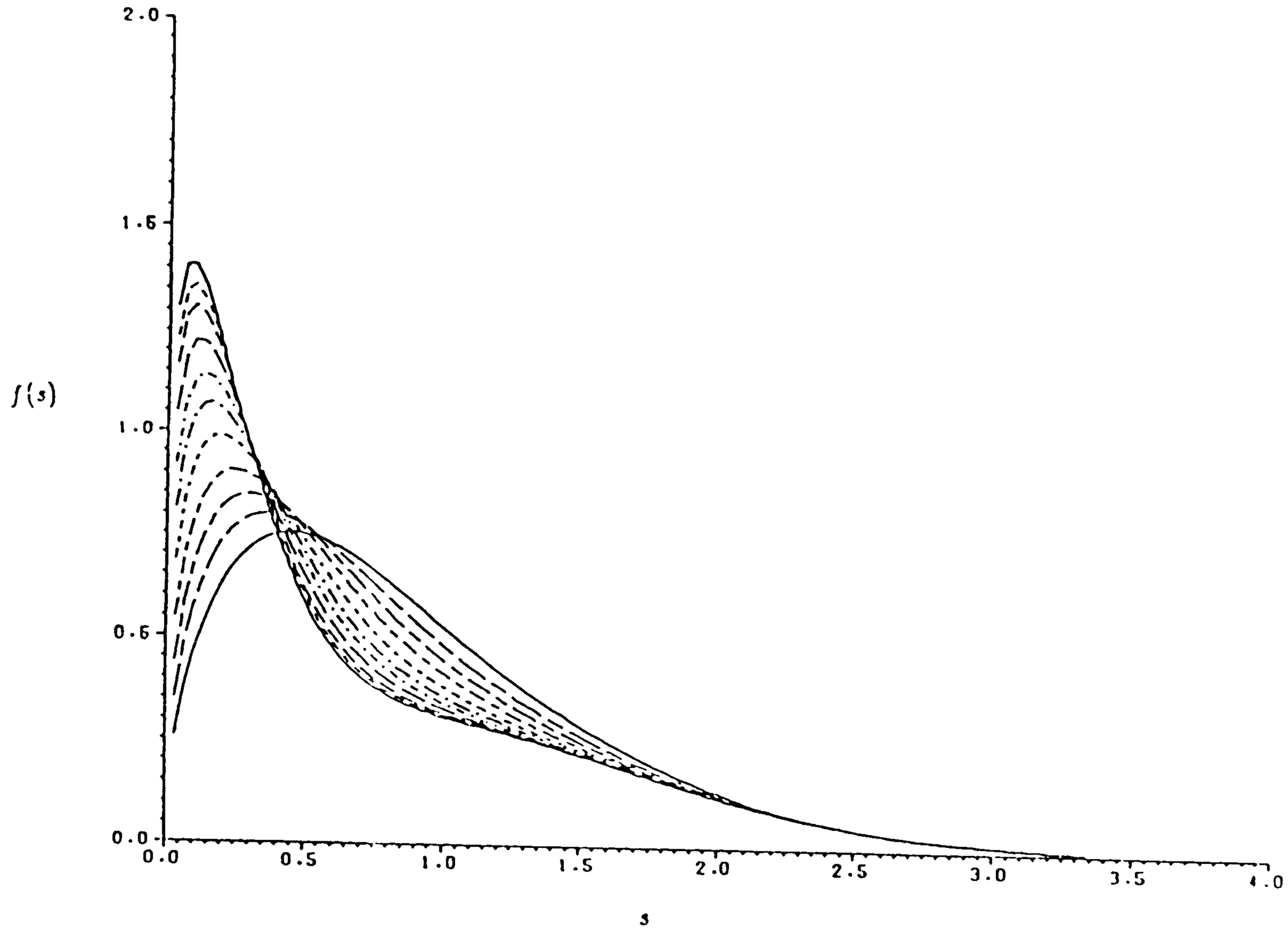

Fig. 5.15 Illustration of model 1 for 11 spectra

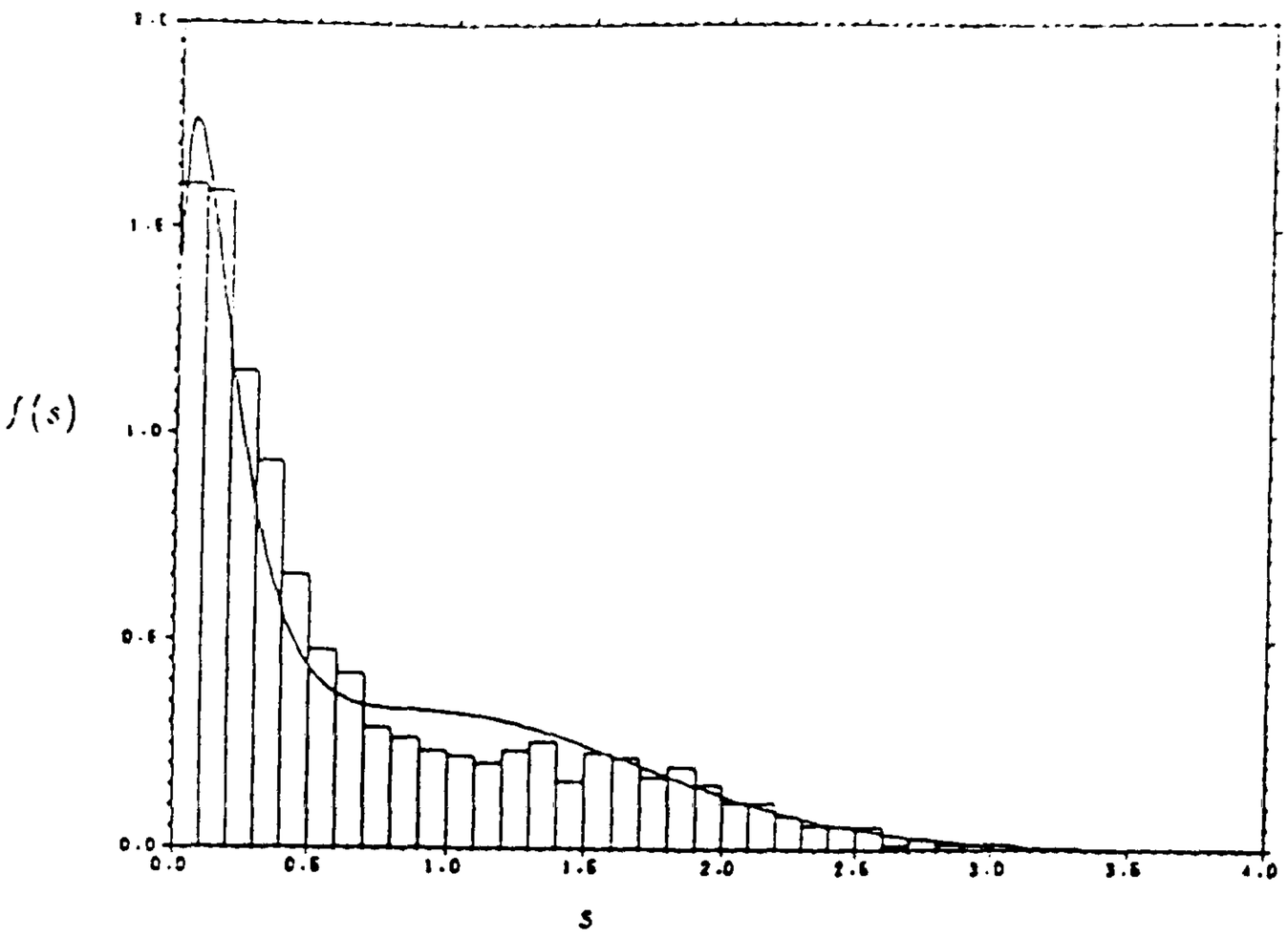

Fig. 5.16 Proposed model2 for $f(s)$ for spectra 1, 6 and 11

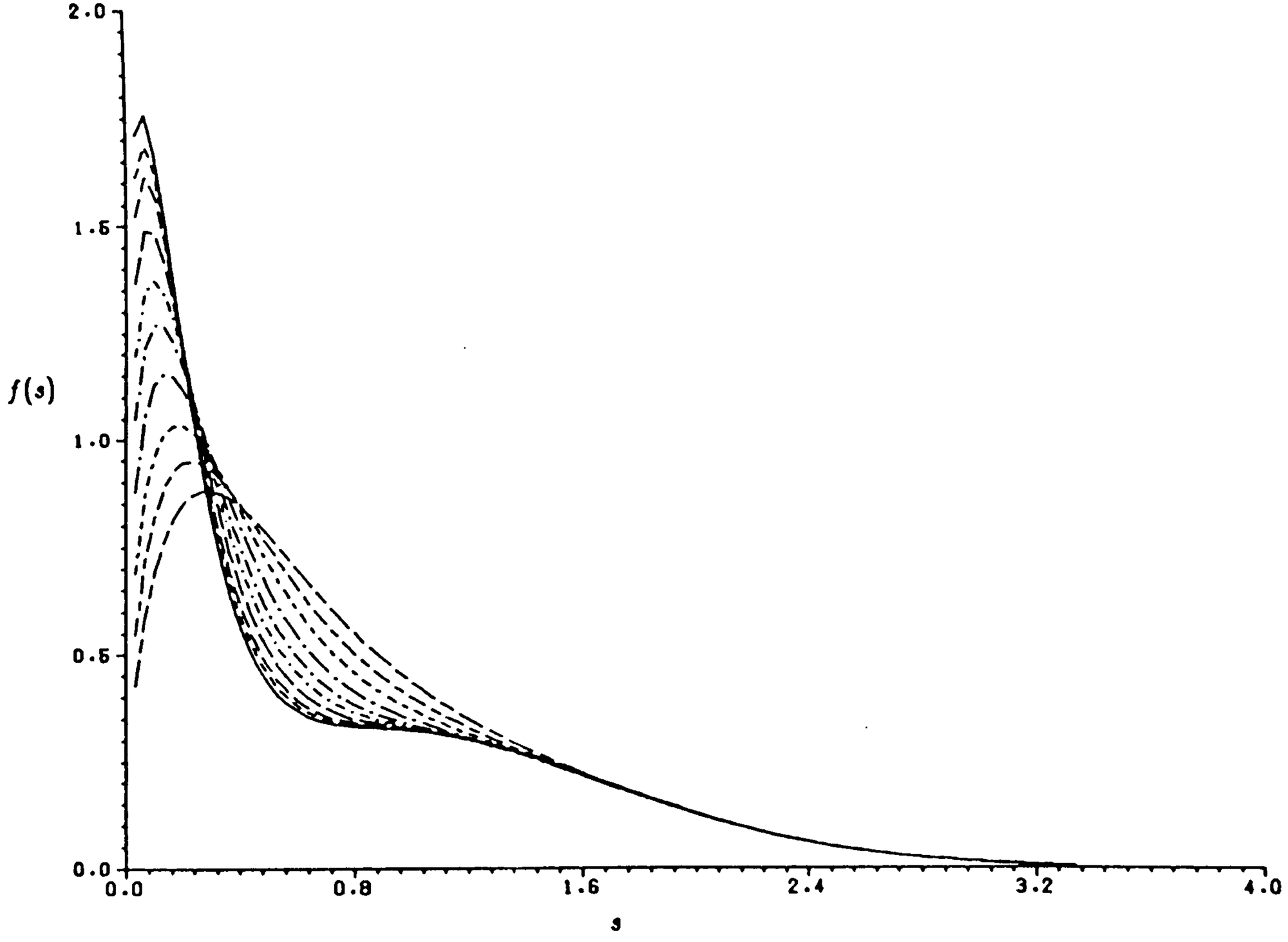

Fig. 5.17 Illustration of model 2 for 11 spectra

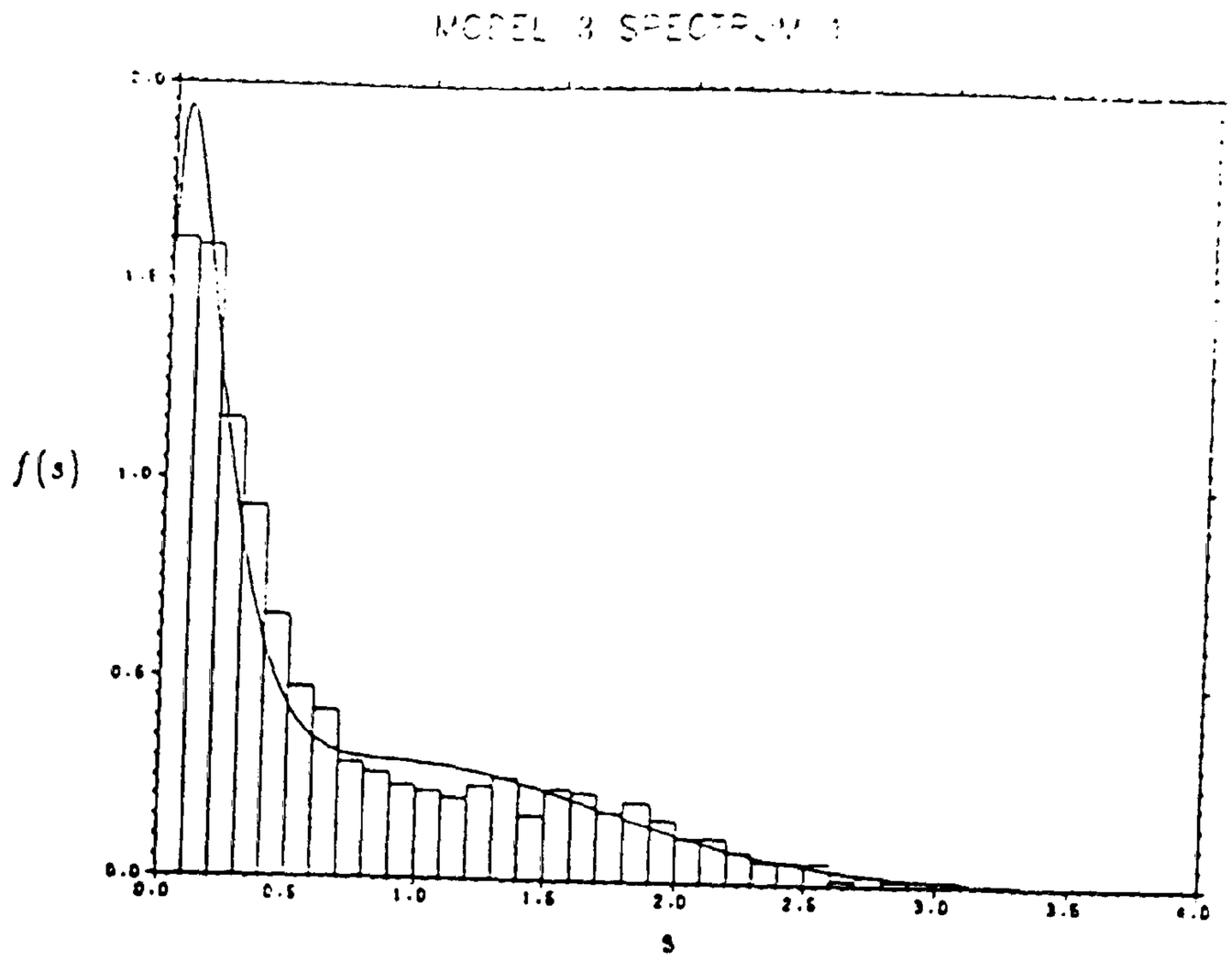

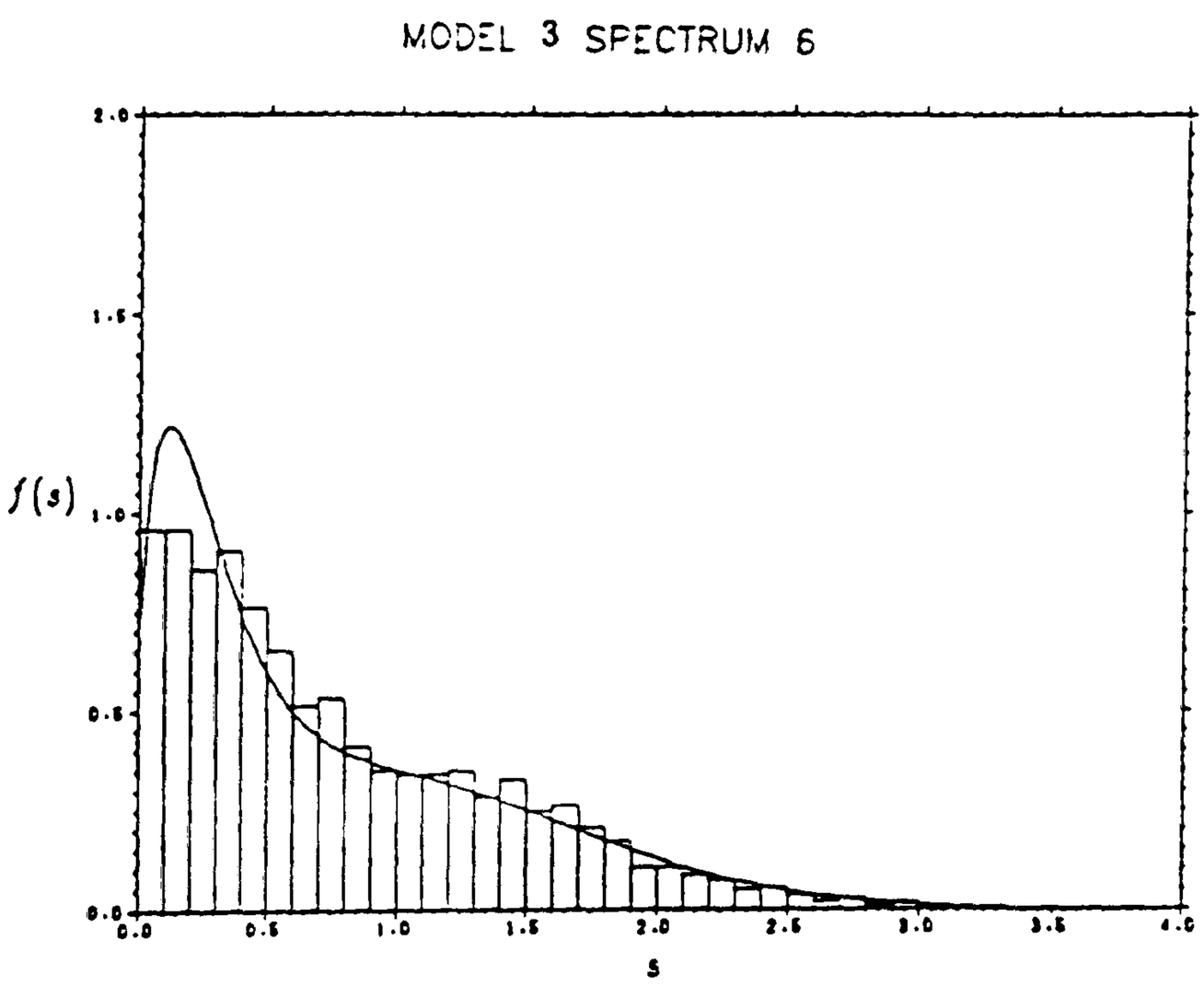

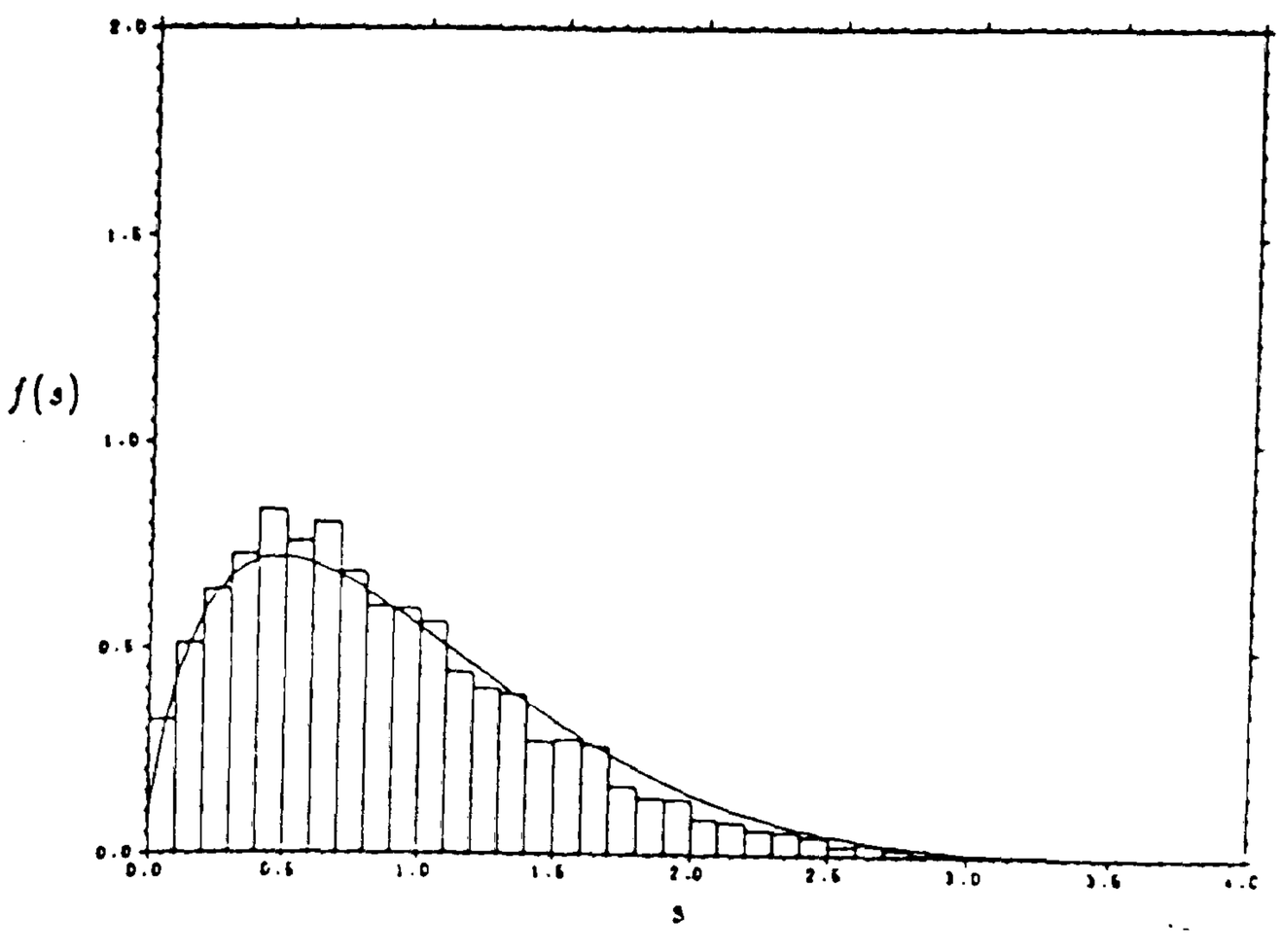

Fig. 5.18 Proposed model 3 for $f(s)$ for spectra 1, 6 and 11

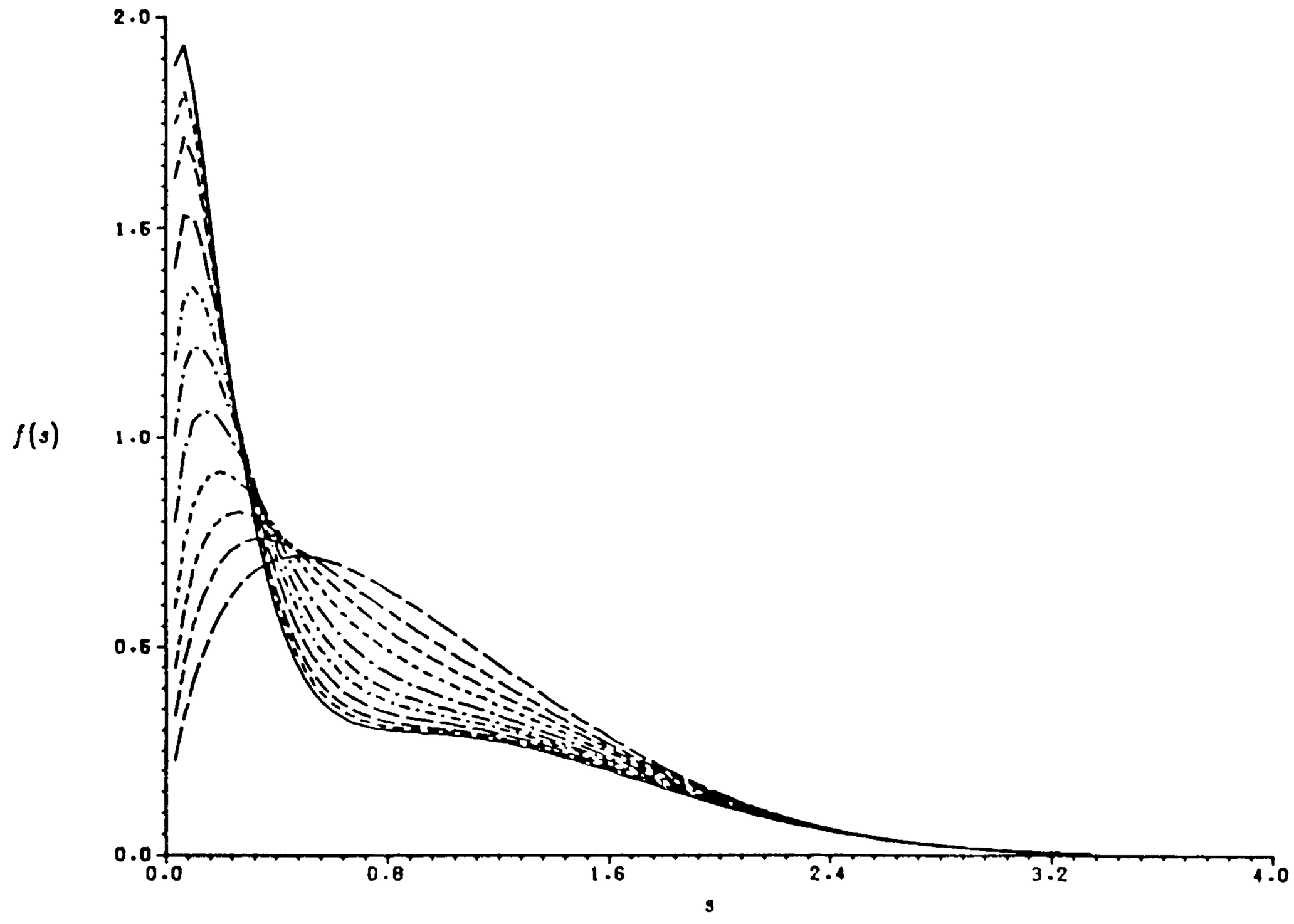

Fig. 5.19 Illustration of model 3 for 11 spectra

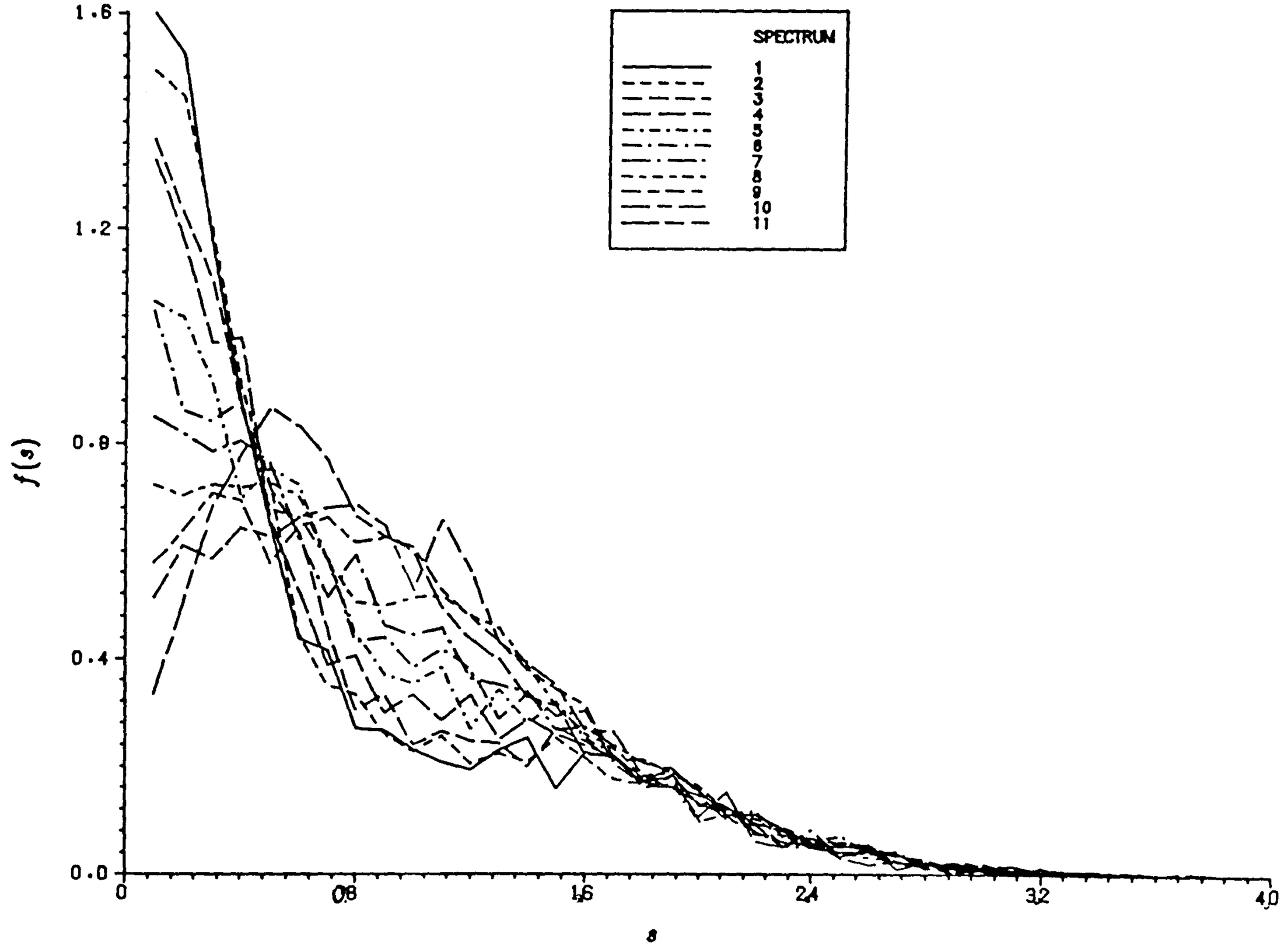

Fig. 5.20 Frequencies of stress range from 11 spectra by simulation

TABLE 5.2 AUTOREGRESSIVE SIMULATION COEFFICIENTS OF RANDOM SERIES FOR 11 SPECTRA

	SPECTRUM 1	SPECTRUM 2	SPECTRUM 3
C 1	.22195597E+01	.43596186E+01	−.54319752E+01
C 2	−.89279409E+00	−.37024955E+01	.27239687E+01
C 3	.17843752E+01	.66567558E+01	.64038869E+01
C 4	.86574840E+00	−.50045888E+01	−.56461503E+01
C 5	.84602944E+00	.12560300E+02	−.96244603E+01
C 6	.21213429E+01	−.67256164E+01	.83231390E+01
C 7	−.74607237E−01	.11949634E+02	.26793993E+01
C 8	.31308190E+01	−.88191068E+01	.47916828E+01
C 9	−.95033244E+00	.12075649E+02	−.14274985E+02
C10	.36249152E+01	−.31945820E+01	.51045124E+01
C11	−.11590285E+01	.59659972E+01	.30609078E+01
C12	.33144677E+01	−.29441320E+01	.23949255E+01
C13	−.18968115E+00	−.44695371E+01	.52977296E+00
C14	.21291455E+01	.58374733E+01	−.13655515E+02
C15	.20337297E+01	−.68537373E+01	.75652150E+01
C16	.34949681E+00	.89363123E+01	−.13539096E+02
C17	.49182070E+01	−.15948901E+02	.12381792E+02
C18	−.15069894E+01	.82330921E+01	−.17267271E+02
C19	.72254354E+01	−.75286016E+01	.13836015E+01
C20	−.28747074E+01	.13595720E+02	−.14102117E+02
C21	.75167778E+01	−.28031301E+01	.54317105E+01
C22	−.33127112E+01	.24454157E+01	−.10890727E+01
C23	.48695745E+01	.21567583E+01	.13362583E+01
C24	−.26018828E+01	.66358953E+01	−.93721561E+00
C25	−.41818144E+00	.12996328E+02	.97602926E+00
C26	−.71529199E+00	−.11401671E+01	.72665590E+01
C27	−.65259969E+01	.27076230E+00	.39607484E+01
C28	.22389022E+01	−.69527597E+01	.89948412E+01
C29	−.10586370E+02	.40276817E+01	−.59837117E+01
C30	.59258403E+01	−.20201586E+01	−.57927897E+00
C31	−.99966660E+01	−.62718320E+01	−.11759034E+02
C32	.94862630E+01	−.14345439E+02	−.48883738E+00
C33	−.41049500E+01	−.66689481E+01	−.11570960E+02
C34	.11251214E+02	.20031257E+00	−.85805045E+01
C35	.46871099E+01	.85334773E+01	−.10941593E+02
C36	.89746363E+01	.19205815E+01	−.49139498E+01
C37	.11483311E+02	.58574905E+01	.42770277E+01
C38	.10731270E+01	.89738637E+01	.10997897E+02
C39	.11569944E+02	.17596727E+02	.16059196E+02
C40	−.11276552E+02	.16855274E+02	.10289205E+02
C41	.42228051E+01	.28844072E+01	.79931761E+01
C42	−.22534950E+02	−.11453167E+01	.23621679E+01
C43	−.50107944E+01	−.15484181E+02	.41150721E+00
C44	−.24026113E+02	−.10520067E+02	−.15340359E+02
C45	−.67075152E+01	−.20838537E+02	−.18630592E+02
C46	−.96349136E+01	−.16010077E+02	−.28283146E+02
C47	.45068547E+01	−.12372968E+02	−.18671676E+02
C48	.15930728E+02	−.57502315E+01	−.11857375E+01
C49	.21098494E+02	.10878917E+02	.20895071E+02
C50	.33682661E+02	.21259605E+02	.32866259E+02
C51	.23011784E+02	.39498715E+02	.20145061E+02
C52	.21551421E+02	.34738657E+02	.54923533E+01
C53	−.40137435E+01	.65291603E+01	−.11526303E+02
C54	−.18454085E+02	−.20124825E+02	−.24990900E+02
C55	−.40114274E+02	−.37453541E+02	−.15804116E+02

C56	−.40433731E+02	−.19870039E+02	−.77474114E−01
C57	−.31555955E+02	−.22710133E+01	−.20029455E+01
C58	.65562723E+01	−.40037545E+01	.11316519E+02
C59	.29096122E+02	.24467232E+02	.32304270E+01
C60	.58894149E+02	.21816409E+02	−.55825299E+01

	SPECTRUM 4	SPECTRUM 5	SPECTRUM 6
C 1	.66023968E+00	.14789169E+02	−.59087183E+01
C 2	−.31231285E+02	.73159841E+00	.78092079E+01
C 3	.16529962E+01	−.85014664E+01	−.10831273E+02
C 4	−.80072523E+01	.78126208E+01	−.42889763E+01
C 5	−.30675174E+01	.16754135E+01	.40454072E+01
C 6	.37503702E+01	−.45412393E+01	−.18916215E+01
C 7	.14014840E+02	−.35365306E+01	−.55255944E+01
C 8	.28855199E+02	.34968944E+00	−.31918515E+01
C 9	.51688419E+01	.98905417E+01	.77833709E+01
C10	.46791594E+01	.62645396E+01	−.63905438E+00
C11	−.25044298E+02	.21053429E+01	.34845778E+01
C12	−.10292497E+02	.28715477E+01	−.89317244E+01
C13	−.26494551E+02	−.12411240E+00	.72819233E+01
C14	−.48323612E+01	.76904064E+00	−.41386299E+01
C15	−.80476071E+01	−.85171848E+01	−.50504182E+00
C16	.15363834E+02	−.12316040E+02	−.72806903E+01
C17	.15490487E+02	−.66644268E+01	−.73406285E+01
C18	.15645037E+02	−.58270947E+00	.57401911E+01
C19	.35366911E+01	.16691990E+02	−.52334172E+01
C20	−.96092084E+01	.12118685E+02	.94787781E+01
C21	−.62290052E+01	.17967376E+02	−.77583747E+01
C22	−.96179849E+01	.17647956E+01	.10675601E+02
C23	.43097285E+01	−.89104135E+00	−.19772687E+01
C24	−.55598871E+01	−.16024235E+02	.64968586E+01
C25	.35454915E+01	−.15601853E+02	−.77705194E+01
C26	−.85523767E+01	−.13174774E+02	−.46633989E+01
C27	.17725308E+01	.17885845E+01	−.86625176E+01
C28	−.69511866E+01	.12748655E+02	−.12134392E+01
C29	.21451653E+01	.14944072E+02	−.29132571E+01
C30	−.14299767E+01	.73199666E+01	.11367420E+01
C31	.74265951E+01	−.53645830E+01	.12582384E+01
C32	.50617535E+01	−.38192797E+01	.53246177E+01
C33	.25726682E+01	−.42488174E+01	.87955235E+01
C34	−.56918116E+01	.12384194E+02	.15414304E+01
C35	−.93636665E+01	−.29282592E+00	.11797189E+01
C36	−.40280144E+01	.80974390E+01	−.12063035E+02
C37	.29543172E+01	−.16062371E+02	−.37174770E+01
C38	.81860030E+01	.26816145E+01	−.90265205E+01
C39	.15941811E+01	−.94853666E+01	.19985618E+01
C40	−.60171878E+01	.11889290E+02	−.15862226E+01
C41	−.10130675E+02	−.64060296E+00	.46233165E+01
C42	−.42103947E+01	.48730446E+01	.52967195E+01
C43	.51890521E+01	−.28232719E+00	.70797690E+01
C44	.73022356E+01	−.32823125E+00	.26239518E+01
C45	.35992138E+01	.87924810E+01	−.60100805E+01
C46	−.67786196E+01	−.26296032E+01	−.12601156E+02
C47	−.67743003E+01	.69587516E+01	−.10248409E+02
C48	−.53235709E+01	−.10071859E+02	−.92446140E+00
C49	.43198867E+01	.36381806E+01	.99219710E+01
C50	.23914674E+01	−.48374703E+01	.11527445E+02
C51	.15308794E+01	.58740382E+01	.35282265E+01
C52	−.69082022E+01	.11931635E+01	−.63120883E+01

C53	−.49691900E+01	.16026043E+00	−.12382843E+02
C54	−.43945801E+01	.16220188E+01	−.71000770E+01
C55	.15174638E+01	−.21797668E+01	−.31732603E+00
C56	.41982855E+00	.64822040E+01	.53079110E+01
C57	−.43688584E+00	−.34681818E−01	.42872007E+01
C58	−.30496345E+01	.65774846E+01	−.10794793E+01
C59	−.32164557E+01	−.20168030E+01	−.26235669E+01
C60	−.48560165E−01	.24120900E+01	−.58511973E+01

	SPECTRUM 7	SPECTRUM 8	SPECTRUM 9
C 1	.94512742E+01	.11163073E+02	−.34723564E+01
C 2	−.38728211E+01	.13658505E+01	.30450729E+01
C 3	−.40956489E+01	−.10415224E+02	−.31390039E+01
C 4	.10686421E+02	−.12041144E+01	−.48156676E+00
C 5	.12693963E+00	.34497981E+01	−.40032509E+01
C 6	.69308367E+00	.66815256E+01	.37095639E+01
C 7	−.51498555E+01	.44074358E+01	−.24602307E+01
C 8	.25711199E+01	−.26895953E+01	−.49241897E+00
C 9	.31459102E+01	−.27059035E+01	−.22147404E+01
C10	.15538093E+00	−.29944187E+01	.20077934E+01
C11	−.15456882E+01	.92668203E+00	.94366590E+00
C12	−.72828237E+00	.42063357E+01	−.15629857E+01
C13	.29623311E+01	.32838802E+01	−.28792487E+01
C14	.41404294E+01	.29003291E+01	.13368330E+01
C15	.24014020E+00	−.71241283E+00	.99664849E+00
C16	−.69089946E+00	−.28562819E+01	−.18937742E+01
C17	−.16374659E+01	−.10800922E+01	−.19922993E+01
C18	.83033778E+00	−.29341142E+01	−.27975299E+00
C19	.21745364E+01	.39312104E+01	.22377358E+01
C20	−.24391324E+01	−.42515179E+00	−.40883502E+01
C21	.16805496E+01	.53587498E+01	.45763313E+01
C22	−.42866024E+01	−.16387669E+01	−.57795306E+01
C23	.80801477E+01	.14543807E+01	.23127720E+01
C24	−.16972215E+01	−.32911578E+01	−.15120162E+01
C25	.80748573E+01	−.51228092E+00	.26072625E+01
C26	−.57038680E+01	−.61936900E+00	−.35887153E+01
C27	.33472674E+01	.16218380E+01	−.40405920E+00
C28	−.36222982E+01	.29943416E+01	.19098304E+01
C29	.15872572E+01	.21474938E+01	−.20015472E+01
C30	−.10818805E+01	.25495159E+01	.35669218E+01
C31	−.42720019E+01	−.15606537E+01	−.42492512E+01
C32	.25256372E+01	.52275050E+00	.22308634E+01
C33	−.24773278E+01	−.49378816E+01	−.21506991E+01
C34	.11352000E+02	.23088672E+01	.17308615E+01
C35	−.14769124E+01	−.45674332E+01	−.12265101E+01
C36	.83991605E+01	.67420812E+01	−.37498243E+00
C37	−.74467760E+01	−.32038133E+01	−.34602892E+01
C38	.32042062E+01	.78716426E+01	.17884227E+01
C39	−.61735874E+01	−.36395525E+01	.78506521E+00
C40	.10481041E+01	.41907642E+01	−.17785666E+01
C41	−.47547120E+01	−.35161655E+01	.21077965E+01
C42	−.16268944E+01	−.70188807E−01	−.33481660E+01
C43	.24463351E+01	.75146046E−01	.29053709E+01
C44	.58940140E+01	−.18131306E+01	−.86965168E+00
C45	.11029059E+02	.50069483E+01	.83405554E+00
C46	.22736891E+01	−.24092531E+01	−.31897067E+01
C47	−.17629162E+01	.64927090E+01	−.26836623E+01
C48	−.11509012E+02	−.35597043E+01	.60179133E+00
C49	−.62630178E+01	.38206814E+01	.25008147E+01

C50	−.60575116E+00	−.36166654E+01	.28669137E+01
C51	.81168640E+01	.59334868E+00	−.55499516E+00
C52	.97498866E+01	−.90430359E+00	−.29641686E+01
C53	.34432685E+01	−.43622918E+00	−.45548853E+01
C54	−.91194749E+00	.32446318E+01	−.44417995E+00
C55	−.69460944E+01	−.19167372E+00	.10019723E+01
C56	−.11669124E+01	.50544632E+01	.36636381E+01
C57	−.16037500E+00	−.43344137E+00	−.39954704E+00
C58	.66029167E+01	.44235940E+01	−.16908182E+01
C59	.31157642E+01	−.88746488E+00	−.25633691E+01
C60	.37942944E+01	.15573107E+01	−.34060271E+01

	SPECTRUM 10	SPECTRUM 11
C 1	.35556027E+01	−.94079987E+00
C 2	.22668981E+01	.14734507E+00
C 3	−.24943079E+01	−.61343607E+00
C 4	−.21132625E+01	.20827761E+00
C 5	.22426889E+01	−.25958088E+00
C 6	.80801478E+00	−.16240363E+00
C 7	.71106022E+00	−.10512348E+00
C 8	.48397473E+00	−.38038253E+00
C 9	−.10716136E+01	−.12783613E−01
C10	.44277471E+00	−.92699672E−01
C11	.33056004E+00	−.15834679E+00
C12	.11707647E+00	−.84511467E−01
C13	.96382443E+00	.73817392E−01
C14	−.16751147E+00	.33771694E−03
C15	.28529645E+00	−.30310398E+00
C16	.81107280E−01	.17773703E+00
C17	.52849949E−01	−.43764172E+00
C18	−.10287048E+00	.52215184E−01
C19	.75870855E+00	.11247977E−01
C20	−.89654932E+00	−.46908755E+00
C21	.15074423E+01	.39530847E+00
C22	−.13384554E+01	−.28384946E+00
C23	.15886247E+01	−.17865104E+00
C24	−.11062462E+01	.42256705E+00
C25	.12945572E+01	−.89729639E+00
C26	−.82002573E+00	.84390225E+00
C27	.12025505E+01	−.13441097E+01
C28	−.81828068E+00	.98192156E+00
C29	.12066705E+01	−.95381385E+00
C30	−.65596884E+00	.41683201E+00
C31	.72502302E+00	−.52399863E+00
C32	.12558540E+00	.47761789E+00
C33	−.33501573E+00	−.39497063E+00
C34	.12638246E+01	−.78238328E−01
C35	−.13144809E+01	.51712888E+00
C36	.20496485E+01	−.82071771E+00
C37	−.16198919E+01	.62478653E+00
C38	.21651172E+01	−.88243760E+00
C39	−.14396654E+01	.90231583E+00
C40	.19508985E+01	−.14476077E+01
C41	−.13014897E+01	.11659421E+01
C42	.17529668E+01	−.10786237E+01
C43	−.11339201E+01	.50658623E+00
C44	.13115205E+01	−.44512682E+00
C45	−.34266046E+00	−.34719483E−01
C46	.16715807E+00	.34701949E−03

C47	.11280740E+01	−.23005468E+00
C48	−.14249730E+01	−.33654477E−01
C49	.23978485E+01	−.42115100E+00
C50	−.24008425E+01	.40000479E+00
C51	.25742040E+01	−.63219170E+00
C52	−.18785231E+01	.36229095E+00
C53	.16148130E+01	−.54088520E+00
C54	−.15613677E+00	.23675895E+00
C55	.23084398E+00	−.40537614E+00
C56	.15680216E+01	.36434825E−01
C57	−.67563276E+00	−.43424279E+00
C58	.20828747E+01	−.68744752E−01
C59	−.79444245E+00	−.13268398E+00
C60	.14443427E+01	−.59419656E+00

Chapter 6

Deterministic Fatigue Analysis

Nomenclature

a	crack size
a_1, b_1, a_2, b_2, fw	parameters in the stress range pdf constructed in Chapter 5
an_i	fraction of time for spectrum i
C	constant in Paris' Law
$f(.)$	pdf
$E(P)$	peak rate defined in Eqn. (6.42)
F	threshold filter
I	irregularity factor $\sqrt{1-\epsilon^2}$
k	number of stress ranges
$\triangle K$	stress intensity factor range
$\triangle K_{th}$	stress intensity factor range threshold
K_c	fracture toughness
K_{max} and K_{min}	maximum and minimum stress intensity factor
m	constant in Paris' Law
n	number of cycles
N	number of cycles to failure
pdf	probability density function
r	yield zone size
r_{peak}	yield zone size from peak load
R	stress ratio
S	stress range
s	normalised stress range $s = \frac{S}{2\sigma_x}$
S_{re}	equivalent stress range
S_h	normalised equivalent stress range
t	time
t_u	iteration unit
w	crack section thickness
Y	geometry factor

ϵ	bandwidth (see Chapter 5)
η	peak amplitude of a stochastic process
λ	$= \frac{damage\ from\ rainflow\ calculation}{damage\ from narrow\ band\ approximation}$
σ_x	root mean square of the stochastic process

Other symbols are defined in the text.

6.1 Introduction

6.1.1 General remarks

This chapter aims to discuss the basic fatigue mechanism and especially the influence of random loading on the fatigue process. It is necessary to examine the fatigue crack growth deterministically before a reliability analysis of fatigue can be conducted.

Fatigue is a very complex process. Even after years of research and engineering experience, a large scatter in the prediction of failure still exists. This is partly due to the stochastic nature of the fatigue process and partly due to limited knowledge. By using the present level of understanding of the fatigue process and admitting the existence of some uncertainties, a general pattern of fatigue crack growth can be drawn.

6.1.2 Fatigue mechanism

When an engineering component is subjected to repeated applications of loads much less than its static strength, it may develop a crack or cracks and, if the loading is continued, some of these cracks may grow and ultimately lead to complete rupture. This phenomenon is termed fatigue.

In chapter 3, distinction has been made between fatigue crack growth process and a fracture process. The main difference between these two processes is the crack growth mechanism. The process of fatigue can be divided into three stages or regimes:

(a) Nucleation or crack initiation, i.e. the primary stage. This stage starts with the first load cycle and ends when a technically detectable crack is present. When the strain ranges imposed upon the material by repeated loads is greater than that which the material can accommodate by elastic deformation, usually in some critical region corresponding to a high stress concentration or local weakness, a microcrack can be produced by continued deformation. This stage takes a high proportion of life in low amplitude fatigue.

(b) Crack propagation, i.e. the secondary stage. This stage can have two phases. Phase I is in the form of slip band growth. Phase II is in the form of crack growth with direction normal to the maximum stress. The basic mechanism of fatigue crack growth is that of striation formation with variations on this basic mechanism dependent on micro-structure, ductility, stress intensity range and the environment etc.

(c) Rapid crack growth and eventual failure by fracture or some other limiting states. This is the final stage and the failure criteria are important to establish the failure functions for reliability analysis.

6.1.3 Factors affecting fatigue

Usually, a fatigue experiment will have results with a certain amount of scattering for different types of specimen or even for the same type of specimen. This is partly due to the probabilistic nature of fatigue process and partly due to the fact that fatigue behaviour is dependent on many factors.

The major factors which affect fatigue behaviour are:[6.1]

(1) type and nature of loading
(2) geometry of component
(3) surface finish and directional properties
(4) stress or strain concentrations
(5) mean stress or strain
(6) environmental effects
(7) metallurgical factors and material properties
(8) strain rate and frequency effects

6.1.4 Scope of fatigue analysis in this study

While it is ideal in a fatigue analysis to include as many factors as possible, an experiment in the laboratory is subjected to many constraints and only some of the factors having predominant influence are studied. The analytical models built from experimental data cannot possibly include all the factors. The aim of this study is to build up a methodology for the reliability analysis of fatigue and fracture. Some limitations have been imposed although more factors can be taken into account in future studies. This study has provided a methodology for calculating fatigue crack growth using present knowledge. It is assumed that:

1) The loading is medium frequency low amplitude (for example, the stochastic loading caused by waves in offshore structures).

2) The material is structural steel; thus valid experimental results for structural steel can be used.

3) The crack or defect is pre-existing, (e.g. in typical welded joints). The analysis of fatigue is therefore concerned only with fatigue crack propagation. For structural steel which has low strength and high fracture toughness the crack propagation stage occupies a relatively long proportion of fatigue life.

4) The structural component is a typical welded joint of an offshore structure. The crack is found in the toe of the weldment of the joint. Y factors are calculated from 2-dimensional finite element computation[6.2]. For a typical cruciform joint, the Y factors are listed in Table 6.1 and plotted in Fig. 6.1.

5) Environmental effects are ignored (e.g. corrosion fatigue). However, in practical situations it should not be ignored.

6) Only a one-directional stress is considered. Again like the fifth assumption, in practical situations, further extension to a multi-directional stress system is needed.

7) Temperature effects are ignored.

8) The material (e.g. BS4360 50D) chosen for study is not sensitive to stress ratio changes between -1 and 0.85 in experiments [6.3] so that residual stress effects can be ignored. However, for general material, residual stress effects i.e. their distributions in the crack extension sections, and their influence on crack growth rate through the stress ratio and threshold effect remain to be problems to be researched.

The probabilistic nature of fatigue is to be studied in the next chapter.

6.2 Fatigue Under Constant Amplitude Loading

As discussed in section 6.1.2, the fatigue crack growth process can be divided into three regimes depending on the size of the crack. It has been found that there is an empirical relationship between $\triangle K$ and crack growth rate da/dn[6.1], [6.4], [6.5]. In view of this, the fatigue crack growth process can be divided into three regimes according to the value of $\triangle K$. The relationship between $\triangle K$ and da/dn is illustrated in Fig. 6.2[6.1].

6.2.1 Fatigue limit or threshold value

In regime (a) $\triangle K$ is small. stress ranges below a certain threshold level will not cause cracks to propagate. The threshold value of $\triangle K$ is often taken as a material property. This threshold value is named $\triangle K_{th}$.

The threshold effects can be modelled in a number of ways. In reliability study (chapter 7), threshold value is to be treated as a statistical variable rather than as a deterministic value. One of the ways to model the threshold effect is to use a variable high pass filter[6.2].

$$\frac{da}{dn} = F(\frac{da}{dn})_{(with\ no\ threshold\ effects)} \tag{6.1}$$

In this thesis, for simplicity the filter is given the form:

$$F = 0 \qquad \triangle K \leq \triangle K_{th} \tag{6.2}$$

$$F = 1 \qquad \Delta K_{th} \leq \Delta K \tag{6.3}$$

The fatigue threshold is reflected in the S-N curve as the lower limit stress range for unlimited crack life[6.4].

6.2.2 Paris' Law

In the intermediate region of fatigue crack growth, i.e. after the threshold region and before the rapid crack growth with K_{max} near K_{1c} , Paris had reviewed the then previous models of crack growth rate da/dn, and found that the general trend is[6.5]:

$$\frac{da}{dn} = C\Delta K^m \tag{6.4}$$

where C, m are empirical material constants.

$$\Delta K = K_{max} - K_{min} = \Delta\sigma Y\sqrt{\pi a} \tag{6.5}$$

This equation was developed from empirical results and found wide applications. Many modifications of this relationship can also be found.

6.2.3 Forman equation

In regime (c) fatigue crack will experience rapid growth when K is approaching K_c. To include the regime (c) into the general Paris' Law, Forman *et al* proposed the equation[6.6]:

$$\frac{da}{dn} = \frac{C\Delta K^m}{(1-R)K_c - \Delta K} \tag{6.5}$$

where K_c is the fracture toughness and R is the stress ratio.

This equation takes the fracture toughness and the stress ratio into account and has been proved by several research laboratories to give a reasonable approximation to test results for many aircraft structural materials, e.g. [6.7].

Further refinement has been made to take account of the threshold effects [6.8]:

$$\frac{da}{dn} = \frac{C(\Delta K^m - \Delta K_{th}^m)}{(1-R)K_c - \Delta K} \tag{6.6}$$

where ΔK_{th} is the threshold level of stress intensity factor range.

These more complex forms have some experimental support, but none has yet become established as the best available . The Paris' Law has the advantage of being neat and simple. The factors being ignored by Paris' Law can be treated as uncertainties in a reliability analysis and thus structural integrity can be studied in a general format.

6.3 Fatigue Under Random Loading

6.3.1 General remarks

When a structure is subjected to random loading, cracks in structural components will experience changing stress amplitude. The stress interaction will have effects such as retardation and acceleration of crack growth.

Various load interaction effects on the crack growth behaviour under random loading have been observed by many investigators. The following list is a summary of the significant effects[6.9]:

1) tensile overload causes retardation in general .
2) greater retardation is caused by:
    a. increasing the magnitude of the overload
    b. repeating the overload
    c. blocks of overload instead of single overload.
3) after an overload, the crack growth rate may have a short increase and then gradually reduce to its lowest point before recovering to the baseline. It is called delayed retardation.
4) compressive loads in compression-tension load cycles cause subsequent acceleration of crack growth.
5) compressive loads in tension-compression load cycles reduce the retardation effect caused by previous tensile overload.
6) in step loading, a high-low sequence has similar results to the overload effect, but a low-high sequence has little influence on the crack growth rate.

The process of stress interaction is so complex that different quantitative models have been developed that give only an approximate correlation with the real mechanism. However, each of those models takes only some of the factors of influence into account, so that there is no complete agreement with the experimental results. Those models can be classified into two groups, although overlap may exist:

1) yield zone model, which is based on the yield zone size created by the load history[6.10] [6.11].

2) closure model, which is based on the closure caused by the crack surface deformation, which defines the crack opening or contact stress, occurring within the yield zone [6.12].

6.3.2 Yield zone models

1) *WHEELER MODEL*

The Wheeler model predicts retardation by reducing the crack growth rate through analysis of the plastic zone created by the overload and the plastic zone size due to the present load[6.10].

$$\frac{da}{dn}(spectrum) = Cp\frac{da}{dn}(baseline) \tag{6.7}$$

where

$$Cp = \begin{cases} (\frac{r_y}{r_{peak}})^m & r_y < r_{peak} \quad inside\ the\ peak\ load\ plastic\ zone \\ 1 & r_y \geq r_{peak} \quad outside\ the\ peak\ load\ plastic\ zone \end{cases}$$

m is a empirically determined constant from data fitting.

r_y and r_{peak} are the yield zone size for the present load and the peak load.

The simplicity of this model makes it popular and refined versions have been made over the years.

2) *WILLENBORG MODEL*

In the Willenborg model[6.11], the retardation is accounted for by a reduction in the stress intensity factor and by truncating the minimum effective stress intensity factor for stresses below zero.

$$\frac{da}{dn} = C\triangle K^m_{spectrum} \tag{6.8}$$

where C and m are stress ratio dependent.

$$\triangle K_{spectrum} = (K_{max} - K_{ret}, K_{min} - K_{ret}) \tag{6.10}$$

$$K_{ret} = \begin{cases} K_{peak} - K_{max} & r_y < r_{peak} \quad inside\ the\ peak\ load\ plastic\ zone \\ 0 & r_y \geq r_{peak} \quad outside\ the\ peak\ load\ plastic\ zone \end{cases} \tag{6.11}$$

$$R = \frac{K_{max} - K_{ret}}{K_{min} - K_{ret}} \tag{6.10}$$

The yield zone models assume that retardation effects only exist in the overload plastic zone (opz) while experimental evidence has shown that the retardation zone is beyond the opz. Both models predict the maximum retardation immediately after an overload while in reality maximum retardation is observed sometime after the overload. The effects of compressive overloads, and multiple

overloads are not considered in the yield zone models. These models are used for their convenience and fit for the particular type of data used.

6.3.3 Crack closure models

In 1969, Elber[6.12] found that crack closure can occur with the permanent tensile plastic deformation left in the wake of the propagating crack even in the cyclic loading process. The crack growth rate for even constant amplitude loading should be decided not only by the stress intensity factor range ΔK but also by the so called crack opening load influenced by residual plastic deformation.

For fatigue cracks under cyclic tensile loads, the plastic zone formed by the increasing part of the loading cycle is named as *forward yield zone* and the one by the unloading part as *reversed yield zone* embedded in the former. In the forward yield zone, permanent sets of plastic tensile straining occur which will subsequently experience compressive actions by the surrounding elastic matrix during unloading. The material in the vicinity of the crack tip is in a state of plastic tensile strain and the compressive stress. This state is then called the residual deformation.

With residual deformation, the sides of the crack ahead of the tip will be forced into contact so that the crack will not be open until some level called the crack opening stress. After overloading the overload residual deformation increases the crack opening stress. The crack growth rate will retard until the normal residual deformation state ahead of the crack tip is recovered.

Also it is found that the overload will cause excessive residual deformation as well as bigger front blunting in the crack tip region than the following low stress amplitude cycles [6.13]. The big crack front blunting can increase the crack opening load. Therefore the delayed retardation can be explained in the way that immediately after overload the blunting effects are dominant and decrease with the advance of the crack until the residual deformation has a dominant effect.

It was later found that this discovery can help to explain the stress interaction effect due to variable amplitude loading and also the threshold concept[6.14]. As for threshold effects under random loading, they are different from that under constant amplitude loading. Under constant amplitude loading, the crack opening stress can be assumed to be a constant, and so can the threshold value. Under random loading, due to the change of crack tip state, the crack opening stress can be lower or higher than that under constant amplitude loading.

6.3.4 Discussion

An impressive amount of work has been devoted to investigate stress interaction effects. Literature on some of the main developments can be found in ASTM STP 743, 687, 677, 637, 595[6.15], [6.9],[6.14],[6.16],[6.17].

The models based on yield zone size are constructed to relate parameters in the model and the

calculated yield zone to the experimental data. These types of models are easy to adopt and efficient under some circumstances. The model based on the crack opening concept has a better physical explanation but needs more data acquisition and computer effort. The crack opening concept can also help to explain the threshold phenomenon under random loading. Various models originating from these two models have been developed.

However, no ideal solution for general practical application has been provided. Each model has its own limitations.

6.4 Equivalent Stress Range

6.4.1 General remarks

For some materials like offshore structural steel the stress interaction effects are less serious. Certain alternative approaches can be used to reduce the effort required to calculate random stress interaction, for conventional fatigue analysis. In engineering practice the concept of equivalent stress range is used to replace the variable amplitude loading by simpler constant amplitude loading giving rise to equivalent damage. Some empirical formula have been proposed by Wirsching, Dover and Hancock from analytical and simulation studies [6.18] [6.19] [6.20] [6.21] [6.22].

6.4.2 Equivalent stress range concept

In a variable amplitude loading process, the crack initiation and crack growth processes are inevitably complex. Fatigue data are usually based upon stress amplitudes or stress ranges in a cycle. In other words, the stress amplitudes or stress ranges in a cycle are used to describe the fatigue damages. By definition, the amplitude is the difference between the peak and the mean and the stress range is the algebraic difference between the maximum and minimum stress in the cycle. Normally, some damage accumulation rules are used to calculate the effect of a variable amplitude loading process on fatigue performance.

One of the damage accumulation rules is Miner's Rule [6.23]. By ignoring the crack growth non-linearity and sequence effects, Miner assumed a linear damage summation:

$$D = \sum_{i=1}^{k} D_i = \sum_{i=1}^{k} \frac{n_i}{N_i} \tag{6.12}$$

where n_i is the number of cycles for stress range S_i while N_i is the number of cycles to failure for stress range S_i.

Usually, D is set equal to 1 for failure. In the more general case, D can be a random variable [6.24]. From fracture mechanics theory, the crack growth for constant amplitude loading in the intermediate

regime (i.e. moderate values of $\triangle K$)can follow the Paris law.

$$da = CS^m Y^m (\pi a)^{\frac{m}{2}} dn \tag{6.13}$$

or

$$\frac{da}{(\pi a)^{\frac{m}{2}} Y^m C} = S^m dn \tag{6.14}$$

Integrating both sides of equation (6.14) for constant S, we have:

$$\int_{a_0}^{a_f} \frac{da}{(\pi a)^{\frac{m}{2}} Y^m C} = NS^m \tag{6.15}$$

where a_0 is the initial crack size, a_f is the crack size failure criterion and N is the number of cycles to failure.

If

$$K_m = \int_{a_0}^{a_f} \frac{da}{(\pi a)^{\frac{m}{2}} Y^m C} \tag{6.16}$$

then

$$NS^m = K_m \tag{6.17}$$

This is the form for S-N curve, i.e.

$$N = \frac{K_m}{S^m} \tag{6.18}$$

For variable amplitude loading, the damage caused by each stress range S_i is:

$$D_i = \frac{n_i}{N_i} = \frac{n_i S_i^m}{K_m} \tag{6.19}$$

where n_i is the number of cycles for S_i.

By the linear summation rule, we have

$$D = \sum_{i=1}^{k} D_i = \sum_{i=1}^{k} \frac{n_i S_i^m}{K_m} \tag{6.20}$$

If K_m does not change with different S_i,

then

$$D = \frac{\sum_{i=1}^{k} n_i S_i^m}{K_m} \tag{6.21}$$

If we define

$$S_{re} = [\sum_{i=1}^{k} (\frac{n_i}{n}) S_i^m]^{\frac{1}{m}} = (\int_0^{\infty} S_i^m f(S_i) dS_i)^{\frac{1}{m}} \tag{6.22}$$

with $n = \sum_{i=1}^{k} n_i$

then

$$D = \frac{{S_{re}}^m n}{K_m} \tag{6.23}$$

When $D = 1, n$ should be equal to N, i.e. in the final failure, then

$$N = \frac{K_m}{{S_{re}}^m} \tag{6.24}$$

By comparing equation (6.24) with equation (6.18), S_{re} can replace the variable amplitude loading fatigue in the constant amplitude loading S-N curve. S_{re} is then called the equivalent stress range.

Yamada and Albrech [6.25] have reported that the equivalent stress range concepts and Miner's rule become a special case of the fracture mechanics approach to fatigue under the following conditions:

1) All stress ranges considered are above the threshold value.

2) The fatigue life consists of crack propagation only.

3) Sequence effects resulting from the loading process are negligible.

4) The slope of the cyclic crack growth rate curve is the same as the absolute value of the inverse slope of the S-N curve.

However from experience, the above conditions are not strictly necessary for the concept of equivalent stress range to be valid in fatigue studies for most situations.

6.4.3 Literature review of empirical equivalent stress range models

For a stationary narrow-band Gaussian load process, each peak is associated with a trough with approximately the same amplitude. The stress range is thus double the peak amplitude. Therefore, the distribution of stress ranges is the same as the peak distribution with amplitude equal to half of the value of the stress range.

From probability theory, the distribution of peaks for a narrow- band and stationary Gaussian process is the Rayleigh distribution[6.26], thus from Rayleigh distribution, the pdf of peak amplitude η is:

$$f(\eta) = \frac{\eta}{\sigma_x{}^2} e^{-\frac{\eta^2}{2\sigma_x{}^2}} \tag{6.25}$$

Hence, from equation (6.22), putting S = 2η , and

$$\frac{n_i}{n} = f(\eta)\ d\eta \tag{6.26}$$

gives

$$S_{re} = [\int_0^\infty f(\eta)(2\eta)^m\ d\eta]^{\frac{1}{m}} \tag{6.27}$$

$$S_{re} = 2\sqrt{2}\{\Gamma(\frac{m}{2}+1)\}^{\frac{1}{m}}\sigma_x \tag{6.28}$$

By normalisation, i.e. dividing by the RMS of the process

$$S_h = 2\sqrt{2}\{\Gamma(\frac{m}{2}+1)\}^{\frac{1}{m}} \tag{6.29}$$

When the spectrum is not ideal narrow band the peak pdf will not be in such a form as equation (6.25). As a result, the normalised equivalent stress range obtained from (6.27) will not be of the form of equation (6.29).

Wirsching and Light presented simulation results from rainflow analysis and found an empirical correction factor λ could be used to relate the damage rate by rainflow analysis to damage rate by Rayleigh approximation .

The question then is to have some spectrum parameters to provide a simple method of estimating the rainflow prediction of fatigue life.

By least square regression, Wirsching[6.18] has managed to obtain a empirical formula for λ .

$$\lambda = g + (1-g)(1-\epsilon)^b \tag{6.30}$$

where

$$\begin{cases} g = & 0.962 - 0.033m \\ b = & 1.587m - 2.323 \end{cases} \tag{6.31}$$

and so that

$$S_h = 2\sqrt{2}[\lambda\Gamma(\frac{m}{2}+1)]^{\frac{1}{m}} \tag{6.32}$$

Chaudhury and Dover[6.21] proposed an equation of S_h valued between the narrow band approximation and the broad band approximation .

They have:

$$S_h = 2\sqrt{2}[\frac{\epsilon^{m+2}}{2\sqrt{\pi}}\Gamma(\frac{m+1}{2}) + \frac{3}{4}\ I\ \Gamma(\frac{m}{2}+1)]^{\frac{1}{m}} \tag{6.33}$$

A modified version of the above model by Kam and Dover[6.27] replaced the second term in the right side of the above equation with a error function, $erf(\epsilon, m)$, which is related to the bandwidth parameters ϵ and m.

$$S_h = 2\sqrt{2}[\frac{\epsilon^{m+2}}{2\sqrt{\pi}}\Gamma(\frac{m+1}{2}) + (1+erf(\epsilon,m))\frac{I}{2}\Gamma(\frac{m}{2}+1)]^{\frac{1}{m}} \tag{6.34}$$

By a polynomial fit with the error function it is found that:

$$erf(I,m) = 0.3012I + 0.4916I^2 + 0.9181I^3 - 2.3534I^4 - 3.3307I^5$$

$$+15.6524I^6 - 10.7846I^7 \qquad for\ 0.13 < I < 0.96 \tag{6.35}$$

$$erf(I,m) = 1 \quad for\ \ 0.96 \leq I \tag{6.36}$$

Also, Hancock proposed two forms of S_h[6.22],

Model A:

$$S_h = \sqrt{2}\ [I\ \Gamma(\frac{m}{2}+1)]^{\frac{1}{m}} \tag{6.33}$$

and model B:

$$S_h = \delta\ [\Gamma(\frac{m}{u}+1)]^{\frac{1}{m}} \tag{6.37}$$

$$\text{where}\ \ \delta = \sqrt{2}(2-\epsilon^2)$$

$$u = 2 - \epsilon^2$$

The S_h values from all those models are shown in Fig. 6.3, 6.4, 6.5, 6.6, 6.7 for the 11 spectra given in Chapter 5, for a range of values of the Paris' Law parameter m.

Using the method of autoregressive simulation shown in Chapter 5, the loading process on a crack has been reproduced and counted by the rainflow method as discussed in Chapter 5. Then these stress ranges were converted to equivalent stress ranges by Eqn (6.27). For each calculation, 9,000 data points were generated in the autoregressive simulation. Results of S_h are shown in Fig. 6.8 with each curve representing one of the 11 spectra.

All the approximations are based on one or the other theoretical analysis. The reason for the empiricism of S_h is the difficulties in getting the distribution of $f(S)$. This impediment can be overcome with the new semi-empirical stress range probabilistic distribution models described in chapter 5.

6.4.4 Equivalent stress range from the stress range pdf models

Chapter 5 has proposed three separate equations for the normalised stress range distribution $f(s)$, which show very good agreement with the rainflow stress range results from 9,000 time interval points, with the time interval equal to $\frac{1}{2f_{max}}$, where f_{max} is the maximum frequency in Hertz. In this way $f(s)$ can be directly related to spectrum parameters. The solutions of $f(s)$ therefore provide some new forms of S_h by integration from (6.22).

From models for $f(s)$ in chapter 5 with stress range $S = 2 \times \sigma_x \times s$, the equivalent stress range is

$$S_{re} = 2\sigma_x[\Gamma(1+\frac{m}{b_1}){a_1}^{-\frac{m}{b_1}} f_W + \Gamma(1+\frac{m}{b_2}){a_2}^{-\frac{m}{b_2}}(1-f_W)]^{\frac{1}{m}} \tag{6.38}$$

Then the normalised equivalent stress

$$S_h = 2[\Gamma(1+\frac{m}{b_1}){a_1}^{-\frac{m}{b_1}} f_W + \Gamma(1+\frac{m}{b_2}){a_2}^{-\frac{m}{b_2}}(1-f_W)]^{\frac{1}{m}} \tag{6.39}$$

The equivalent stress ranges obtained from these three models in Chapter 5 are shown in Fig. 6.9, 6.10, 6.11.

6.4.5 Comparison and Comments

From Eqn. (6.22), the equivalent stress range is the summation or integration over the whole range of stress ranges to the mth power. As such, the equivalent stress range can be treated as a kind of mathematical criterion for the accuracy of the proposed $f(s)$ in Chapter 5.

Comparing each of the models with the simulated results (Fig. 6.8) and among one another, some observations can be made:

(1) All the semi-empirical models for S_h from [6.18], [6.21], [6.22], [6.27] show conservative results.

(2) All the three models calculated from the semi-empirical stress range distributions of the present work give a better fit for S_h with the simulated results and all are more or less conservative.

Some detailed comparisons are as follows:

1) Wirsching's Model

As the first tentative model for S_h for random loading, this model pointed a general trend for S_h to relate to m and bandwidth but this model is overconservative. When $m \leq 2$, this model gives high S_h for wide bandwidth and low S_h for narrow band, which is in contrast to the simulated results.

2) Hancock model A

This model has improved from Wirsching's model greatly. More distinct differences can be observed for each spectrum and the accuracy has increased. However, it still gives very conservative estimates.

3) Hancock model B

The distinguishing feature of this model is the overlapping of S_h curves when $m \simeq 6$. This feature can be compared with the simulated results which intersect when $m \simeq 4$.

4) Chaudhury and Dover's model

This model has increase accuracy from Hancock's models in most cases. This model assumes that the distribution of rainflow stress ranges in a stochastic process follows the distributions of peaks which is the combination of Rayleigh (narrow band) and Gaussian (white noise)[6.21].

5) Kam and Dover's model

This model has improved the accuracy of the model by Chaudhury and Dover but still bases their stress range distribution from rainflow counting on the distribution of peak amplitude. As such, the distribution from peaks should have a greater value of S_h than the one from rainflow counted stress ranges.

6) Models from stress range pdf from Chapter 5

Model 1 for S_h has the largest values and is thus most conservative. Model 2 for S_h is is closer to the simulated results for most of the cases than model 1. In model 3 the S_h curves not only have the closest results to simulation S_h among the three models but also have an overlapping region of S_h curves for the 11 spectra when $m \simeq 4$ which is the same as for the simulation results.

The S_h values from the different models for $f(s)$ can serve as a measurement to judge the accuracy of $f(s)$. The values of S_h with higher values of m are more sensitive to the estimation of $f(s)$ in the larger s part because the larger s can have a much higher percentage of S_h when m becomes big. It can be seen that in model 3 $f(s)$ has a good fit in the higher m region and thus provides the

best estimation for the large s part of stress range pdf. Overall, when $m \leq 3$, all three models have similar results which fit well.

6.5. Equivalent Block Loading

One of the other applications for the stress range probability distribution models is the calculation of equivalent block loading. Because the stress ranges frequencies for the discretised period of stationary loading can be easily obtained from the proposed stress range probability distribution models, the numbers of stress ranges over a long non-stationary period can just be accumulated as follows.

Having obtained the probability density functions of stress ranges for a single response spectrum, it is a straightforward procedure to extend this to block loading (which is defined here as the addition of the same range of stress cycles for different loading conditions or seastates).

$$\text{Number of cycles for stress range } S_i = \text{probability density of stress range } S_i \times$$
$$\text{peak rate of the process} \times \text{fraction of total time } \times dS_i \tag{6.40}$$

where

$$dS_i = S_{i+1} - S_i$$

From our models in chapter 5, $f(s)$ can be obtained for response spectra. For S_i

$$f(S_i)dS_i = f(s_i)ds_i \tag{5.41}$$

If $n(S_i)$ denote the cycle numbers of S_i, and the peak rate (i.e. the number of peaks per unit time, which is equal to the number of cycles per unit time) is:

$$E(P) = \sqrt{\frac{m_4}{m_2}} \tag{6.42}$$

where m_4 and m_2 are the spectral moments defined in chapter 5, then

$$n(S_i) = f(s_i) \times E(P) \times t \times ds_i \tag{6.43}$$

If over a period, several seastates occur

$$n(S_i) = \sum_{j=1}^{k} f(s_i)_j E(P)_j t_j ds_i \tag{6.44}$$

where k is the number of seastates.

Therefore the frequency for stress range S_i over the whole range of spectra would be:

$$f(S_i) = \frac{n(S_i)}{\sum_{i=1}^{\infty} n(S_i)} \tag{6.45}$$

6.6 Fatigue Crack Growth Calculation

6.6.1 Fatigue crack growth calculation procedure

For fatigue crack growth under random loading with high frequency and low amplitude (e.g. offshore wave loading), the calculation can be divided into two groups: 1) directly considering stress interaction effects, 2) indirectly considering stress interaction effects. Section 6.3.2 and section 6.3.3 have reviewed some proposed models to calculate stress interaction directly.

Due to the complexity of the stress interaction problem and lack of experimental data on stress interaction influence on structural steel, no direct consideration of the stress interaction effect has been taken in this study. Instead, fatigue crack growth has been calculated by the equivalent stress range approach, which assumes that the crack growth follows Miner's rule over the period of interest as presented in section 6.4, with additional considerations of threshold effects.

To summarise, for structures under stochastic loading the procedure for calculating the crack growth is as follows:

1) Give information describing the initial flaw geometry.

2) Find $Y(a)$. For any short period of time, the crack increment is assumed to be small so that Y can be assumed to be constant. Also for each small period Miner's rule should be followed.

3) Give information of material properties, e.g. $\sigma_y, K_{1c}, C, m,$ and$\triangle K_{th}$. If stress interaction effects are ignored and Paris' Law is used to calculate crack growth, K_{1c} and σ_y will not affect the crack growth.

4) Define the stochastic loading process either by analytical spectra or numerical forms as discussed in chapter 5.

5) Assume that stress interaction effect can be ignored so that equivalent stress range can be used for calculation of crack growth as the cyclic loading. S_{re} can be obtained from equation (6.38).

6) The number of cycles for spectrum i, i.e. for equivalent stress range S_{re_i} for a period of time t_i is:

$$n_i = E(P)_i \times t_i \tag{6.46}$$

7) For stress range S_{re_i}, determine the range of stress intensity factor $\triangle K_i$.

8) Check whether $\triangle K_i$ exceeds the threshold $\triangle K_{th}$ and if so, compute the increment of crack growth from Paris' Law. i.e.

$$a_{new} = [a_{old}^{(2-m)/2} + \frac{2-m}{2} C Y^m F S_{re_i}^m \pi^{\frac{m}{2}} n_i]^{\frac{2}{2-m}} \tag{6.47}$$

$$= f(a_{old}, Y, C, m, S_{re_i}, n_i)$$

9) Reset $a_{old} = a_{new}$, and repeat step 2 to 4 for all the seastate equivalent stress ranges that will be encountered over the period considered.

6.6.2 Example

The above procedure is used in the following example:

1) Crack geometry:

A typical welded cruciform joint is studied. The Y factors are obtained from 2 dimensional finite element calculation. The stress concentration in this way is automatically considered. The initial flaw is taken as $a_0 = 2$ mm and situated at the toe of the attachment weld. The section thickness w=40mm.

2) Y factor:

$Y(a)$ can be obtained from the piecewise-cubic polynomial fitted to the normalised stress intensity factor data, (see Fig 6.1 finite element output).

3) Material properties:

$C = 0.0001315(895.4)^{-m}$ *for* K in (N mm$^{-3/2}$)

$m = 3.0$

$\triangle K_{th} = 90\text{Nmm}^{-3/2}$

$K_{1c} = 300\text{MPa}\sqrt{\text{m}}$

$\sigma_y = 375$ MPa

4) Loading process:

The loading process is defined by 11 spectra provided by Wirsching[6.24].

5) Stress range:

Model 3 of the constructed stress range pdf in chapter 5 has demonstrated to fit well with the simulated results. Therefore equivalent stress ranges can be calculated from Eqn. (6.38) with a_1, b_1, a_2, b_2 and f_w from model 3.

6) Number of cycles:

It is difficult with the data given by Wirsching to decide how long a seastate last in real situations. However, the fraction of time, namely an_i, for each seastate is given. So for an iteration period of total time t for all these spectra, $t_i = t \times an_i$ for spectrum i. Thus n_i can be obtained from Eqn. (6.46).

Step 7),8),9) can be carried out accordingly. The crack growth curve is shown in Fig. 6.13.

It is not practical in a reliability calculation to conduct a cycle by cycle calculation for any step in the R-F algorithm while the changing Y factor limit the Miner's rule applicable only to a small period of time. In order to avoid excessive computation and maintain accuracy, an appropriate iteration unit t_u should be found for reliability analysis.

By taking one iteration as from minimum stress range to the maximum stress range the crack growth curves are shown in Fig. 6.12, in which for spectrum i in each iteration:

$$n_i = t_u \times E(P)_i \times an_i \tag{6.48}$$

It can be seen from Fig. 6.12 that for iteration unit smaller or equal to 10^5, very little difference can be observed. Therefore it can be stated that 10^5 can be taken as iteration unit with acceptable crack growth curve.

Care should be taken that the nonlinearity of crack growth is subjected to the Y factor , C and m. The result of appropriate iteration unit may deviate from the Miner's rule in some other circumstances.

6.7 Conclusions

In this Chapter, the problems of fatigue calculation for reliability analysis are discussed. To narrow the wide range of fatigue problems to a particular case, the cracks in offshore platform joints under wave loading are studied in detail.

For crack growth under random loading, the complexity of stress interaction effects have not yet been fully understood. The equivalent stress range concept has been used for its simplicity and good agreement with experimental results.

By using the stress range distribution models from chapter 5, the equivalent stress ranges obtained are found to have much better agreement with simulation results than previous empirical models by Wirsching, Hancock and Dover *et al*[2.18], [2.21], [2.22], [2.27]. The great improvement in accuracy is due to a more fundamental treatment of the equivalent stress range as the result of better estimation of stress range pdf from the rainflow counting method.

Fatigue crack growth based on cycle by cycle calculation, is not practical for a reliability analysis, which will require the fatigue crack growth calculation many times for the convergence of reliability index. It is found from crack growth calculation that cycle by cycle calculation is not necessary to have an acceptable crack growth curve if the total cycle numbers per iteration for the whole 11 seastates example is less than 10^5. In this way an efficient crack growth calculation can be achieved.

Table 6.1 Y factor for a cruciform joint

a/t	Y
.001	5.6017
.002	4.4524
.004	3.5523
.008	2.8437
.010	2.6550
.020	2.1491
.040	1.7723
.060	1.6098
.080	1.5289
.100	1.4838
.120	1.4513
.140	1.4464
.160	1.4513
.180	1.4639
.200	1.4786
.300	1.6565
.400	1.9738
.500	2.4211

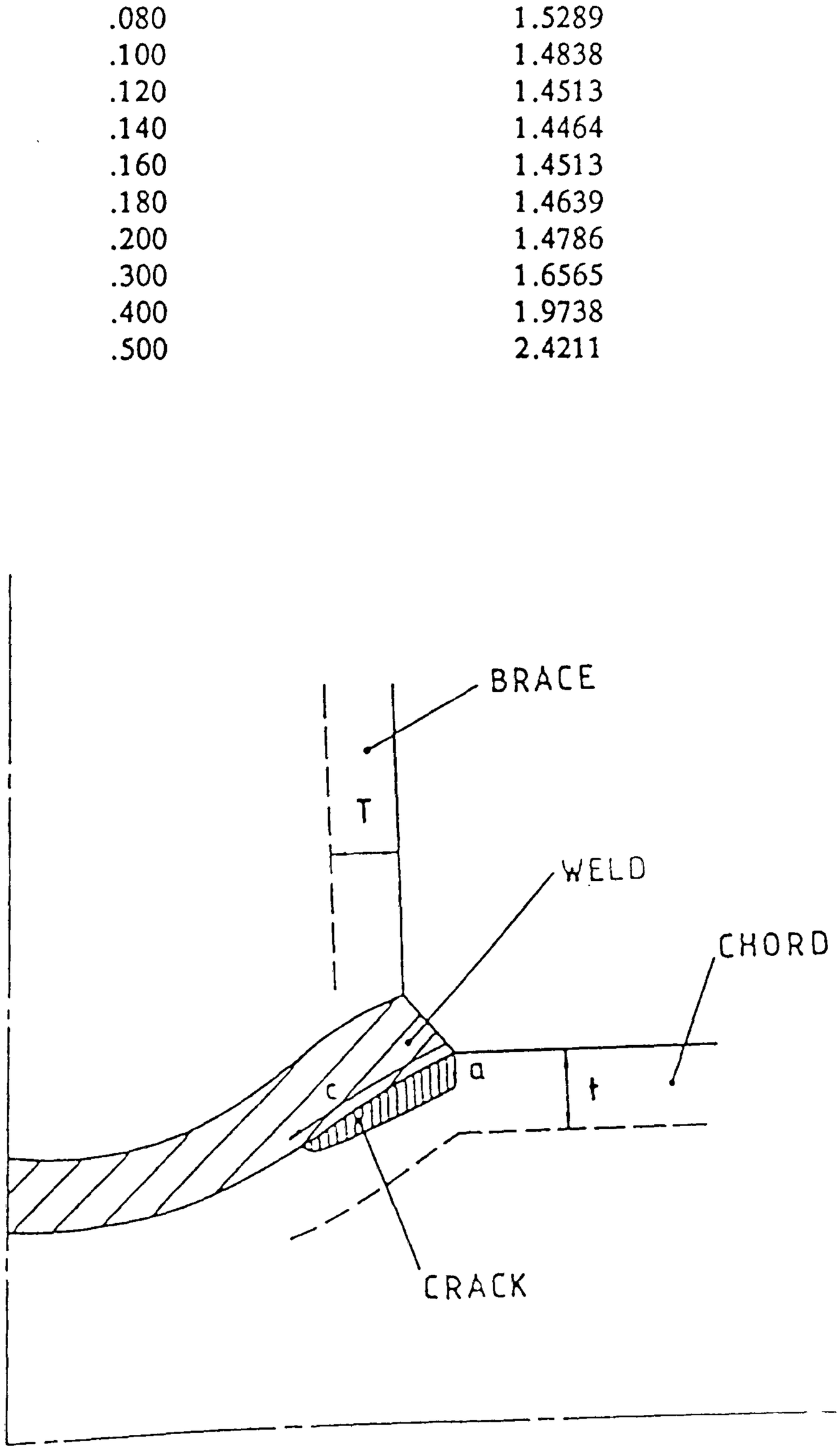

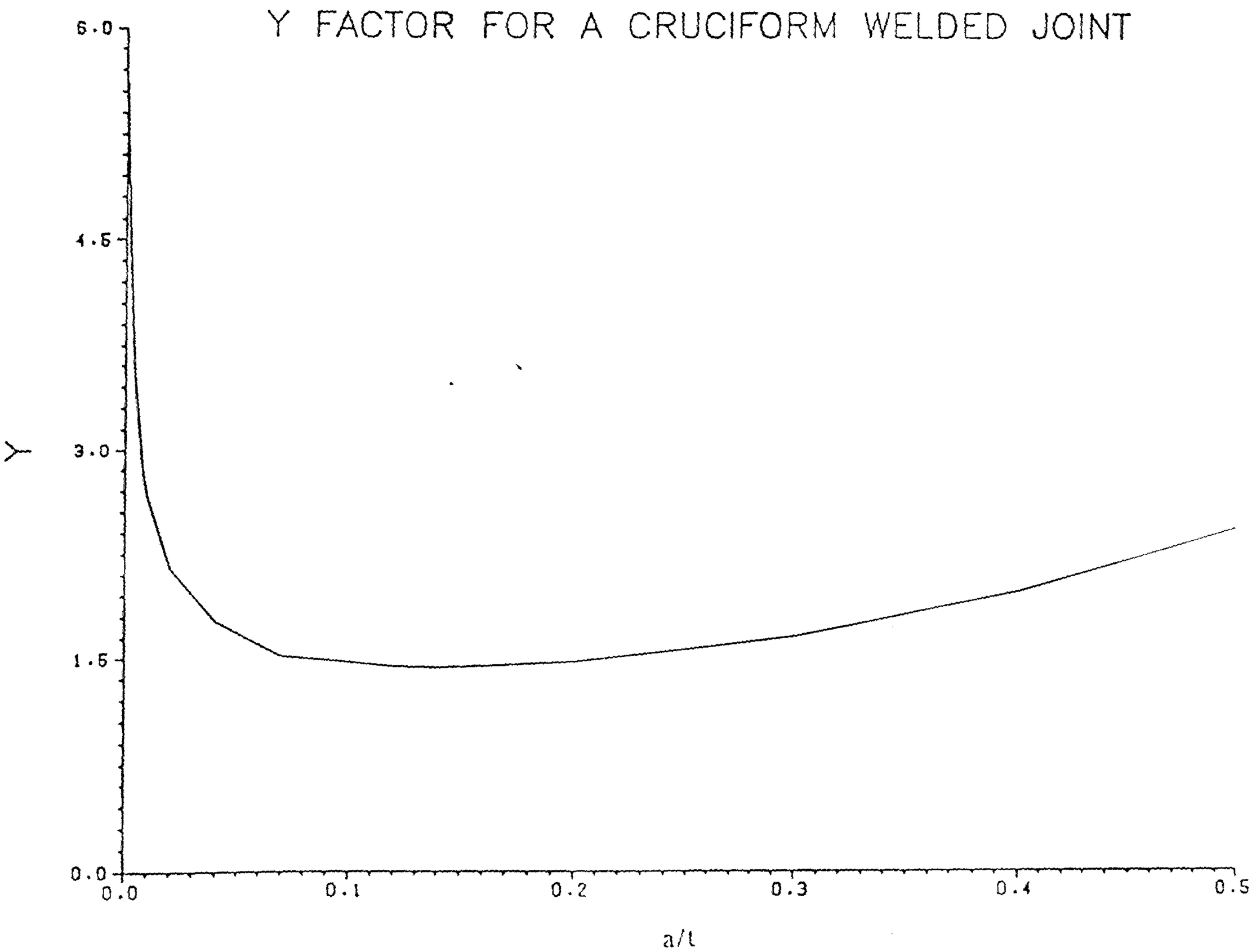

Fig. 6.1 Y factor for a cruciform weld joint

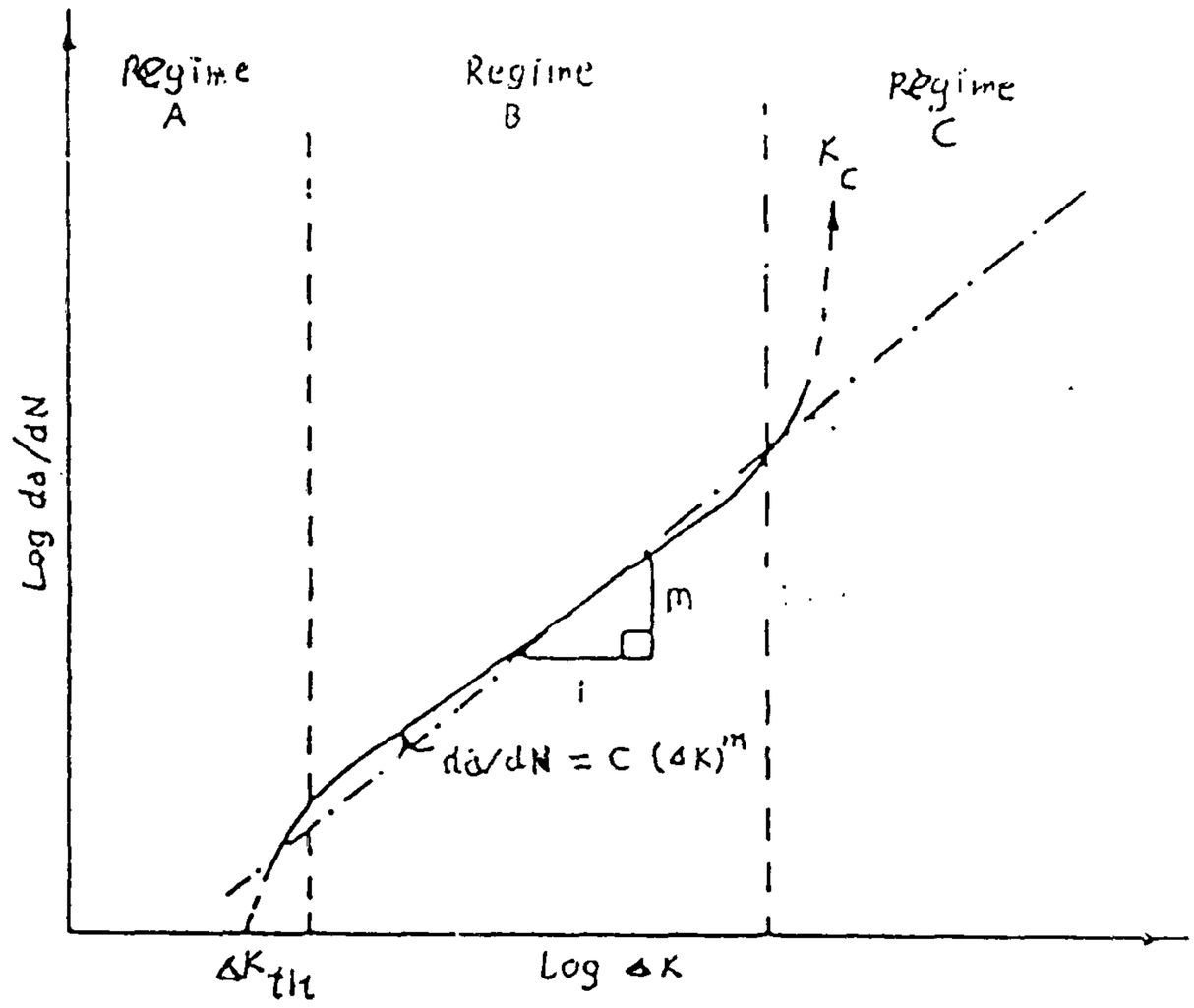

Fig. 6.2 Relationship between $\frac{da}{dn}$ and ΔK

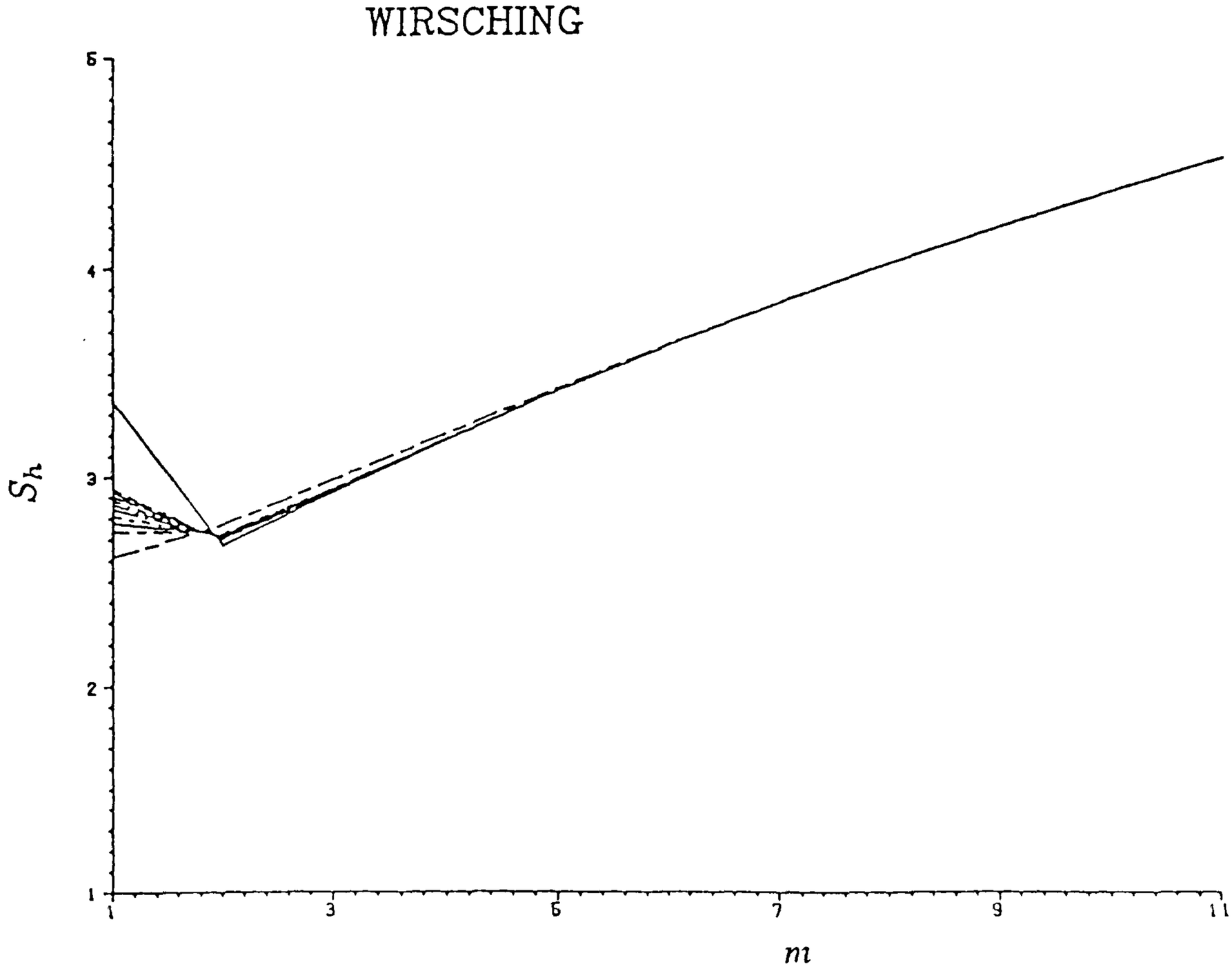

Fig. 6.3 Normalised equivalent stress range from Wirsching

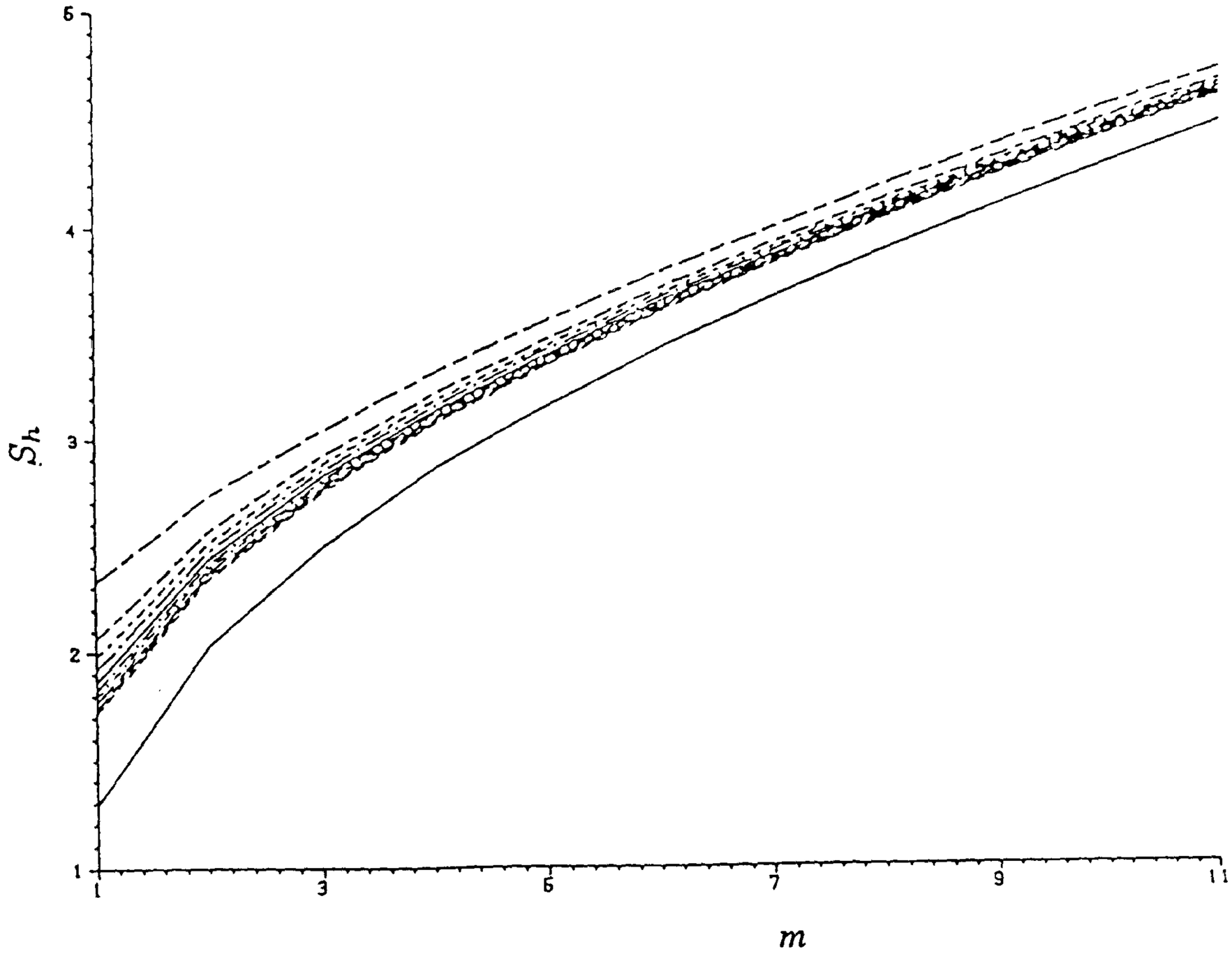

Fig. 6.4 Normalised equivalent stress range from Hancock (A)

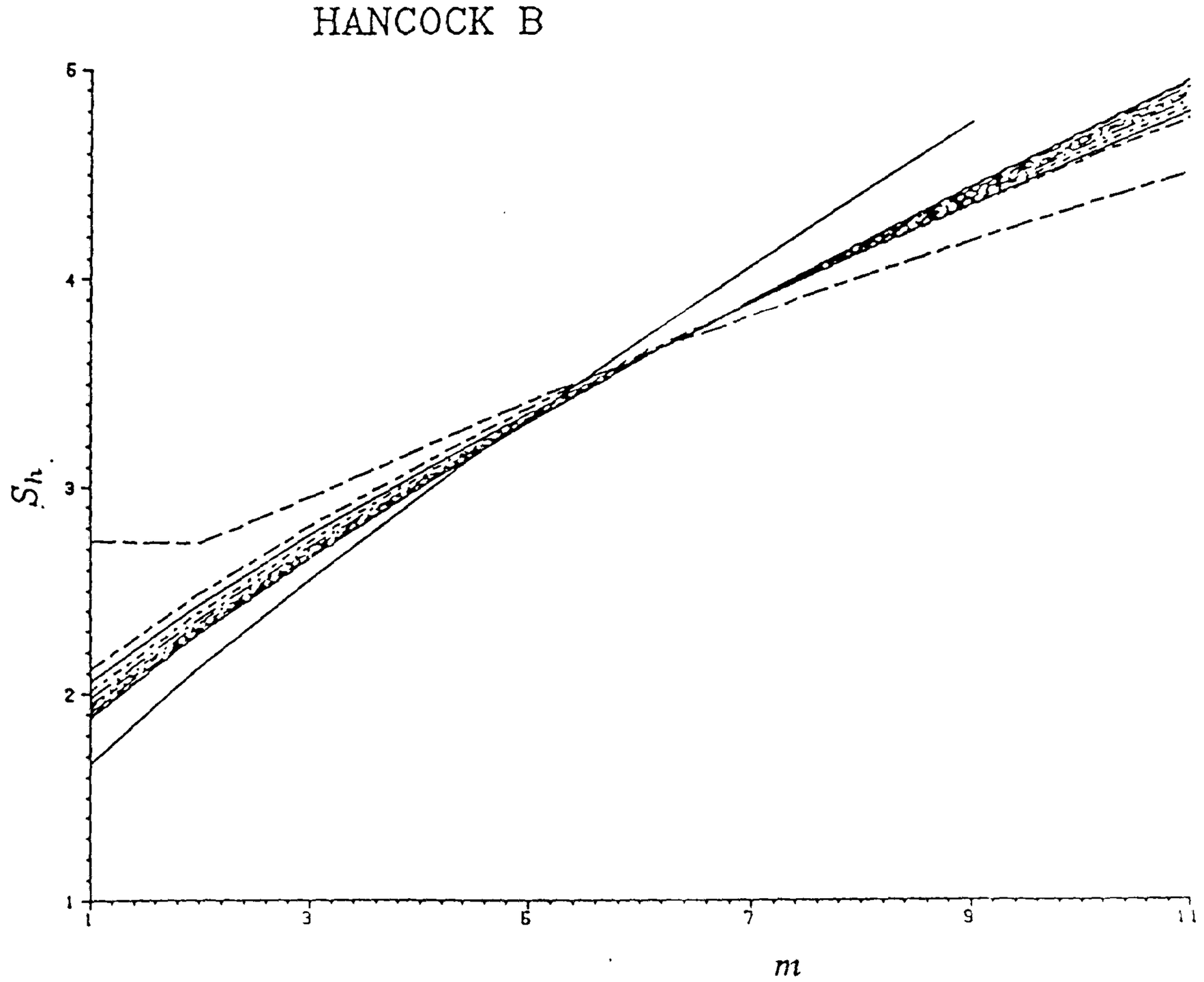

Fig. 6.5 Normalised equivalent stress range from Hancock (B)

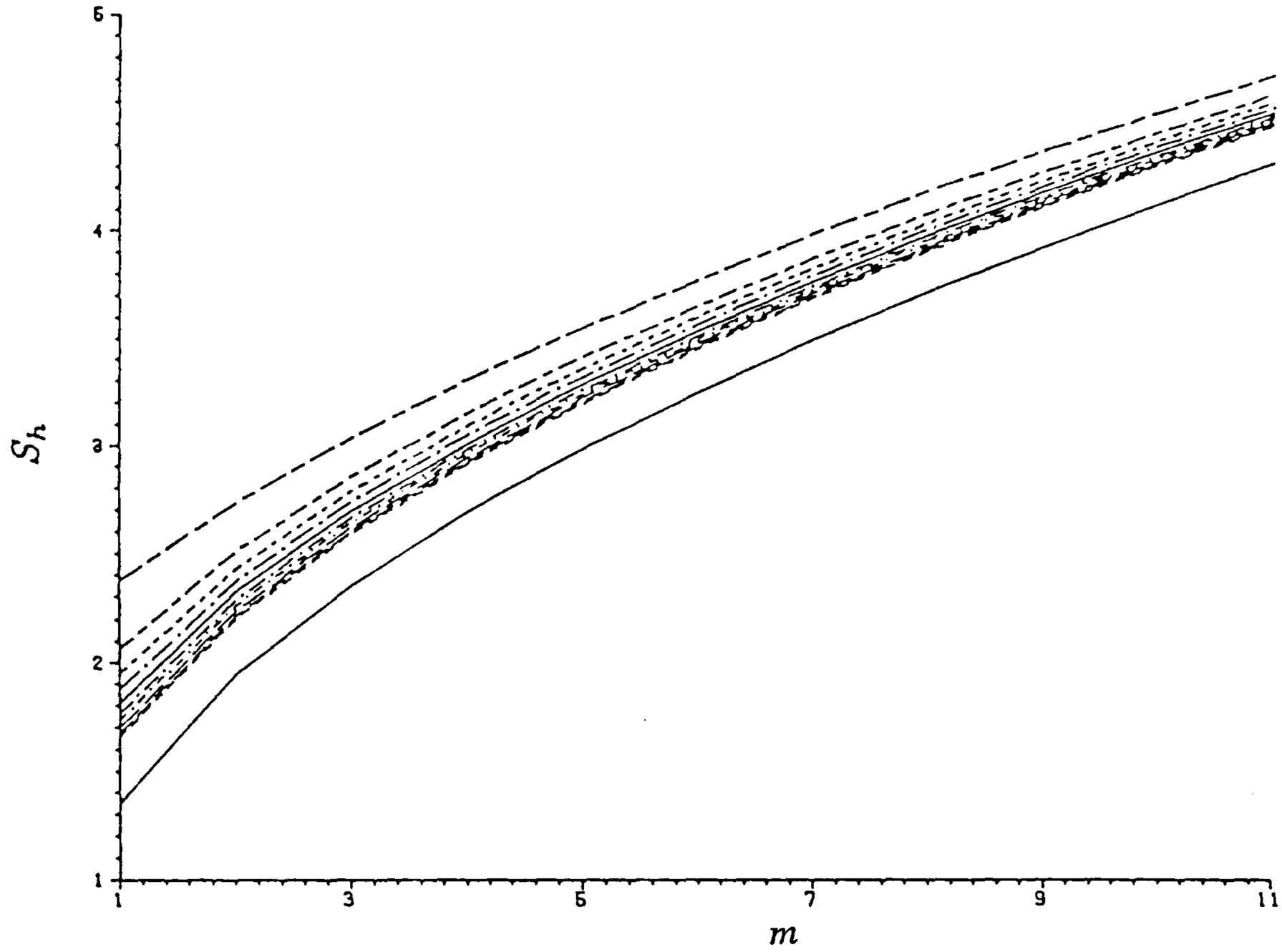

Fig. 6.6 Normalised equivalent stress range from Chaudhury and Dover

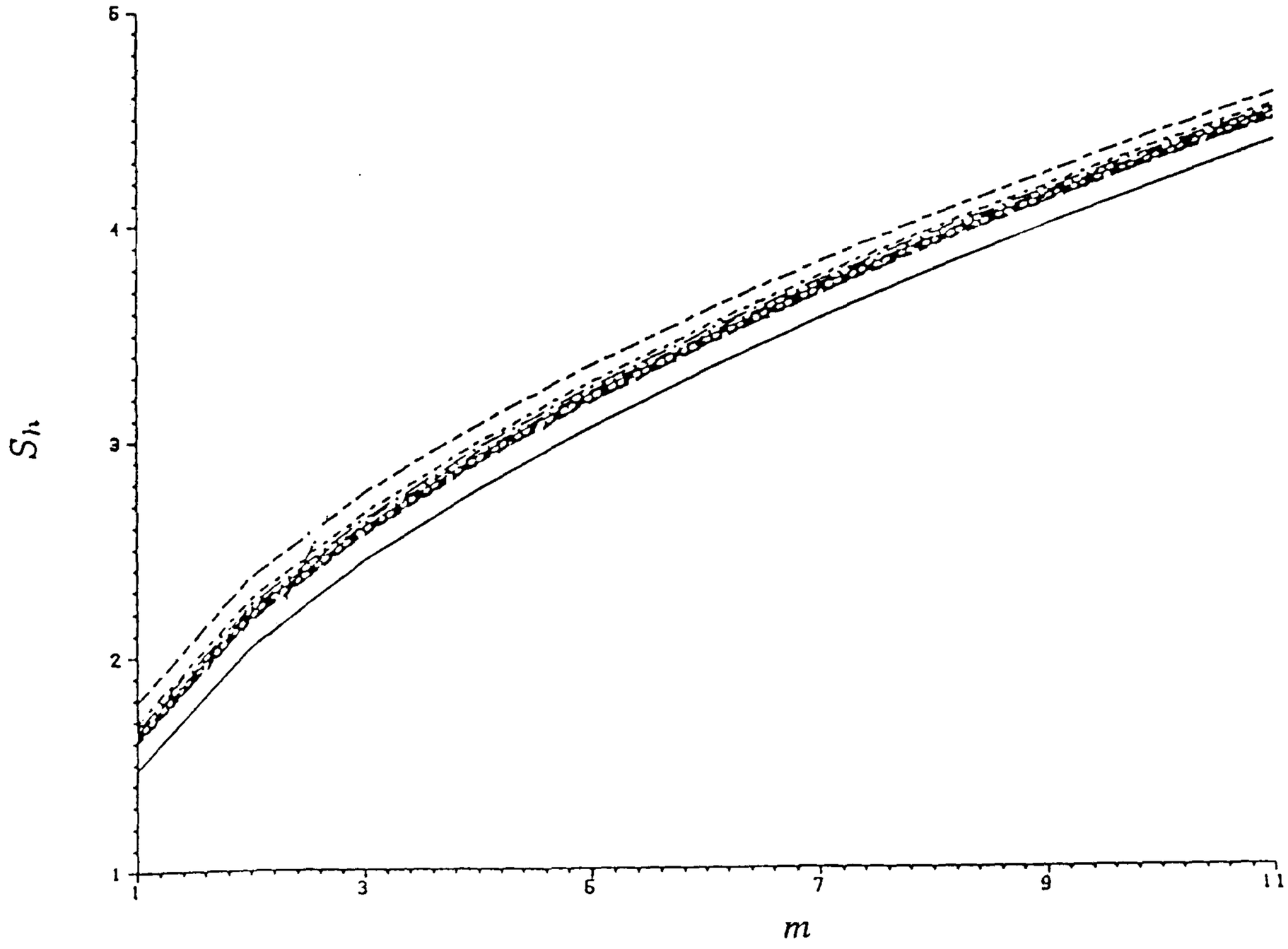

Fig. 6.7 Normalised equivalent stress range from Kam and Dover

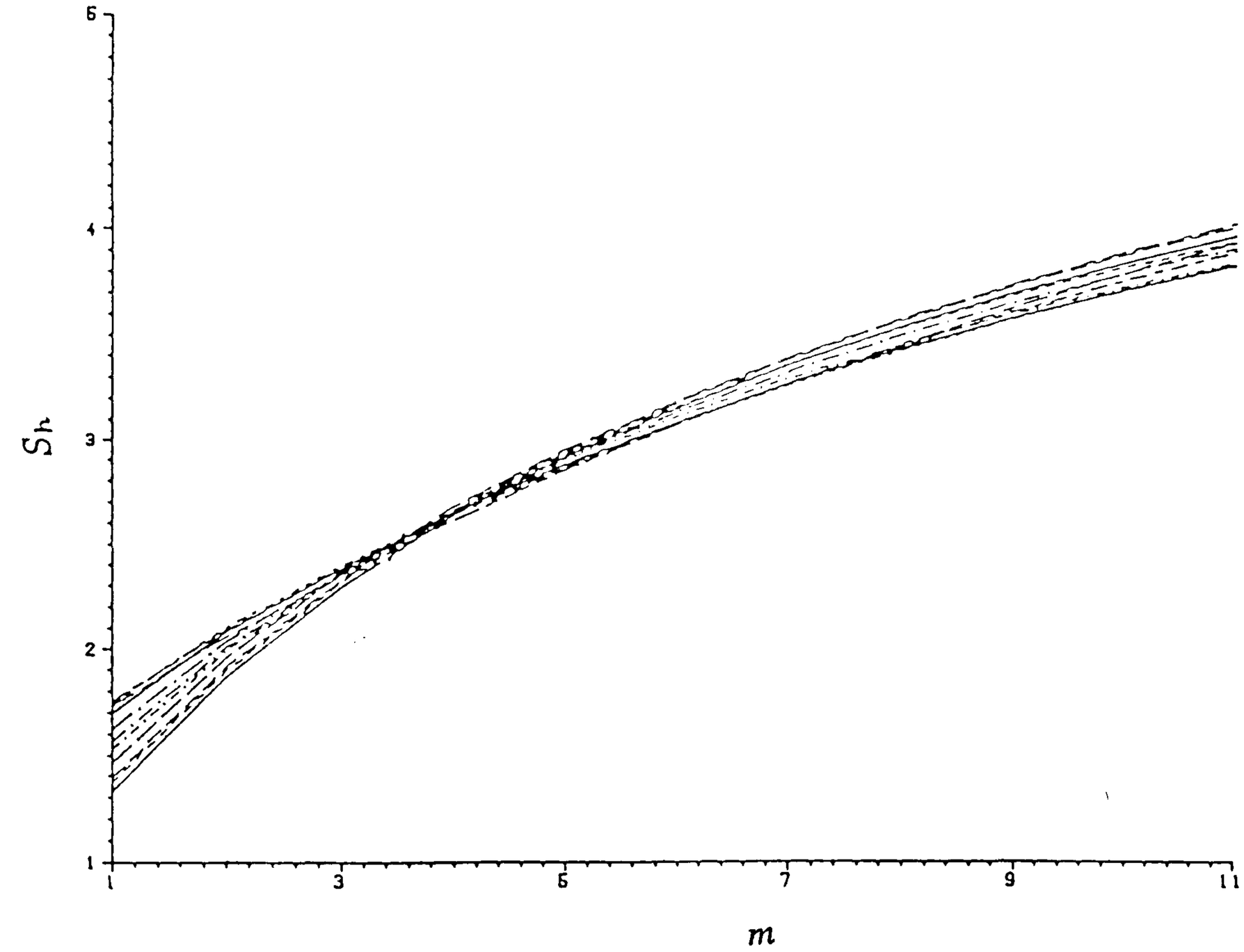

Fig. 6.8 Normalised equivalent stress range from simulation

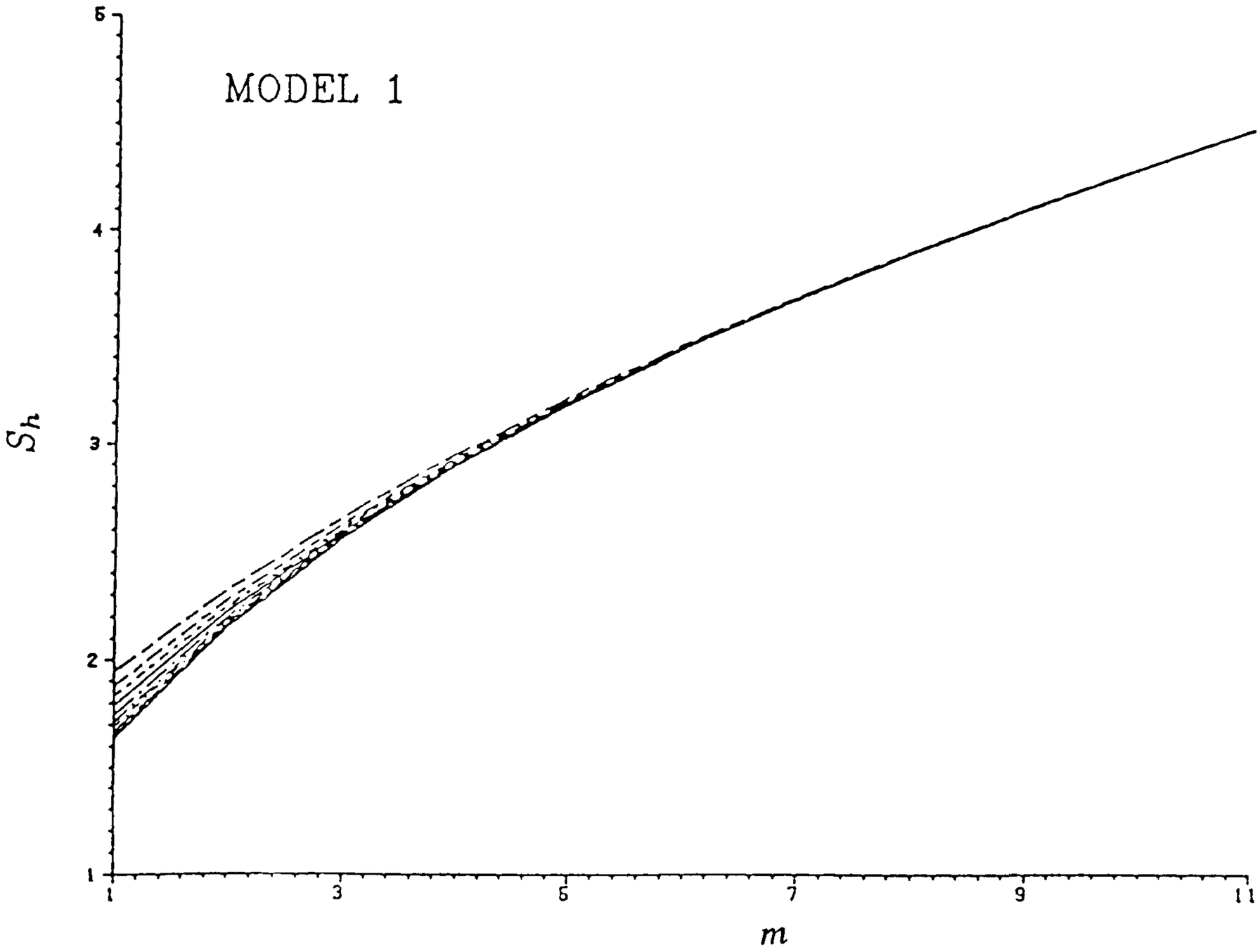

Fig. 6.9 Normalised equivalent stress range from Model 1

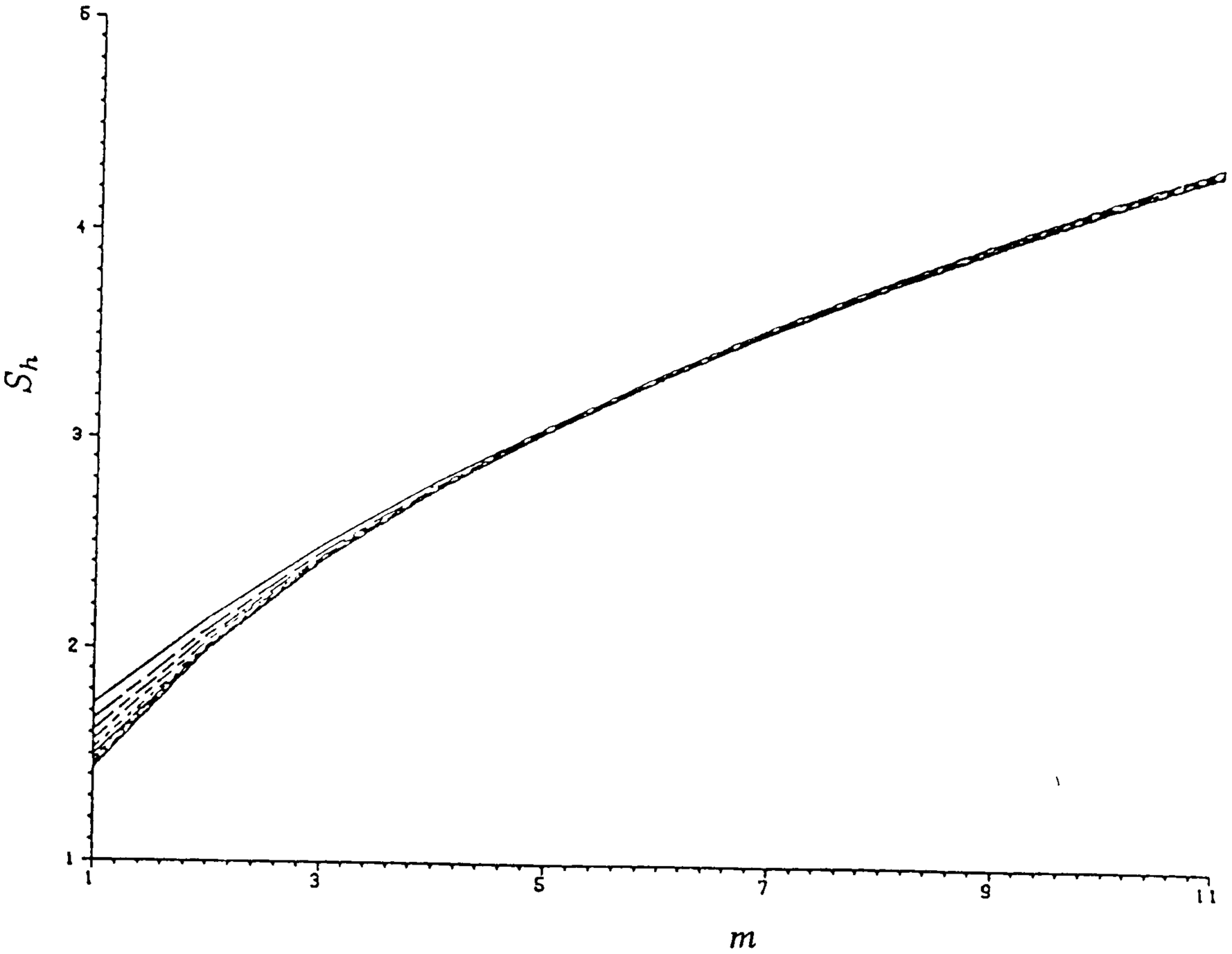

Fig. 6.10 Normalised equivalent stress range from Model 2

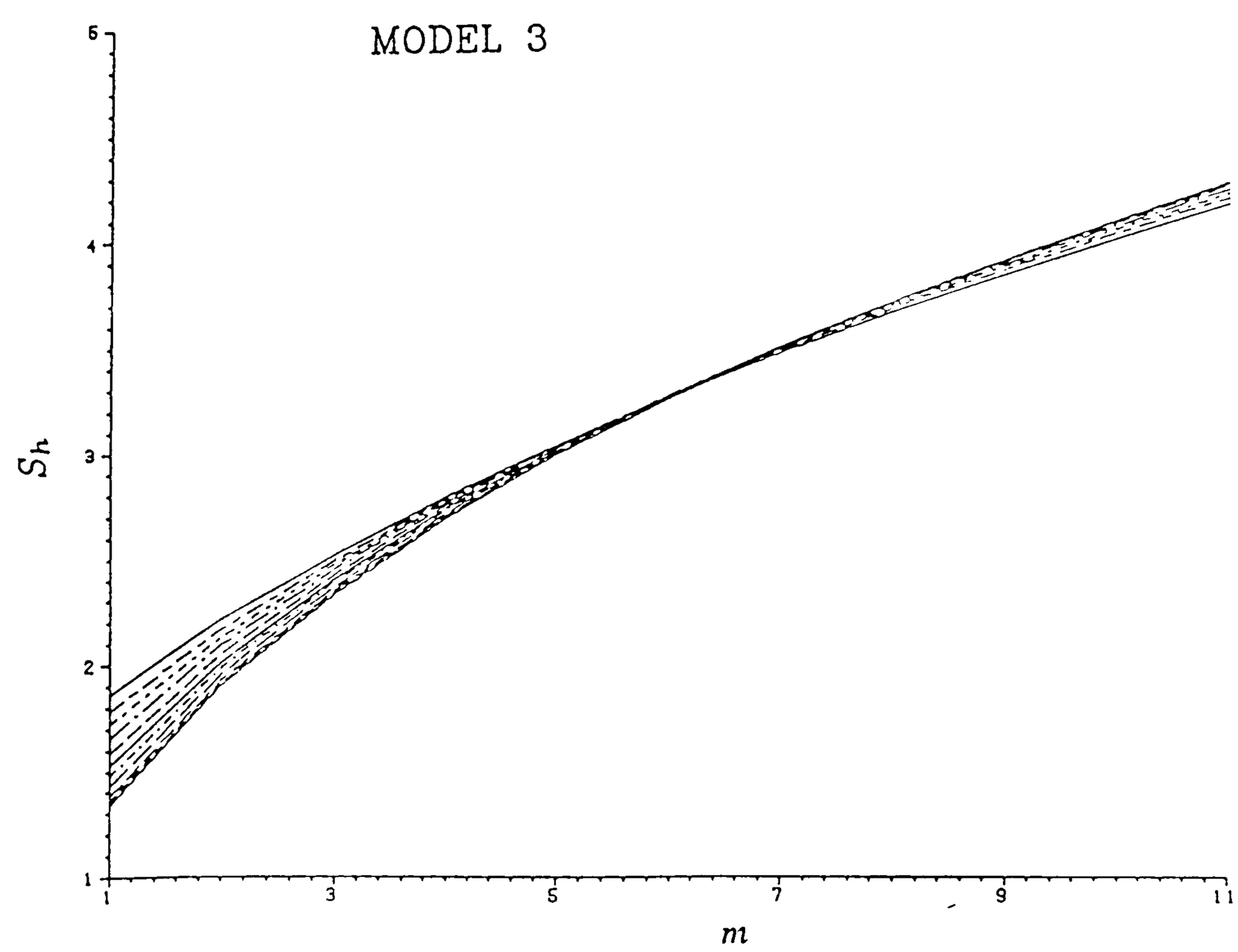

Fig. 6.11 Normalised equivalent stress range from Model 3

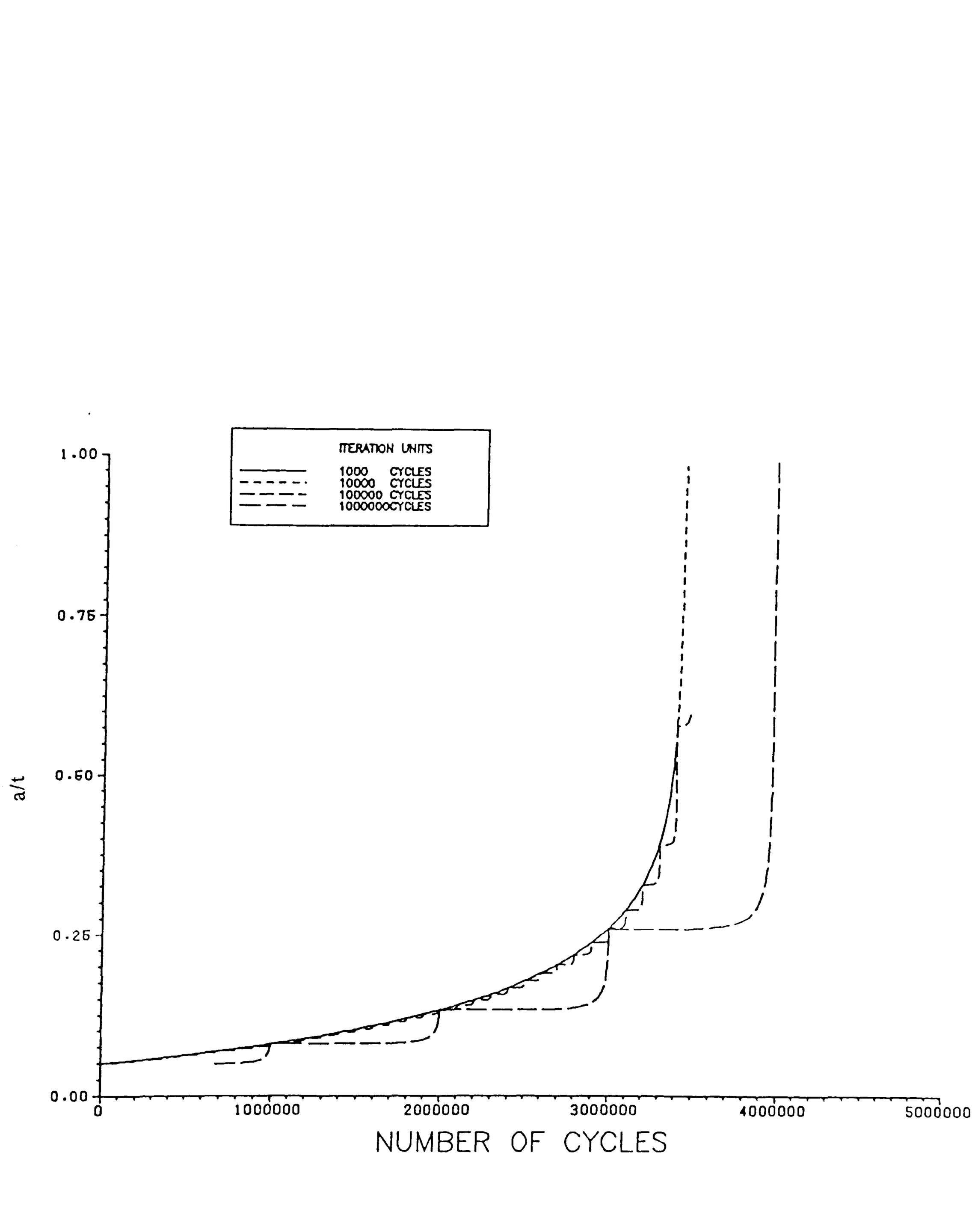

Fig 6.12 Fatigue crack growth curve

Chapter 7

The Reliability Assessment Of Cracked Components Failing By Brittle Fracture Or Plastic Collapse Following Fatigue Under Random Loading

Nomenclature

a	crack size
a_i	initial crack size
a_{new}	crack size after fatigue crack growth
C	Paris' law material constant C=$C_0 10^{F_c}$
$E(P)$	peak rate
F_c	parameter in Paris' Law
f	frequency in Hz
f_n	natural frequency in Hz
H_s	significant wave height
K	stress intensity factor
K_{1c}	fracture toughness
m	Paris' law material constant
$P(n_i)$	probability of occurrence of seastate i
$\mathbf{P}_i$	transition matrix
S	equivalent stress range
S_p	parameter defined by Eqn.(7.13)
SCF	stress concentration factor
t	time
T	time unit=2,500,000 seconds
T_D	dominant period
Y	geometry shape factor
σ_{max}	maximum stress
σ_y	yield stress
σ_u	ultimate stress

Other symbols are defined in the text.

7.1 Introduction

This chapter has incorporated the studies in previous Chapters to form a methodology for the overall reliability analysis of cracked structural components under stochastic fatigue and fracture. This Chapter should be read in conjunction with all previous Chapters.

Structural reliability theory has been discussed in chapter 2. Deterministic fracture mechanics and fatigue have been discussed in Chapters 3 and 5. Leading from those theories, the failure functions for the final failure of cracked components under tensile stress are defined by the R6 method in particular R6 rev. 3. The uncertainties in the random variables which appear in the failure function are discussed both in chapter 3 and chapter 4. Following chapter 2 and chapter 3, reliability analysis is conducted for some examples in chapter 4. A reliability computation procedure for the combined fracture and fatigue problem is also presented in chapter 4. In fatigue analysis random loading data is often obtained by approximation. However in chapter 5, a rainflow stress range probability distribution function for spectral loading is presented which closely agrees with simulation results. This model can further facilitate parametric study in reliability analysis. Chapter 6 discussed the deterministic fatigue process and defined solutions for the analysis of fatigue problem in this thesis. A crack growth calculation procedure was also presented in chapter 6.

It is assumed in this chapter that a cracked component is subjected to random cyclic loading, for instance, ocean wave loading for a given period of time. A reliability analysis is conducted to calculate the probability of failure at the end of that period by assuming the occurrence of an extreme load. The output includes sensitivity factors, design points, coefficients of correlation of linearised failure modes for fracture and plastic collapse, and an approximate probability of failure as shown in Table 7.1.

The methodology for a reliability analysis of fatigue and fracture for cracked components includes 1) modelling of basic variables 2) construction of failure functions 3) reliability computation. Since some of the tasks for constructing such a methodology have been discussed in previous chapters, the scope of this chapter will be to:

1) discuss the statistical fatigue process

2) review previous work on modelling of stochastic fatigue process

3) construct failure functions for the failure of the cracked component following fatigue

4) choose the probability distributions for the basic variables

5) undertake a reliability analysis for some examples.

7.2 The Statistical Nature of The Fatigue Process

In chapter 6, the basic fatigue crack growth mechanism is discussed. Factors influencing the fatigue process have been discussed in detail. Each factor is subject to variation in practical situations. Therefore fatigue laboratory results cannot be taken as deterministic values.

The variables normally used for fatigue analysis of a structural defect include:

1) initial state of the crack

2) geometry of the structural component or system

3) external loading e.g. wind, traffic, wave

4) factors affecting the response to the loading, e.g. mass, stiffness, direction, inertial force, stress concentration, drag force if the source is fluid, continuity mechanism etc.

5) material properties, slope of S-N curve in S-N approach; C, m, ΔK_{th}, K_{1c} etc.

However, at the fundamental level, even if the values in categories 1 to 5 above are fixed as deterministic, the fatigue crack develop process is still a stochastic process as shown in typical laboratory tests where the test conditions are well controlled[7.1]. This indicates that the fatigue process itself is a stochastic process. Recalling discussions in Chapters 2, 3, 4 and 6, the main factors contributing to the variation of crack growth rate are:

1) inhomogeneity of material e.g. inclusions in welds, voids in polycrystal, and notches and crack opening stress.

2) crack irregularity. Stress intensity factors used for fatigue study are usually K in the K_I (i.e. mode I). The actual crack front does not extend uniformly across the thickness of a test specimen due to microstructural differences and the state of the stress; hence the cracks may grow in a non-symmetric manner

3) the threshold value is a nominal one to account for a complicated process which may include 1) stage I crack growth 2) crack opening process 3) crack tip blunting 4) change of fracture mode

4) random loading stress interaction effect

5) uncertainties in the nominal material properties

6) uncertainties in the final fracture model

7) measurement errors in experimental tests whether by the secant method or polynomial method.

7.3 Stochastic Models of The Fatigue Process

The fatigue process has been modelled as a stochastic process in different ways. The main models proposed have been at two extremes: 1) statistical analysis of laboratory records or simulated data to predict the stochastic fatigue process (Kozin[7.2], Yang[7.3]), and 2) engineering models based on a deterministic governing equation for fatigue crack growth and statistical distribution of the basic variables (Baker[7.4], Wirsching[7.5]).

The crack growth equation can be written as

$$\frac{da(t)}{dt} = x(t)g(a(t)) \tag{7.1}$$

where $a(t)$ denotes the crack size at time t, $g(a(t))$ is the usual deterministic equation governing the crack growth rate.

Yang[7.3] has treated $x(t)$ as a random pulse train to simulate the stochastic crack growth.

$$x(t) = \sum_{k=1}^{N(t)} Z_k w(t, \tau_k) \tag{7.2}$$

where N(t) = a homogeneous Poisson counting process giving the total number of pulses that arrive within the time interval [-∞ , τ_k],

τ_k = arrival time of the k^{th} pulse

Z_k = random amplitude of the k^{th} pulse independent for different k.

$$w(t,\tau) = \begin{cases} 1, & 0 < t - \tau \leq \Delta \\ 0 & otherwise \end{cases} \tag{7.3}$$

The probability distribution of the random time to reach a given crack size and its statistical moments, and probability distribution of random crack size at any time, with additional assumption of $a(t)$ as a Markov process, can be obtained from the above equations.

There are two extremes for this model a) the process is fully uncorrelated for any two different times. In this case, the variability of random time to reach a specific crack size would be a minimum. b) $z = x(t)$ is treated as a random variable as opposed to a random process. In this case, there will be the largest variability of random time to reach a specific crack size. Yang has assumed this to be a lognormal distribution . Also in a later study[7.6] Yang has replaced the Markov process approximation by a cumulant-neglect closure model.

However, these mathematical attempts seem to somehow lack convincing physical arguments.

The Kozin-Bogdanoff model[7.2] [7.6] uses the concept of *duty cycle* , which is a repetitive period of time in the operational life of the component in which damage can accumulate, to discretise the real stress cycles into a series of duty cycles.

In the Kozin-Bogdanoff(B) model, the stochastic process of interest is the cumulative damage (CD) for a large number of data sets in the fatigue life, fatigue crack growth and wear. The state of damage is only considered at the end of the duty cycle. The damage during one duty cycle is assumed to be non-negative, and the state of damage at time t is given by the vector:

$$\mathbf{p}_t = [p_1(t), p_2(t), ..., p_b(t)] \tag{7.4}$$

where $p_i(t)$ is the probability that damage is in state i at time t. b denotes the defined state of failure and $\sum_{i=1}^{b} p_i(t) = 1$.

If we assume an initial damage state vector $\mathbf{p}_0, \mathbf{p}_t$then follows from Markov chain :

$$\mathbf{p}_t = \mathbf{p}_0\mathbf{P}_1\mathbf{P}_2, ..., \mathbf{P}_t \tag{7.5}$$

The statistical characteristics can be derived thereafter.

The above models all need data acquisition for special specimens and extensive statistical analysis. These are not yet generally available.

One important approach for engineering reliability analysis is to start with deterministic crack growth and failure functions and then introduce random quantities into the model parameters. (Baker[7.4], Madsen[7.7], Wirsching[7.5])

In previous chapters of this thesis the fracture mechanics parameters have been fully discussed and the random loading process has been modelled successfully. From literature and past experience, material parameters appearing in the crack growth equations can be treated as random variable and given appropriate types of distributions. In this way, we can have a consistent approach for a reliability study.

7.4 Modelling of Statistical Variables

7.4.1 Loading variables

Chapter 5 has analysed the stress range distribution under random loading and proposed three similar models for stress range distribution under spectrum loading.

In chapter 6, the equivalent stress ranges are modelled for stochastic wave loading. The seastate spectrum parameters are taken as deterministic values. The transfer function from the seastate spectrum to the response spectrum can include a number of factors. In this thesis, only the fundamental natural frequency is taken as statistical variable as an example. The structural natural frequency depends on many factors (mass, stiffness, the joint flexibility, the pile foundation etc.). Due to the dominant effect of the first mode on the structural vibration, only the first mode natural frequency is considered. The uncertainties in natural frequency are recognised by assuming a coefficient of variation of 0.15 with a normal distribution.

For the stress response in a welded joint, the stress concentration factor should be introduced to take account the discontinuities at the joint. However, in this study the Y factors calculated from finite element analysis have already included the stress concentration effect. The Y factors are give in Table 6.1.

The reliability of the joint is calculated at the end of a stochastic fatigue growth period at which it is assumed that some peak load will be applied to the structure. It is assumed that the peak loading acting upon the cracked component will have a normal distribution with mean of 140 MPa and a coefficient of variation of 0.1.

However, this is not very realistic and attempts should be made to improve this part of the model in future research.

7.4.2 Initial crack size

The initial crack state is assumed to be the same as discussed in Chapter 6 for typical offshore welding joints. The crack size is assumed to be normally distributed with a coefficient of variation (COV) of 10%.

7.4.3 Material properties

The probability distribution of yield stress and fracture toughness have been discussed in Chapter 4. For fatigue a few extra material properties are required: 1) threshold value 2) Paris parameters C and m.

The deterministic value of threshold stress intensity factor range has been discussed in Chapter 6.

It is assumed that the mean values of the threshold filter ΔK_{th} is equal to 90 N/mm $^{3/2}$ and the standard deviation is equal to 15 N/mm$^{3/2}$.

The factors C and m depend on materials. According to a probabilistic study by Snijder *et al* [7.8], the mean values for weld metal are m=2.6 and $C_0 = 0.8833\ 10^{-12}$ (N,mm). The factor m is taken to be deterministic. The factor C is assumed to be log-normal:

$$C = C_0 10^{F_c} (\text{Nmm}) \tag{7.6}$$

where F_c is normally distributed with mean value equal to 0 and standard deviation equal to 0.102.

Table 7.2 shows the statistical modelling of all the variables in a fatigue and fracture process under random loading for a typical steel of BS4360 50D steel.

Table 7.2 Reliability calculation input

Variable	Distribution	Values	Reference
K_{1c}	normal	COV=.1	Chapter 4
Y	deterministic	function of a	Chapter 6
$\Delta\sigma$	governed by response spectra		Chapter 5
Sea state parameters	deterministic range		Chapter 5
f_n	deterministic	$\mu_{f_n} = 0.34$ Hz	Chapter 5
	or normal	$\sigma_{f_n} = 0.05$ Hz	Chapter 7
σ_{max}	normal	$\mu = 140$ MPa COV=.1	Chapter 7
σ_y	lognormal	$\mu = 360$MPa $\sigma = 30$ MPa	Chapter 4
L_r^{max}	deterministic	1.225	Chapter 4
m	deterministic	2.6	Chapter 6
C_0	deterministic	$0.8833\ 10^{-12}$	Chapter 7
F_c	normal	$\mu = 0\ \sigma = 0.102$	Chapter 7
ΔK_{th}	normal	$\mu = 90\text{N/mm}^{3/2}\ \sigma = 15\text{N/mm}^{3/2}$	Chapter 6
a_i	normal	COV=0.1	
T	deterministic	2,500,000 seconds per unit	Chapter 7
w	deterministic	40 mm	Chapter 6

7.5 Failure Functions

7.5.1 Conventional failure function

If failure is defined as the state in which the cracked component cannot sustain the extreme loading and therefore fails by rupture or plastic collapse at the end of the fatigue crack growth, a straightforward form of failure function can be constructed as follows:

1) calculate crack size a_{new} after fatigue growth

2) determine K_r and L_r with $a = a_{new}$ from R6 FAD..

3) for fracture failure mode, in the R6 FAD, the failure assessment line is assumed to be $K_r = K(L_r)$, then, the failure function is:

$$g_1(\mathbf{X}) = K(L_r) - K_r \tag{7.7}$$

for plastic collapse failure mode:

$$g_2(\mathbf{X}) = L_r^{max} - L_r \tag{7.8}$$

In a reliability analysis, the amount of computer time required for convergence in the R-F algorithm depends partly on the local shape of the failure surface. In the case of fatigue and fracture reliability analysis if the above failure functions are used, each iteration will involve time spent in calculating fatigue crack growth for determining the derivative of all the fatigue related variables including $F_c, \Delta\sigma, f_n, \Delta K_{th}, a$. Therefore, in each iteration fatigue crack growth needs to be calculated 4 or 5 times. Hence, it is important to find a suitable failure function which converges quickly.

In this study, it was found that the failure functions given by Eqn.(7.7) and Eqn. (7.8) often take many iterations to converge and in some cases convergence was not achieved. Eqn.(7.7) and (7.8) are not suitable for all cases, and more suitable failure functions are defined below.

7.5.2 Alternative failure functions

For the same definition of failure state as in section 7.5.1, alternative failure functions can be constructed as follows:

a. for fracture failure mode:

1) calculate crack size a_{new} after fatigue growth

2) calculate critical crack size a_{crit}

3)

$$g(\mathbf{X}) = a_{crit} - a_{new} \tag{7.9}$$

b. for plastic collapse failure mode, in addition to Eqn. (7.9):

1) calculate crack size a_{new} after fatigue growth

2) calculate L_r with $a = a_{new}$

3) for yield load=$\sigma_y(w - a)$,

$$g(\mathbf{X}) = L_r^{max}\sigma_y(1 - \frac{a_{new}}{w}) - \sigma \tag{7.10}$$

or

$$g(\mathbf{X}) = L_r^{max}/L_r - 1 \tag{7.11}$$

Eqn. (7.7) and Eqn. (7.9) represent the same physical failure states with different mathematical expressions. Eqn. (7.7) relates the state of the cracked component of crack size a_{new} to its relevant position in the R6 FAD. Whereas Eqn. (7.9) compares the component crack size after fatigue, a_{new} with the critical crack size obtained from R6 FAD, thus ensuring that the failure surface is not influenced by the local shape of the R6 FAD. Eqn. (7.10) compares the applied stress with maximum stress allowing for crack growth thus avoiding the difficulty in defining failure by Eqn.(7.8). Eqn. (7.11) is obtained by dividing both sides of Eqn. (7.10) by σ.

For the examples given in section 7.6, the failure functions from Eqn.(7.9) and (7.10) were found to give a much faster convergence to the reliability index. Normally, only 4 to 5 iterations were needed for convergence. It was observed that the longer the fatigue loading period is, the more iterations are generally needed. This can be explained by the fact that the longer the fatigue time, the more scattering of fatigue crack growth is expected.

7.6 Examples

7.6.1. Data preparation

A series of examples has been chosen to demonstrate the use of the models for probabilistic fatigue and fracture analysis. The crack has been assumed to be found in a cruciform welded joint of an offshore platform. The Y factors are given in Table 6.1.

For the purpose of reliability analysis under fatigue it has been necessary to define a time unit. This time unit has been chosen as 2,500,000 seconds, about one month, during which time it is assumed that all the seastates defined in the probabilistic study by Wirsching occur for the correct proportion of time. It is difficult to know, however, the real time interval corresponding to 1 time unit for a real offshore platform since all the very low seastates are not included in the model. When the time unit is zero, failure occurs without fatigue crack growth.

First, assuming the structural natural frequency has a deterministic value of 0.34 Hz, with COV for a_i and K_{1c} provided in Table 7.2, the mean values are given by:

Table 7.3 Example cases

Case	μ_{a_i}(mm)	$\mu_{K_{1c}}$(MPa $\sqrt{\text{m}}$)
Case 1	2	50
Case 2	4	50
Case 3	6	50
Case 4	4	70
Case 5	4	90

Together, cases 1, 2, 3 serve for a comparison of reliability with differences only in the statistical properties of a_i; whereas cases 2, 4, 5 serve for a comparison of reliability with differences only in the statistical properties of K_{1c}.

7.6.2 Probability of failure

The same procedure as discussed in chapter 4 in the flow chart of program RAFF has been used to conduct a reliability analysis but with changes in the failure functions as discussed in section 7.5. As demonstrated in chapter 4, second order reliability methods were found to make only minimal difference to first order reliability results. Hence in this analysis, second order reliability estimates are not calculated. In fact, in the process of determining reliabilities, the author has tried some examples but no meaningful differences were found between FORM and SORM.

Fig. 7.1 shows the the relationship between probability of failure and time (represented by the selected time unit) for cases 1, 2 and 3, with the same statistical properties of K_{1c} but different a_i.

As expected, as the mean value of a_i increases the probability of failure increases.

Fig. 7.2 shows the relationship between probability of failure with time for cases 2, 4 and 5 with the same statistical properties of a_i but different K_{1c}. As the mean value of K_{1c} increases the probability of failure decreases. It can also be seen that as the time increases, very little difference in the probability of failure can be found between case 4 and case 5. This is because the failure probability is governed by the fatigue crack growth and not the fracture parameters. The relationship of $P(f)$ with time in the fracture mode alone for cases 2,4, 5 is shown in Fig. 7.3. For the plastic collapse failure mode, K_{1c} does not appear in the failure function so that the value of K_{1c} has no influence on the probability of failure. So for plastic collapse failure mode, case 2, case 4 and case 5 have the same relationship between time and $P(f)$, as shown in Fig. 7.4.

The probabilities of failure calculated from Ditlevsen's bounds for the two failure modes are only slightly bigger than those from fracture failure modes alone. The reasons are that 1) the contributions of failure probabilities from the plastic collapse failure mode are low when $T \leq 2$; 2) when $T > 2$ although the contributions from the plastic collapse failure mode increase dramatically, the correlation between these two failure modes is very high (see Fig. 7.5). The coefficient of correlation ρ is determined from Eqn. (2.66).

As time increases, the fatigue variables have more and more influence on the probability of failure while the non-fatigue variables become less important. This explains the closeness of $P(f)$in Fig. 7.3 for case 4 and case 5 even with different K_{1c}. For case 1, fracture failure mode is still dominant due to small K_{1c}. These parametric relationships can be further explained in the sensitivity analysis in the next section.

7.6.3 Sensitivity analysis

Fig. 7.6 to Fig 7.10 show the sensitivity factors for the variables for cases 1 to 5. Resistance variables such as K_{1c}, σ_y and ΔK_{th} have negative values while loading variables such as σ, a and F_c have positive values. As α_i^2 is used to judge their relative contributions to failure probability, only the absolute values of α_i should be compared. The general trend is that the sensitivity factors of the fatigue variables such as a, F_c and ΔK_{th} increase with time and the sensitivity factors of the non-fatigue variables K_{1c}, σ_y, σ decrease as time increases.

Sensitivity factor for a_i

Generally the sensitivity factor for initial crack size increases with time. Comparing case 1, case 2, and case 3, one can see also that when the μ_{a_i} increases from 2mm to 6mm, the sensitivity factor of a_i increases by a large amount. Therefore in a structural safety assessment it is important to determine initial crack size by inspection. And in the quality control process, it is important to ensure a low initial crack size during fabrication.

Sensitivity factor for σ_y

The small sensitivity factors for σ_y in these cases are partly due to the large mean value and small coefficient of variation. The component fails mainly by fatigue and fracture. The role of σ_y in the fracture failure function is to introduce an element of yielding fracture mechanics. The small sensitivity factor for σ_y also implies that LEFM is sufficient to conduct a reliability analysis in these fatigue cases.

Sensitivity factor for F_c of the Paris parameter

F_c is a fatigue crack growth parameter. The longer the fatigue crack has time to grow, the more influential the variation of F_c is, as shown in all the figures.

Sensitivity factor for K_{1c}

Like σ_y, K_{1c} is a non-fatigue material property when using the Paris' Law for fatigue calculation. In other fatigue crack growth formulae, e.g. Forman's equation, K_{1c} can affect the crack growth rate especially in the final stages. In these examples, the Paris Law is used to calculate fatigue crack growth. With the increase of time, the sensitivity factor for K_{1c} decreases quickly, especially for case 4 and case 5 where the sudden drop of sensitivity factor for K_{1c} at $T = 3$ can be seen. The insignificant role of K_{1c} in long term fatigue failure explains why in some approaches to fatigue the K_{1c} variable is ignored, for instance in the S-N approach.

Sensitivity factor for σ_{max}

In this study, it is assumed that after a period of fatigue, a maximum stress with a mean of 140 MPa and having a normal distribution are applied to the component. However, improvements in the way that the maximum stress is treated needs further research.

Within the limit of the examples, the maximum stress has medium sensitivity factors. When time increases, the sensitivity factor for σ_{max} decreases, because of the increased importance of fatigue crack growth.

Sensitivity factor for ΔK_{th}

In these examples, fatigue crack growth has been calculated from the equivalent stress ranges for the 11 seastates. The 11 equivalent stress ranges calculated for the 11 seastates discussed in chapter 5 are obviously discontinuous. In 5 of the examples studied, the sensitivity factors for ΔK_{th} appear to be either zero or reasonable large negative values and have no clear trend. This is because ΔK_{th} only cuts off very small ΔK values below the threshold and thus it influences the fatigue crack growth process in the intermediate region and final failure very little. The threshold factor may have a more meaningful role in the crack initiation stage.

7.6.4 Natural frequency as a statistical variable

From case 1 up to case 5, assumptions are made that the fundamental structural natural frequency has a deterministic value of 0.34 Hz. In an offshore structure, the pile foundations which provide the stiffness of the structure are quite uncertain. In addition, the part of the structure above ground will inevitably have uncertainties in mass and stiffness as well. The masses and the stiffnesses of all the components determine the natural frequency of the system. Therefore it is of interest to investigate the structural reliability with variable natural frequency. Because the cyclic fatigue loading can be directly determined from the models in chapter 5, it is also straightforward to do that.

Fig. 7. 11 shows the variations of spectral response functions from $f_n = 0.02$ to $f_n = 0.41$ with wave loading spectral parameter $H_s = 8.38$ $T_D = 12.7$. The maximum spectral amplitude is achieved at a natural frequency about the value of resonance. The double peak spectra cannot be seen in the figure due to the very high near resonance spectral amplitude. For the purpose of demonstrating the response spectra with double peaks, Fig. 7.12 is drawn to show the variations of spectral functions from $f_n = 0.25$ to $f_n = 0.43$. Care should be taken when comparing Fig. 7.11 and Fig. 7.12 as the maximum amplitude in Fig. 7.11 is much larger than the maximum amplitude in Fig. 7.12. As the maximum amplitude increases the energy density calculated from the response spectrum increases. These two figures show the fact that the closer the natural frequency gets to the excitation frequency, the larger the energy density of the response process becomes. Therefore, the value of f_n has great influence over the response spectral properties especially when f_n approaches the resonance value.

The cyclic fatigue loading is generated from the response spectrum. The peak rates and the equivalent stress ranges can then be calculated from spectral properties. Hence, the fatigue damage can be calculated. The change of natural frequency will change the equivalent stress range and the peak rate. Fig. 7.13 shows the relationship $E(P)$ and the equivalent stress range for $f_n = 0.225, 0.25, 0.275, 0.30$. In Fig. 7.13, as f_n increases, equivalent stress range $E(P)$ increases i.e. the loading process has a lower amplitude but higher frequency for a fixed period of time. From the Paris' Law:

$$\frac{da}{dN} = CS^m Y^m \pi^{m/2} a^{m/2} \tag{7.11}$$

$$\triangle a = CS^m Y^m \pi^{m/2} a^{m/2} \triangle N \tag{7.12}$$

where

$$\triangle N = E(P) \times t$$

If for spectrum i, the equivalent stress range is S_i, the crack extension da will be proportional to $S_i^m E(P)_i$ due to change in natural frequency. S_i can be directly calculated from spectral properties from Eqn. (6.38).

Fig. 7.14 demonstrates the variation of $S_i^m E(P)_i$ from $f_n = 0.01$ to $f_n = 0.4$ for the 11 spectra in chapter 5. Furthermore if all 11 spectral have their probability of occurrence $P(n_i)$ as presented by Wirsching and as given in Table 5.1, and Y is assumed to be constant for a short extension of crack size, and it is defined such that

$$S_p = \sum_{i=1}^{11} E_i(P) S_i^m P(n_i) \tag{7.13}$$

then

$$\Delta a = C Y^m \pi^{m/2} a^{m/2} t S_p \tag{7.14}$$

i.e. Δa is proportional to S_p for a fixed time and crack size.

Fig. 7.15 shows the relationship between f_n and S_p.

Fig 7.16 compares the probabilities of failure between case 2 with variable f_n and with deterministic f_n. It can be seen that the introduction of natural frequency can increase the probability of failure to a large extent. However for small times, the difference is small as well, because the crack has experienced only a small amount of fatigue crack growth.

Fig 7.17 shows the sensitivity factor variation with time when natural frequency is treated a statistical variable. With an increase in time, the sensitivity factor for natural frequency increases dramatically to be close to 1. This is obviously due to the strong influence of natural frequency on the fatigue cyclic loading and may be partly due to the COV of f_n which is high (0.15) in this example.

7.7 Conclusions

In this Chapter, a methodology for determining the reliability of a cracked component subjected to random loading has been developed and demonstrated. Failure by brittle fracture and plastic collapse are both treated . A number of examples have been studied in detail and the sensitivity of the failure probability to each of the input variables has been examined. The following conclusions can be drawn:

1) A number of alternative failure functions have been considered for component failure under the action of fatigue. Of these, the functions which involve a comparison of the critical crack size with the crack size after fatigue have been found to be the most efficient when used with the Rackwitz-Fiessler algorithm.

2) The examples have shown that with increased exposure to fatigue loading, the sensitivity factors of fatigue related variables $a_i, F_c \Delta K_{th}$ increase. The opposite is true for non-fatigue variables σ, K_{1c}, σ_y. Therefore, with increasing time, the fatigue related variables become dominant in determining the probability of failure.

3) With increased exposure to fatigue loading, the absolute magnitude of sensitivity factors of σ_y and K_{1c} can decrease to near zero. This fact demonstrates that the variations of yield stress and fracture toughness have little influence on the probability of failure in the long term fatigue of a cracked component. Thus, LEFM may be justifiable for used in a fatigue fracture analysis.

4) Natural frequency variations can have a great influence on the cyclic fatigue loading and thus on the probability of failure of cracked components. The variation of natural frequency could be dominant in determining the probability of failure of cracked components for long term fatigue problems. When the natural frequency of the structure is close to the peak of the seastate, the equivalent stress range of the loading process increases, but the number of cycles decreases. Hence, the sum of $S_i^m E(P)_i P(n_i)$, to which the crack extension is proportional, can have a much larger value. The probability of failure by fatigue and fracture can be increased by the variation of natural frequency as the deterministic value.

Table 7.1 Output Example Of Case 2

Variable name	pdf type	mean value	standard deviation	maxima	minima	math. symbol
CRACKSIZE	NORMAL	.4000E+01	.4000E+00	.4000E+02	.4000E-01	a
Y STRESS	LOGNOR	.3860E+03	.3000E+02	.3860E+04	.3860E+02	σ_y
PARISM	NORMAL	.2600E+01	.0000E+00	.2600E+01	.2600E+01	m
PARISC	NORMAL	.8833E-12	.0000E+00	.8833E-11	.8833E-11	C
PARISFC	NORMAL	.0000E+00	.1020E+00	.1000E+01	-.1000E+01	F_c
K1C	NORMAL	.5000E+02	.5000E+01	.5000E+03	.5000E+00	K_{1c}
WIDTH	NORMAL	.4000E+02	.0000E+00	.4000E+02	.4000E+02	w
RESTRESS	NORMAL	.0000E+00	.0000E+00	.0000E+00	.0000E+00	σ_{res}
MAXSTRESS	NORMAL	.1400E+03	.1400E+02	.1400E+04	.1400E+01	σ
NAT FREQ	NORMAL	.3400E+00	.0000E+00	.3000E+01	.3000E-01	f_n
THRESH DK	NORMAL	.9000E+02	.1500E+02	.9000E+03	.9000E+01	$\triangle K_{th}$

```
MODE 1 ITERATION =  4   MODE 2 ITERATION =  5
RHO= .353079E+00
 .274077E-05 < FIRST ORDER PF <  .274077E-05
PROBABILITY OF FAILURE  OF MODE 1 FROM FORM=   .274077E-05
PROBABILITY OF FAILURE  OF MODE 2 FROM FORM=   .263616E-23
SENSITIVITY FACTOR OF  CRACKSIZE  =   .177098E+00
SENSITIVITY FACTOR OF  Y STRESS   =  -.491182E-01
SENSITIVITY FACTOR OF  PARISM     =   .000000E+00
SENSITIVITY FACTOR OF  PARISC     =   .000000E+00
SENSITIVITY FACTOR OF  PARISFC    =   .000000E+00
SENSITIVITY FACTOR OF     K1C     =  -.857548E+00
SENSITIVITY FACTOR OF  WIDTH      =   .000000E+00
SENSITIVITY FACTOR OF  RESTRESS   =   .000000E+00
SENSITIVITY FACTOR OF  MAXSTRESS  =   .480453E+00
SENSITIVITY FACTOR OF  NAT FREQ   =   .000000E+00
SENSITIVITY FACTOR OF  THRESH DK  =   .000000E+00
TOTAL LOAD CYCLES=   0
DESIGN POINT COORDINATES
LR    = .505635E+00    KR      = .956915E+00
BEETA  = .454566E+01
CRACK INCREMENT=  .000000E+00 mm
```

```
MODE 1 ITERATION =  4   MODE 2 ITERATION =  5
RHO= .379103E+00
 .915936E-05 < FIRST ORDER PF <  .915936E-05
PROBABILITY OF FAILURE  OF MODE 1 FROM FORM=   .915936E-05
PROBABILITY OF FAILURE  OF MODE 2 FROM FORM=   .131716E-22
SENSITIVITY FACTOR OF  CRACKSIZE  =   .231431E+00
SENSITIVITY FACTOR OF  Y STRESS   =  -.525785E-01
SENSITIVITY FACTOR OF  PARISM     =   .000000E+00
SENSITIVITY FACTOR OF  PARISC     =   .000000E+00
SENSITIVITY FACTOR OF  PARISFC    =   .732589E-01
SENSITIVITY FACTOR OF     K1C     =  -.831791E+00
SENSITIVITY FACTOR OF  WIDTH      =   .000000E+00
SENSITIVITY FACTOR OF  RESTRESS   =   .000000E+00
SENSITIVITY FACTOR OF  MAXSTRESS  =   .496420E+00
SENSITIVITY FACTOR OF  NAT FREQ   =   .000000E+00
```

```
SENSITIVITY FACTOR OF  THRESH DK  =    .000000E+00
TOTAL LOAD CYCLES=    .800814E+06
DESIGN POINT COORDINATES
LR    = .512651E+00     KR      = .955298E+00
BEETA  = .428461E+01
CRACK INCREMENT=   .731732E+00 mm
-----------------------------------------------------------------
MODE 1 ITERATION =  5    MODE 2 ITERATION = 23
RHO= .489225E+00
 .121830E-03 < FIRST ORDER PF <  .121830E-03
PROBABILITY OF FAILURE  OF MODE 1 FROM FORM=    .121830E-03
PROBABILITY OF FAILURE  OF MODE 2 FROM FORM=    .167070E-20
SENSITIVITY FACTOR OF  CRACKSIZE  =    .315726E+00
SENSITIVITY FACTOR OF  Y STRESS   =   -.572318E-01
SENSITIVITY FACTOR OF  PARISM     =    .000000E+00
SENSITIVITY FACTOR OF  PARISC     =    .000000E+00
SENSITIVITY FACTOR OF  PARISFC    =    .310069E+00
SENSITIVITY FACTOR OF     K1C     =   -.734110E+00
SENSITIVITY FACTOR OF  WIDTH      =    .000000E+00
SENSITIVITY FACTOR OF  RESTRESS   =    .000000E+00
SENSITIVITY FACTOR OF  MAXSTRESS  =    .511842E+00
SENSITIVITY FACTOR OF  NAT FREQ   =    .000000E+00
SENSITIVITY FACTOR OF  THRESH DK  =   -.540241E+00
TOTAL LOAD CYCLES=    .160163E+07
DESIGN POINT COORDINATES
LR    = .525705E+00     KR      = .952139E+00
BEETA  = .366890E+01
CRACK INCREMENT=   .291156E+01 mm
-----------------------------------------------------------------
MODE 1 ITERATION =  7    MODE 2 ITERATION = 23
RHO= .774348E+00
 .262453E-02 < FIRST ORDER PF <  .262453E-02
PROBABILITY OF FAILURE  OF MODE 1 FROM FORM=    .254066E-02
PROBABILITY OF FAILURE  OF MODE 2 FROM FORM=    .231107E-03
SENSITIVITY FACTOR OF  CRACKSIZE  =    .390591E+00
SENSITIVITY FACTOR OF  Y STRESS   =   -.460485E-01
SENSITIVITY FACTOR OF  PARISM     =    .000000E+00
SENSITIVITY FACTOR OF  PARISC     =    .000000E+00
SENSITIVITY FACTOR OF  PARISFC    =    .675677E+00
SENSITIVITY FACTOR OF     K1C     =   -.467138E+00
SENSITIVITY FACTOR OF  WIDTH      =    .000000E+00
SENSITIVITY FACTOR OF  RESTRESS   =    .000000E+00
SENSITIVITY FACTOR OF  MAXSTRESS  =    .412991E+00
SENSITIVITY FACTOR OF  NAT FREQ   =    .000000E+00
SENSITIVITY FACTOR OF  THRESH DK  =   -.672337E+00
TOTAL LOAD CYCLES=    .240244E+07
DESIGN POINT COORDINATES
LR    = .536211E+00     KR      = .949447E+00
BEETA  = .280184E+01
CRACK INCREMENT=   .237602E+02 mm
-----------------------------------------------------------------
MODE 1 ITERATION = 10    MODE 2 ITERATION = 30
RHO= .919639E+00
 .331724E-01 < FIRST ORDER PF <  .331724E-01
PROBABILITY OF FAILURE  OF MODE 1 FROM FORM=    .331238E-01
```

```
PROBABILITY OF FAILURE  OF MODE 2 FROM FORM=    .518820E-02
SENSITIVITY FACTOR OF  CRACKSIZE  =    .396238E+00
SENSITIVITY FACTOR OF  Y STRESS   =   -.299134E-01
SENSITIVITY FACTOR OF  PARISM     =    .000000E+00
SENSITIVITY FACTOR OF  PARISC     =    .000000E+00
SENSITIVITY FACTOR OF  PARISFC    =    .831031E+00
SENSITIVITY FACTOR OF     K1C     =   -.269292E+00
SENSITIVITY FACTOR OF  WIDTH      =    .000000E+00
SENSITIVITY FACTOR OF  RESTRESS   =    .000000E+00
SENSITIVITY FACTOR OF  MAXSTRESS  =    .281016E+00
SENSITIVITY FACTOR OF  NAT FREQ   =    .000000E+00
SENSITIVITY FACTOR OF  THRESH DK  =   -.589790E+00
TOTAL LOAD CYCLES=    .320325E+07
DESIGN POINT COORDINATES
LR    = .537363E+00     KR      = .949144E+00
BEETA  = .183674E+01
CRACK INCREMENT=   .249973E+02 mm
-------------------------------------------------------------------
MODE 1 ITERATION =  6    MODE 2 ITERATION = 31
RHO= .871506E+00
 .145981E+00 < FIRST ORDER PF <  .145947E+00
PROBABILITY OF FAILURE  OF MODE 1 FROM FORM=    .145981E+00
PROBABILITY OF FAILURE  OF MODE 2 FROM FORM=    .346585E-01
SENSITIVITY FACTOR OF  CRACKSIZE  =    .395129E+00
SENSITIVITY FACTOR OF  Y STRESS   =   -.233748E-01
SENSITIVITY FACTOR OF  PARISM     =    .000000E+00
SENSITIVITY FACTOR OF  PARISC     =    .000000E+00
SENSITIVITY FACTOR OF  PARISFC    =    .863957E+00
SENSITIVITY FACTOR OF     K1C     =   -.210108E+00
SENSITIVITY FACTOR OF  WIDTH      =    .000000E+00
SENSITIVITY FACTOR OF  RESTRESS   =    .000000E+00
SENSITIVITY FACTOR OF  MAXSTRESS  =    .229697E+00
SENSITIVITY FACTOR OF  NAT FREQ   =    .000000E+00
SENSITIVITY FACTOR OF  THRESH DK  =   -.722627E+00
TOTAL LOAD CYCLES=    .400407E+07
DESIGN POINT COORDINATES
LR    = .534878E+00     KR      = .949796E+00
BEETA  = .105383E+01
CRACK INCREMENT=   .135203E+02 mm
-------------------------------------------------------------------
```

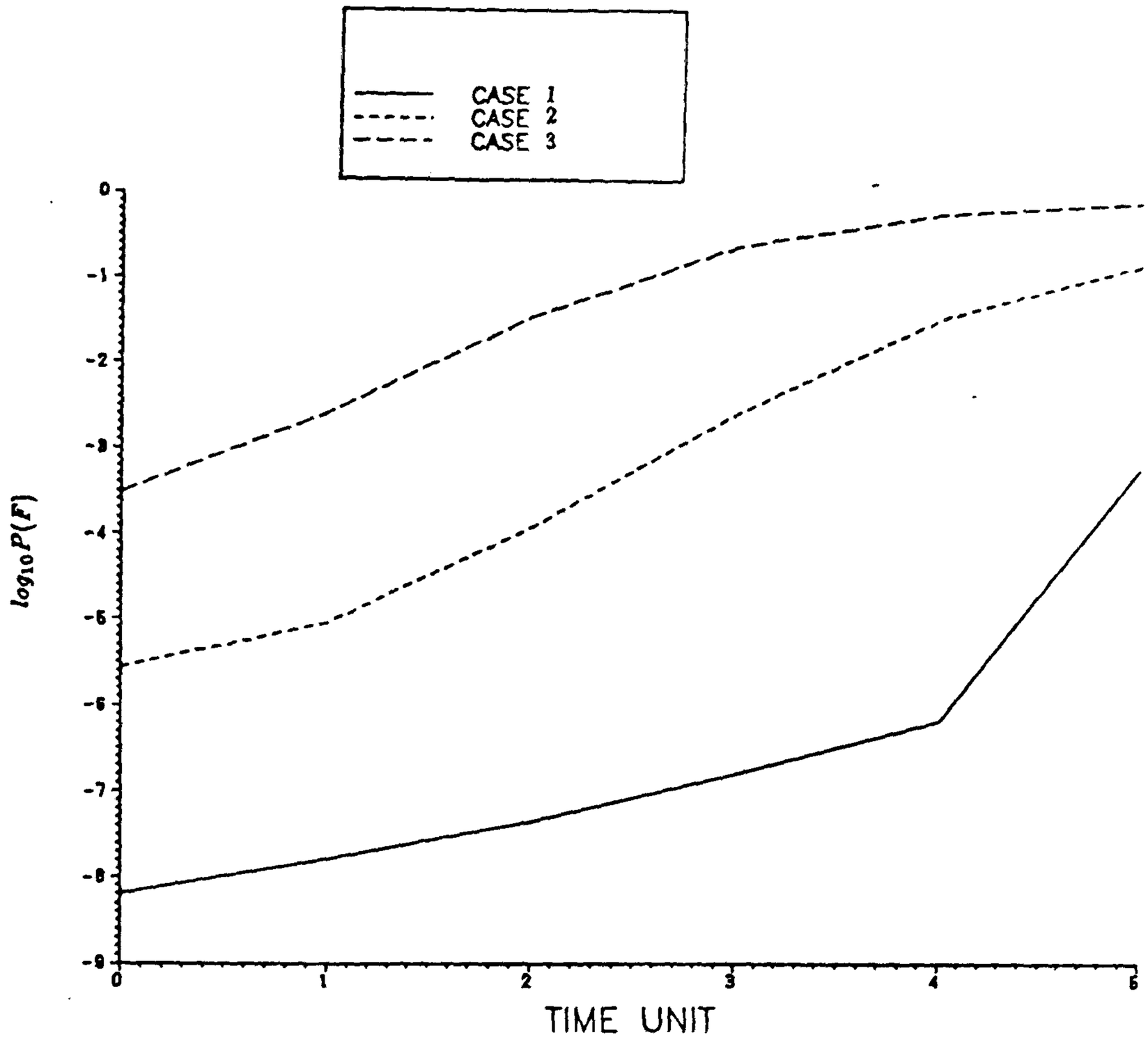

Fig. 7.1 The relationship of $log_{10}P(f)$ with time for cases 1, 2, 3

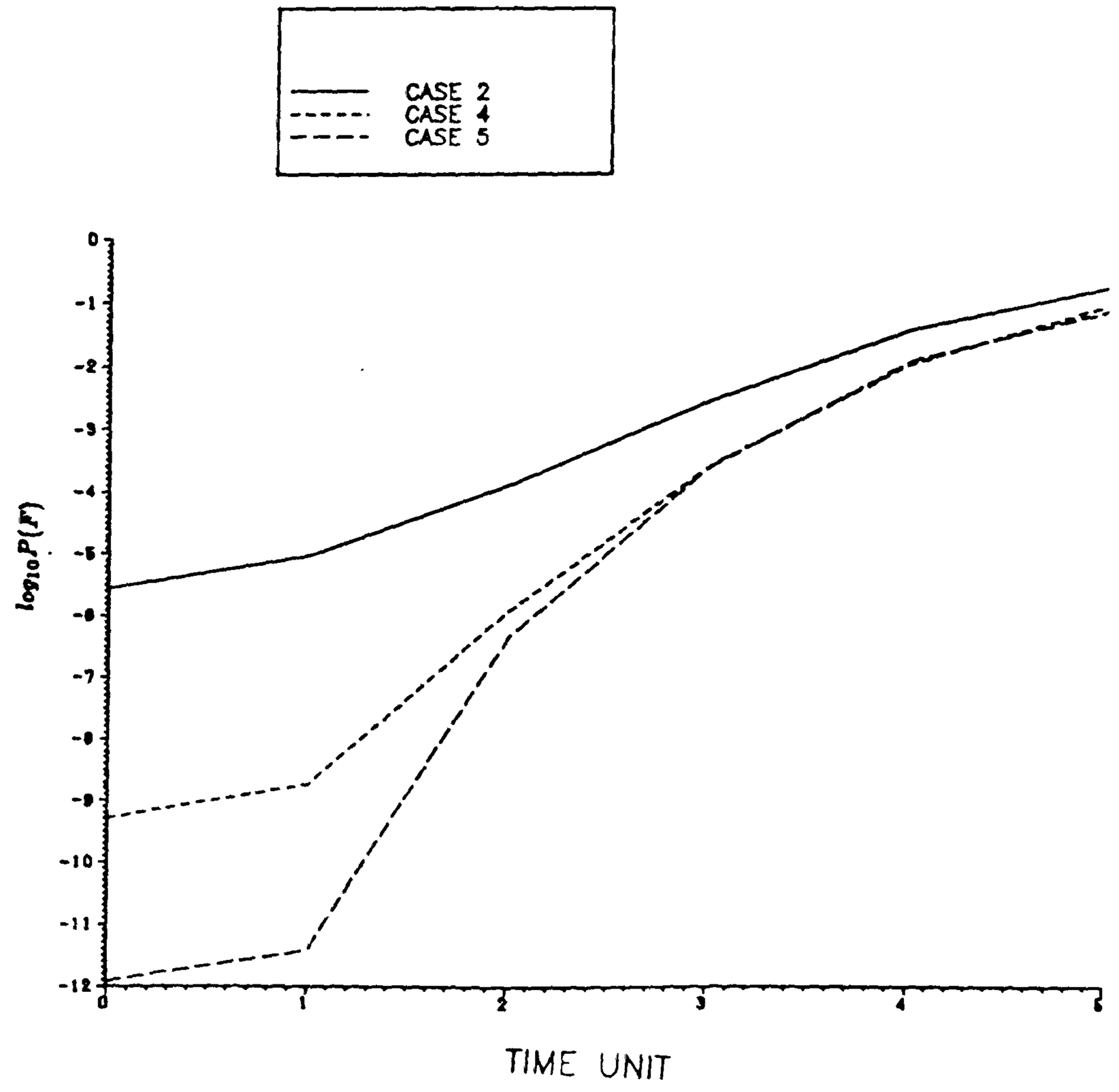

Fig. 7.2 The relationship of $log_{10}P(f)$ with time for cases 2, 4, 5

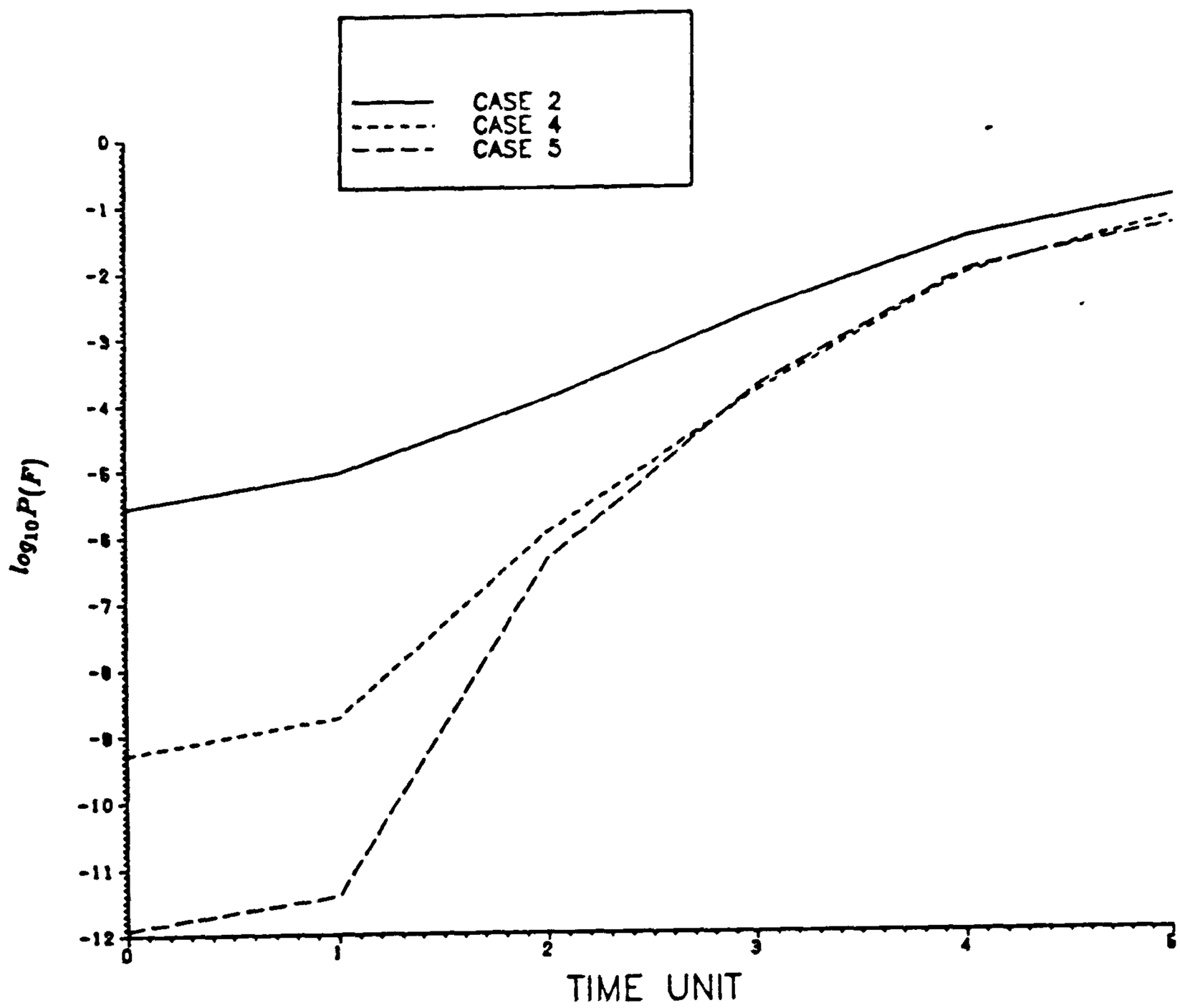

Fig. 7.3 The relationship of $log_{10}P(f)$ with time in the fracture mode for cases 2, 4, 5

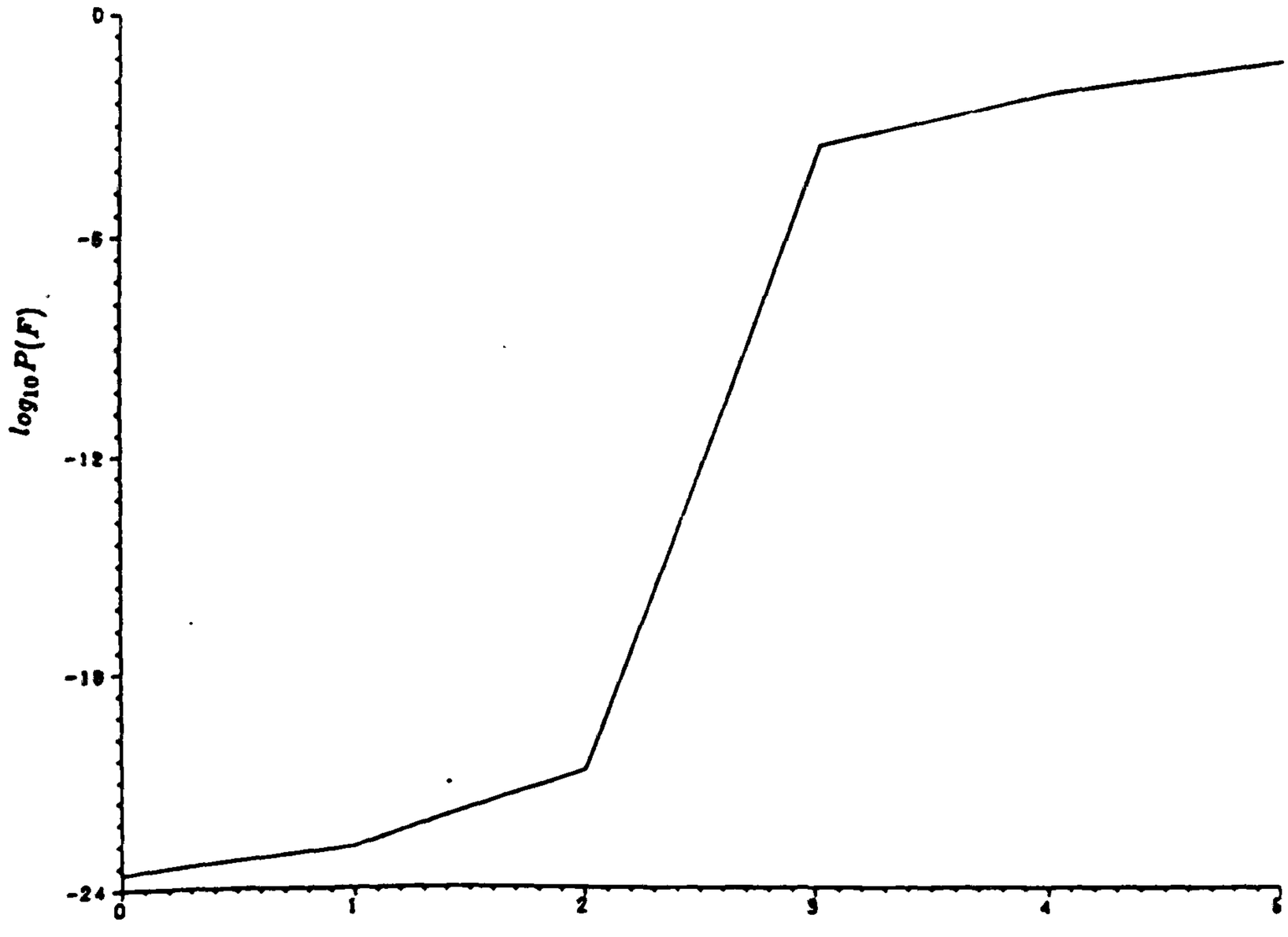

Fig. 7.4 The relationship of $log_{10}P(f)$ with time in the plastic collapse mode for cases 2,4, 5.

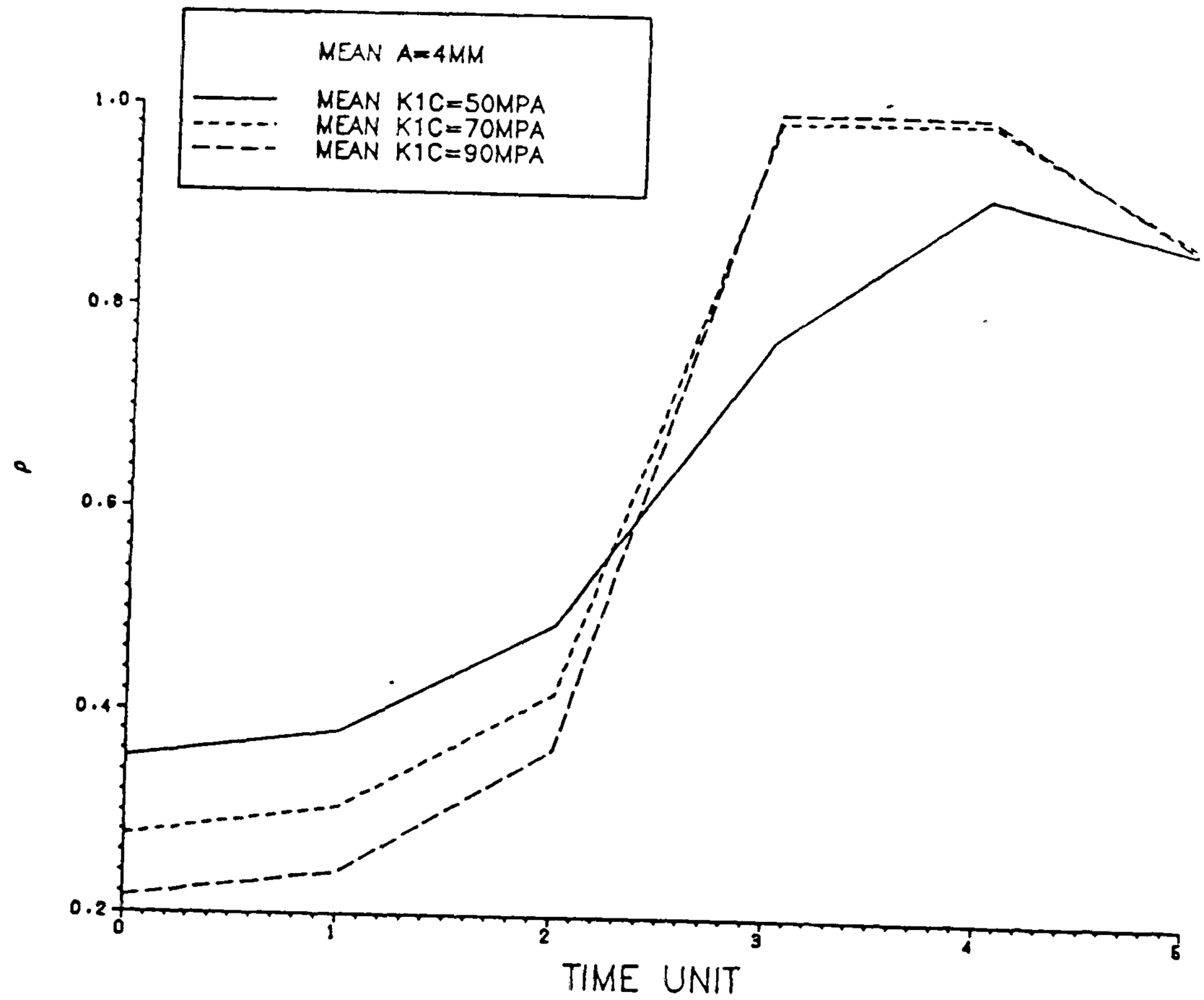

Fig. 7.5 The relationship of coefficient of failure modes correlation ρ with time.

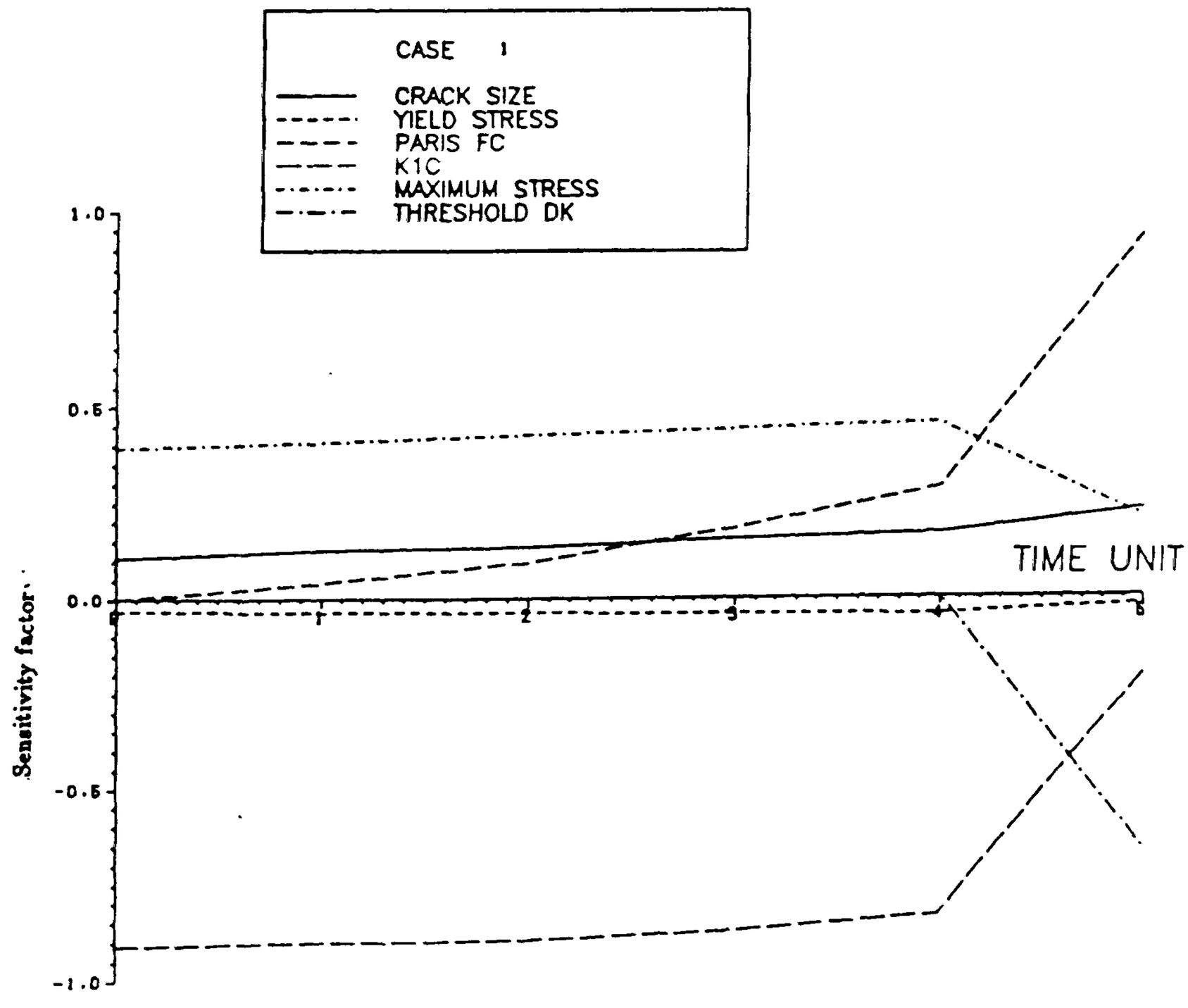

Fig. 7.6 The sensitivity factors from case 1

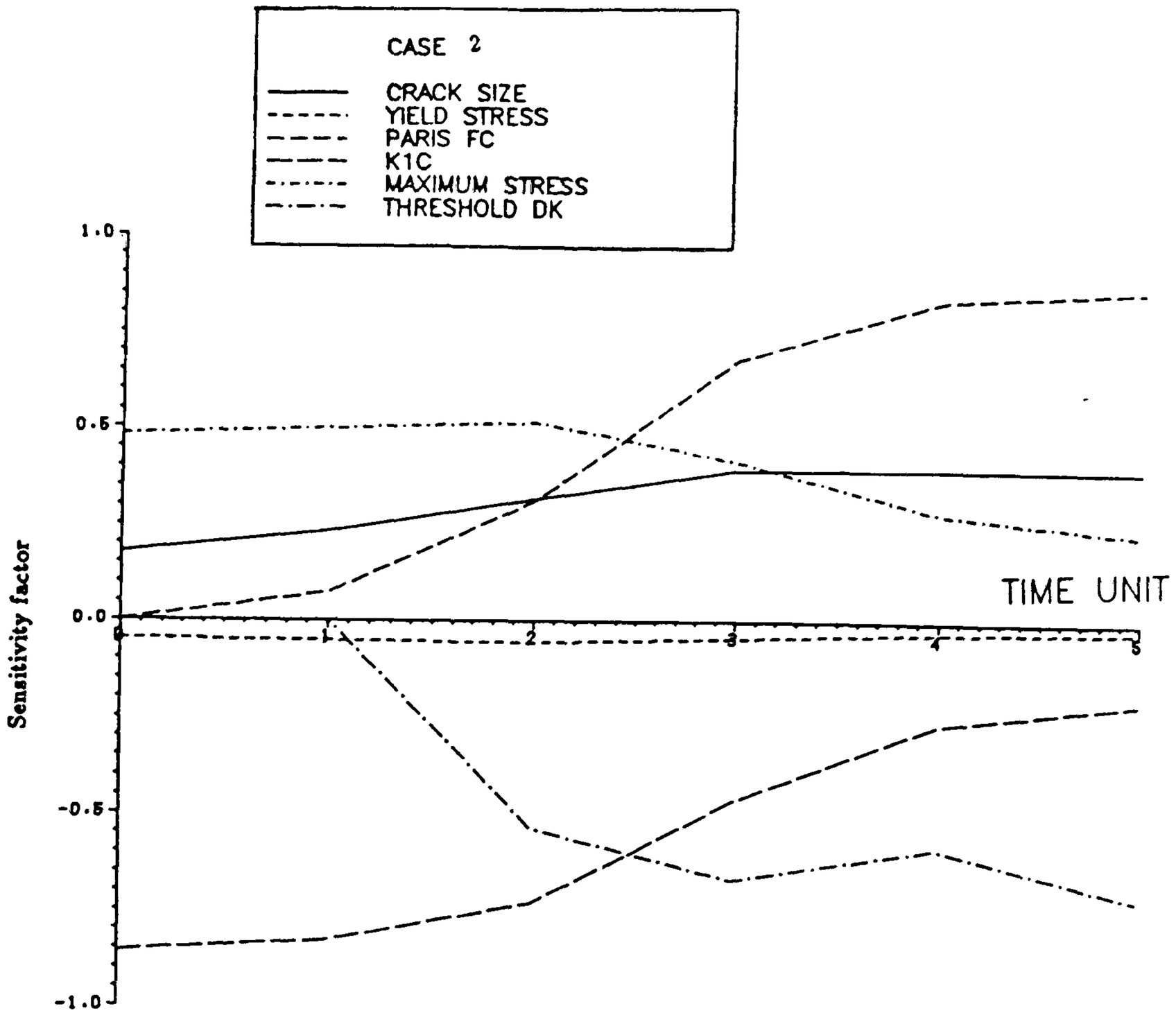

Fig. 7.7 The sensitivity factors from case 2

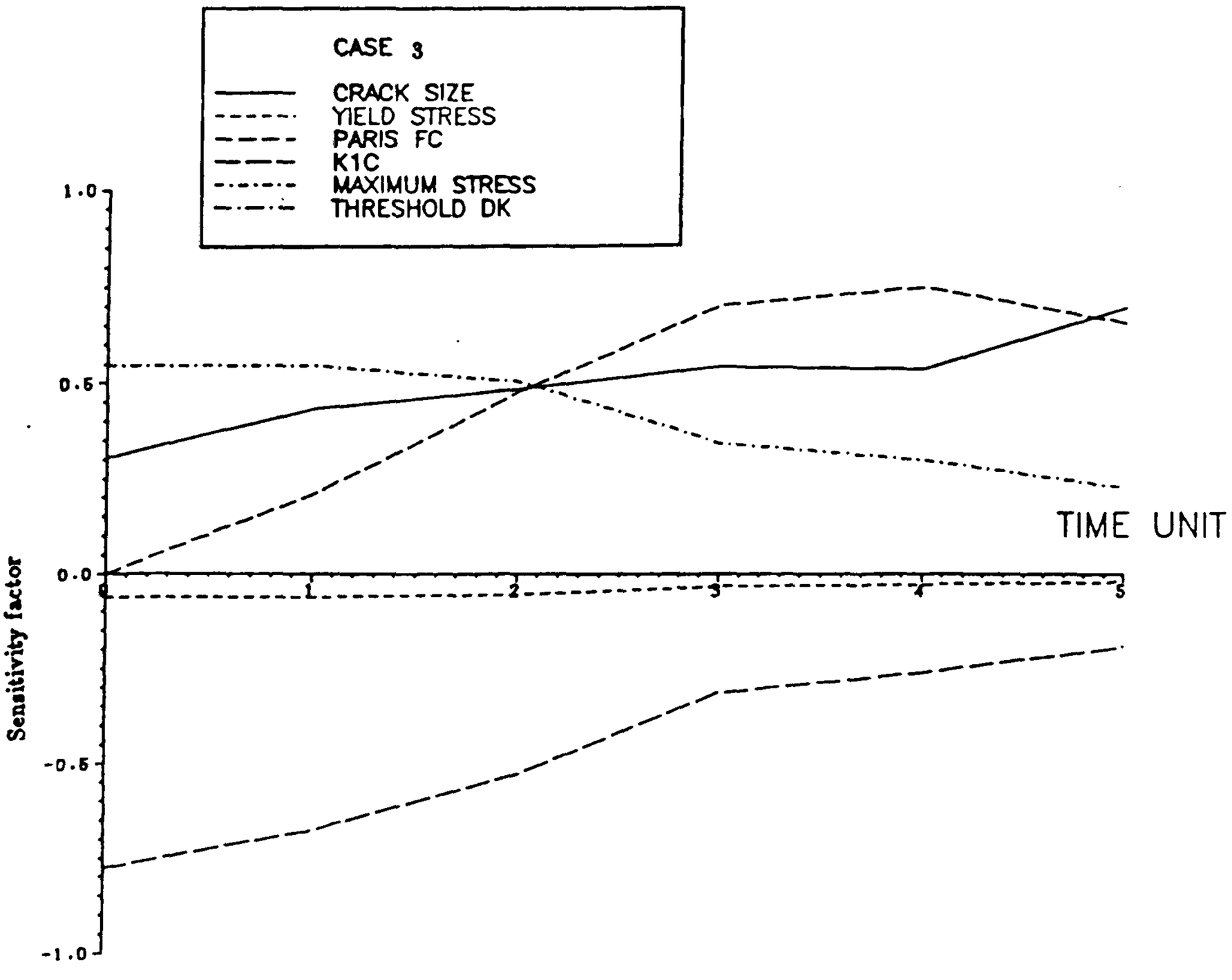

Fig. 7.8 The sensitivity factors from case 3

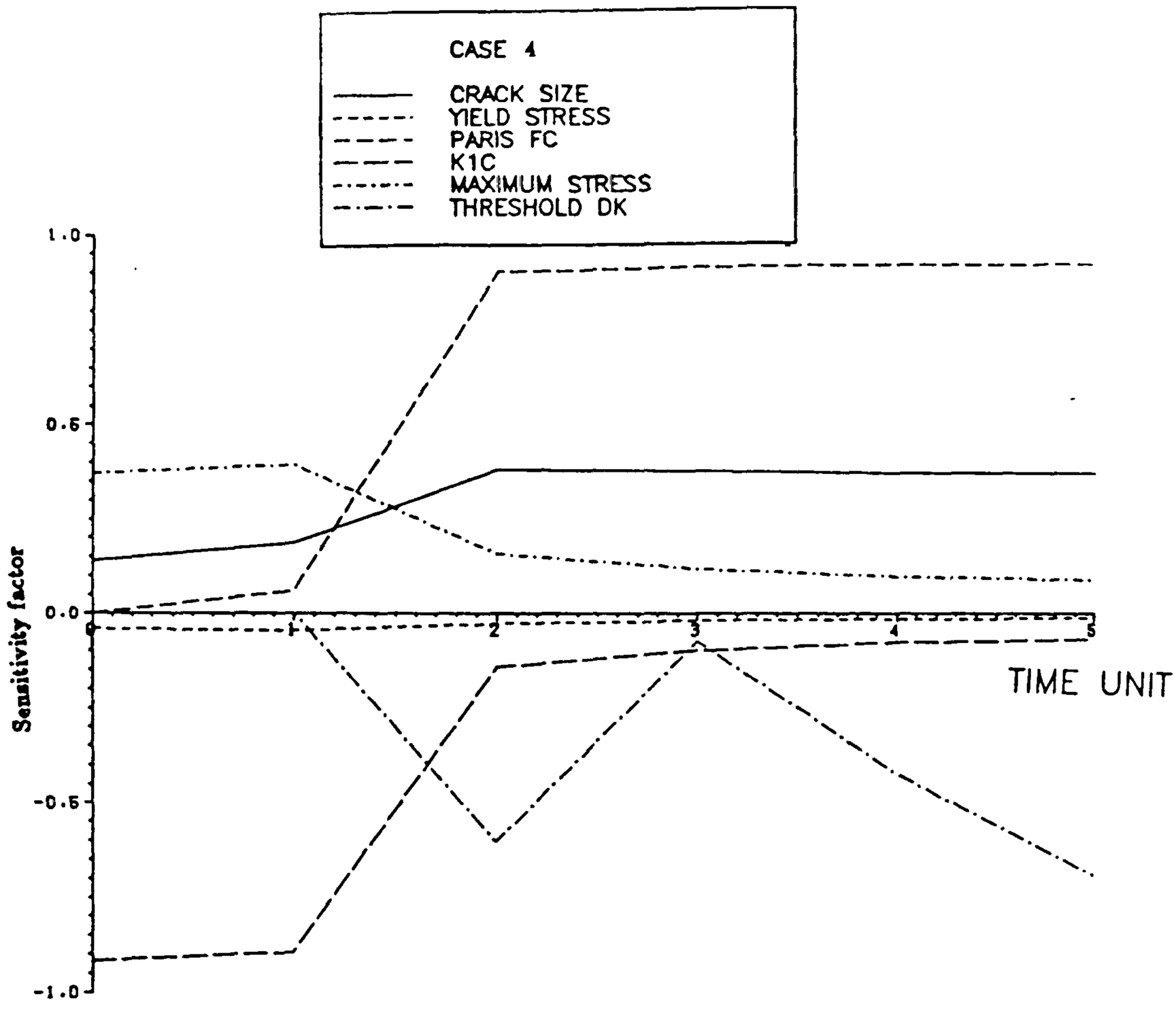

Fig. 7.9 The sensitivity factors from case 4

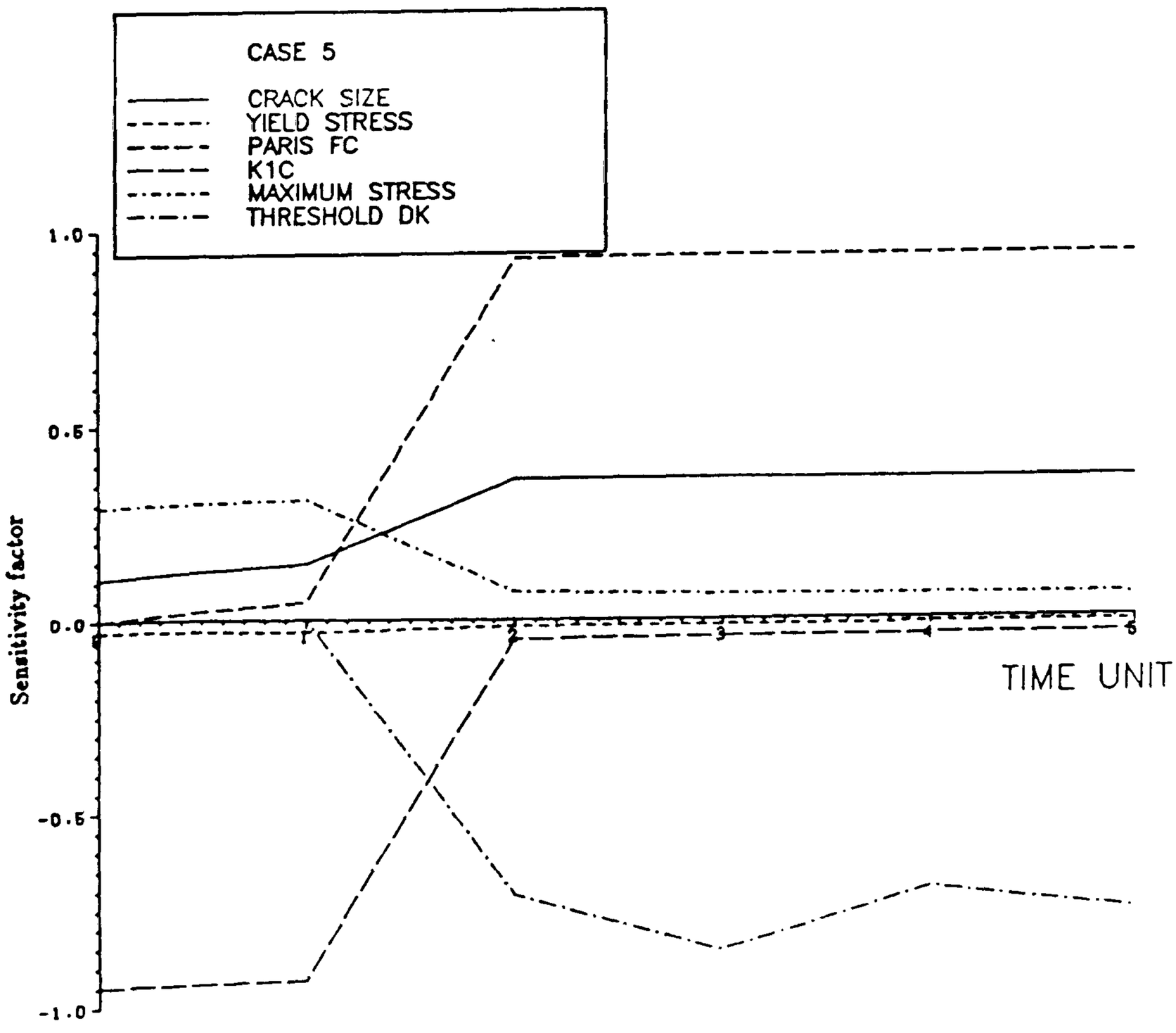

Fig. 7.10 The sensitivity factors from case 5

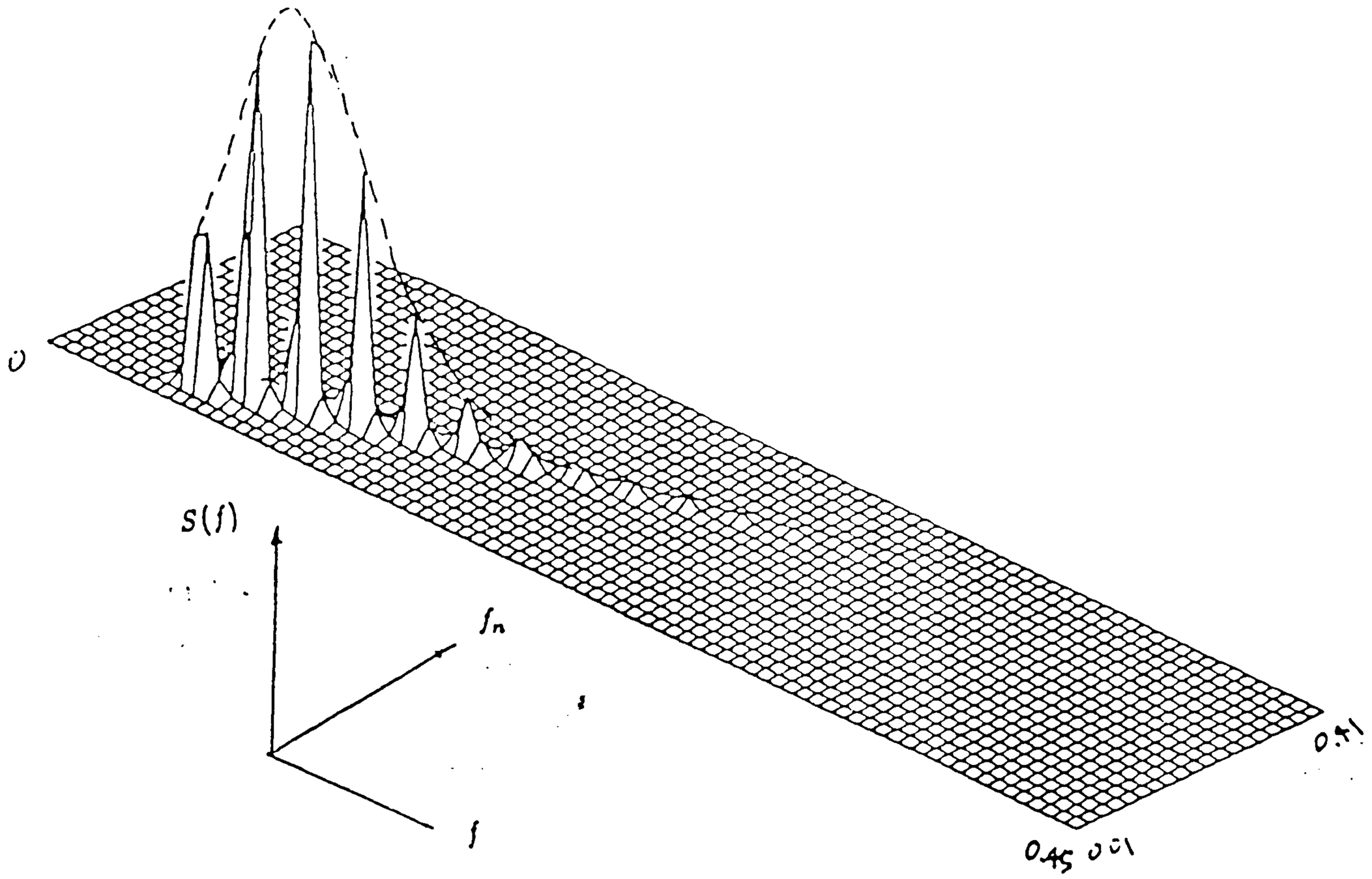

Fig. 7.11 The variations of spectral functions from $f_n = 0.02$ to $f_n = 0.4$ with wave loading spectral parameter $H_s = 8.38$ $T_D = 12.7$

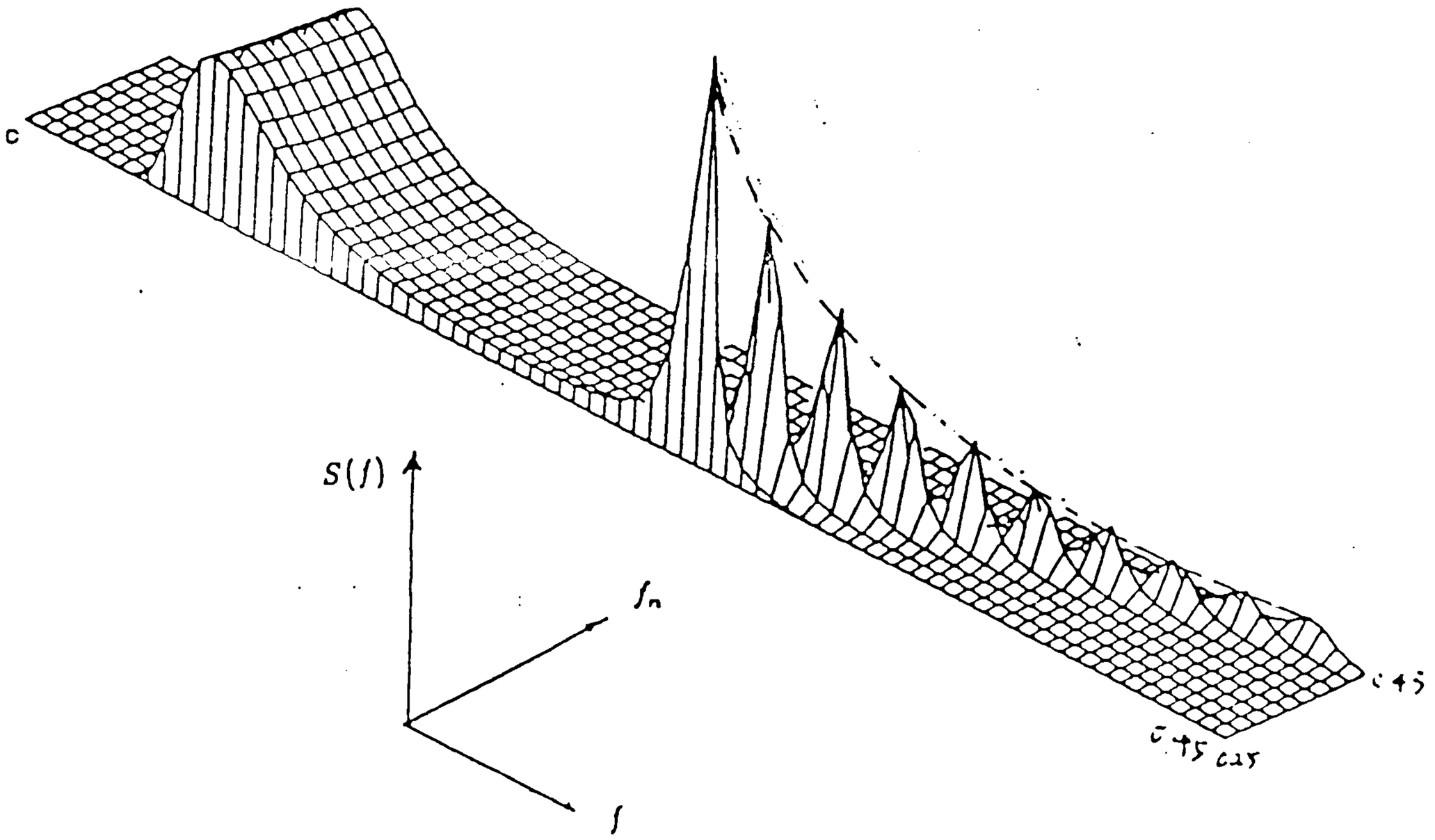

Fig. 7.12 The variations of spectral functions from $f_n = 0.25$ to $f_n = 0.43$

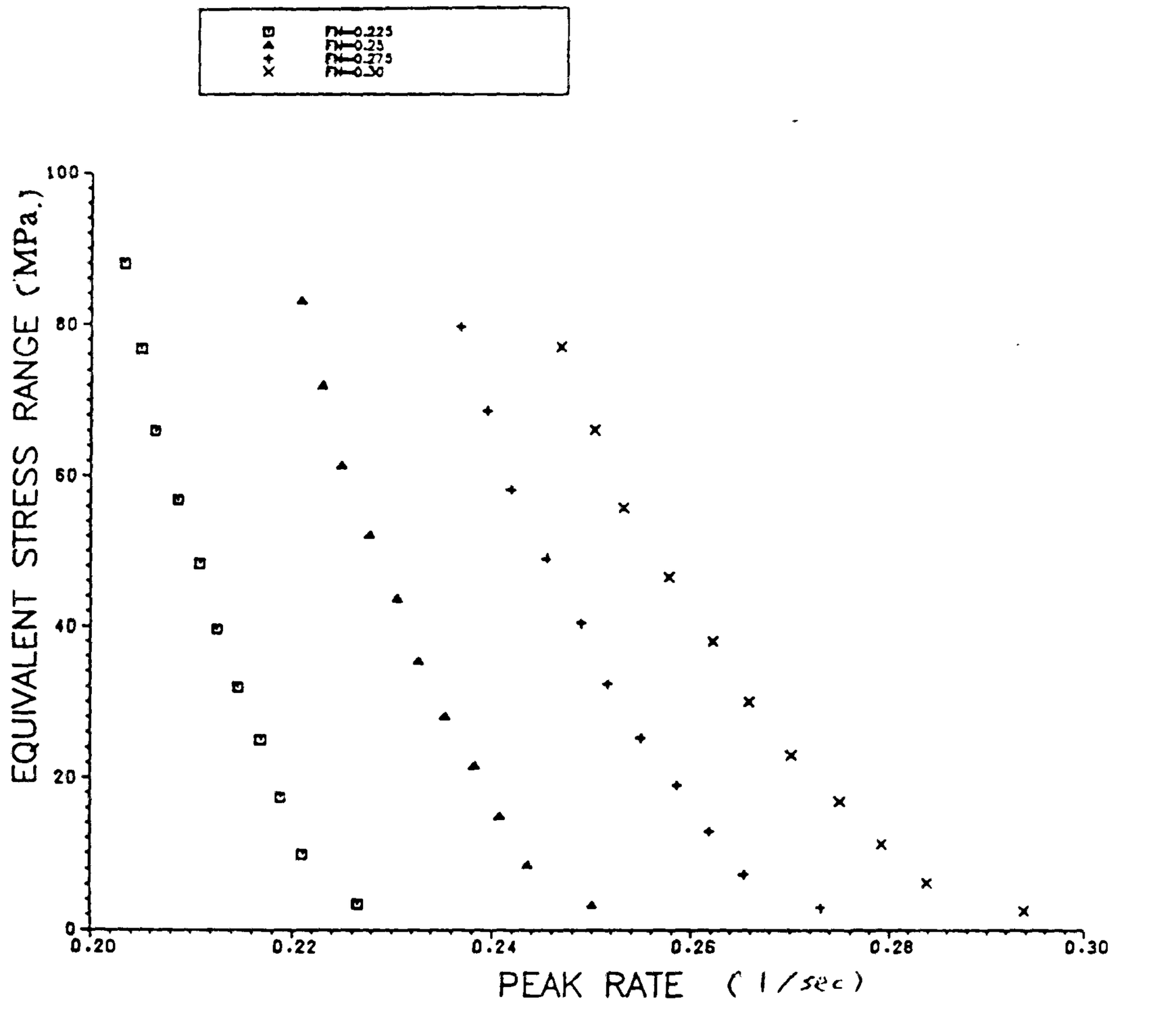

Fig. 7.13 The relationship of $E(P)$ and S for $f_n = 0.225, 0.25, 0.275, 0.30$.

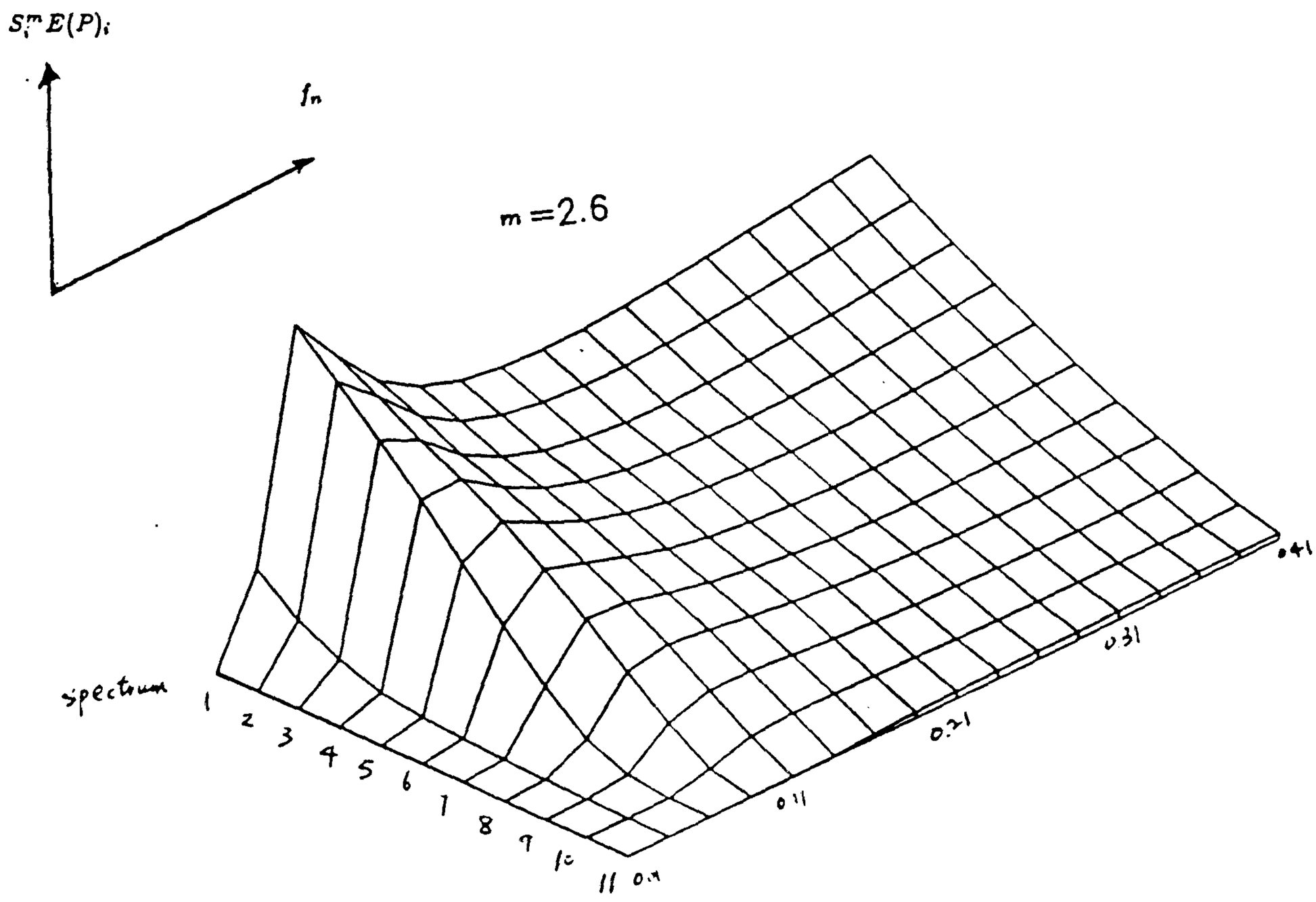

Fig. 7.14 The variation of $S_i^m E(P)_i$ from $f_n = 0.01$ to $f_n = 0.41$ for the 11 spectra

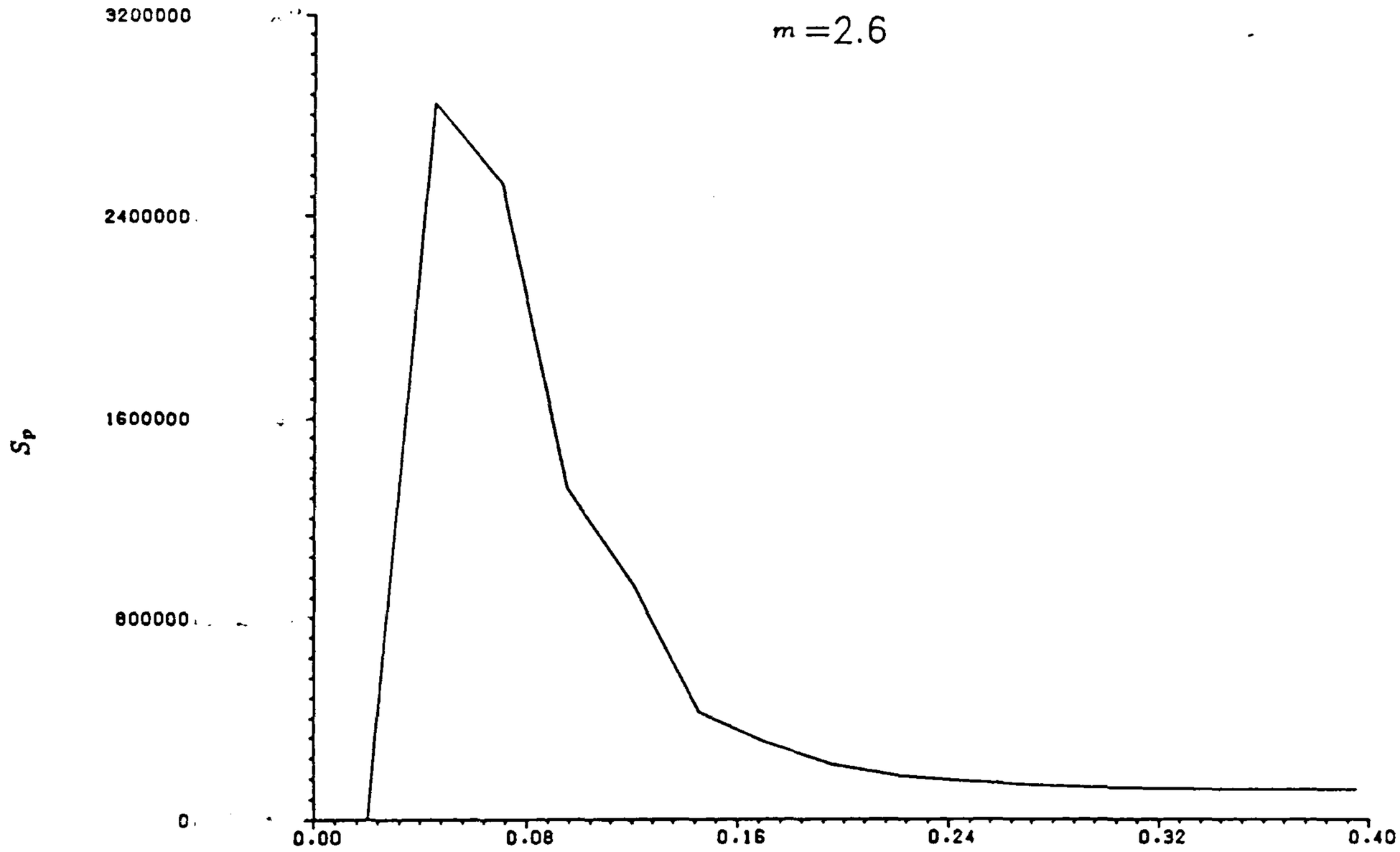

Fig. 7.15 The relationship between f_n and S_p

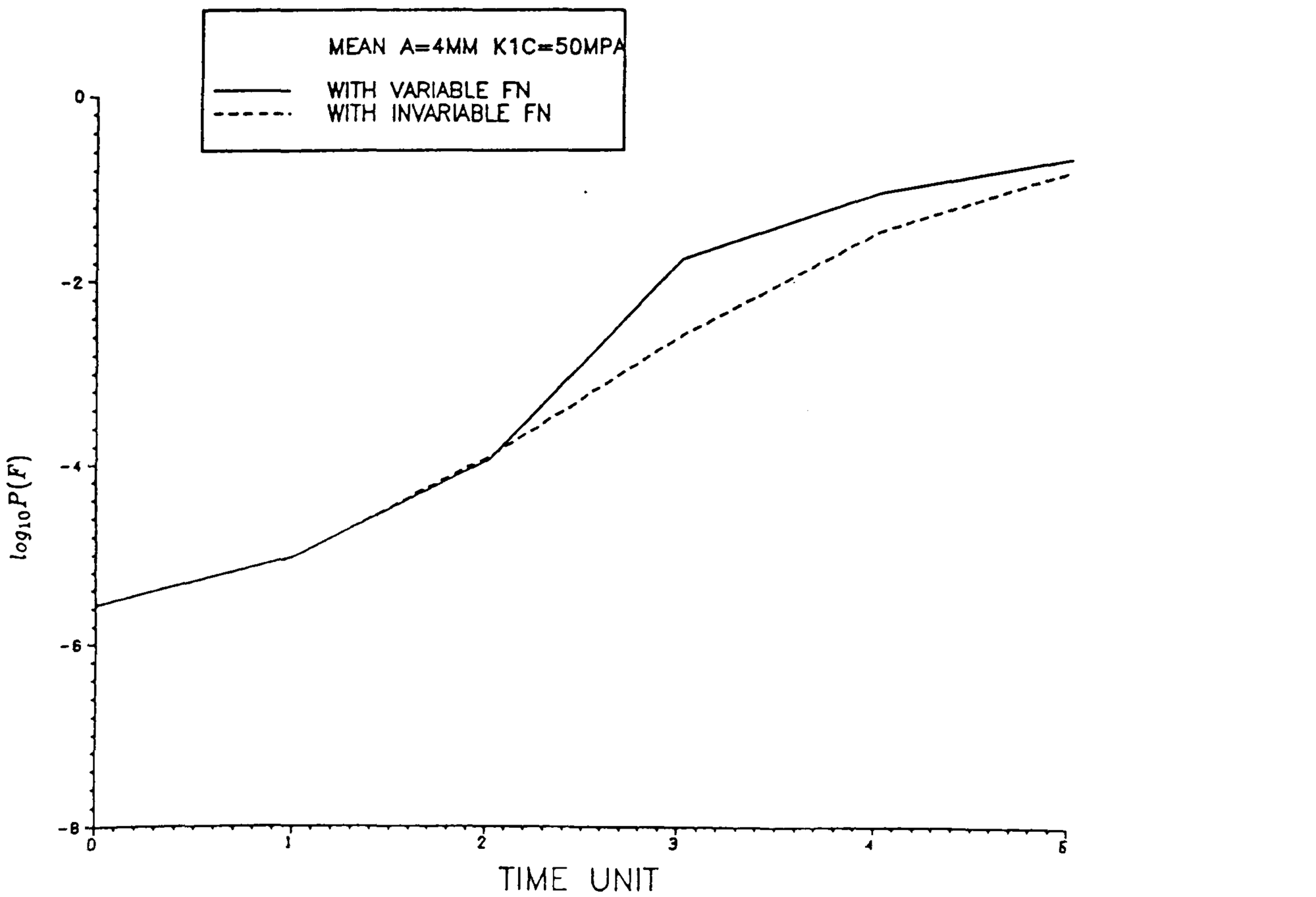

Fig. 7.16 The probabilities of failure of case 2 with variable f_n and with deterministic f_n.

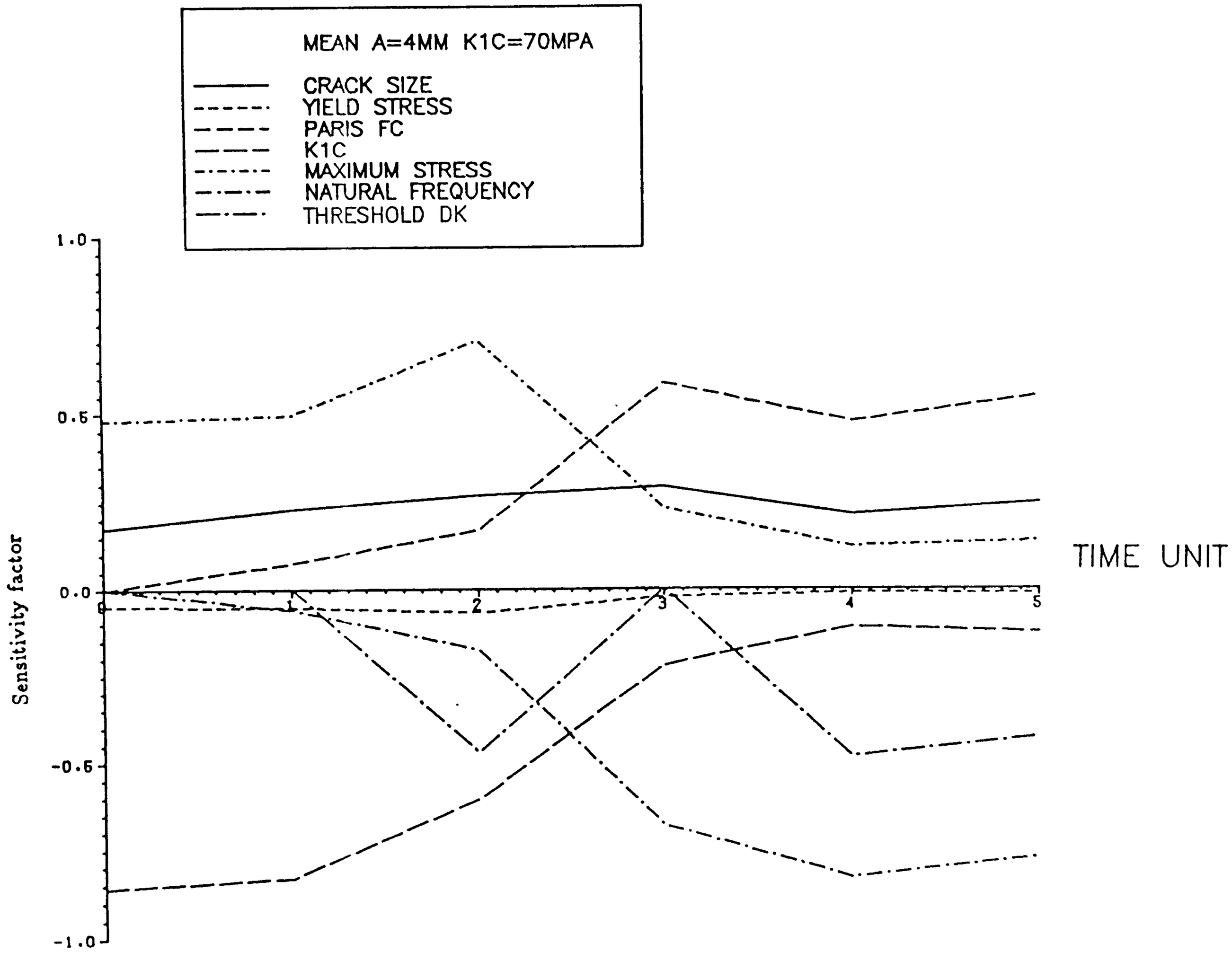

Fig. 7.17 The sensitivity factors with f_n being a statistical variable for case 2

Chapter 8

Conclusions And Scope For Future Work

8.1

8.1 Conclusions

This thesis has developed a methodology for the reliability analysis of cracked structural steel components under the action of random loading. This study has linked fracture mechanics, fatigue analysis, the probabilistic analysis of loading and reliability analysis into a single procedure for integrity assessment.

Chapter 2 has reviewed the development of structural reliability theory and has proposed a refinement for the finite difference scheme for second-order reliability analysis. Because the only important properties for second-order derivatives are those at the design point, the finite difference scheme for calculating those properties can be simplified. The number of points at which it is necessary to calculate the value of the safety margin can be reduced by a factor of about four.

Chapter 3 has reviewed fracture mechanics theory for setting up a failure criterion for a critical crack state. The uncertainties in basic variables affecting fracture are discussed. Several design methods are presented. In particular, the R6 method has been evaluated and has been selected as the failure criterion to determine the critical crack state. This is failure either by fracture or plastic collapse.

Chapter 4 provides a thorough study of the reliability of a cracked component under non-cyclic loading. The component can fail by brittle fracture for brittle material, ductile fracture for ductile material or plastic collapse for any material. The tedious manual procedure in the R6 method to determine the instability load for ductile material has been replaced by an efficient computer interactive procedure. From the reliability analyses undertaken in this chapter, a number of findings can be mentioned:

1) For the examples studied, the difference between the values of the reliability calculated using first-order and second-order methods is small.

2) The safety factor or load factor alone cannot give a satisfactory indication of component safety. The safety should be assessed by reliability calculation.

3) The sensitivity factors for yield stress and fracture toughness change gradually from the linear elastic region where the fracture toughness variables are dominant to the plastic collapse region where yield stress is dominant.

4) There are large differences in the computed reliabilities with and without ductile tearing, which means that the reserve strength of a structural component arising from ductility cannot be ignored. However, the probability of failure is not sensitive to variations in the slope of the J-R curve in these cases.

5) The plastic collapse failure mode has a very important role in governing the probability of failure, especially with ductile crack growth.

Chapter 5 has studied the probability distribution of stress range derived from the rainflow counting method under stochastic loading. Under these conditions, the structural response is random and the stresses induced follow a stochastic process. Often, for short periods of time, the response process is assumed to be stationary. In a fatigue study, the rainflow counting method for variable amplitude loading is generally assumed to be the best method among the three that are often used, i.e. the range pair method, the peak counting method and rainflow method. However, the rainflow method involves response process simulation from given information, either in numerical form or from an analytical spectrum, and then counting cycle by cycle.

Chapter 5 has shown that the stress range distribution derived from the rainflow method can be modelled as a function of spectral properties, and consisting of two Weibull functions. A series of stress range probability functions have been built which closely agree with the simulated stress range data. In this thesis, the combined Weibull distribution technique has only been applied to offshore spectra, although it is likely to be applicable to a wide range of random loading cases. By using this model, if one has a response spectrum in either numerical form or analytical form, one can obtain the stress range probability density function directly from properties of the stress spectrum without going through the time-consuming process of simulation and cycle counting.

Chapter 6 has analysed fatigue problems deterministically. To narrow down a wide range of fatigue problems, the crack development in a welded joint of an offshore platform under wave loading is studied in detail. Chapter 6 also reviews fatigue crack growth calculation under random loading. The complexity of stress interaction is yet to be fully understood. The practical model for crack growth under random loading is still the Paris'Law with certain modifications in regime (a) by introducing a threshold value. However, the stress range counting process should be the rainflow method in order to have a prediction method that gives results close to the actual experimental results. The equivalent stress range concept has been used both for its simplicity and good agreement with experimental results.

By using the stress range probability density functions in Chapter 5 the equivalent stress range has been calculated. The applications of stress range probability functions in the calculation of equivalent stress range was shown to give satisfactory results, in comparison with simulated results and other empirical models. To calculate the crack growth, the cycle by cycle calculation is the most precise but the least efficient. The cycle by cycle calculation is not necessary when the stress interaction effects are ignored and the Y factor can be treated as a constant for a short period of time, to keep Miner's rule applicable. Direct cycle by cycle calculation is not practical in reliability calculations. It is demonstrated that the cycle by cycle calculation can be replaced by a reasonably large number of cycles (up to 10^5) without affecting the accuracy of the results.

Chapter 7 has incorporated the work from previous chapters and has described the reliability analysis of cracked components failing by fracture or plastic collapse following fatigue under random loading. It is found that the long-term fatigue reliability is not sensitive to non-fatigue variables including

yield stress and fracture toughness. However, sensitivity to fatigue related variable like Paris' Law parameters, ΔK_{th}, increase with the increase in exposure time to fatigue loading. This implies that the use of LEFM is justifiable in many cases. Also in this study, it has been shown that the uncertainties in the natural frequency of the structure can have a dominant effect on the reliability of the system.

As discussed in chapter 1, reliability methods are being developed for the use in rational safety assessment. These theories are based on the probabilistic study of the basic variables and the chance combination of these quantities in causing failure. In conclusion, this work has advanced reliability theory and its applications in three different directions:

1) the probabilistic study of basic variables in fatigue and fracture problems, especially the loading variable;

2) the development of suitable failure functions for the reliability analysis of fatigue and fracture under the action of random loading or monotonic loading;

3) the development of suitable reliability calculation procedures for fatigue and fracture problems.

8.2 Scope For Future Work

This thesis has in a way raised more questions than it has solved. However as a direct result of this work further research can be briefly listed below:

1) the extension of the probabilistic methods to the treatment of structural systems;

2) the physical nature of fatigue and fracture problems in a probabilistic manner, e.g. stress interaction effects, stochastic fatigue modelling, crack instability problems etc.;

3) direct applications e.g. design safety, fatigue prediction, safety assessment for existing structures, maintenance strategies.

REFERENCES:

Chapter 1

1.1 Duddeck, H., The role of research models and technical models in engineering science, Proceedings, ICOSSAR'77, Ed. H. Kupfer *et al*, Werner Verlag, Du..sseldorf, 1977, pp.115-118

1.2 Baker, M.J. and Wyatt, T.A., Methods of reliability analysis for Jacket platforms, Paper 84, BOSS 1979

Chapter 2

2.1 Freudenthal , A.M., The safety of structures, Trans. ASCE, Vol. 112, 1947

2.2 BSI BS 449, Addendum No. 1 Part 2, Specification for the use of cold formed steel sections in buildings, 1969

2.3 BSI BS5400, Structural use of steelwork in building, 1985

2.4 CIRIA, Rationalisation of safety and serviceability factors in structural codes, CIRIA Report No. 63 London, 1977

2.5 Gates, R. S. , An elastic plastic probability fracture mechanics methodology, CEGB SWR/SSD/0260/83 Job No. 01-80, 1983

2.6 Cornell , C.A., A probability based structural code, Journal of the American Concrete Institute, Vol. 66 , No. 12, 1969

2.7 Hasofer, A.M. and Lind, N.C., Exact and invariant second moment code format, ASCE EM DIV., Vol. 100, 1974

2.8 Ditlevsen, O, Structural reliability and the invariance problem, Research report No. 22, Solid Mechanics Division, University of Waterloo, Waterloo, Canada, 1973

2.9 Madsen, H.O., Krenk,S. and Lind, N.C., Methods of structural safety, Prentice-Hall, 1986

2.10 Thoft-Christensen,P. and Baker,M.J., Structural reliability theory and its applications, Springer-Verlag, 1982

2.11 Blockley, D.I., The nature of structural design and safety, Ellis Harwood, Chichester, 1980.

2.12 Ang, A. H-S. and Tang, W. H., Probability concepts in engineering planning and design, Vol. 1 Basic principles, John Wiley and Sons, Inc. 1975

2.13 Bogdanoff, J.L. A new cumulative damage model, J. of Applied mechanics, Vol. 45 pp. 246-257, 1978

2.14 Rackwitz, R. and Fiessler, B., Structural reliability under combined random load sequences, Computers and structures, Vol. 9, pp. 489-94, 1978

2.15 Rosenblatt,M., Remarks on a multivariate transformation, The Annals of mathematical statistics, Vol. 23, 1952

2.16 Fiessler, B., Neumann , H.-J. and Rackwitz, R., Quadratic limit states in structural reliability, ASCE, EM div. Vol. 100 pp. 111-121 1974

2.17 Tvedt, L., Two second order approximation to the failure probability, Veritas report RDIV/20-004-83, Des norske Veritas, Oslo, Norway, 1983

2.18 Breitung, K., Asymptotic approximations for multinormal integrals, ASCE EM div Vol 110 No 3, 1984

2.19 Thorpe, J.A., Elementary topics in differential geometry, Springer, New York, N.Y., 1979

2.20 Chen.X and Lind,N.C., Fast probability integration by three-parameter normal tail approximation, Structural Safety, Vol. 1 pp269-276, 1983

2.21 Wu,Y.T. and Wirsching,P.H., New algorithm for structural reliability estimation, ASCE EM div. , Vol. 113 No. 9, Sept. 1987

2.22 Madsen,H.O., Omission sensitivity factors, Structural safety, Vol. 3 pp195-229, 1986

2.23 R/H/R6 - Rev. 3, Assessment of the Integrity of Structures Containing Defects, CEGB, Nov. 1985

2.24 Ditlevsen,O. Narrow reliability bounds for structural systems, J. Struct. Mech. Vol. 7 No. 4 pp. 453-72, 1979

2.25 Ang, A. H-S. and Tang, W. H., Probability concepts in engineering planning and design, Vol. 2 Decision, risk and reliability, John Wiley and Sons, Inc., 1984

Chapter 3

3.1 Latzko, D.G.H.,(ed.) Post-yield fracture mechanics, Pub. app. sci., 1984(2nd ed.)

3.2 Sih, G.C., Handbook of stress intensity factor for researchers and engineers, Institute of fracture and solid mechanics, Lehigh University, Bethlehem, Pa.,1973.

3.3 Griffith, A.A., The phenomena of rupture and flow in solids, Phil. Trans. R. Soc., London, A, Vol. 221, 1921

3.4 Irwin, G.R., Analysis of stress and strains near the end of a crack traversing a plate, Trans. ASME, J. of Applied mechanics. Vol. 24, 1957.

3.5 ASTM E399-78, Standard test method for plane strain fracture toughness of metallic materials, Annual book of ASTM standards, 1979.

3.6 Brown,W.F. Jr. and Srawley, J.E., Plane strain crack toughness testing of high strength metallic materials. ASTM STP 410, 1967.

3.7 BSI, BS 5447, Methods of test for plane strain fracture toughness (K_{1c}) of metallic materials, UK, 1978.

3.8 Rolfe, S.T. and Barsom,J.M., Fracture and fatigue control in structures: Applications of fracture mechanics, Prentice-Hall, Inc. 1977. pp. 178

3.9 Ibid., pp. 180

3.10 Ibid., pp. 184

3.11 Irwin, G.R., Fracture, Handbuch der Physik, VI, pp. 551-90, Springer-verlag, Heidelberg, 1958.

3.12 Dugdale, D.S., Yielding of steel sheets containing slits, J. Mech. phys. solids, Vol. 8 pp. 100-8, 1960

3.13 Newman, J.R., A Review and Assessment of The Stress-Intensity Factors for Surface Cracks, Chang , J.B. (ed.) ASTM STP 687

3.14 Sinclair, G.B. and Chambers, A.E., Strength size effects and fracture mechanics: what does the physical evidence say?, Engineering fracture mechanics Vol. 26 pp. 279-310, 1987

3.15 BSI PD 6493:1980, Guidance on some methods for the derivation of acceptance levels for defects in fusion welded joints.

3.16 Burdekin, F.M. and Stones , D.E. W., The crack opening displacement approach fracture mechanics in yielding materials, J. Strain Anal. Vol. 1 pp. 145-53, 1966

3.17 Rice, J.R., Paris, P.C. and Merkle, J.G., Some further results on J-integral analysis and estimates, ASTM STP 536, 1973

3.18 Hutchinson, J.W., Singular behaviour at end of tensile crack in hardening material, J. Mech. Phys. Solids. Vol. 16 pp. 13-31, 1968

3.19 Rice, J.R. and Rosengren, G.F., Plane strain deformation near crack tip in power-law hardening material, J. Mech. Phys. Solids. Vol. 16 pp. 1-12, 1968

3.20 Hutchinson, J. W., Crack tip singularity fields in nonlinear fracture mechanics: A survey of current state, ICF 81, pp. 2669-683, 1981

3.21 McMeeking, R.m. and Pars, D.M., A criterion for J-dominance of crack-tip fields in large scale yielding, Elastic-plastic fracture, Landes, J.D.and Begley, J.A. (ed.) ASTM STP 668, 1979

3.22 Shih, C.F., Relationship between the J-integral and crack opening displacement for stationary and extending cracks, J. Mech. Phys. Solids, Vol 29, pp. 305-26, 1981

3.23 Sumpter ,J.D.G. and Turner, C.E., Design using elastic-plastic fracture mechanics, Int. J. Fract. Vol. 12 pp. 861-73, 1976.

3.24 Paris, P.L., Ernst, H. and Turner,C.E., A J-integral approach to development of factors., Fracture mechanics: Twelfth conference, ASTM STP 700, pp. 338-50

3.25 Rice, J.R. *etal*, Some further results of J integral analysis and estimates, Progress in flaw growth and fracture toughness testing, ASTM STP 536, pp. 231-45, 1973.

3.26 Clark, G.A. and Landes, J.D. Evaluation of the J integral analysis for the compact specimen considering axial force as well as bending effects, J. pres. vess. tech., pp. 286-92. ,1974.

3.27 Ersnt, H.A. *etal*, Estimation of J-Integral and tearing modules T from a single specimen test record, Fracture mechanics 13th conference, ASTM STP 743, pp. 476-502, 1981.

3.28 Ernst, H.A., Material resistance and instability beyond J-controlled crack growth, Elastic plastic fracture: second symposium, Vol. I , 1983.

3.29 Dowling, A.R. and Townley, C. H. A., Int. J. of press. vess. and piping, Vol. 3 1975

3.30 See 2.23

3.31 Kumar, V. and Shih, C.F., Fully plastic crack solutions, estimation scheme, and stability analysis for the compact specimen, Fracture mechanics: twelfth conference, ASTM STP 700, 1980

3.32 Neale, B.K., Curry,D.A., Green,G., Haigh, J.R. and Akhurst, K.N., A procedure for the determination of the fracture resistance of ductile steels, Int. J. of press. vess. and piping Vol. 20, 1985

3.33 Ainsworth, R.A., Dowling,A.R., Milne,I., Stewart,A.T., Revision 3 of R6 its background and validity, Fracture control of engineering structures - ECF 6, 1986

3.34 Newman , Loss (ed.), Elastic Plastic Fracture Mechanics Technology, ASTM STP 896, 1985

3.35 Rhee, H.C. and Salama, M.M., Application of Fracture Mechanics Method to Offshore Structural Crack Instability Analysis , OTC 5023, 1985

3.36 Ainsworth, R. A., The treatment of thermal and residual stresses in fracture assessments, Engineering fracture mechanics, 1987

3.37 Milne,I., Failure analysis in the presence of ductile crack growth, Material science and engineering, Vol. 39, pp. 65-79, 1979

3.38 Turner, C.E. Description of stable and unstable crack growth in the elastic-plastic regime in terms of J_r resistance curves, Fracture mechanics. ASTM STP 677 pp. 614-28, 1979

Chapter 4

4.1 Larsson, Lars. Hannes(ed.) , Elastic plastic Fracture Mechanics, Proc. of the 4th Adv. Seminar on Frac. Mech., Joint Research Center, Ispra, Italy 24-28 Oct. 1983 pp. 8

4.2 See 2.5

4.3 OED/STM/87/10125/N, Job No. 00-27 , CEGB OED STB (midland area) , Statistical Analysis of Fracture Toughness Data, Dec. 1987

4.4 See 2.10

4.5 The Welding Institute, Size Measurement and Characterisation of weld defects by Ultrasonic Testing - part 2: Planar defects in ferritic steel, W I Report 3527/100/80/

4.6 R/H/R6 - Rev. 2 , Assessment of the Integrity of Structures Containing Defects, 1982, Appendix 5

4.7 Newman.Jr., J.C. A Review and Assessment of The Stress-Intensity Factors for Surface Cracks, Chang , J.B. (ed.) ASTM STP 687

4.8 See 3.37

4.9 Milne, I., Calculating the Load Bearing Capacity of A Structure Failing by Ductile Crack Growth, Advances in Fracture Research, Fracture 81, 5th Int. Conf. on Frac. Mech. , Cannes, France, 29 March - 3 April, 1981

Chapter 5

5.1 Cartwight, D.E. and Longuest-Higgins, M.S., The statistical distribution of the maxima of a random function, Proceeding of the Royal Society, Vol. 237 pp212-232, 1956

5.2 Lin, Y.K, Probabilistic theory of structural dynamics, Mcgraw-Hill, 1976

5.3 Nerzic, R. and lebas, G., Uncertaities in wave loading from full-scale measurement, BOSS 88 pp. 1399-412

5.4 Wirshing, P. H. and Prasthofer, P.H., Preliminary dynamic assessment of deep water platforms, J. of the Structural Div. (ASCE), July,1976

5.5 Wirsching, P.H. and Light, M.C., Fatigue under wide band random stresses, J. of the structural div. (ASCE)Vol. 106, July. 1980

5.6 Lutes, D.L., Corazao, M., Hu, S., J. and Zimmerman, J., Stochastic fatigue damage accumulation, J. of the Structural Div. (ASCE), Nov. 1984

5.7 Chaudhury, G.K and Dover, W.D, Fatigue analysis of offshore platform subject to seawave loadings, Int. J of Fatigue, Jan. 1985

5.8 Wirsching, P.H. and Shehara, A.M., Fatigue under wide band random stresses using the rainflow method, J. of Engng. Mater. Technol. (Trans. ASME), July 1977

5.9 Corazao, M., Stress ranges prduced by stochastic loads, Thesis presented to Rice Univ. at Houston, Tex., In partial fulfilment of the requirements for the degree of the master of science, 1981

5.10 Zimmerman, J.J., Stochastic stress history simulation for fatigue analysis, Thesis presented to Rice Univ. at Houston, Tex., In partial fulfilment of the requirements for the degree of the master of science, 1983

5.11 See 2.10

5.12 Pierson, W.J. and Moskowitz, L., A proposed spectral form of fully developed wide seas based on the similarity theory of S.A.Kitaigordskii., J. of Geophsical Reserch, Vol. 69 No. 24. Dec. 1964

5.13 Hasselmann, K. *et al.*, Measurement of Wind-Wave Growth and swell Decay during the Joint North Sea Wave Project(JONSWAP), Deutsches Hydrogrphisches Zeitschrift, Hamburg, Reihe A(8) Nr. 12.

5.14 Karadeniz, H., Spectral analysis and stochstic fatigue reliability calculation of the offshore steel structure, Report, Delft Univ. of Techno., Dept. of Civ. Eng. April, 1983

5.15 Brabbia, C.A. and Walker, S., Dynamic analysis of offshore structures, Newnes-Butterworths, London, 1979

5.16 Shinozuka, M. and JAN, C.-M., Simulation of multi-dimensional random processes, J. of the Acoustical society of America, Jan. 1972

5.17 Yang, J.N., Simulation of the random envelope processes, J. of sound and vibration, Vol. 21, No. 1, 1972

5.18 May, H.I., A study of the effect of yield on the dynamic response of tall structures to wind loading, Ph.D. Thesis to the Univ. of London, Dept. Of Civ. Eng., Imperial College, 1988

5.19 Anagnostides, G., Design of economical means of enhancing the energy absorption of steel braced frame structures, Ph.D. Thesis to the Univ. of London, Dept. of Civ. Eng., Imperial College, 1988

5.20 Clough, R.W. and Penzien, J., Dynamics of structures, McGraw-Hill, 1975

5.21 Matsuishi, M. and Endo, T., Fatigue of metals subjected to varying stresses, The Japan Society of Mechanical Engineers, Fukuoka, Japan, March, 1968

5.22 Lind, N.C., Krenk, S. and Madsen, H.O., Safety of structures, Prentice Hall Inc., 1985

5.23 Dowling, N.E., Fatigue failure prediction for complicated stress-strain histories, J. of materials, JMLSA Vol. 7 No. 1, March 1972

5.24 Rice, J.R. and Beer, F.P., On the distribution of rises and falls in a continuous random process Journal of Basic Engineering, Trans. ASME D Vol. 87 June, 1965

5.25 Borgman, L. E., Wave Forces on Piling for narrow-band spectra, J. of the waterways and harbors div. ASCE, Vol. 91, 1965

5.26 Moa, G. and Crandall, S. H., Extremes of morison-type wave loading on a single pile, J. of mechanical design, ASME, Vol. 99, 1973

5.27 Rychlik, I., A new definition of the rainflow cycle counting method Int. J. of fatigue Vol. 9 Feb. 1987

5.28 Lindgren,G. and Rychlik, I., Rain flow cycle distribution for fatigue life prediction under Gaussian load precesses, Fatigue and fracture of Engng. Mater. and struct., Vol. 10 No. 3, 1987

5.29 Ford, D.G., Range-mean-pair Exceedences in Stationary Gaussian Processes Reliability and Optimisation of Structural Systems, Edited by P. Thoft-Christensen, Springer-verlag

5.30 Wirsching, P.H., Fatigue reliability in welded joints of offshore structures, Int. J. Fatigue, April, 1980

5.31 Ang, A.H-S and Tang W.H., Probability Concepts in Engineering Planning and Design Vol. 1 pp274, 1975

Chapter 6

6.1 Duggan,T.V. and Byrne, J., Fatigue as a design criterion (2nd ed.) Macmillan, 1979

6.2 Baker, M.J., Probabilistic fracture analysis of typical lower hull welded joints, Final report, Dept. of Civ. Eng. Imperial College, 1984

6.3 Glinka, G., Dharmavasan, S. and Dover, W.D. An analysis of the efeect of residual stress on the initiation and fatigue crack growth in tubular joints, Steel in marine structures, ed. by Noordhoek, C. and de Back, J., 1987.

6.4 Osgood,C.C., Fatigue Design (2nd ed.) Pergamon press, 1982

6.5 Paris, P.C., The Fracture Mechanics Approach to Fatigue. Fatigue, An Interdisciplinary Approach, Edited by J.J.Burke, N.L.Reed, and V.Weiss, Syracuse Univ. Press, 1964

6.6 Forman, R.G., Kearney, V.E. and Engle, R.M., Numerical analysis of crack propagation in cyclic loaded structures, ASME paper No. 66-WA/ Met 4, 1964

6.7 Schütz, W., The prediction of fatigue life in thr crack initiation and propagation stage- a state of the art survey, Engineering fracture mechanics Vol. 11 pp. 405-21, 1979

6.8 Schütz, W. and Oberparleiter, W., Ermittlung des unteren Grenzwertes F..ur den Rissfortschritt

bei Flugzeugbauwerkstoffen. IABG-Bericht TF-583, 1976

6.9 Chang, J.B.(ed.) Part through fatigue life prediction ASTM STP 687, 1979

6.10 Wheeler, D.E., Fatigue growth under spectrum loading, General dynamics, Rep. FZM 5602, 1970

6.11 Willenborg, J., Engle, R. M. and Wood, H. A., A crack growth retardation model using an effective stress concept, AFFDL TM-71-1FBR, 1971

6.12 Elber,W. Fatigue crack propagation under random loading: An analysis considering crack closure, Proc. Tech. session of the 11th ICAF-Meeting, Stockholm, 1969

6.13 de Koning, A.U., A simple crack closure model for prediction of fatigue crack growth rates under variable-amplitude loading, ASTM, STP 743, 1981

6.14 Nowack, H. *et al*, Sequence effects on fatigue crack propagation; mechanical and microstructural contributions, ASTM STP 677, 1979.

6.15 Chang, J.B., Engle, R.M. and Stolpestad, J. Fatigue crack growth behaviour and life predictions for 2219-T851 aluminium subjected to variable-amplitude loadings, ASTM STP 743, 1981

6.16 Dill, H.D. and Saff, C.R., Analysis of crack growth following compressive high loads based on crack surface displacements and contact analysis, ASTM STP 637, 1977

6.17 Schijve, J. Observations on the prediction of fatigue crack growth propagation under variable-amplitude loading, ASTM STP 595, 1976

6.18 Wirsching, P.H and Light, M.C., Fatigue under wide band random stresses, J. of the Structural Div. (ASCE)Vol. 106, July. 1980

6.19 Hibberd, R.D. and Dover, W.D., The analysis of random load fatigue crack propagation, Fracture 1977, Vol. 2, ICF 4, Waterloo, Canada, 1977

6.20 Dover, W.D., Variable amplitude fatigue of welded structures, Conf. on fracture mechanics, Cambridge, 1979.

6.21 Chaudhury , G.K. and Dover, W.D., Fatigue analysis of offshore platforms subject to seawave loadings, Int J Fatigue Vol. 7, pp. 13-9, 1985

6.22 Hancock, J.W. and Huang, X. W., A reliability analysis of fatigue crack growth under random loading, Final report of the cohesive programme of research and development into the fatigue of

offshore structures (July 83-June 85). Marine technology directorate Ltd., Dec., 1985,

6.23 Miner, M.A., Estimation Fatigue Life with Particular Emphasis on Cumulative Damage, Metal Fatigue edited by B. Sines and J.L.Waisman, McGraw-Hill Publishing Co., Inc., New York, 1959

6.24 Wirsching, P.H., Fatigue Reliability for Offshore Structures, J. of the Structural Div. (ASCE), Vol. 110 Oct., 1984

6.25 Yamada, K. and Albrecht, P., Fatigue behaviour of two flange details, J. of the Structural Div. (ASCE), Vol. 193 Apr., 1977

6.26 See 5.1

6.27 Kam, J.C.P., and Dover,W.D., Fast fatigue assessment procedure for offshore structures under random stress history, Proc. Institn Civ. Engrs, Part 2 , Vol. 85, Dec., 1988

6.28 BSI PD6493 1980

Chapter 7

7.1 Virkler , D.A., Hilberry, B.M. and Goel, P.K., The statistical nature of fatigue crack propagation J. Of Engineering Material and Technology ASME, Vol. 101 1979 pp. 148-153

7.2 Bogdanoff, J.L., and Kozin, I., A new cumulative damage model, Part 4. J. Appl. Mech., Vol. 47, 1980

7.3 Lin. Y. K., and Yang, J. N., On stochastic moments of fatigue crack propagation, J. Eng. Frac. Mech., Vol. 18, 1983 pp. 243-256

7.4 See 6.2

7.5 Wirsching, P.H., Fatigue Reliability in welded joints of offshore structures Int. J. Fatigue April 1980

7.6 Eggwertz, S and Lind, N.C. (Ed.), Probabilistic Methods in the mechanics of solids and structures IUTAM Symposium Stockholm, Sweden Springer-Verlag June 19-21, 1984

7.7 Madsen, H.O. Skojong, R and Moghtaderi-Zadeh, M., Experience on probabilistic Fatigue Analysis of Offshore Structures BOSS 85

7.8 Snijder, H.H. , Gijsbers, F.B.J., Gijkstra, O.D., and ter Avest, F.J., Probabilistic fracture mechanics approach of fatigue and brittle fracture in tubular joints, "Steel in marine structures", edited by Noordhoek, C. and de Back,J. Elsiever Science Publishers B.V. , Amsterdam, 1987